Development and non-equilibrium functions of a supramolecular oscillator



Michael G. Howlett

Wolfson College

A thesis presented in partial fulfilment of the requirements
for the award of the degree of

Doctor of Philosophy
of the
University of Oxford

Department of Chemistry

Hilary Term 2023

Declaration

This thesis describes work conducted in the Chemistry Research Laboratory, Oxford between February 2019 and March 2023, under the supervision of Professor Stephen Fletcher. The thesis is entirely my own work except where otherwise indicated and acknowledged. It has not been submitted for any other degree at this university or at any other institution.

Michael G. Howlett

Acknowledgements

I am hugely grateful to Steve for granting me such independence whilst exploring such an exciting research topic and for drilling into me the importance of brevity in writing – advice that I will have to ignore here as I acknowledge all of the wonderful people who have supported me.

I must pay tribute to some of those who played key roles before I began in the Fletcher group. Namely, Jordi Burés who set me on the path towards autocatalysis, Kat Badiola who, at the perfect point in time, introduced me to the mindset for practical kinetic analysis, and Martin Smith, who was a supportive mentor whilst we worked together.

Sarah and Rob were the first Fletcher group members I met and I owe them my thanks for inspiring me to join, and specifically Rob for enduring my countless questions whilst I found my feet.

To the brave souls who joined me in working on so-called 'scam chemistry' (a.k.a blue skies research), Roshni, Muffin, Lukas and Zhiheng, I hope you enjoyed team oscillator as much as I enjoyed mentoring you, and I'm sure you've all got exciting times ahead.

As we all emerged from a pandemic in the middle years of my studies, it was the social core of the group at the time who truly kept me sane and who selflessly joined me in supporting the local pubs. David, I think my life expectancy will skyrocket once I stop sharing a lab with you, but you've made me laugh every single day and I wouldn't have had it any other way. Martin, I know you're an NPC, but despite your programming (Input: Yes, I have food for today.) you're simultaneously the most infuriating and nicest person I know. Conor, you're an absolute hero and your energy brought a lot of joy to the group. Likewise, Milky, thank you for being the Positivity Coach of the bay and for tolerating an absurd nickname for so long.

Special thanks go to Ton who was with me during some of the most challenging times and contributed significantly not only to this thesis but how I grew during my time in Oxford. I am grateful to you for being a dear friend, a role model and the best person I could have hoped to work with.

To all of the other Fletcher group members who provided good advice and good laughs, whether our time as lab mates was long or short, thank you for putting up with me when the UPLC had a tantrum and for teaching me many things beyond my own project. In the early years this bunch included Elias, Reece, Lucy, Wieland, Joseph, Elena and Masha; later on it was Yan, Violeta, Sourabh, Florian, Ke and Tilly who helped me towards the finish line with their company.

I'd like to thank the Kukura group, particularly Eric, Manish and Jack, for always being so welcoming and for making sure I didn't break anything expensive.

These acknowledgements wouldn't be complete without mentioning several people outside the research team who, each in their own way, helped keep me going and provided perspectives and distractions when things were tough. Thank you, Alex, George, Andrew, Jeroen, Ryan, Johnny and the ultimate frisbee community for all of your friendship during this chapter of my life.

The greatest discovery of my time in Oxford has been my partner, Laura. You are an endless source of dark humour, wisdom and love, and I am humbled to have someone so supportive by my side.

Lastly, I thank my parents for all of their love since I left home a decade ago, I know you've been cheering me on every step of the way.

Abstract

Lipids are an important class of chemicals which appear simple in isolation, but collectively show complex supramolecular dynamics. Biology uses lipids ubiquitously and this thesis demonstrates ways in which chemical systems of lipids can emulate traits found in living systems. The primary theme of this thesis is how synthetic, metastable lipids can generate unexpected complexity, for example through emergent selection mechanisms and unique chemically oscillating systems.

Chapter 1 gives a general introduction to self-reproducing lipids both in the context of prebiotic chemistry and as a source of valuable systems-level behaviour. Physical autocatalysis is introduced and presented as a central principle in origins of life research and for related applications. Special consideration is given towards the generation of structural complexity and out-of-equilibrium concepts, both which are important hallmarks of life.

Chapter 2 describes an investigation into competition between self-reproducing lipids. Mixtures of lipids which continuously form and breakdown over time revealed two selection mechanisms, one of which involved an unexpected reaction pathway for some lipids, at the expense of competitors. This work showed new ways that simple chemicals may have become dominant species in prebiotic environments.

Chapter 3 introduces a unique supramolecular oscillator based upon autocatalytic micelles. The development of this system and its core principles are discussed in detail. Supported by high resolution kinetics and other control experiments, the underpinning mechanism of the oscillator is explored. This system has several properties which set it apart from other chemical oscillators and will be a source of interesting chemical systems in the future.

In Chapter 4, the responsivity of the oscillator is used to transduce information in waves of chemical concentration. Fine control over the frequency and period over the waveforms is shown.

Chapter 5 uses the oscillator to guide the transport of chemical cargo between phases, as a demonstration of the potential spatiotemporal control that is possible with such systems.

Abbreviations and notes

Ar	aryl
br	broad
CAC	critical aggregation constant
cat.	catalytic
CMC	critical micelle concentration
CSTR	continuously stirred tank reactor
DLS	dynamic light scattering
DMAP	4-dimethylaminopyridine
DMSO	dimethylsulfoxide
DOSY	diffusion ordered spectroscopy
EDC	1-ethyl-3-(3-dimethylaminopropyl)carbodiimide
eq.	equivalents
ES	electrospray ionisation
g	grams
h	hours
HEPES	4-(2-hydroxyethyl)-1-piperazineethanesulfonic acid
HPLC	high performance liquid chromatography
HRMS	high resolution mass spectrometry
Hz	hertz
iSCAT	interferometric scattering microscopy
J	coupling constant
L	litre
M	molar concentration
MES	2-morpholinoethanesulfonic acid
min	minute

mol	mole
MPC	2-methacryloyloxyethyl phosphorylcholine
NMR	nuclear magnetic resonance
Ph	phenyl
pH	decimal logarithm of the reciprocal of the hydrogen ion activity
R	variable chemical moiety
rpm	revolutions per minute
TFA	trifluoroacetic acid
TLC	thin layer chromatography
TRIS	tris(hydroxymethyl)aminomethane
UPLC	ultra high performance chromatography
UV	ultraviolet
δ	chemical shift
λ	wavelength
°C	degrees Celsius

Notes:

This thesis has been compiled in an 'integrated' format based upon work written up for publication. Where necessary, additional discussion has been included for background and to link the chapters. Details of these manuscripts may be found in the statements appended to each chapter.

The compound numbers reset to 1 at the start of Chapter 2, with consistent numbering between Chapters 2-6. A separate reference list is also provided for each chapter.

Contents

Declaration iii

Acknowledgements iv

Abstract vi

Abbreviations and notes vii

Chapter 1 2

General introduction 2

1.1 Origins of life research 2

1.1.1 Defining and understanding life 3

1.1.2 Theories on the origin of life 3

1.1.3 Molecular reproduction through autocatalysis 5

1.1.4 Physical autocatalysis 8

1.1.5 Opportunities and limitations of physical autocatalysis 8

1.1.6 Mechanistic considerations of physical autocatalysis 9

1.1.7 A special (prebiotic) role for lipids 11

1.1.8 Autopoiesis 12

1.2 Self-reproducing lipid models 13

1.2.1 Early autopoietic systems 13

1.2.2 Complexity-building autocatalytic lipid systems 16

1.2.3 Visualising supramolecular systems with iSCAT 23

1.2.4 Out-of-equilibrium autocatalytic lipid systems 25

1.2.5 Competition and selection in autocatalytic lipid systems 34

1.3 Beyond self-reproduction 40

1.4 Thesis outline 44

References 45

Chapter 2 53

Competition Between Self-Reproducing Lipids 53

2.1 Introduction 53

2.2 Aims 55

2.3 Results and Discussion 56

2.3.1 System overview 56

2.3.2 Reactivity trends established in non-competition reactions 57

2.3.3 Species succession by intrinsic structural factors 61

2.3.4 Unexpected selection effects with increased compositional complexity 63

2.3.5 A dynamic selection mechanism through metathesis 66

2.3.6 Dynamic covalent activation 69

2.4 Conclusions 70

References 71

Chapter 3 78

A Supramolecular Chemical Oscillator 78

3.1 Introduction 78

3.1.1 Oscillations in the natural world 78

3.1.2 Requirements and rationale for designing oscillators 78

3.1.3 Synthetic oscillators 79

3.2 Aims 83
3.3 Results and Discussion 83
3.3.1 System overview 83
3.3.2 Initial experiments and optimisation 84
3.3.3 Mechanistic descriptions of the system 87
3.3.4 Supramolecular investigations by iSCAT 92
3.3.5 Mechanistic investigations 94
3.3.6 Control of the oscillations 105
3.4 Conclusions and outlook 107
References 108
Chapter 4 115
Information transduction via controllable chemical waves 115
4.1 Introduction 115
4.1.1 Communicating information by different means 115
4.1.2 Oscillators for information transduction 116
4.2 Aims 117
4.3 Results and Discussion 117
4.3.1 System overview 117
4.3.2 A waveform generator 118
4.3.3 Signalling via chemical waves 121
2.4 Conclusions 126
References 127

Chapter 5 131

Oscillation-mediated mass transport 131

5.1 Introduction 131

5.1.1 Controlled transport of molecules 131

5.1.2 Coupling processes to oscillations 131

5.2 Aims 132

5.3 Results and Discussion 132

5.3.1 Initial findings: coupling oscillations to the uptake of chemicals 132

5.3.2 Re-optimisation of the oscillator in a new vessel 134

5.3.3 Proof of concept and reproducibility 136

5.3.3 Transport of hydrophobic cargo 139

5.3.4 Transport directionality 143

5.3.5 Transport-directed reactivity 145

5.4 Conclusions 151

References 152

Chapter 6 157

Conclusions and outlook 157

6.1 Remarks on physical autocatalysis 157

6.2 Chapter 2: Competition between self-reproducing lipids 157

6.3 Chapter 3: A supramolecular chemical oscillator 159

6.4 Chapter 4: Information transduction via controllable chemical waves 160

6.5 Chapter 5: Oscillation-mediated mass transport 160

6.6 Ongoing work 162
6.6.1 Aerobically driven oscillations 162
6.6.2 Oscillating vesicle populations 163
6.7 Describing future models of life 165
6.8 Outlook 167
References 169
Chapter 7 173
Experimental section 173
7.1 General experimental 173
General information 173
Buffer preparation 173
UPLC analysis of reaction samples 174
7.2 Supplementary data for Chapter 2 175
7.2.1 Synthesis of compounds 175
7.2.2 NMR data 184
7.2.3 Procedures for kinetic experiments 199
7.2.4 UPLC methods 200
7.2.5 Aggregate characterisation 213
7.3 Supplementary data for Chapter 3 221
7.3.1 Synthesis of compounds 221
7.3.2 NMR data 225
7.3.3 Procedures for kinetic experiments 231

7.2.4 Control experiments 232

7.2.5 iSCAT and other characterisation of the aggregates 234

7.4 Supplementary data for Chapter 4 240

7.4.1 Synthesis of compounds 240

7.4.2 Procedures for kinetic experiments 240

7.5 Supplementary data for Chapter 5 242

7.5.1 Procedures for kinetic experiments 242

Chapter 1

General introduction

Chapter 1

General introduction

Parts of this chapter are in press at Nature Reviews Chemistry: '(Self-)reproducing lipid systems: from autocatalysis to survival of the fittest'.

1.1 Origins of life research

Origins of life research is widely regarded as 'big picture science' that has attracted a broad range of theoreticians and experimentalists for decades. There has also been significant recent interest from newer academic groups and it seems likely to continue to be explored well into the future. However, despite sustained attention over many years, and next generation researchers applying the latest scientific approaches and tools, the transition from 'chemistry' to 'biology' remains mysterious.

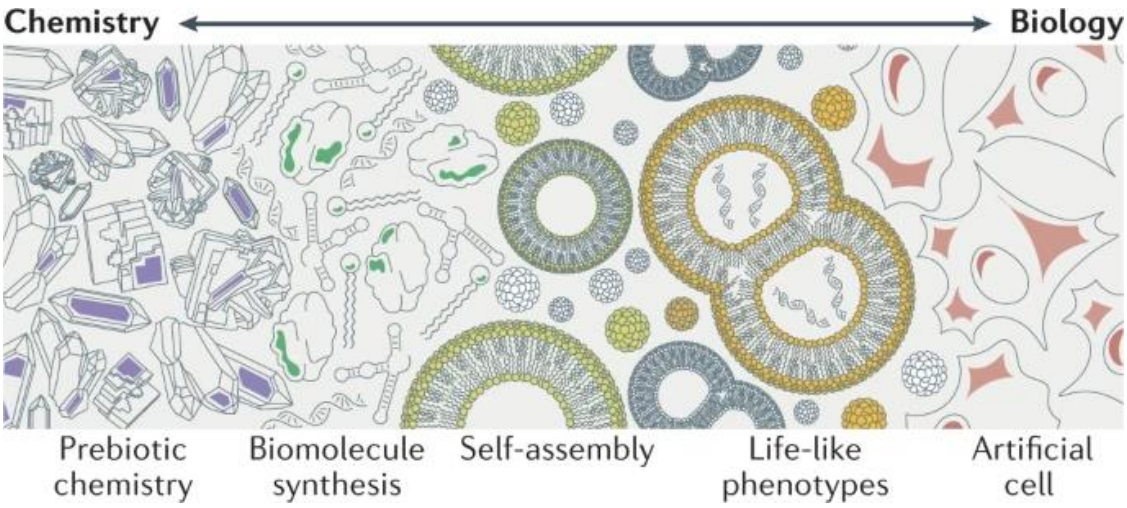

Figure 1.1: Representation of the transition from inanimate chemical beginnings to contemporary biology. Reproduced from Podolsky and Devaraj[1]

1.1.1 Defining and understanding life

Life is remarkably hard to define, and experts might joke that this is its most universally accepted trait – a precise and wholly accepted definition of life is elusive.[2-5] Both 'top-down' and 'bottom-up' strategies to understanding primitive life have been extensively explored – advancing the capabilities of synthetic cells,[6,7] our understanding of prebiotic synthesis,[8-12] and highlighting the importance of studying complex systems.[13-18] However, mimicking biological phenomena and producing the building blocks of (present-day) life from simple chemistry is quite different from making living systems and there appear to be significant technological and conceptual barriers to generating life from inanimate chemicals.

A major problem in 'bottom-up' origins of the life research is that if you generated a primitive living system you probably would not realise it. While problems with defining 'life' are well known, how to experimentally measure and characterize it are likely much more confounding. The challenge of producing a tractable system with sufficient intricacy to show life-like properties and recognising when the threshold for 'life' is met, is considerable. A second problem can be appreciated by considering just how much complexity was gradually built up to form the earliest living systems. The historical pathway from chemical simplicity to biological complexity is relatively traceless and knowing absolutely when and why specific early functional systems thrived is likely beyond our reach. Despite the problems of 'bottom-up' approaches to generating life forms, there is value in seeking the minimal chemical ingredients necessary to model living systems and understanding how increasing complexity emerged and became self-sustaining and reproducing.

1.1.2 Theories on the origin of life

How chemical systems capable of self-maintenance came to be organized and the timeline of their development is *the* question of the emergence of life. Two contrasting theories towards addressing this have steadily gained popularity.

The first, a replicator-first scenario modelled on modern day RNA, posits that rudimentary but competent template molecules were able to catalyse their own formation and eventually had a

metabolic network formed around them, followed by a cell-like structure.[19-24] Improved understanding of the genetic code and catalytic roles for nucleic acids have provided support for this viewpoint.[25,26] However, many researchers have pointed out theoretical difficulties with this model, the most obvious being that it requires a starting point involving highly specialised molecules and very low replication error.[27-29]

An alternative idea is that simple compartments appeared first, and there potentially existed a 'lipid world' as a starting point for prebiotic reproduction.[14,28,30,31] These compartments may have been oil-in-water droplets, coacervates or bounded by self-assembled membranes. The basic idea is that life arose from a population of self-assembling aggregates which can undergo a form of evolution based upon changing composition and resulting function. This container could then establish internal self-sustaining reaction networks that build up the complexity of the entity over time.

By concentrating chemicals within the compartment's interior and insulating early reactions from the environment, a population of privileged guest molecules may have emerged. These little containers may occasionally contain efficient catalysts for the synthesis of more complicated structures (to the benefit of the boundary or its contents). In time, enough catalysts may randomly accumulate such that the system can maintain its own components in a statistically consistent fashion, and even outlast other proto-metabolic systems competing for resources (Figure 1.2).[32-34] This crude process could then transition, by natural selection, to one involving evolved functional assemblies and modern information carriers (e.g. enzymes and DNA).[28]

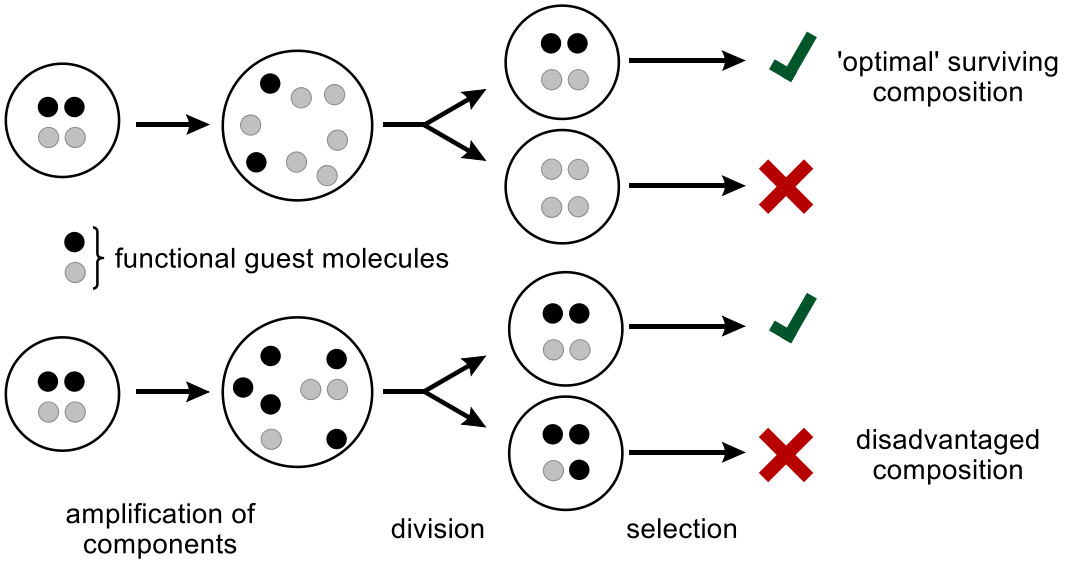

Figure 1.2: Statistical group selection of compartmentalised protocells. Compartments containing functional catalytic molecules uptake material from their environment and multiply their contents, also growing the container. These enlarged compartments then split into daughter 'cells' which have a new internal composition that is statistically determined. These different compositions may be more or less capable of the reactions that sustain them (metabolism), leading to selection between the protocell offspring.[32-34]

In this scenario the physical boundary is clearly beneficial and is key to defining the living unit and protecting it from external factors. One might even ask, without separation from its environment within a boundary, how could life exist? The study of nano- and microscale compartments such as micelles and vesicles is therefore one of the major focuses in the field of prebiotic chemistry. Research in this area has implications which strengthen a compartment-first outlook.

As it stands, no theory or sequence of events has achieved complete dominance or consensus.

1.1.3 Molecular reproduction through autocatalysis

The ability to self-reproduce is fundamental to living things. Organisms can be viewed as complex chemical systems organized to promote reproduction and sustainability. By generating offspring, the population of a species can propagate and evolve. Present-day biological reproduction involves highly evolved biological machinery (RNA and proteins) but at some point reproduction must have used different, and simpler, mechanisms.

Chemical self-reproduction can be accomplished using autocatalysis. An autocatalytic reaction is one where the product acts as a catalyst for its own formation.[35-37] These systems are characterized

principally by a positive correlation between product concentration and reaction rate. This typically results in a sigmoidal concentration-time curve (see Figure 1.3) and an induction period which can be removed by adding product of the reaction to the reaction (seeding).

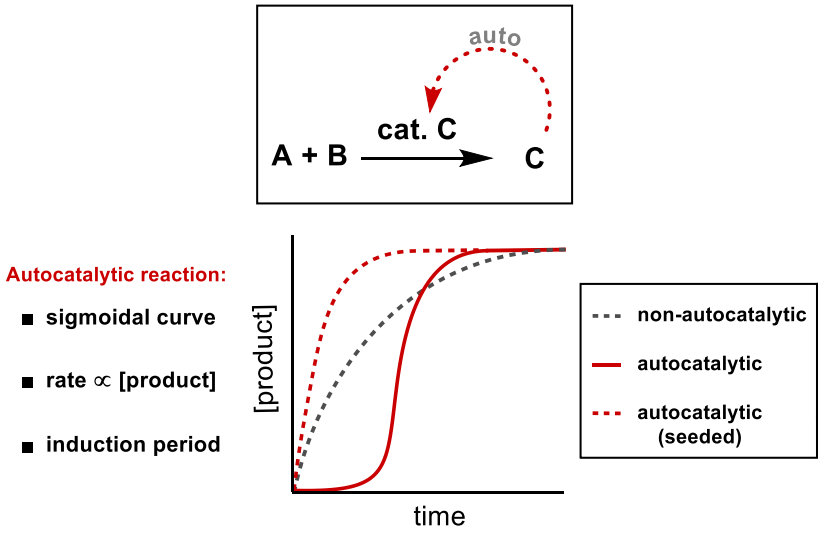

Figure 1.3: Features and kinetics of a generic autocatalytic reaction, with (dashed red line) and without (solid red line) product seeding, compared to a hypothetical non-autocatalytic reaction (dashed grey line).

Autocatalytic processes have been implicated as essential in the emergence of life and being relevant to many current natural processes.[35-38] From chemical systems aimed at mimicking life-like processes to contemporary organisms, all life relies upon autocatalysis in some form. This is true at the easily observable macroscopic level, where members of a species make new beings, at the biochemical level where information polymers like DNA can propagate information in time, and where the building blocks for living systems, such as lipids, are constructed.

While there are many trivial systems that show autocatalytic effects,[35,36,39,40] only autocatalytic systems that may be relevant to the origins of life and emergent properties are discussed here – such autocatalytic systems can be broadly classified by their mechanism of action: network, template or physical autocatalysis (see Figure 1.4).[35]

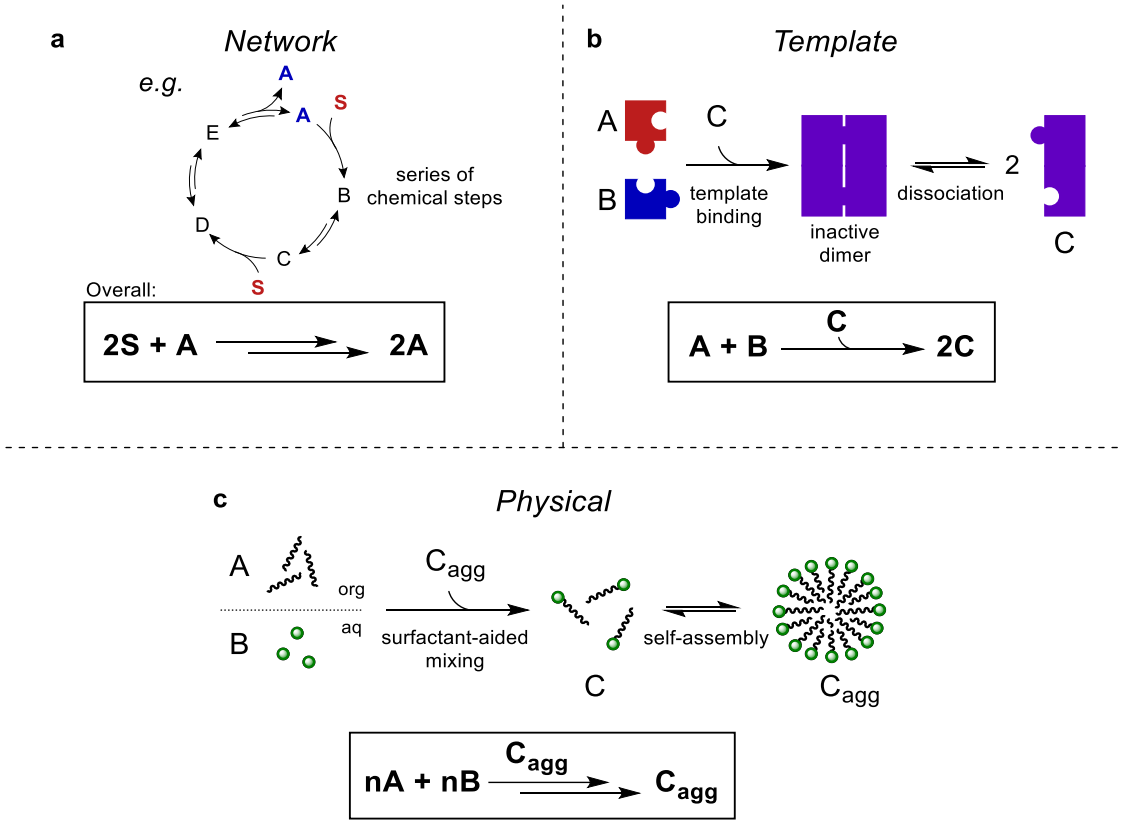

Figure 1.4: Classes of chemical autocatalysis a) A metabolic example of network autocatalysis modelled on the formose reaction (other networks possible) where the autocatalyst (A) is consumed and then regenerated in later reactions, b) template autocatalysis showing formation and dissociation of the product dimer, c) physical autocatalysis which involves enhanced phase transfer of reagents (A + B), promoted by an aggregate (agg) of the product C.

Network catalysis typically involves a series of chemical reactions which consume a compound and produce the same compound downstream, resulting in net production of the autocatalyst. This class is represented by metabolic examples such as the formose reaction,[41,42] the reverse citric acid cycle,[43,44] and also complex inorganic networks such as the Belousov-Zhabotinski reaction (Figure 1.4a).[45-47] Template autocatalysis is roughly the mechanism used by nucleic acids in genetic replication and is likely the autocatalytic mechanism most familiar to chemists and biologists. A template replicator functions by bringing its own precursors together, thereby raising their effective concentration. After reaction, an inactive dimer complex is formed which must dissociate in order to be involved in further replication (Figure 1.4b). Numerous chemical systems operating by this mechanism – inspired by biology –have been reported, with varying degrees of efficiency and complexity.[35,36,48-52]

1.1.4 Physical autocatalysis

A third class of autocatalysis, which is key to much of the chemistry in this thesis, is physical autocatalysis. Here the autocatalyst is not always an individual, well-defined product molecule but is instead something that causes a physical change to the system. In most reported cases the catalyst is a supramolecular aggregate that facilitates formation of its own building blocks (Figure 1.4c). For example, this can be surfactant formation from phase-separated reagents, leading to micelles which allow the starting materials to better mix and react interfacially.

Besides systems forming supramolecular aggregates, physical autocatalysis has also been seen in cosolvent,[53-55] hydrotrope[56] and phase-transfer catalyst[35] forming reactions. Because of this generality, physically autocatalytic effects may appear unexpectedly in some systems and may be harder to recognise than other autocatalytic processes. For a broader overview of autocatalytic systems, the reader is directed to an earlier review on the topic.[35]

1.1.5 Opportunities and limitations of physical autocatalysis

Physical autocatalysts are not affected by product inhibition, which often impacts reproduction efficiency in template replication. Also in contrast to template replicators, elaborate starting materials are not required to create physical autocatalysts. The spontaneity and ability to use readily available materials hints at the relevance of self-reproducing lipids to the origins of life as it provides a means for self-reproduction to readily emerge from a range of different staring conditions.

Physical autocatalysts are inherently non-'faithful' in their mode of action and, in theory, could catalyse any biphasic reaction. This gives autocatalytic lipids a broad capability to show cross-catalytic behaviour and to establish feedback networks.

There is an unusually challenging level of experimental sensitivity inherent in physically autocatalytic reactions. Reactions involving phase changes are sensitive to additional variables in addition to those seen in homogenous reactions. This is exacerbated with non-linear kinetics, where small changes can amplify and lead to drastically different outcomes. Important variables that we

have observed in our own work include: stirring rate, vessel and stir bar geometry, temperature, reaction volume, interfacial area, presence of surfactant impurities/byproducts, disturbances by sampling reactions and pH. All of these factors can influence the reproducibility of the biphasic systems under study. The reactions are 'repeatable' in that the same overall effect is observed when all major variables are well considered (*e.g.* temperature, stirring rate), but are not highly controllable as sometimes inexplicable or overlooked parameters, such as the precise positioning of the reaction vessel relative to the stirring apparatus, can lead to different kinetic profiles for individual experiments. This can lead to frustrating degrees of qualitative-quantitative reproducibility, which can slow progress.

1.1.6 Mechanistic considerations of physical autocatalysis

Physical autocatalysis operates under heterogeneous conditions and involves the transfer of material between phases. The autocatalyst increases mixing between the phases by solubilising the hydrophobic component in the aqueous layer. This enables more efficient interaction of the reagents and thereby increases the rate of biphasic reactions. Physical autocatalysis can be brought about by many different types of systems, including hydrotrope and cosolvent forming reactions, not just the surfactant forming reactions featured heavily in this thesis. In fact, there are likely many different mechanisms that could occur in surfactant forming autocatalysis alone.

Theoretical analysis of reported autocatalytic micelles and vesicles has been carried out by Mavelli and co-workers,[57] Maestro,[58] Mavelli and Luisi[59] and Coveney and co-workers.[60,61] This work aimed to describe the non-linear kinetics observed in such systems and the models broadly matched the experimental trends seen. The observed kinetics were ascribed to a rate limiting interfacial-surface reaction. There was also a strong dependence of rate upon the critical aggregation concentration (CAC) of the supramolecular species, highlighting the importance of self-assembled compartments.

When analysing a micelle-forming system Micheau and co-workers dispute the micellar catalysis interpretation (green pathway, Figure 1.5). They instead propose a phase-transfer catalysis (PTC)

model where hydrophobic reactants are solubilised by the micelles but are released before reacting in the bulk aqueous phase, instead of at the micelle boundary (red pathway, Figure 1.5).[53,62] While this distinction is subtle it may be relevant to whether these systems are 'autopoietic'.

Both micellar catalysis and phase transfer catalysis involve the uptake of reactants (**A**) into the aqueous phase via partitioning into an interfacial region (**1.** in Figure 1.5) and association with the surfactant assembly (**2.**). In the PTC scenario, the reactant is released (**3.**) and will react in the bulk aqueous media (**4.** $\mathbf{A_{aq} + B_{aq} \rightarrow C_{aq}}$) whereas in the micellar catalysis model the reaction occurs at or within the micelle boundary (**5**.). The alternative PTC model accounts for the experimental observations well and agrees with earlier models that micelles solubilise substrate in the aqueous phase. However, Micheau *et al.* suggest that prior theoretical work was not capable of discriminating between micellar and phase-transfer catalysis. In fact, their data suggest that the role of the micelles is solely restricted to transport, followed by reaction in the bulk aqueous instead of at or in the micelles themselves.

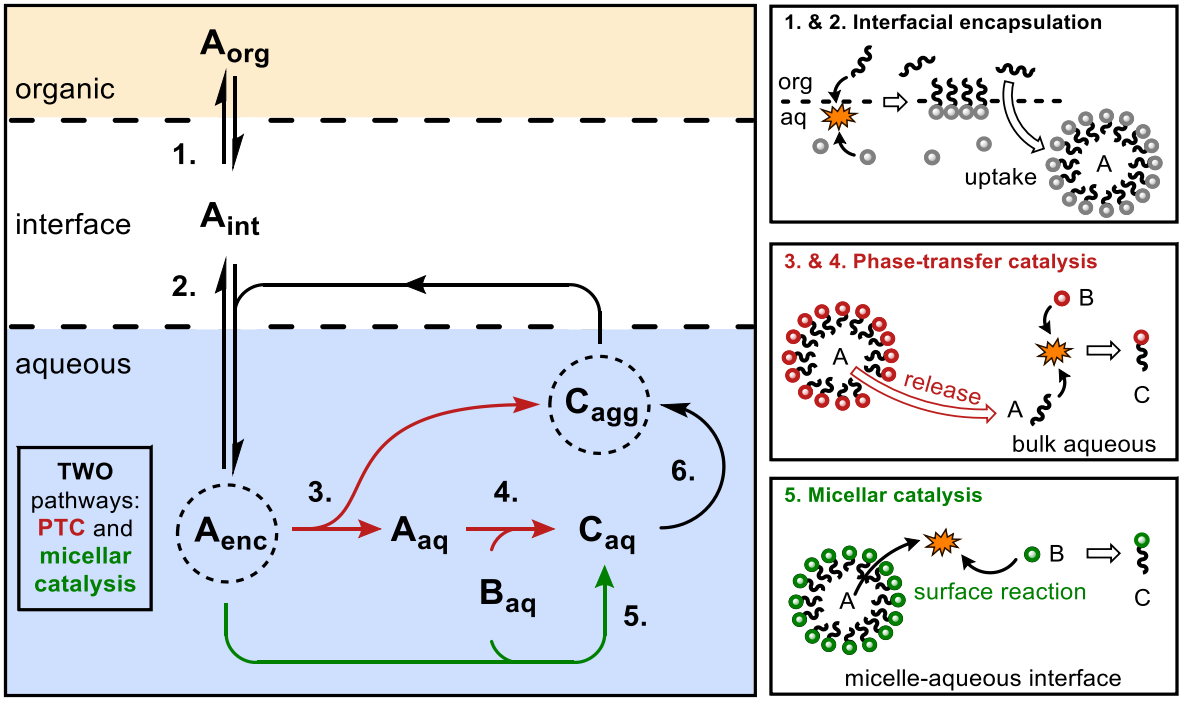

Figure 1.5: Mechanistic overview of micellar catalysis versus phase transfer catalysis (PTC). Note the different location of the reaction $A_{aq} + B_{aq} \rightarrow C_{aq}$ in the two pathways. 1. reactant A_{org} entering interfacial region, 2. uptake of A_{int} by micellar compartments into aqueous, 3. release of A_{aq}, 4. reaction in bulk aqueous phase, 5. reaction on the surface of micelle, 6. self-assembly of any monomers

Definitively demonstrating that a particular mechanistic pathway is occurring is challenging because of the kinetic similarity of the two scenarios, the highly dynamic nature of self-assembled lipids and the sensitivity of biphasic catalysis to experimental conditions. It is of course possible that both pathways could be occurring to different extents under different sets of conditions.

These systems are difficult to study and there are limits on what can be achieved in performing classical 'physical organic chemistry' type studies because of their heterogeneity and sensitivity. However, experimental evidence for the micellar catalysis pathway has been found in some systems examined by diffusion ordered spectroscopy (DOSY). By comparing diffusion rates of small molecules (such as surfactants below their CAC and hydrophobic substrates) and supramolecular assemblies, which are larger and diffuse slower, it can be determined if there is an interaction (*i.e.* uptake or binding) between these components. Specific cases of DOSY analysis, in support of micellar catalysis, have been reported by the Giuseppone and Fletcher groups.[63-65]

1.1.7 A special (prebiotic) role for lipids

Discussion on autocatalytic reactions relevant to life's origins tends to downplay coverage of non-template mechanisms – often simply stating that such work is outside the scope of the article or review.[36,48,49,66] This means that the advances in lipid replicators have not been well highlighted and put into context. Autocatalytic lipid systems show many unique features that have not been well explored or understood, perhaps because of the practical and theoretical difficulties in studying such systems (*vide infra*). Many researchers have considered micelles and vesicles to be relevant to primitive life-forms as lipids are capable of compartmentalisation, self-reproduction and the transmission of compositional information.[30,67-70] The simplicity of lipids' mode of action (spontaneous self-assembly in water) and their (perhaps surprising) functional capabilities suggest they may have been important at the earliest stages of self-organisation and metabolism. The diversity of possible lipid species presents other reasons for their study. Structures composed of mixtures of lipids have been found to be more robust to environmental conditions than structures

with a simpler composition.[71-73] This effect suggests mechanisms for how cooperation between autocatalytic lipids could stabilise early protocells.

Counterintuitively, autocatalysts which can promote the formation of other species and have global effects are more likely to form a complex enough system to 'survive' in a prebiotic scenario. This is because before evolved biomolecules existed, collective means of selection (cross-catalysis and feedback networks) were likely more important than chemical recognition at the individual level. As lipids can, in theory, cross-catalyse any biphasic reaction, they are a potentially central to providing the mechanism and compositional variety for collective, system-level evolution.

Molecules capable of carrying information in chemistry and biology are traditionally thought to be limited to RNA or DNA and similar classes of compounds – not lipids. However, the compositional information contained within heterogeneous lipid mixtures has been compared to sequence based information of biopolymers, with experimental backing.[70,74-76] Walde, Lenhert and Lancet argue that recognition of lipid aptamers could provide a missing link for evolution with micelle and vesicle-type reproducing systems (Figure 1.6). These developments strengthen the role for lipids in early life and a possible 'lipid world' scenario.

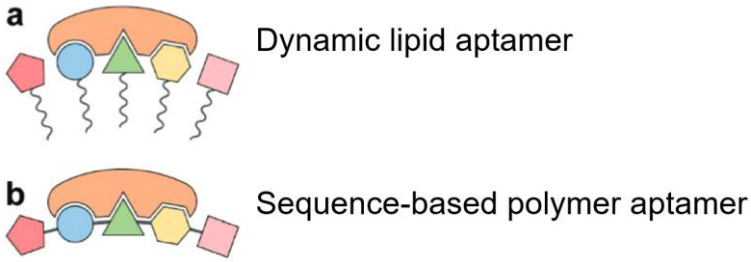

Figure 1.6: A target molecule recognizes aptamers formed from a) lipid headgroups and from b) threaded biopolymer groups (*e.g.* oligopeptides). Adapted from Lancet et al.[70]

1.1.8 Autopoiesis

Autopoiesis is a concept that attempts to define life minimally and was theoretically formulated by Varela and Maturana.[3,77] An autopoietic system is a closed structure which is capable of producing itself by generating all of its components, including the boundary which defines it.[3,77-79] It is conceptually interesting because it focusses on the self-organisation of processes that sustain the

living unit as a whole, rather than characterizing living things by commonly observed but possibly extrinsic features such as movement or evolution.

Self-generation and a boundary with its environment are key features of autopoietic systems. The organisational network that can exist in such a system is illustrated in Figure 1.7. For the case of micellar systems, a surfactant's molecular properties enable organisation into micelles, the micelles facilitate synthesis which, in turn, produce components of the system. Autopoietic micelles have obvious analogies to cellular structures (and are indeed an attempt to mimic these) and can be considered protocells, which are synthetic entities with some characteristics of cells.[80]

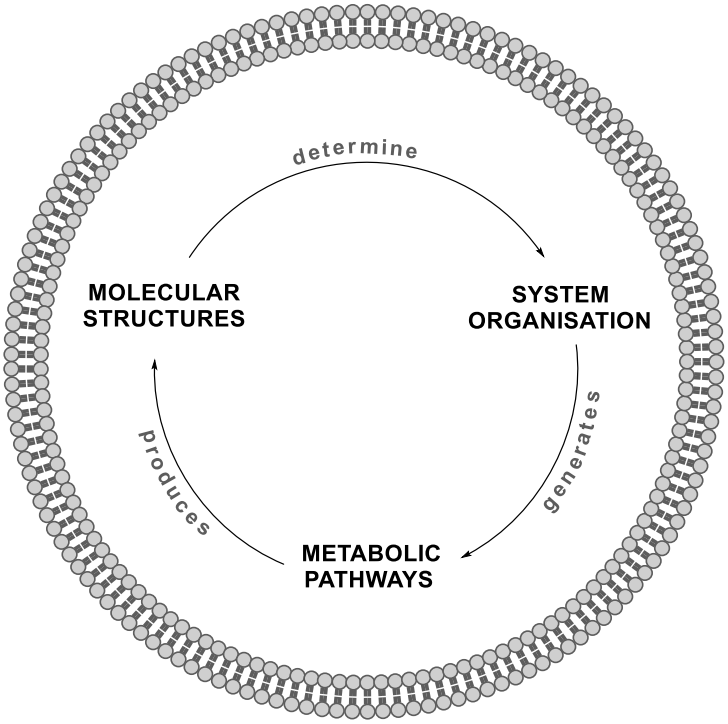

Figure 1.7. Autopoietic organization leading to the self-production of a self-contained circular network of processes. In the case of reproducing micelles, the molecular properties of the amphiphiles determine the self-assembled structure, which then facilitates metabolic processes such as the synthesis of the amphiphile components. Adapted from Fleischaker[79] and Luisi.[81]

1.2 Self-reproducing lipid models

1.2.1 Early autopoietic systems

The Luisi group was the first to experimentally explore how physical autocatalysis may be relevant to the origins of life and in 1990 reported a self-reproducing system of reverse micelles.[78] The

system used a surfactant (50 mM sodium octanoate) and aqueous LiOH in a 9:1 (v/v) mixture of isooctane/1-octanol. The alcohol is essential for making stable reverse micelles, and partitions between the micelle layer and the bulk solvent. LiOH is localized in the aqueous interior of the compartments and octyl octanoate is preferentially in the organic phase (see Figure 1.8a) although some of it will be present at the micellar interface. Hydrolysis of the ester precursor at the micelle interface produces new octanoate monomers, which self-assemble, and so the reaction increases the number of reverse micelles. In this way, the reverse micelles promote their own formation in a biphasic system. Experiments in the absence of sodium octanoate gave no hydrolysis, supporting the autocatalytic role of the micelles and the localisation of the reaction within them.

Luisi's work on simple self-replicating (or self-reproducing – *vide infra*) chemical systems was an attempt to make synthetic autopoietic systems, and was explicitly linked to the theoretical work on autopoiesis and minimal definitions of life.[3,77,82] Overall, his extensive body of work has been enormously influential to prebiotic chemistry.

Several similar systems from the Luisi group were reported in the 1990s, and while the first reports were quite conceptual, better characterized systems with more thorough kinetic information were reported in later work. The synthetic autopoietic systems of the late 20th century focused almost exclusively on self-assembling fatty acid amphiphiles. The octanoate monomer was studied extensively and could be accessed by chemical and enzymatic hydrolysis and by oxidation, giving rise to micelles and reverse micelles depending upon the conditions. Luisi's initial follow up systems demonstrated a degree of generality but all relied on the use of preformed micelles which encapsulated one of the reactants, as opposed to de novo micelle synthesis.[83] Autocatalytic micelles that did not require the presence of preformed aggregates were reported in 1992.[84] The biphasic hydrolysis of ethyl octanoate showed truly remarkable non-linear effects when the concentration of product monomers was followed in time (Figure 1.8b-c).

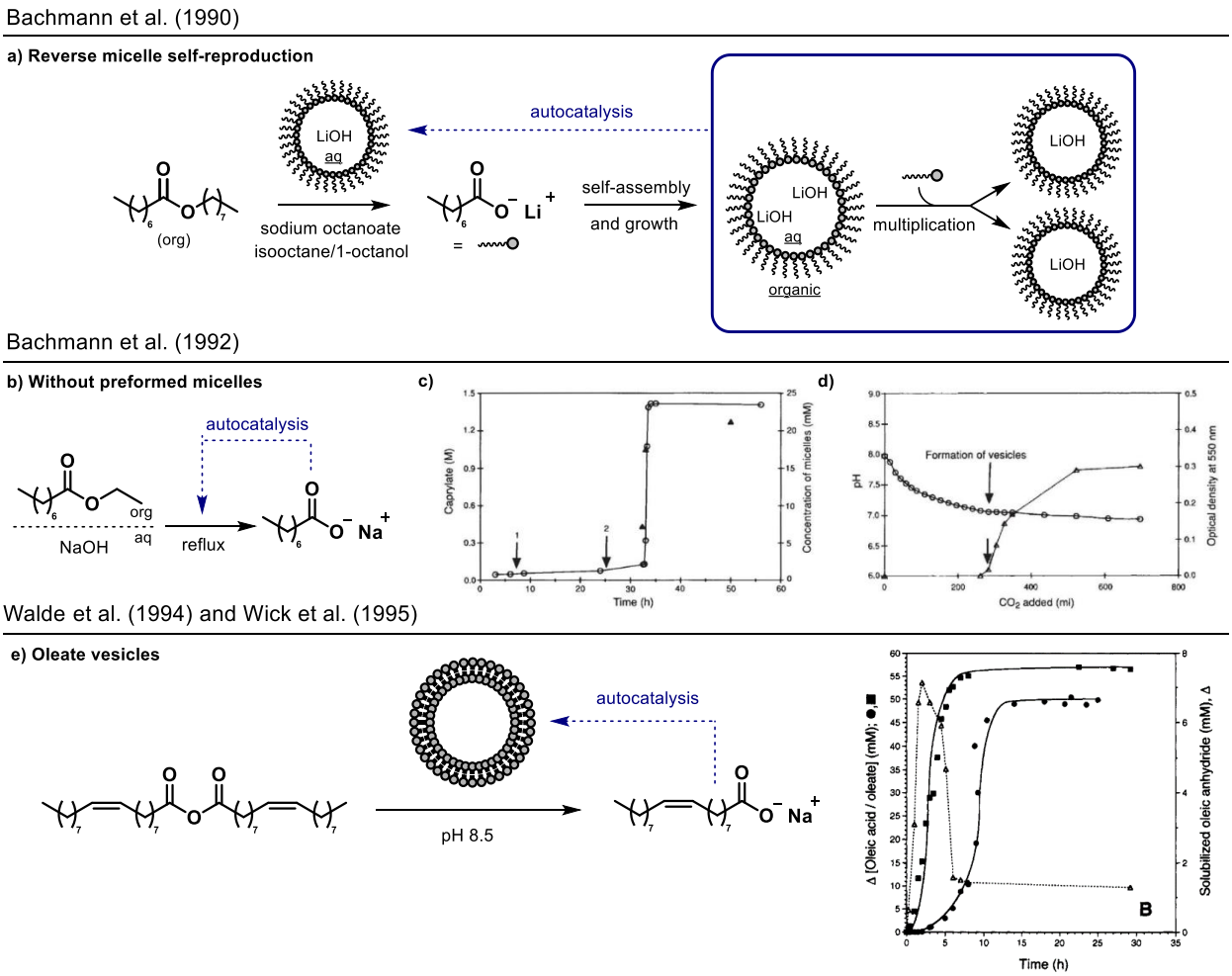

Figure 1.8: Autopoietic systems from Luisi and co-workers based upon micelle and vesicle compartments. a) Luisi's earliest self-reproducing autopoietic system involving alkaline hydrolysis of fatty esters to form reverse micelles. Oxidation of 1-octanol by sodium permanganate and enzymatic hydrolysis of trioctanoyl glycerol were also used in later simple systems to form the octanoate surfactant in a biphasic reaction; b-c) Biphasic hydrolysis of ethyl octanoate without preformed micelles showed a dramatic non-linear effect. Octanoate concentration (circles) and micelle concentration (triangles) increase over time as ethyl octanoate is hydrolysed by aq. NaOH (3M). Onset of exponential growth was regulated by increasing the stirring from 150 rpm to 450 rpm (arrow 1) or by seeding the reaction with 20 mM sodium octanoate (arrow 2), d) A micelle to vesicle transition triggered by the introduction of CO2 to a solution of sodium octanoate micelles, lowering the pH (circles) and increasing the turbidity of the mixture (triangles); e) Using longer chain oleate monomers, autopoietic vesicles could be generated and visualized by microscopy. Graph shows the hydrolysis of oleic anhydride by alkaline buffer (pH = 8.5) over time, forming oleic acid/oleate as measured by FTIR spectroscopy (initial concentration of oleic acid/oleate, 0 mM (filled circles) and 20 mM (filled squares). The concentration of oleic anhydride (in 20 mM seeded experiment) is represented by triangles). Inset images show vesicle birth processes in a 50 mM solution of sodium oleate in alkaline buffer (pH 8.5) when oleic anhydride is introduced. Adapted from the work of the Luisi group.[78,84-86]

Stirring is one of many physical factors that would emerge as important in 'physical' autocatalysis and here, stirring clearly impacts the onset of the exponential growth (see arrow 1, Figure 1.8c). Faster kinetics were also observed when the reaction was seeded with the micellar product (growth onset at arrow 2, Figure 1.8c). The octanoate system was sensitive to environmental changes; the

micelles could transition to vesicles by adding carbon dioxide which lowered the pH to 7 (Figure 1.8d).

Vesicles are attractive as prebiotic models due to their closer analogy to bilayer cell membranes than micelles and ability to hold an internal aqueous compartment. Using a longer chain fatty acid, vesicles could be produced directly. The kinetics of the biphasic reaction between oleic anhydride and an alkaline aqueous layer are shown in Figure 1.8e and clearly exhibit autocatalytic reaction kinetics and growth in terms of number and size of the aggregates formed.[85] Stable giant vesicles could also be produced that undergo birthing events observable by light microscopy, providing support to the general idea that internal self-reproduction is occurring (Figure 1.8e).[86]

Although most early examples of physical autocatalysis involved fatty acid-derived systems, Kust and Rathman demonstrated physical autocatalysis by oxidation of tertiary amines to form N-oxide amphiphiles in 1995 (Figure 1.9).[87]

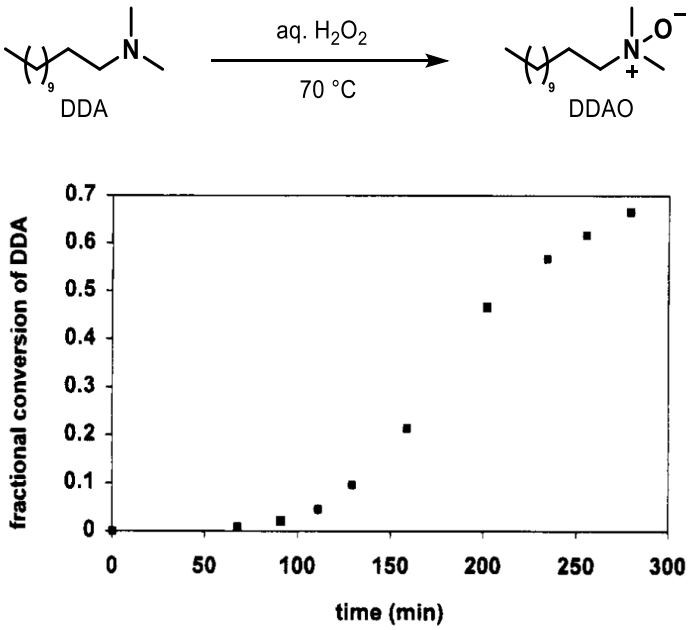

Figure 1.9: Oxidation of aliphatic amines shows (physical) autocatalysis. Reproduced from Kust and Rathman[87]

1.2.2 Complexity-building autocatalytic lipid systems

One clear attribute of life is the construction of complex structures from simple precursors. The pioneering autopoietic systems that use fatty ester hydrolysis are entirely ‘catabolic’ systems,

meaning that they tend towards simpler molecular components. Bissette and co-workers have argued that physical autocatalysis involving bond cleavage processes was limiting as molecular complexity was always being reduced – which is quite the opposite of how living matter organizes itself.[64,88] It was proposed that bond-forming autocatalytic reactions could be used to build-up molecular complexity (see Figure 1.10). Bond formation between precursors (*i.e.* 'anabolic' chemistry) may be more relevant to understanding how to build complexity in a life-like way from relatively simple precursors. Such systems may lose some of their 'prebiotic relevance' if simple fatty acid lipids are viewed as being particularly important to study, but bond forming reactions would, at least in principle, provide access to a wide variety of new autopoietic systems. Anabolic systems would also enable combinatorial synthesis and competition experiments, where mixtures of starting materials are used, so that processes like selection and evolution might be observed. Also, it seems likely that systems built from simple but diverse components are well placed to give rise to emergent phenomena. This is due to the complexity that can arise from combinatorial interactions and the promiscuity of these simple building blocks, both of which can contribute to a wide range of outcomes.

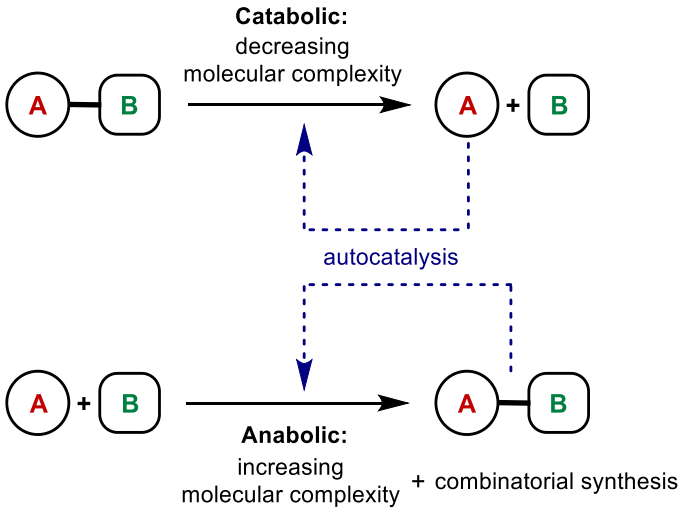

Figure 1.10: Bond breaking and bond forming processes in building molecular complexity. Anabolic, bond forming processes may provide promising routes to building life-like complexity.

In an impressive example of self-reproduction driven by bond-forming reactions, Sugawara and co-workers reported imine-based amphiphiles which self-assemble into giant vesicles. The reversible

reaction between aldehyde **1** and amine **2** gives imine surfactant **3** (Figure 1.11a).[89] Formation of this surfactant is facilitated by a membrane-bound imidazole catalyst **4**. As the catalyst is not a product of a self-reproduction process the system is 'autoinductive' rather than 'autocatalytic'.[37]

There are several design features here to note. For example, **1′** is selectively activated within the vesicle by membrane-bound **4**, the location of which was determined using a tethered fluorescent dye and optical microscopy. Microscopy showed the generation of new vesicles within existing vesicles, which were described as birthing and peeling processes. As the reaction to form the building blocks of the vesicle, and the production of new compartments both occur in a parent vesicle, it is a synthetic autopoietic system.

A related system aimed at making a minimal self-reproducing cell by incorporating DNA was reported by Sugawara in 2011 (Figure 1.11b).[90] Hybrid giant vesicles, composed of a cationic double tailed amphiphiles, were produced *in situ* and were stabilized by additional phospholipid to tolerate polymerase chain reaction conditions. Amplification of DNA within the vesicle promotes both the growth and division of the vesicles, demonstrating feedback between internal processes and propagation of the autopoietic unit. This work may give insight into how primitive lipid-based life forms could outcompete others based on their composition.

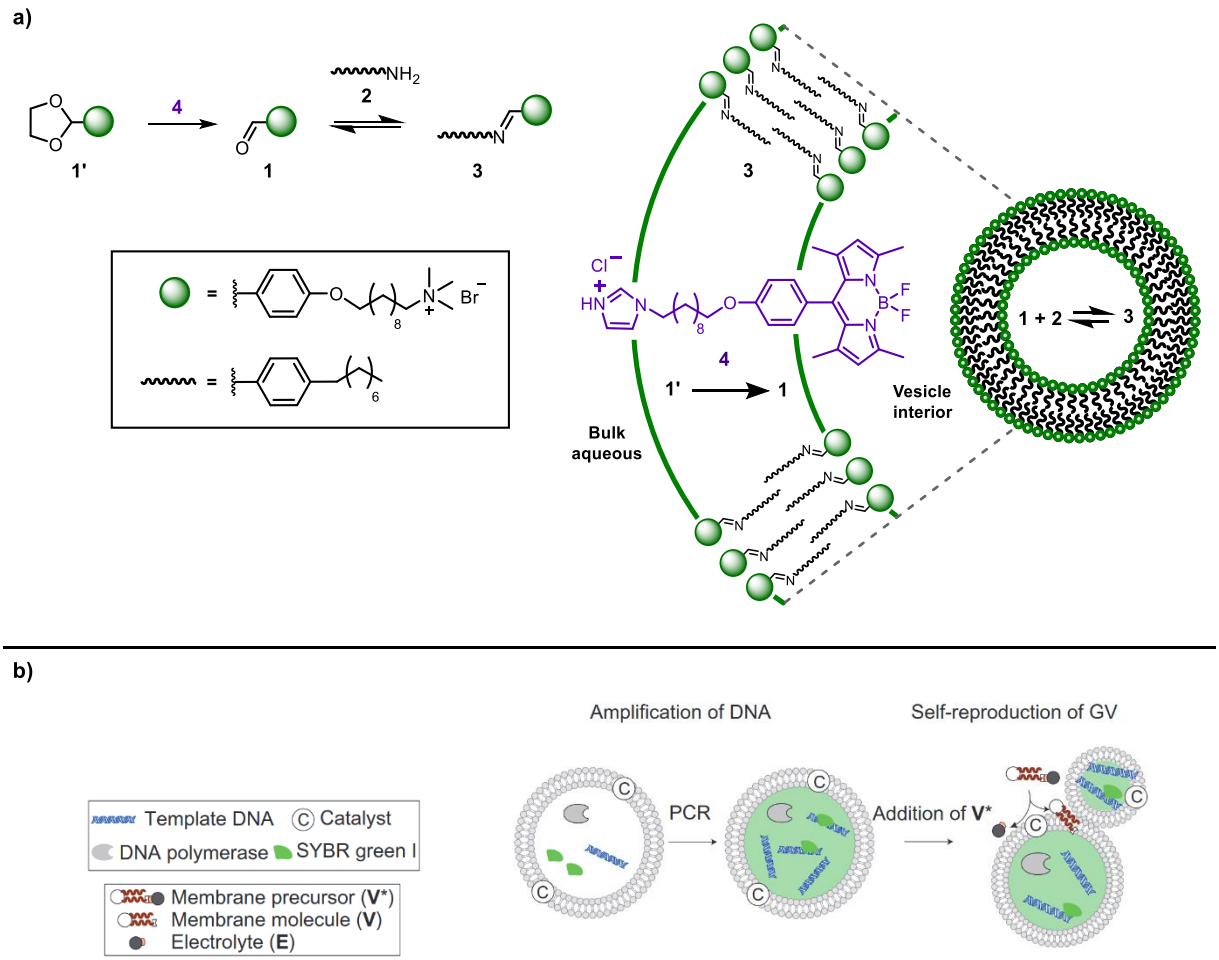

Figure 1.11: Self-reproducing systems based upon reversible imine chemistry. a) Using a membrane bound catalyst, vesicle precursors are activated for reaction and then promote the formation of new vesicles within the parent vesicle, b) Incorporating DNA into autopoietic vesicles resulted in positive feedback between the PCR and vesicle growth and division. Adapted from Kurihara et al.[90]

There is a fundamental difference between what can be achieved with reversible and irreversible chemical reactions. Autocatalytic processes which are initiated by effectively irreversible chemistry could be used to explore out-of-equilibrium systems. Such systems might exhibit new phenomena and allow for the kinetic discrimination between autocatalysts based upon their catalytic efficiency, rather than just thermodynamic stability.

In 2014 Bissette et al. reported examples of physical autocatalysis driven by irreversible bond-forming reactions (Figure 1.12).[64] Their first generation system involved hexanethiol and a phosphatidylcholine-derived Michael acceptor (MPC) to produce a self-assembling phospholipid **5a** under basic conditions. Kinetic analysis revealed a sigmoidal reaction profile and the removal of the lag period when the reaction is seeded with product, confirming autocatalysis.

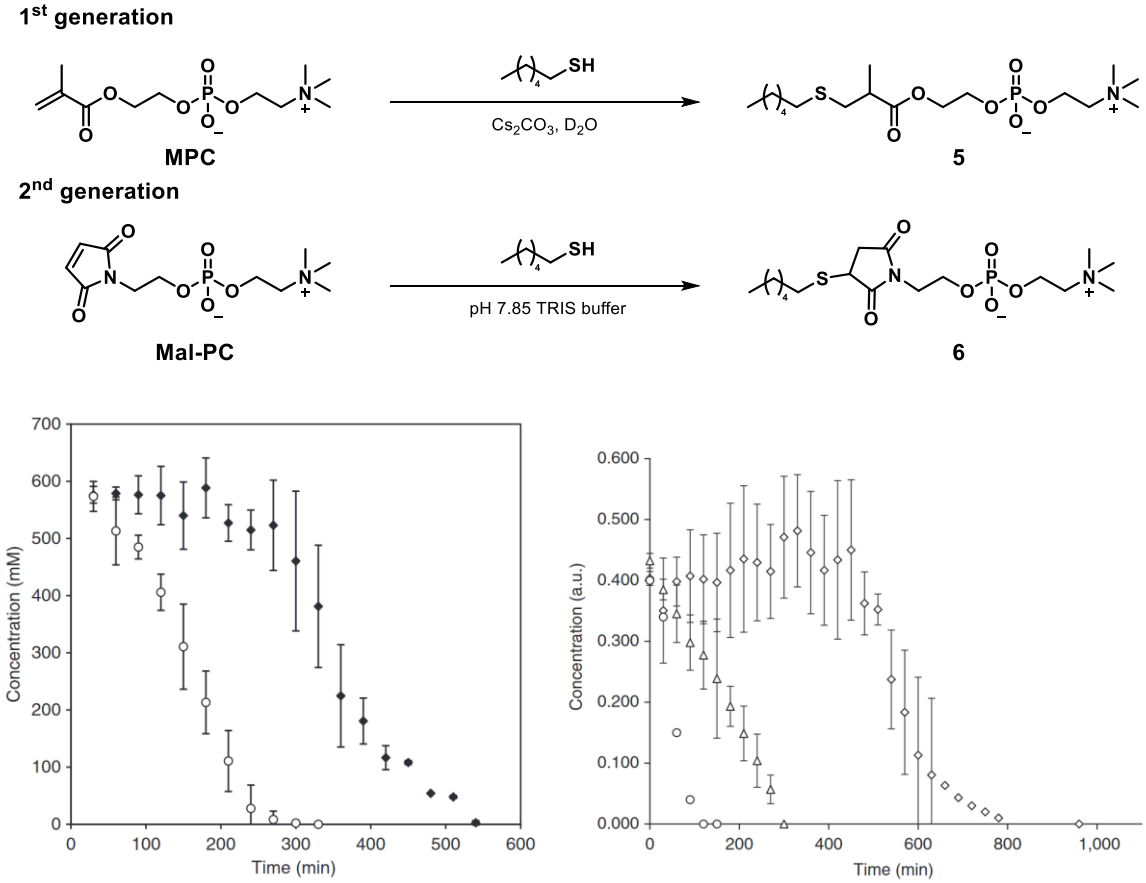

Figure 1.12: Irreversible bond formation used in synthetic physically autocatalytic systems. Left: 1st generation reaction profile showing MPC consumption over time monitored by ^{1}H NMR spectroscopy (filled diamonds: unseeded reaction between MPC and 1-hexanethiol showing a lag period, unfilled circles: the same reaction seeded with 20 mol% phospholipid **5a**). Right: 2nd generation reaction profile showing Mal-PC consumption over time by ^{1}H NMR spectroscopy (unfilled diamonds: unseeded reaction between Mal-PC and hexanethiol, unfilled triangles: reaction between Mal-PC and hexanethiol with 20 mol% phospholipid **6**, unfilled circles: reaction between Mal-PC and hexanethiol with 70 mol% of **6**). Data points are the mean of three experiments and error bars show the standard deviation. Reproduced from Bissette et al.[64]

Due to the highly alkaline conditions required for the conjugate addition, significant competitive hydrolysis of the ester linkage was observed which complicated analysis. The use of a second generation system featuring a more reactive maleimide acceptor (Mal-PC) allowed the reaction to occur under milder conditions (pH ~7.8).

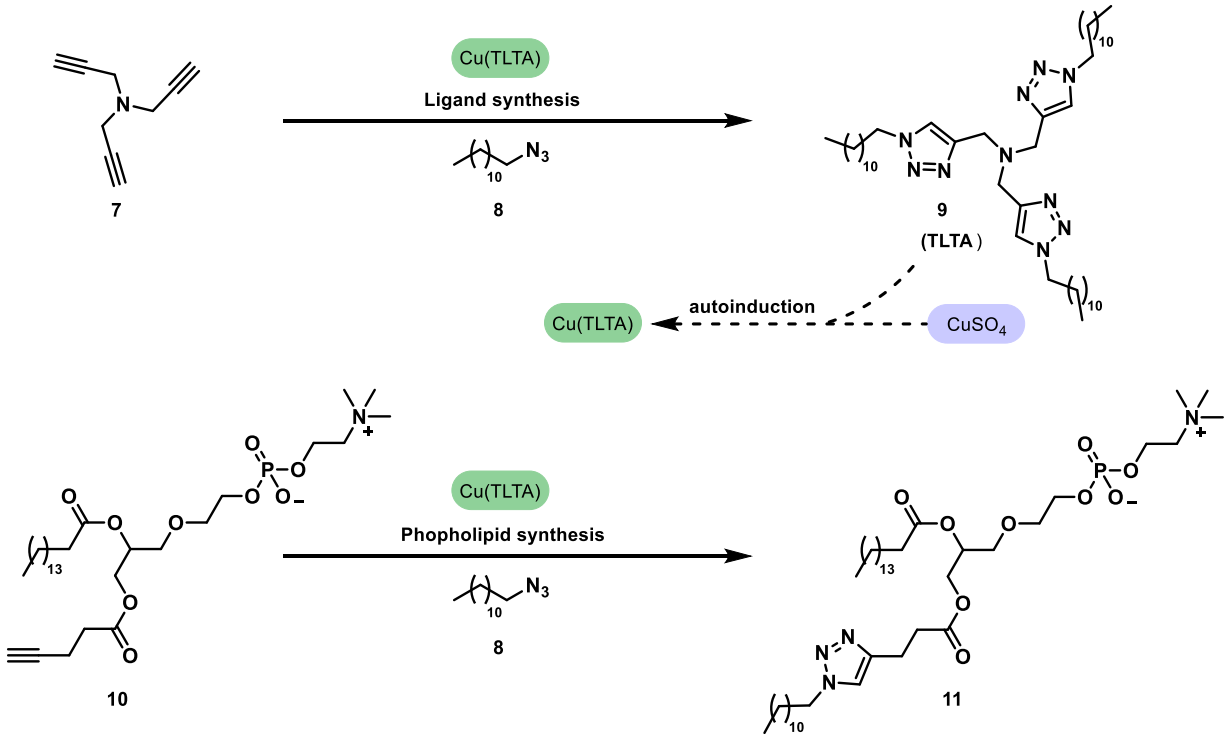

Figure 1.13: Self-reproducing lipids formed by the copper-catalysed azide-alkyne cycloaddition (CuAAC) between **8** and **10** to give **11**. Simultaneous production of ligand **9** (TLTA) by CuAAC provides a rate enhancement over time.

Devaraj and co-workers developed a self-reproducing catalyst system through the clever use of a class of rapid bond-forming reactions, copper-catalysed azide-alkyne cycloadditions (CuAACs).[91,92] Triazole ligands such as **9** can promote and be produced by CuAACs, enhancing their own formation (Figure 1.13). Hence, the production of **9** in the presence of copper, alkyne (**7**) and azide (**8**) substrates leads to a rate enhancement over time. As the ligand is not a catalyst itself and the rate acceleration is limited by the metal catalyst loading, this is probably best described as an autoinductive process. In the reported system, the copper-ligand complex simultaneously facilitates a second CuAAC reaction between **8** and **10** (see Figure 1.13). This forms self-assembling triazole phospholipid **11** which can form vesicles. There was also evidence that the formed vesicles sequester the catalyst complex and are capable of division to give daughter vesicles which can then grow, driven by the internal CuAAC.

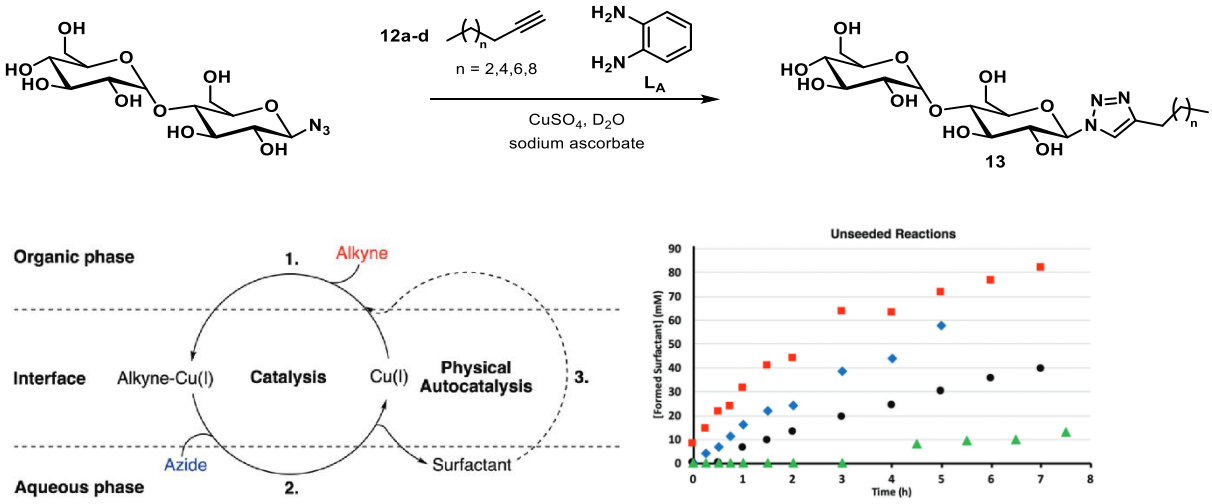

Figure 1.14: Physically autocatalytic CuAAC system where the rate of micelle formation can increase independently of copper catalyst concentration. Changing the hydrophobicity of the alkyne partner **12** resulted in differences in the onset and rate of micelle formation. Adapted from Post et al.[93]

CuAAC was also used by Post et al. in the biphasic coupling of hydrophobic alkynes (**12a-d**) and hydrophilic maltose azide (Figure 1.14).[93] This reaction produces micelles whose formation show autocatalytic features including a lag period and rate acceleration upon seeding with the product. Being the result of an interfacial reaction, the product amphiphiles (**13**) can enhance phase transfer in the reaction independently of [Cu], autocatalytically promoting their own formation.

Variation of the alkyne coupling partners revealed a negative correlation between chain length and CuAAC reaction rate, with a delayed onset for the most hydrophobic alkynes **12a-b** (n = 6, 8, Figure 1.13) Moreover, DOSY NMR studies showed that the alkynes strongly associated with the micelles, an observation consistent with a micellar catalysis mechanism (*cf.* phase transfer catalysis).

Because the copper-phenylenediamine complex initially used in this system is quite soluble in water, where the cycloaddition reaction occurs could not be determined. Later work showed that when the location of the copper complex is controlled, this affects the reaction network (Figure 1.15).[94]

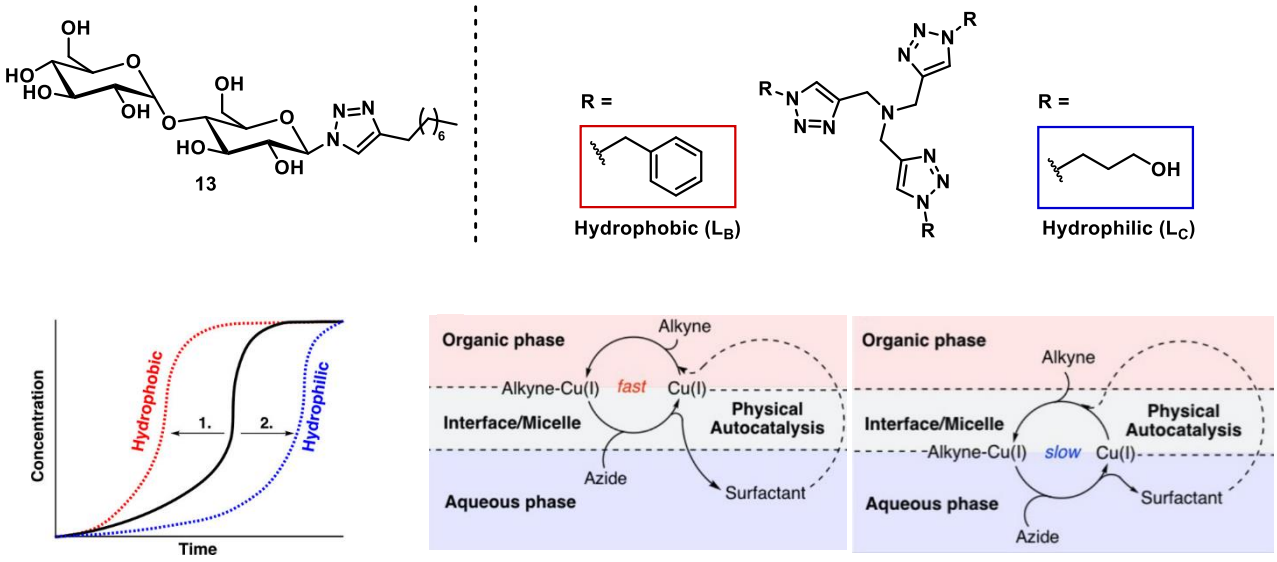

Figure 1.15: The kinetics of a physically autocatalytic CuAAC can be controlled by the localation of the catalyst. Micelle formation could be accelerated when using hydrophobic triazole ligand $\mathbf{L_B}$ and slowed by using hydrophilic ligand $\mathbf{L_C}$. Adapted from Post et al.[94]

Changing the hydrophobicity of the catalyst complex provided a handle to tune the overall reaction kinetics: using the hydrophobic Cu-$\mathbf{L_B}$ complex promoted the retention of the catalyst in the organic phase and accelerated turnover whereas using the hydrophilic Cu-$\mathbf{L_C}$ slowed the reaction as the catalyst was more strongly phase separated from the alkyne substrate (Figure 1.15). Based upon control experiments and using combinations of different polarity alkynes, azides and catalysts they proposed a predictive phase model which rationalised the results.

1.2.3 Visualising supramolecular systems with iSCAT

Gaining insight into how physical autocatalytic systems work is inherently challenging because they are highly dynamic, operate under heterogeneous conditions, and involve supramolecular aggregates that are poorly defined and sensitive to a wide range of variables. Monomer formation and/or the disappearance of starting material can be followed at the molecular level by routine NMR spectroscopic or HPLC analysis of reaction aliquots. For supramolecular aggregates analysis is more complicated. Classical optical microscopy can be used to observe large aggregates such as giant vesicles but is not viable for particles on the nanoscale, as seen in micelle-forming systems. Likewise, electron microscopy isn't well suited for analysis of these systems due to the typically

harsh conditions for sample preparation and the way it which it perturbs a sensitive chemical system.

In 2016, Ortega-Arroyo, Kukura and collaborators used a type of super-resolution imaging called interferometric scattering microscopy (iSCAT) to study self-reproducing micelles.[95,96] Using iSCAT, nanoscale particles binding to a glass surface can be monitored and quantified to achieve the real-time, label free analysis of supramolecular structures produced in a physical autocatalytic reaction.[97] The above thiol-ene reaction was modified by using oleyl thiol to produce larger aggregates (R_H ~ 3 nm) allowing the kinetics of phospholipid **5b** formation to be tracked on the supramolecular scale (Figure 1.16a). Reactions were conducted within wells on a microscope slide and videos showing particle formation were recorded. By digitally quantifying the number of particle landing events on the microscope slide in a given time, the supramolecular reaction kinetics could be extracted, showing a characteristic sigmoidal profile (orange data, Figure 1.16b). iSCAT also revealed that seeding the reaction with micelles produced a much higher rate of particle landings on the glass slide from the outset while also removing the lag period (purple data, Figure 1.16b).

Besides measuring solution kinetics, the authors were also able to image the reactive thiol-aqueous interface of biphasic reactions. By focusing on micrometer sized thiol droplets on the microscope slides and recording the reaction with an aqueous solution of MPC, the production of new aggregates could clearly be seen (Figure 1.16c). Near the interface high levels of activity were seen and many lipid aggregates form, and the rate of particle binding was proportional to the proximity to the droplet. These observations lend support to a biphasic mechanism where the reaction occurs at the thiol-water interface by providing *in situ* spatial information that would be difficult to otherwise obtain. Eventually the interface around the droplets breaks down and complex extended lipid structures emerge. While the large number of particles present made isolating individual events difficult, the overall proliferation of the vesicles is consistent with the growth and division of many individual lipid structures.

This work demonstrated the ability to visualize and study with high spatiotemporal resolution a complex system which rapidly generates supramolecular complexity. It also revealed – without labelling the molecules - how tracking single-particle dynamics can help to build understanding of physical autocatalytic reactions.

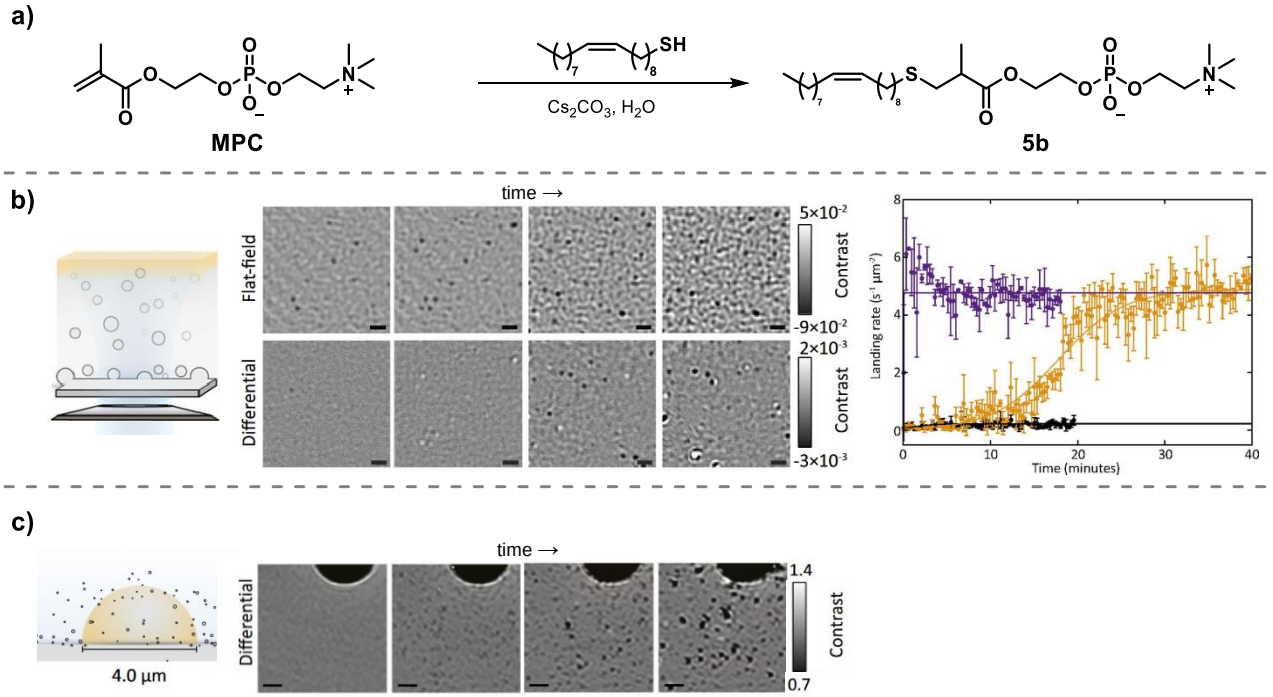

Figure 1.16: Visualization of a physically autocatalytic system using interferometric scattering microscopy (iSCAT). a) Bond forming autocatalytic reaction using oleyl thiol to produce large aggregates; b) Reaction kinetics by iSCAT of the reaction between Michael acceptor MPC and oleyl thiol (orange data) and between MPC and oleyl thiol seeded with phospholipid **5b** (purple data); c) Observing the reactive interface using micrometer sized thiol droplets within an aqueous solution of MPC produced complex extended lipid. All scale bars: 1mm. Adapted from Ortega-Arroyo et al.[97]

1.2.4 Out-of-equilibrium autocatalytic lipid systems

A wide variety of autocatalytic systems have been explored, and while they are fascinating for several reasons, many are limited in what they can achieve – they simply make more of themselves over time. Many autocatalytic reactions are effectively just interesting mechanistic pathways to a thermodynamic product. Systems that aim to model living systems should have access to a non-equilibrium state, and there is growing awareness that chemical systems which operate under thermodynamic control cannot mimic nature and will be much more limited in what can eventually be achieved compared to kinetically controlled systems.[98,99] Introducing (further) non-equilibrium

qualities into autocatalytic systems is a logical yet non-trivial undertaking and has been central to many recent synthetic origins of life research efforts.[38,100]

Developing out-of-equilibrium synthetic systems requires reaction networks to be controlled primarily by kinetics rather than equilibrium thermodynamics. In most of the processes seen above, the kinetic and thermodynamic products are one and the same. In fact, it should be pointed out that the non-linearities seen in physical autocatalysis often arise from slowing down (by phase separation) what would normally be fast reactions, and then using the product in order to open up a viable new reaction pathway. Figure 1.17a shows an energy diagram where thermodynamic ($\mathbf{P_A}$) and kinetic ($\mathbf{P_B}$) products arise from a common starting material **S**. $\mathbf{P_A}$ and $\mathbf{P_B}$ lie on the same energy landscape, and all reactions are reversible, meaning that the thermodynamic product ($\mathbf{P_A}$) will be favoured, given sufficient energy and time.

Irreversible processes should be able to enable kinetic control over autocatalyst formation (and selection between species based upon reproductive efficiency).[88] But in scenarios where the energies and structures of $\mathbf{P_A}$ and $\mathbf{P_B}$ are similar, the respective transition states to access them would also likely be similar and attempting to use a catalyst to favour the kinetic product would likely be challenging and lead to non-generally applicable solutions.

An approach that has emerged as being useful in developing synthetic out-of-equilibrium systems is to make the kinetic product ($\mathbf{P_B}$) metastable. When $\mathbf{P_B}$ is consumed, it does not go back to starting material, but instead gives another product ($\mathbf{P_C}$) (see Figure 1.17b) which introduces irreversibility to the system. By adapting the overall reaction network in this way, the substrate **S** can be channelled along a kinetic reaction coordinate. As a general strategy to control complex reaction networks and access states away from thermodynamic equilibrium, making metastable species and transient materials has attracted considerable attention.[98,101-103] Creating fuelled systems capable of maintaining non-equilibrium states and performing some useful function is an ongoing challenge and has been well reviewed in recent years.[99,104-108]

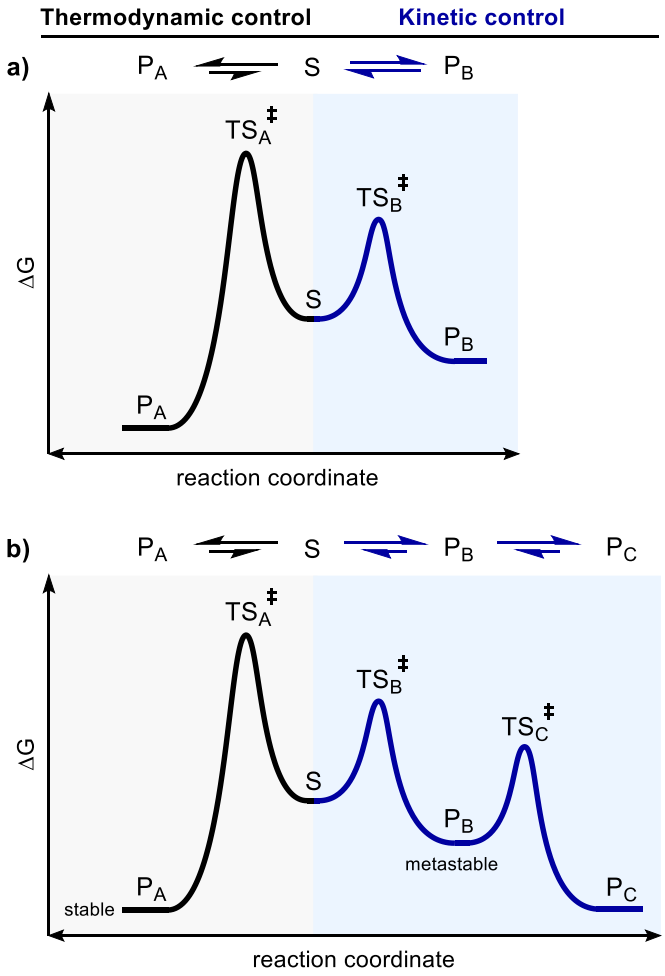

Figure 1.17: a) Energy profiles where a single starting material **S** can react by either a thermodynamically or kinetically controlled process to give products $\mathbf{P_A}$ and $\mathbf{P_B}$, respectively. Importantly, all steps are reversible. Under kinetic control, it is possible to access states which aren't the global energy minimum. b) Introduction of a second reaction step on the kinetic pathway ($\mathbf{P_B}\rightarrow\mathbf{P_C}$) can promote irreversibility in the formation of $\mathbf{P_B}$. Where $\mathbf{P_C} = \mathbf{P_A}$, we have a system with two mechanistic pathways to the same product.

A significant and early example of using multiple kinetically controlled reactions to observe out-of-equilibrium behaviour was achieved in 2001 by Zepik *et al.* who used self-reproducing oleate vesicles to model chemical homeostasis.[109] The system relies on the use of a fatty anhydride, which undergoes two sequential chemical steps which form and then destroy the self-assembling monomer. Alkaline hydrolysis of phase separated oleic anhydride generates metastable vesicles, which are then (simultaneously) degraded by oxidation of the oleate monomer to give a non-amphiphilic thermodynamic product (Figure 1.18). Notably, the oxidising species (OsO_4) was purposely membrane-bound to ensure reaction at the vesicle surface. Depending upon the relative rates of the two reactions, which were controllable, this autopoietic system was able to show three

different outcomes, namely, growth ($rate_{form} > rate_{destr}$), homeostasis ($rate_{form} = rate_{destr}$) and decay ($rate_{form} < rate_{destr}$).

This system's capability to maintain a steady state using orthogonal chemical fuels compares favourably with many state-of-the-art dissipative systems which would come almost two decades later. The homeostatic system is remarkably simple, but it highlights how relying on a catabolic process to form the vesicle limits molecular complexity.

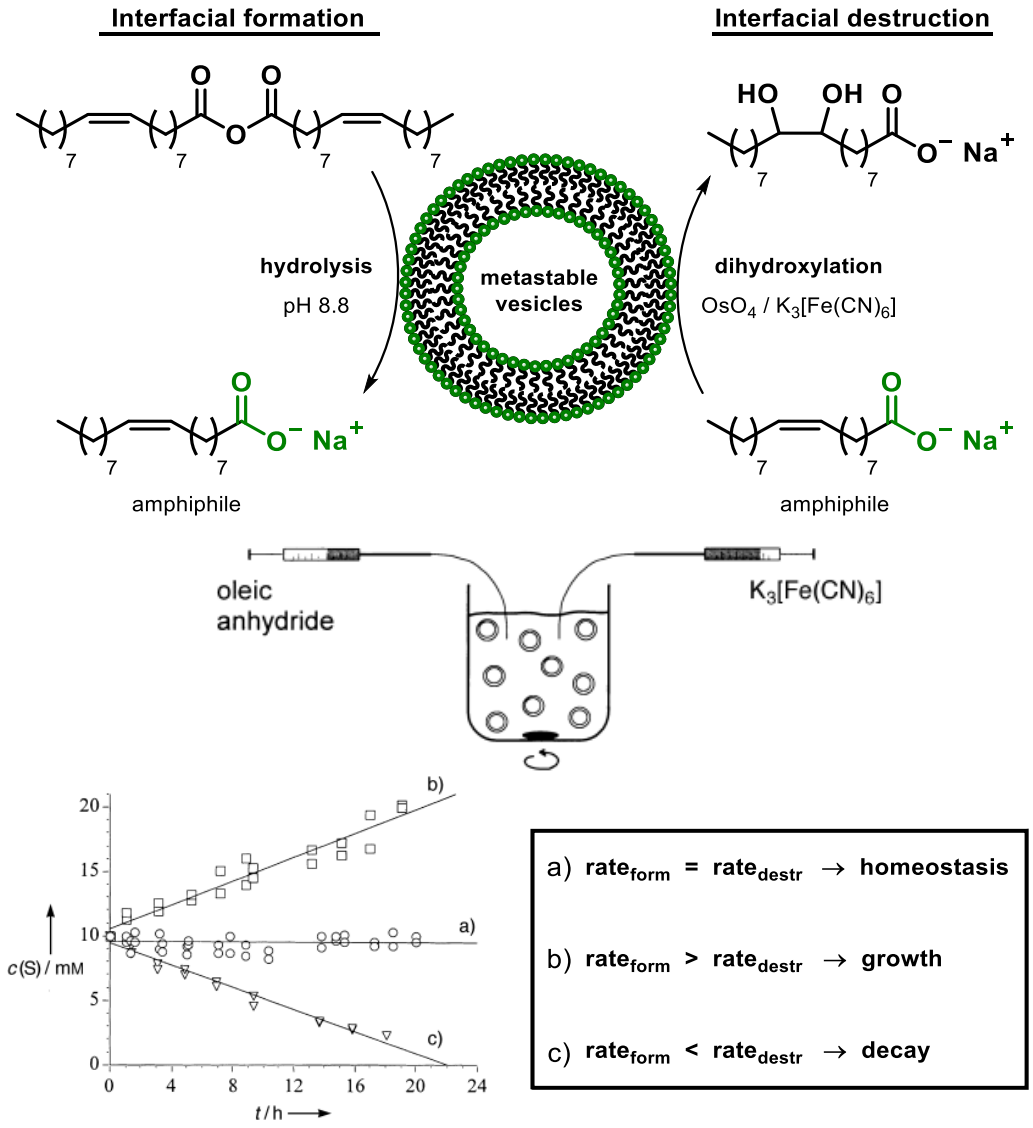

Figure 1.18: Homeostasis in an early out-of-equilibrium system was achieved by simultaneously forming and destroying vesicles. Adapted from Zepik et al.[109]

A catabolic process followed by an irreversible metal catalyzed degradation reaction tends towards creating species with less functionality and almost certainly restricts what could be achieved with

this system in terms of building networks of compounds capable of disparate functions, as found in biological settings. The next section will discuss how incorporating bond-forming reactions into physically autocatalytic systems can open up novel (non-equilibrium) behaviour.

In 2018 Colomer et al. reported a system of transient self-reproducing, self-assembling species. The surfactants here were formed and subsequently consumed under the reaction conditions in an overall irreversible process (see Figure 1.19).[110]

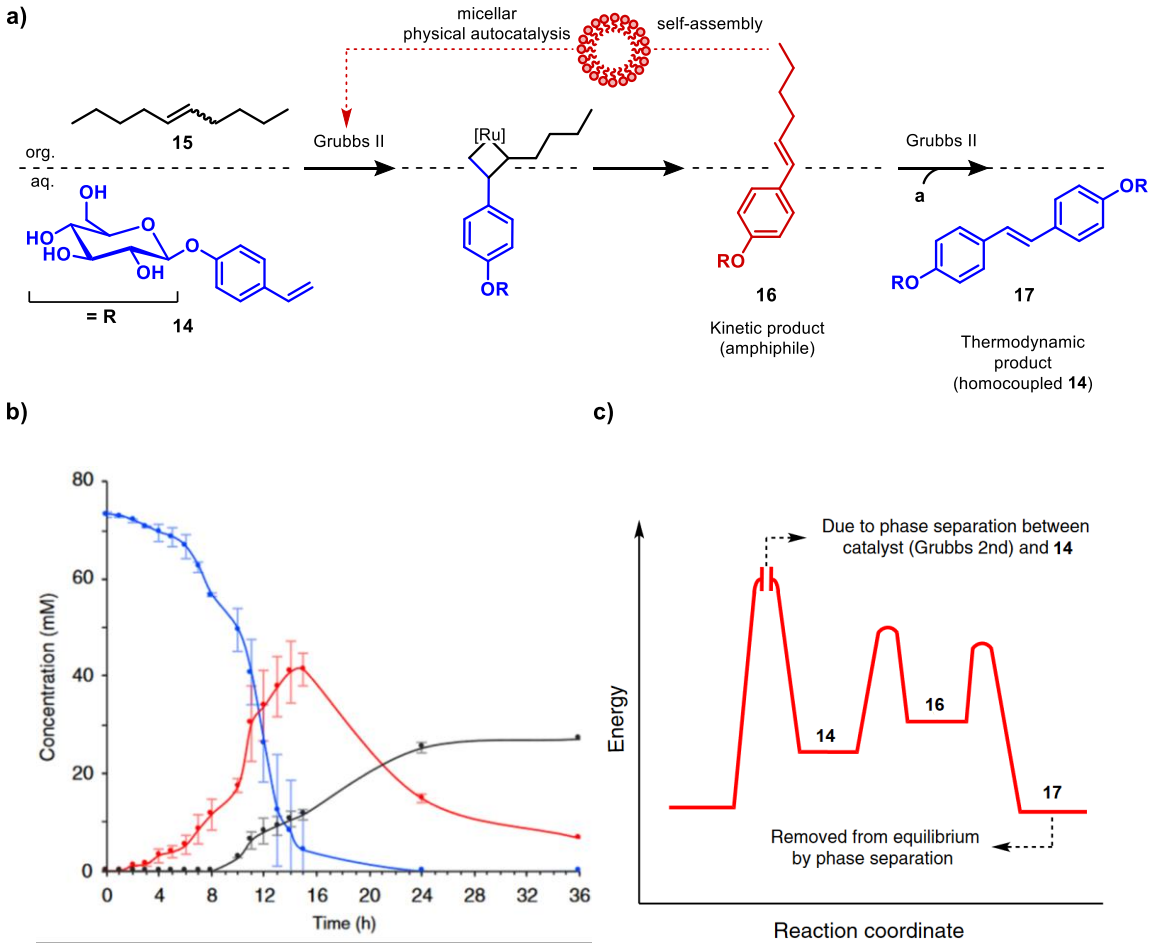

Figure 1.19: A self-reproducing lipid which is both formed and destroyed by alkene metathesis in an overall irreversible process. a) Biphasic reaction between **14** and **15** gives amphiphile **16** which is then broken down to thermodynamic waste product **17**; b) Reaction kinetics; c) Energy profile for the metathesis reactions, highlighting the pathway from **14** to **17** via amphiphile **16**. Adapted from Colomer et al.[110]

Using ruthenium-catalysed cross-metathesis, phase separated alkenes **14** (hydrophilic) and **15** (hydrophobic) are coupled to give metastable product **16**. This species transiently exists in a non-equilibrium state by virtue of its autocatalytic formation and kinetic stability. Rather than replicating

until the reactants are fully consumed, the metastable replicator reaches a maximum population and is then depleted by a second cross-metathesis and moves towards equilibrium, forming thermodynamic waste product **17**. Mechanistic experiments suggest the biphasic setup is responsible for guiding both replicator formation and destruction; due to the phase separation of the ruthenium catalyst from the aqueous phase the reaction requires amphiphilic intermediates and cannot directly homo-couple alkene **14** to give hydrophilic waste product **17**. In addition, the equilibrium is potentially shifted by the removal of **17** into the aqueous phase, driving destruction of amphiphile **16** (Figure 1.19b-c).

While the ability of simple species such as **16** to form self-assembling, self-reproducing structures is remarkable, creating more life-like dynamics requires the ability to sustain dissipative states. In 2019, Morrow and co-workers reported an example of a metastable self-reproducer capable of escaping thermodynamic equilibrium in a persistent and controllable fashion by consuming a chemical fuel (Figure 1.20).[111] Maintaining self-reproducing systems through fuelling has clear analogies with ordered, high energy biological structures which operate out-of-equilibrium. The realization of synthetic systems capable of persisting in out-of-equilibrium states presents the opportunity to learn how to control and use reciprocal feedback systems and the dynamic instability of transient self-replicating species. Understanding how they work may someday prove useful in addressing long term goals such as modelling metabolism and other life-like processes.[108,112,113]

Exploring new 'reactivity space' for physical autocatalysts, this system uses thiol-disulfide exchange reactions between phase separated **18** and **19** to give monomer **20**, which self-assembles into micelles. **20** is destroyed in a second catabolic step where thiol **18** attacks **20**, giving breakdown products **21** and **22**, the equilibrium end point for the system.

Importantly, this equilibrium position can be evaded by the continuous addition of a chemical fuel (H_2O_2) to regenerate the high energy disulfide starting material **19** from **21**. This crucial anabolic step enables the closing of a metabolic cycle (see Figure 1.20a) so that a steady state can be maintained that is responsive to the rate of fuel supply (Figure 1.20b-c). The kinetic asymmetry of

the amphiphile formation, destruction and oxidative recycling steps provides intrinsic irreversibility to the system, meaning that there is a unidirectional substrate flux derived from attempting to regain equilibrium via sequential thermodynamically favourable steps.

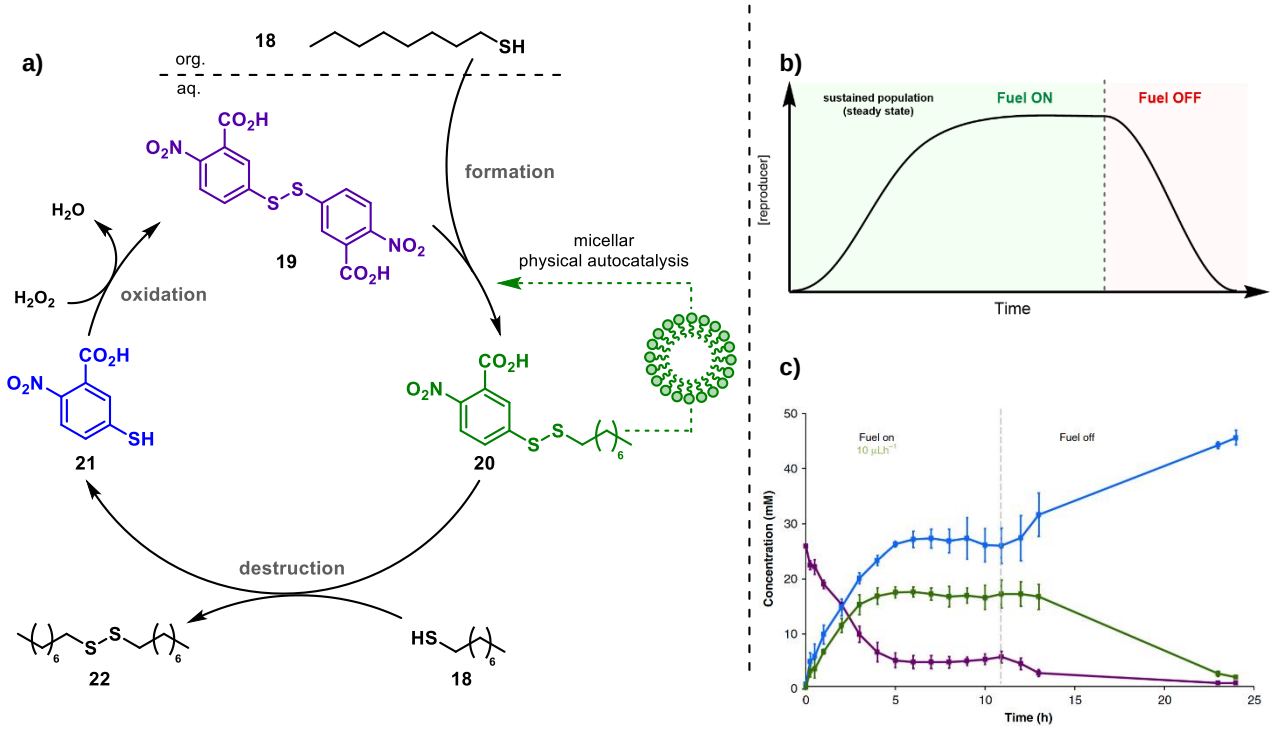

Figure 1.20: Adding chemical fuel to a system of self-reproducing disulfide lipids closes a metabolic cycle and holds the lipids in an out-of-equilibrium in a steady state. a) Metabolic cycle, b-c) A steady state can be maintained with chemical fueling. Blue line: **21**, green line: **20**, purple line: **19**. Adapted from Morrow et al.[111]

Morrow's thiol-disulfide system was used as a case study by Lebedeva and co-workers in developing an iSCAT assay for monitoring supramolecular aggregates under batch conditions. Previous work on monitoring autocatalytic reactions by iSCAT was done by measuring reactions performed directly on microscope coverslips.[97,114] Two biphasic systems were examined – one produces micelle-forming amphiphile **20**, and the other vesicle-forming **23** (Figure 1.21). When aliquots were removed from reactions in round bottomed flasks and added to the microscope coverslip it allowed the study of the onset and evolution of aggregate growth for both systems. For example, Figure 1.21b shows increasing size and polydispersity of **23** over time. This assay allows reactions to be monitored under the conditions that they normally take place (as opposed to on microscope slides), and so they are more representative of how the biphasic aggregate-forming reactions typically occur. In physical autocatalytic reactions – where variables such as stirring rate

and interfacial area are tremendously important – this provides the opportunity to compare supramolecular data directly to molecular level concentration data. It also allows parameters such as temperature and the surface area between phases to be controlled, enabling the study of these variables on these systems. It should of course be considered that there may be supramolecular level events taking place during the process of removing samples and adding them to the iSCAT, but there are several clear advantages over other analysis methods that would require particle labelling or freezing (for example) and it has uniquely high resolution in both space and time. Being able to count the number of particles present and measure their size distribution revealed aspects of the supramolecular assembly process that would be hard to determine by ensemble measurement methods. For example, dynamic light scattering (DLS) and fluorimetry average out data, as opposed to providing information on individual particles which can be visualized and followed in time.

One particularly important observation was the swelling of micelles over time, indicating uptake of hydrophobic precursors into the micelle interior. This provides support for the long-debated *interfacial* mechanism of micelle self-reproduction, as opposed to enhanced dissolution of precursors in the bulk media (see mechanistic discussion above).[53,58,59,62] They were also able to observe that micelle to vesicle transitions were occurring under certain circumstances.

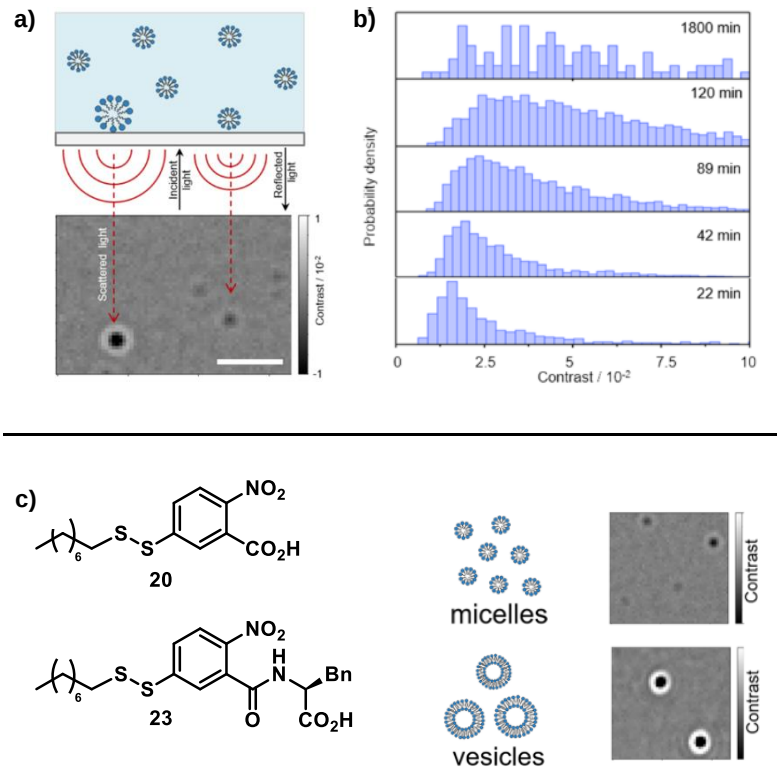

Figure 1.21: An iSCAT assay for the direct visualization of supramolecular particles under native conditions was developed and applied to disulfide lipids. Vesicle and micelle particles of different sizes can be differentiated and counted over time. Adapted from Lebedeva et al.[114]

Vesicles have a closer resemblance to compartmentalized life than micelles and are highly sought protocell models, particularly if they can be combined with other life-like features. Engwerda and co-workers were able to hold self-reproducing vesicles out-of-equilibrium using a chemically fuelled disulfide based system (Figure 1.22),[115] which had some modification from Morrow's system due to higher stability of the vesicle precursors. Reaction of double tailed thiol **24** and **19** gave **25** which forms vesicles according to DLS and iSCAT analysis. However, the catabolic process key to holding the system out of equilibrium was slow here because of the steric effects of the larger thiol. To degrade the thiol effectively and allow construction of a metabolic cycle, a second – coupled – metabolic cycle was created by adding a nucleophilic catalyst (see Figure 1.22). Once the rate of surfactant destruction was sufficient, adding H_2O_2 allowed the vesicles to be held in a 'life-like' steady state.

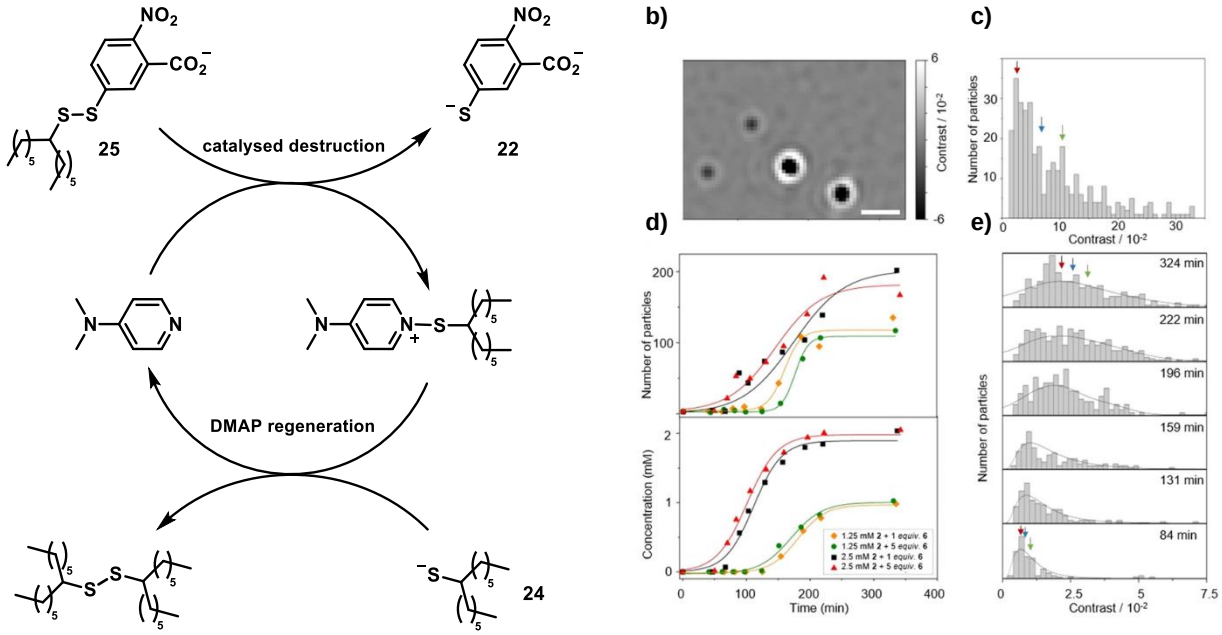

Figure 1.22: Vesicle forming disulfide lipids arise from using a double tailed thiol precursor. a) Reaction network including lipid destruction by the action of DMAP to closes the cycle; b) iSCAT image of **25** aggregates binding to glass surface, measured contrast is proportional to size; c) Histogram of the contrast (size) observed for a solution of **25** in buffer (pH 9 TRIS). Arrows indicate the peak (red), median (blue) and mean (green) contrast; d) Reaction kinetics of the formation of lipid **25**, monitored by iSCAT particle counts (top) and UPLC (bottom); e) Contrast (size) distribution changes over the course of a reaction which forms **25**. Adapted from Engwerda et al.[115]

iSCAT is capable of providing a rich picture of dynamic supramolecular systems in real time. The out-of-equilibrium vesicle study used iSCAT to characterise the vesicles on the nanoscale in isolation (Figure 1.22b-c) and to quantify vesicle counts during reactions (Figure 1.22d-e), allowing kinetic monitoring of out-of-equilibrium reactions at the supramolecular level.

1.2.5 Competition and selection in autocatalytic lipid systems

The development of minimal autocatalytic systems is a necessary stepping stone but can only teach us a limited amount about life's most interesting phenomena. Moreover, if different prebiotic scenarios are to be tested then systems showing selection, variation and evolution must be experimentally attempted.

The 'RNA world' is a widely known prebiotic hypothesis based upon template replicators that can compete for resources. An alternative idea is that cell-like compartments appeared first in a so-called 'lipid world' (see Section 1.1.2). A common perception is that selection and heredity in

autocatalysts are almost always linked to template mechanisms and therefore, determining whether selection between lipid compartments is possible is a key focus for the field, as discussed below. It is not obvious how a dynamic aggregate of lipids could begin to impart selection in a prebiotic model. Acting at the supra- and mesoscale but with relatively limited molecular recognition capabilities, lipid systems which show selection without a template mechanism could have a profound impact on theories of life's origin.

A seminal example of such selection was demonstrated in 2020 using a biphasic system of surfactants both produced and destroyed by ruthenium-catalyzed alkene metathesis.[116] Starting with a mixture of different length hydrophobic alkenes (**15a-c**), a preference was found for forming replicators with shorter tails (Figure 1.23). When reactions were done in a continuously stirred tank reactor (CSTR) to compete for a common hydrophilic building block (**14**) different steady state distributions were found. The setup enables comparison of kinetic factors governing autocatalytic formation under non-equilibrium conditions. The steady state distributions were found to evolve in time depending upon the precursors added to the reaction. Remarkably, no selection is seen when the same reactant mixtures are dissolved in the same phase. The origin of selection is proposed to be the relative solubility of the precursors, which is highly sensitive to minor structural differences.

Later, Myrgorodska and Colomer found that complex oligomerization was observed in related biphasic cross-metathesis processes.[117] When reacting alkene precursors **14**, **14b** and **15a** under homogeneous conditions (9:1 ^{t}BuOH:D_2O) they saw rapid and exclusive formation of products **26a-b**. However, when alkene **15a** was phase separated from an aqueous solution of **14** and **14b**, this caused the diversity of the metathesis products to grow substantially (Figure 1.24). Polymer formation is crucial in biology and relies upon advanced (enzymatic) catalysts to overcome thermodynamic and kinetic limitations in their synthesis.

The work shows how phase separation can be used to alter chemical reactivity and lead to complex phenomena which does not occur when there is no liquid-liquid interface. This results in unique

reactivity patterns and oligomer populations which can change over time, without evolved biological mechanisms.

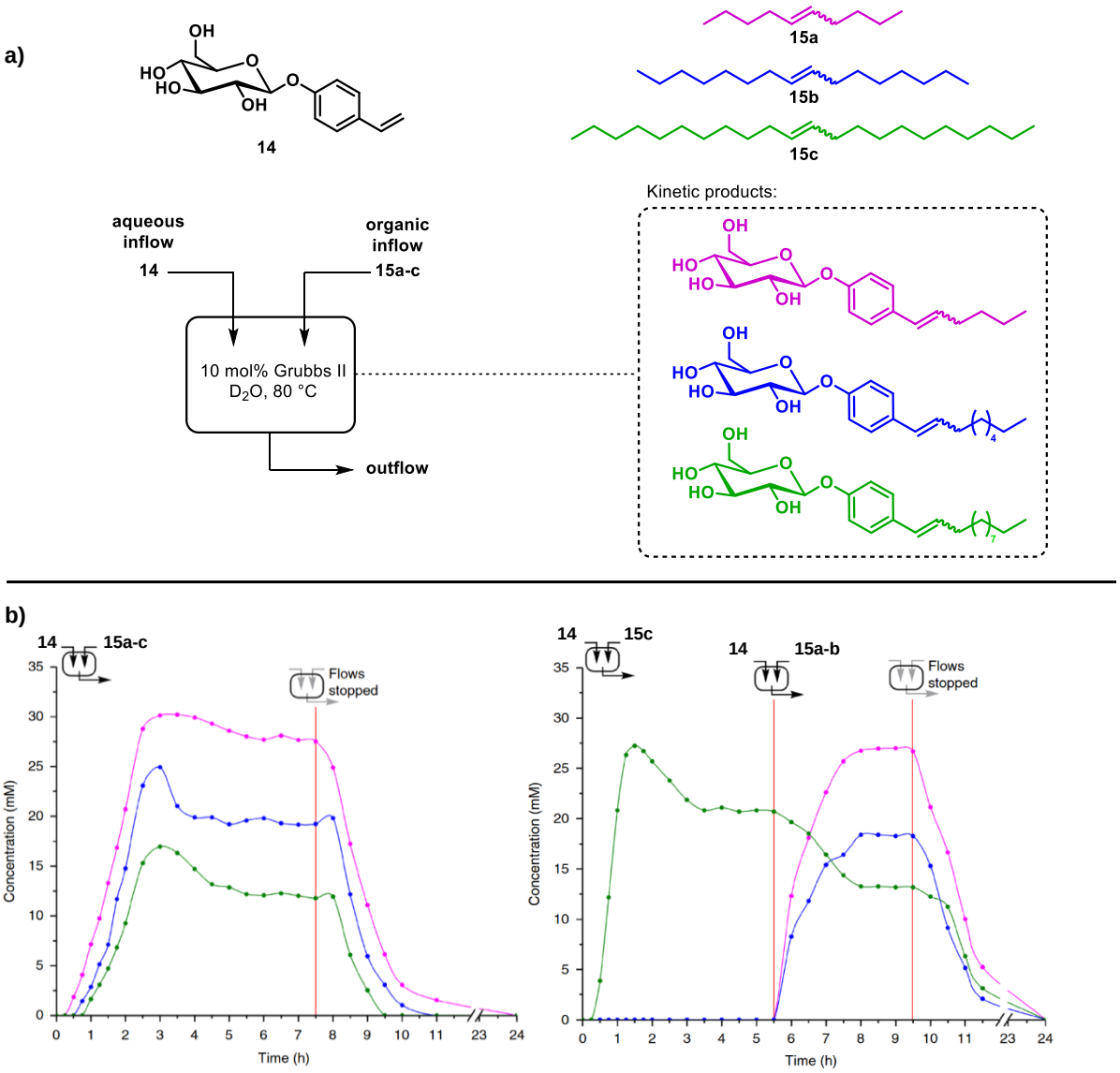

Figure 1.23: Competition between alkene precursors of self-assembling lipids in a CSTR setup showed out-of-equilibrium selection, likely on the basis of precursor solubility. a) Precursors **14** and **15a-c** were continuously added to a reactor and underwent alkene metathesis to produce lipid products; b) Reaction kinetics when combining all the components **14** and **15a-c** showed a preference for different lipids formed; c) when precursors **15a-b** were added to a reacting mixture of **14** and **15c**, the lipid population was responsive to the new composition. Reproduced from Colomer et al.[116]

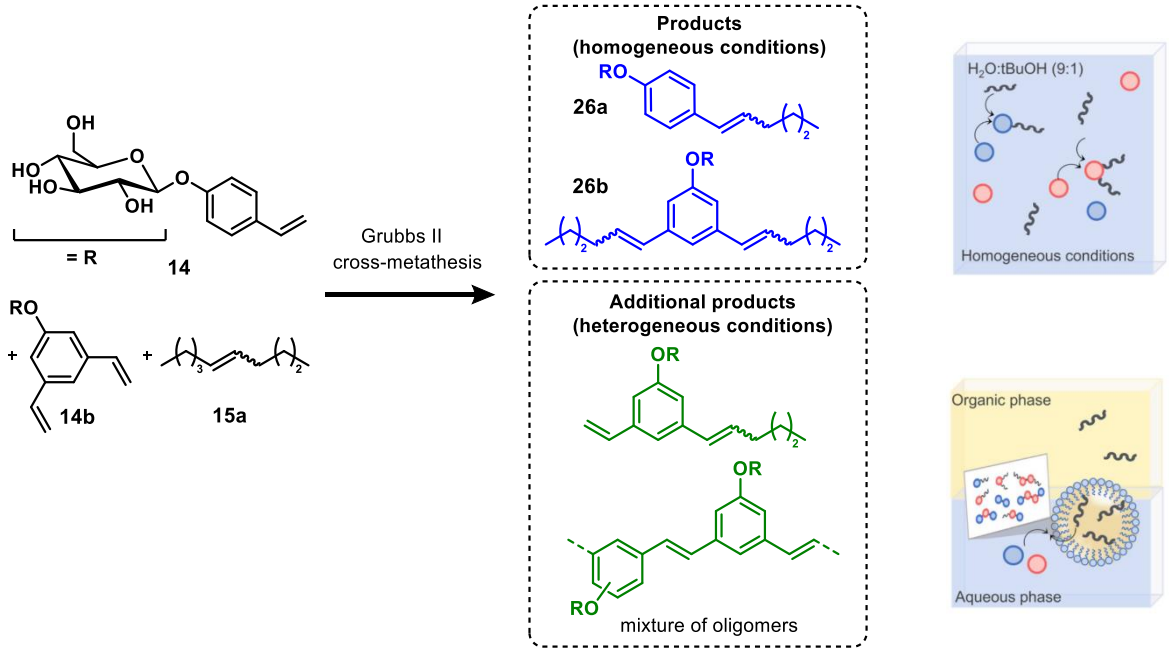

Figure 1.24: Phase separation of precursors gives rise to a diverse population of alkene oligomers that was not accessible under homogenous conditions. Reproduced from Myrgorodska et al.[117]

Arguably, the most sophisticated mechanism of selection in synthetic replicating protocells was reported by Post in 2020. Here the metastable self-reproducing species are phospholipids generated by autocatalytic CuAAC chemistry.[118] Using phase separated building blocks **27-32**, both self-replicating micelles and self-replicating vesicles could be formed by choosing the appropriate hydrophobic azide precursors (Figure 1.25). The micelles/vesicles were held out-of-equilibrium by introducing a destructive hydrolysis step and continuously turning over material in a CSTR.

In competition experiments where micelle and vesicle precursors compete for a common feedstock, the 'winners' were found to vary depending on the pH. Vesicles outcompete micelles under basic conditions, but the micelles were dominant at neutral pH (Figure 1.25b). Vesicles dominate under basic conditions because the vesicles and their component surfactants were more stable to alkaline hydrolysis. The reason micelles were found to outcompete vesicles under neutral conditions is more subtle, and Post and Fletcher proposed an inhibition mechanism where the micelles effectively stop vesicle formation when hydrolysis is insignificant. They propose, based on DOSY studies aimed at seeing supramolecular interactions, that micelles prevent the synthesis of the vesicles by sequestering the CuAAC catalyst (**30**) into the micelles – and that the building blocks of the vesicles

are too large to be taken up by micelles, resulting in segregation of the components necessary for vesicle synthesis (Figure 1.25c). In the same work, vesicles were used as hosts for a organocatalysed aldol reaction between *p*-nitrobenzaldehyde and cyclohexanone. First, a CuAAC was used to create a hydrophobic, membrane bound organocatalyst (Figure 1.25d). Within the vesicles, this catalyst was found to enhance both the *in situ* synthesis of the membrane-bound organocatalyst and the aldol reaction itself, mimicking compartment-supported metabolic processes in a cell.

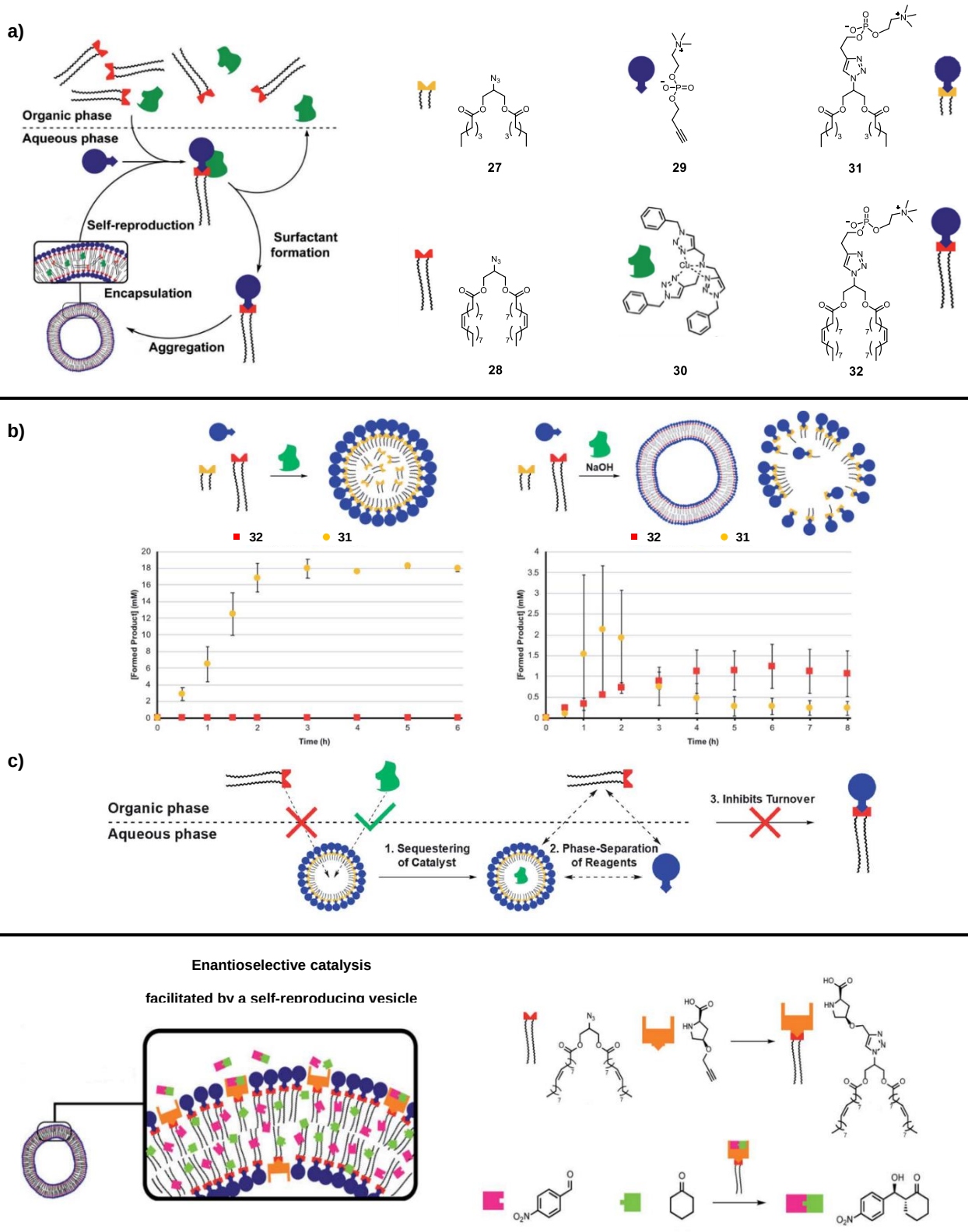

Figure 1.25: Competition between out-of-equilibrium self-reproducing micelles and vesicles shows that different populations dominate under different conditions. a) Autocatalytic micelles and vesicles are formed by the biphasic CuAAC reaction between **27** and **29** to give **31** (micelle forming surfactant) and between **28** and **29** to give **32** (vesicle forming surfactant). b) Precursors **27**, **28** and **29** were combined with a copper catalyst in water and stirred

together to form lipids **31** and **32**. At neutral pH, micelles are the dominant product and almost no vesicles are formed. Under basic conditions, vesicle forming lipids are favoured after a period where micelle precursors dominate. c) Proposed mechanism for selection of micelles: it is thought that the uptake of copper catalyst **30** into micelles phase separates it from precursor **28**, thus inhibiting vesicle production. d) Inclusion of a hydrophobic organocatalyst enabled vesicles to facilitate enantioselective aldol reactions. Vesicle-forming reactions were set up as before, with **28, 29** and $CuSO_4$ catalyst in water. An alkyne-bearing proline unit underwent a CuAAC reaction to form a proline-containing amphiphile which catalysed a model aldol reaction when embedded in vesicles of **32**. Adapted from Post et al.[118]

1.3 Beyond self-reproduction

Exploring catalytic systems that can promote their own formation has demonstrated novel and unexpected results, as discussed above, especially under non-equilibrium and competition conditions. However, how to a harness these new and unusual reactivity patterns to accomplish functions beyond simply making molecules that make more of themselves is a key question. In the three recently reported systems discussed below, fascinating systems-level complexity can be observed by simply mixing two or three different species in water.

Since the concept's introduction by Feynman and popularisation by Drexler,[119,120] 'nanotechnology' has grown into an enormous field, where molecular machines[121,122] have special significance. Drexler famously envisioned a molecular device, or 'assembler', capable of guiding chemical reactions with atomic precision and high efficiency. It was proposed that assemblers would first catalyse their own formation and then become involved in the assembly line-like synthesis of products. Whilst some have come close to this concept by mimicking nature's assemblers,[123] there's plenty to be gained by new interpretations of Drexler's vision. In 2020, Engwerda et al. discovered a catalytic system that shares many features with proposed assemblers; a catalyst promotes its own formation and brings reactants together into a self-assembled space where it constructs polymer products before consuming itself.[124]

Using thiol-disulfide exchange chemistry, (bola)amphiphilic products (**33**) are formed from the reaction between long chain dithiol (**34**) and two equivalents of **19** (Figure 1.26a). During the destruction of **33**, two further equivalents of the thiol are consumed. The alkyl disulfides produced in the destruction step are believed to continue to react with **33**, causing chain growth into disulfide

polymers (**35**). The supramolecular aggregates of **33** aid mixing and localisation of the reagents, facilitating the overall conversion of **34** into **35** before self-destruction of the aggregates upon consumption of the starting materials.

As a transient assembler, **33** has three clear phases to its lifespan: formation, function and destruction (A-C, Figure 1.26b). The average **35** chain length was seen to continuously increase over time. It could also be controlled by introducing a thiol capping agent, allowing selection for different polymer distributions (Figure 1.26c). This work demonstrated how a self-assembling, physically autocatalytic species can facilitate a continuous synthesis process.

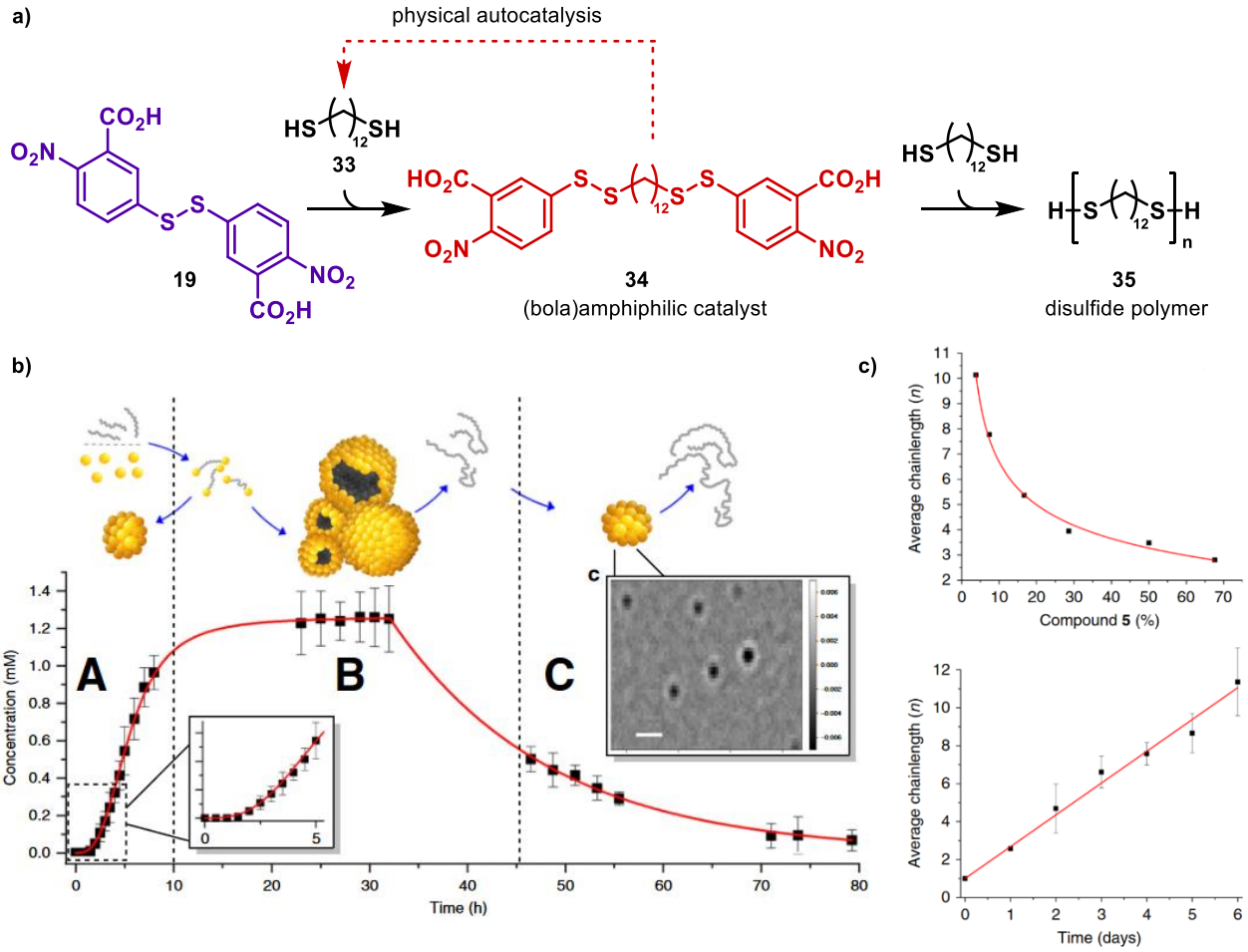

Figure 1.26: A 'molecular assembler' which consists of a supramolecular (bola)amphiphiles (**33**) that assembles itself and continually synthesizes disulfide polymers (**35**) with controllable properties. Reproduced from Engwerda et al[124]

The fact that systems capable of such complexity can be constructed by mixing two different species (**33** and **19**) in water suggests that many new supramolecular systems capable of complex and dynamic functions are simply waiting to be discovered.

A key goal of origins of life research is to demonstrate emergent behaviour across different length scales. This is particularly true for self-assembled non-equilibrium autocatalytic systems, which are likely well suited for observing life-like behaviour. The Katsonis group has a long standing interest in controlling movement in chemical systems and they recently reported a remarkable mutualistic interaction between oil droplet chemotaxis to self-reproduction (Figure 1.27).[125]

When droplets of octanol were added to the autocatalytic reaction between hexanethiol and Michael acceptor MPC, lipid **5a** is formed and coats the oil droplets (Figure 1.27a). Initially, these droplets are static but as the concentration of **5a** grows, it draws octanol away from the bulk droplet into micelles, giving rise to a visible corona (Figure 1.27b). At a threshold concentration of **5a**, termed the critical propulsion concentration (CPC), the droplet interface is sufficiently disrupted by this micellar uptake and a surface tension gradient causes droplet movement via Marangoni propulsion.[126,127] The length of the lag phase before motion depends on the size of the droplets, where higher lipid concentrations are necessary to move larger droplets. The lipid-covered oil droplets move toward areas that are rich in hexanethiol (Figure 1.27c).

In physically autocatalytic systems, interfacial mixing is a critical kinetic factor, and here the motility of the droplets introduces a form of mixing into the system, accelerating biphasic reactivity. The chemotactic oil droplet movement increases the rate of lipid reproduction, so there is reciprocal coupling between molecular level bond-forming chemistry and microscopic level droplet movement. The lipids self-assemble into micelles which cause movement and in return the movement of the oil droplets increases the rate of lipid self-reproduction (Figure 1.27d). Remarkably, the mutualistic interaction between motion and reproduction emerges simply by mixing two chemicals in water and oil, and the authors propose that chemical rate enhancements

driven by motile droplets could be generalizable to other micro-heterogeneous environments such as coacervates and polymer condensates in micellar water.

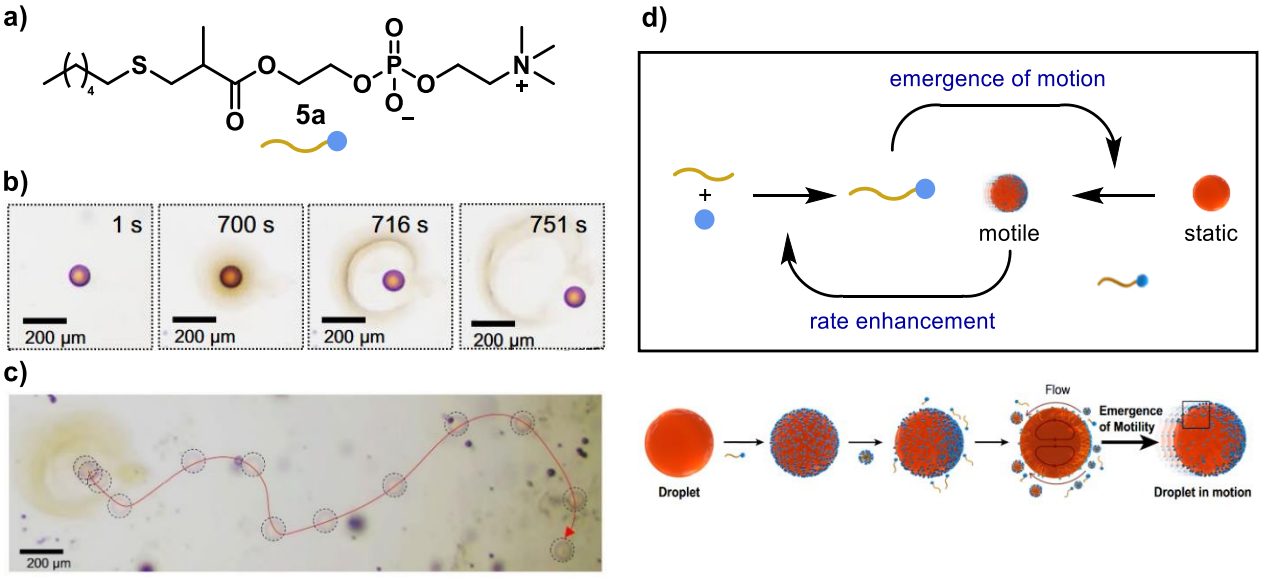

Figure 1.27: Reciprocal coupling between physical autocatalysis and the microscopic movement of oil droplets. Adapted from Babu et al.[125]

Physical autocatalysis may be used as a key design factor in future soft matter based applications, as suggested by the intriguing work of Schwarz and co-workers who produced chemically fueled self-immolative materials,[128] building upon earlier work on dissipative systems.[129,130] The transient materials are based on lipid **36** and anhydride **37** (Figure 1.28), where **37** forms by the EDC fuelled condensation of **36** and produces a phase separated oil emulsion. In aqueous buffer, **37** is steadily hydrolyzed back to **36** over time. The rate of this hydrolysis is related to the solubility of **37** in the water and ordinarily proceeds at a constant rate.[131] However, **36** forms micelles above a critical concentration which accelerates the hydrolysis reaction that leads to their own formation. This autocatalytic and self-triggered degradation of anhydride **37** was recognized as a mechanism to induce a rapid 'off-response' in materials applications. Importantly, this deactivation process could comprise only a fraction of the lifetime of a system, optimizing the utility of the active 'on' state (Figure 1.28). Self-immolative emulsions were tested in two materials: a transparent polyacrylamide gel and a drug-containing hydrogel. Embedding **36** and **37** within these materials provided proof-of-concept for a self-erasing label, which might be useful in future applications such

as for expiry dates or tickets, or new drug delivery platforms where a drug is constantly released followed by a burst phase.

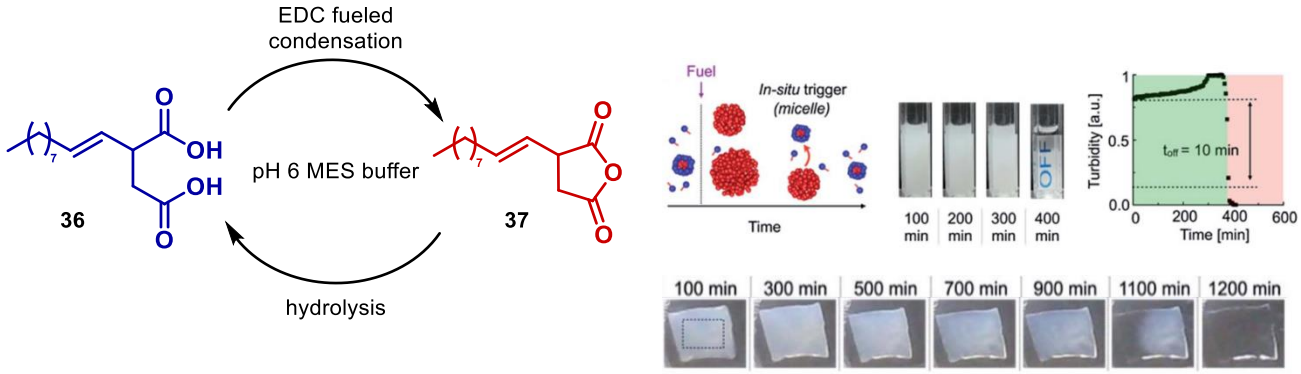

Figure 1.28: Self-immolative materials based upon physically catalytic lipids could enable materials chemistry applications such as a self-erasing labels and controlled drug delivery. Adapted from Schwarz et al.[128]

1.4 Thesis outline

The background given in this chapter aims to show what kinds of roles are available for lipids in chemical systems. Besides their commonplace usage as surfactants, simple lipid molecules are considered to have a potentially central place in theories on the origin of life and also in mimicking life in a functional way. These species can self-assemble, create structures across length scales and can aid their own chemical formation, which is demonstrated throughout the work in this chapter. Even beyond this, many researchers have recently taken greater inspiration from nature and are using lipids to construct functional systems such as in Section 1.3.

The work described in the remainder of this thesis follows these themes, focusing on: lipids in competitive prebiotic scenarios (Chapter 2), oscillating lipid systems (Chapter 3) and the functions that emerge from such non-equilibrium phenomena (Chapters 4 and 5).

References

1 Podolsky, K. A. & Devaraj, N. K. Synthesis of lipid membranes for artificial cells. *Nat. Rev. Chem.* **5**, 676-694 (2021). https://doi.org:10.1038/s41570-021-00303-3

2 Luisi, P. L. About Various Definitions of Life. *Orig. Life Evol. Biosph.* **28**, 613-622 (1998). https://doi.org:10.1023/A:1006517315105

3 Varela, F. G., Maturana, H. R. & Uribe, R. Autopoiesis: The organization of living systems, its characterization and a model. *Biosystems* **5**, 187-196 (1974). https://doi.org:https://doi.org/10.1016/0303-2647(74)90031-8

4 Szostak, J. W. Attempts to Define Life Do Not Help to Understand the Origin of Life. *J. Biomol. Struct. Dyn.* **29**, 599-600 (2012). https://doi.org:10.1080/073911012010524998

5 Cornish-Bowden, A. & Cárdenas, M. L. Contrasting theories of life: Historical context, current theories. In search of an ideal theory. *Biosystems* **188**, 104063 (2020). https://doi.org:https://doi.org/10.1016/j.biosystems.2019.104063

6 Benner, S. A. & Sismour, A. M. Synthetic biology. *Nat. Rev. Genet.* **6**, 533-543 (2005). https://doi.org:10.1038/nrg1637

7 Liu, A. P. & Fletcher, D. A. Biology under construction: in vitro reconstitution of cellular function. *Nat. Rev. Mol. Cell Biol* **10**, 644-650 (2009). https://doi.org:10.1038/nrm2746

8 Powner, M. W., Gerland, B. & Sutherland, J. D. Synthesis of activated pyrimidine ribonucleotides in prebiotically plausible conditions. *Nature* **459**, 239-242 (2009). https://doi.org:10.1038/nature08013

9 Powner, M. W., Sutherland, J. D. & Szostak, J. W. The Origins of Nucleotides. *Synlett* **22**, 1956-1964 (2011).

10 Whitaker, D. & Powner, M. W. Prebiotic nucleic acids need space to grow. *Nat. Commun.* **9**, 5172 (2018). https://doi.org:10.1038/s41467-018-07221-x

11 Patel, B. H., Percivalle, C., Ritson, D. J., Duffy, C. D. & Sutherland, J. D. Common origins of RNA, protein and lipid precursors in a cyanosulfidic protometabolism. *Nat. Chem.* **7**, 301-307 (2015). https://doi.org:10.1038/nchem.2202

12 Miller, S. L. A Production of Amino Acids Under Possible Primitive Earth Conditions. *Science* **117**, 528-529 (1953). https://doi.org:doi:10.1126/science.117.3046.528

13 Mann, S. The Origins of Life: Old Problems, New Chemistries. *Angew. Chem. Int. Ed.* **52**, 155-162 (2013). https://doi.org:https://doi.org/10.1002/anie.201204968

14 Oparin, A. I. *The origin of life on the earth*. 3rd rev. and enl. edn, (Oliver and Boyd, 1957).

15 *The Molecular Origins of Life: Assembling Pieces of the Puzzle*. (Cambridge University Press, 1998).

16 The Origin of Life: Look Up and Look Down. *Astrobiology* **12**, 1087-1092 (2012). https://doi.org:10.1089/ast.2012.0818

17 Woese, C. R. Interpreting the universal phylogenetic tree. *Proc. Natl Acad. Sci.* **97**, 8392-8396 (2000). https://doi.org:doi:10.1073/pnas.97.15.8392

18 Fox, G. E. Origin and Evolution of the Ribosome. *Cold Spring Harb. Perspect. Biol.* **2** (2010). https://doi.org:10.1101/cshperspect.a003483

19 Joyce, G. F. RNA evolution and the origins of life. *Nature* **338**, 217-224 (1989). https://doi.org:10.1038/338217a0

20 Gilbert, W. Origin of life: The RNA world. *Nature* **319**, 618-618 (1986). https://doi.org:10.1038/319618a0

21 Orgel, L. E. Evolution of the genetic apparatus. *J. Mol. Biol.* **38**, 381-393 (1968). https://doi.org:https://doi.org/10.1016/0022-2836(68)90393-8

22 Joyce, G. F. & Szostak, J. W. Protocells and RNA Self-Replication. *Cold Spring Harb. Perspect. Biol.* **10** (2018). https://doi.org:10.1101/cshperspect.a034801

23 Robertson, M. P. & Joyce, G. F. The Origins of the RNA World. *Cold Spring Harb. Perspect. Biol.* **4** (2012). https://doi.org:10.1101/cshperspect.a003608

24 Eigen, M., Gardiner, W., Schuster, P. & Winkler-Oswatitsch, R. The origin of genetic information. *Sci. Am.* **244**, 88-119 (1981).

25 Lincoln, T. A. & Joyce, G. F. Self-Sustained Replication of an RNA Enzyme. *Science* **323**, 1229-1232 (2009). https://doi.org:doi:10.1126/science.1167856

26 Watson, J. D. & Crick, F. H. C. Molecular Structure of Nucleic Acids: A Structure for Deoxyribose Nucleic Acid. *Nature* **171**, 737-738 (1953). https://doi.org:10.1038/171737a0

27 Niesert, U., Harnasch, D. & Bresch, C. Origin of life between scylla and charybdis. *J. Mol. Evol.* **17**, 348-353 (1981). https://doi.org:10.1007/BF01734356

28 Dyson, F. *Origins of Life*. 2 edn, (Cambridge University Press, 1999).

29 Benner, S. A. Paradoxes in the Origin of Life. *Orig. Life Evol. Biosph.* **44**, 339-343 (2014). https://doi.org:10.1007/s11084-014-9379-0

30 Segré, D., Ben-Eli, D., Deamer, D. W. & Lancet, D. The Lipid World. *Orig. Life Evol. Biosph.* **31**, 119-145 (2001). https://doi.org:10.1023/A:1006746807104

31 Kahana, A. & Lancet, D. Self-reproducing catalytic micelles as nanoscopic protocell precursors. *Nat. Rev. Chem.* **5**, 870-878 (2021). https://doi.org:10.1038/s41570-021-00329-7

32 Szathmáry, E. & Maynard Smith, J. From Replicators to Reproducers: the First Major Transitions Leading to Life. *J. Theor. Biol.* **187**, 555-571 (1997). https://doi.org:https://doi.org/10.1006/jtbi.1996.0389

33 Szathmáry, E. The origin of replicators and reproducers. *Philos. Trans. R. Soc. Lond., B, Biol. Sci.* **361**, 1761-1776 (2006). https://doi.org:doi:10.1098/rstb.2006.1912

34 Szathmáry, E. in *Self-Production of Supramolecular Structures: From Synthetic Structures to Models of Minimal Living Systems* (eds Gail R. Fleischaker, Stefano Colonna, & Pier Luigi Luisi) 65-73 (Springer Netherlands, 1994).

35 Bissette, A. J. & Fletcher, S. P. Mechanisms of Autocatalysis. *Angew. Chem. Int. Ed.* **52**, 12800-12826 (2013). https://doi.org:10.1002/anie.201303822

36 Hanopolskyi, A. I., Smaliak, V. A., Novichkov, A. I. & Semenov, S. N. Autocatalysis: Kinetics, Mechanisms and Design. *ChemSystChem* **3** (2021). https://doi.org:10.1002/syst.202000026

37 Blackmond, D. G. An Examination of the Role of Autocatalytic Cycles in the Chemistry of Proposed Primordial Reactions. *Angew. Chem. Int. Ed.* **48**, 386-390 (2009). https://doi.org:10.1002/anie.200804565

38 Ruiz-Mirazo, K., Briones, C. & De La Escosura, A. Prebiotic Systems Chemistry: New Perspectives for the Origins of Life. *Chem. Rev.* **114**, 285-366 (2014). https://doi.org:10.1021/cr2004844

39 Sun, X., Reuther, J. F., Phillips, S. T. & Anslyn, E. V. Coupling Activity-Based Detection, Target Amplification, Colorimetric and Fluorometric Signal Amplification, for Quantitative Chemosensing of Fluoride Generated from Nerve Agents. *Chem. Eur. J.* **23**, 3903-3909 (2017). https://doi.org:https://doi.org/10.1002/chem.201604474

40 Cohen, I. The Bromination of Acetone in Organic Solvents. *J. Am. Chem. Soc.* **52**, 2827-2835 (1930). https://doi.org:10.1021/ja01370a040

41 Breslow, R. On the mechanism of the formose reaction. *Tetrahedron Lett.* **1**, 22-26 (1959). https://doi.org:https://doi.org/10.1016/S0040-4039(01)99487-0

42 Butlerow, A. Formation synthétique d'une substance sucrée. *Comptes rendus l'Académie des Sci.* **53**, 145-147 (1861).

43 Zubarev, D. Y., Rappoport, D. & Aspuru-Guzik, A. Uncertainty of Prebiotic Scenarios: The Case of the Non-Enzymatic Reverse Tricarboxylic Acid Cycle. *Sci. Rep.* **5**, 8009 (2015). https://doi.org:10.1038/srep08009

44 Orgel, L. E. The Implausibility of Metabolic Cycles on the Prebiotic Earth. *PLoS Biol.* **6**, e18 (2008). https://doi.org:10.1371/journal.pbio.0060018

45 Gyorgyi, L., Turanyi, T. & Field, R. J. Mechanistic details of the oscillatory Belousov-Zhabotinskii reaction. *J. Phys. Chem. A* **94**, 7162-7170 (1990). https://doi.org:10.1021/j100381a039

46 Epstein, I. R. & Showalter, K. Nonlinear Chemical Dynamics: Oscillations, Patterns, and Chaos. *J. Phys. Chem. A* **100**, 13132-13147 (1996). https://doi.org:10.1021/jp953547m

47 Hudson, J. L. & Mankin, J. C. Chaos in the Belousov–Zhabotinskii reaction. *J. Chem. Phys.* **74**, 6171-6177 (1981). https://doi.org:10.1063/1.441007

48 Vidonne, A. & Philp, D. Making Molecules Make Themselves – the Chemistry of Artificial Replicators. *Eur. J. Org. Chem.* **2009**, 593-610 (2009). https://doi.org:10.1002/ejoc.200800827
49 Clixby, G. & Twyman, L. Self-replicating systems. *Org. Biomol. Chem.* **14**, 4170-4184 (2016). https://doi.org:10.1039/C6OB00280C
50 Lee, D. H., Granja, J. R., Martinez, J. A., Severin, K. & Ghadiri, M. R. A self-replicating peptide. *Nature* **382**, 525-528 (1996). https://doi.org:10.1038/382525a0
51 Wang, B. & O. Sutherland, I. Self-replication in a Diels–Alder reaction. *Chem. Commun.*, 1495-1496 (1997). https://doi.org:10.1039/A701573I
52 Tjivikua, T., Ballester, P. & Rebek, J. Self-replicating system. *J. Am. Chem. Soc.* **112**, 1249-1250 (1990). https://doi.org:10.1021/ja00159a057
53 Buhse, T., Lavabre, D., Nagarajan, R. & Micheau, J. C. Origin of Autocatalysis in the Biphasic Alkaline Hydrolysis of C-4 to C-8 Ethyl Alkanoates. *J. Phys. Chem. A* **102**, 10552-10559 (1998). https://doi.org:10.1021/jp982765n
54 Chen, M., Jin, Y., Li, J., Zhang, Y. & Li, X. Mechanism and Kinetic Model for Autocatalysis in Liquid–Liquid System: Oxidation of Dibutyl Sulfide with Aqueous Hydrogen Peroxide. *Ind. Eng. Chem. Res.* **56**, 7675-7684 (2017). https://doi.org:10.1021/acs.iecr.7b01416
55 Glatzer, H. J. & Doraiswamy, L. K. Rate enhancements due to autocatalysis and heterogenization in phase transfer catalysis: a comparative study. *Chem. Eng. Sci.* **55**, 5149-5160 (2000). https://doi.org:10.1016/s0009-2509(00)00139-1
56 Chen, X. & Micheau, J. C. Hydrotrope-Induced Autocatalysis in the Biphasic Alkaline Hydrolysis of Aromatic Esters. *J. Colloid Interface Sci.* **249**, 172-179 (2002). https://doi.org:10.1006/jcis.2002.8226
57 Chizmadzhew, Y. A., Maestro, M. & Mavelli, F. A simplified kinetic model for an autopoietic synthesis of micelles. *Chem. Phys. Lett.* **226**, 56-62 (1994). https://doi.org:10.1016/0009-2614(94)00689-x
58 Maestro, M. A kinetic model for an autopoietic synthesis of micelles. *Mol. Eng.* **6**, 391-403 (1996). https://doi.org:10.1007/bf00440411
59 Mavelli, F. & Luisi, P. L. Autopoietic Self-Reproducing Vesicles: A Simplified Kinetic Model. *J. Phys. Chem. A* **100**, 16600-16607 (1996). https://doi.org:10.1021/jp960524e
60 Billingham, J. & Coveney, P. V. Kinetics of self-replicating micelles. *J. Chem. Soc., Faraday Trans.* **90**, 1953 (1994). https://doi.org:10.1039/ft9949001953
61 Coveney, P. V. & Wattis, J. A. D. Becker-Döring model of self-reproducing vesicles. *J. Chem. Soc., Faraday Trans.* **94**, 233-246 (1998). https://doi.org:10.1039/a703483k
62 Buhse, T., Nagarajan, R., Lavabre, D. & Micheau, J. C. Phase-Transfer Model for the Dynamics of "Micellar Autocatalysis". *J. Phys. Chem. A* **101**, 3910-3917 (1997). https://doi.org:10.1021/jp9705838
63 Nguyen, R., Allouche, L., Buhler, E. & Giuseppone, N. Dynamic Combinatorial Evolution within Self-Replicating Supramolecular Assemblies. *Angew. Chem. Int. Ed.* **48**, 1093-1096 (2009). https://doi.org:10.1002/anie.200804602
64 Bissette, A. J., Odell, B. & Fletcher, S. P. Physical autocatalysis driven by a bond-forming thiol–ene reaction. *Nat. Commun.* **5**, 4607 (2014). https://doi.org:10.1038/ncomms5607
65 Morrow, S. M., Bissette, A. J. & Fletcher, S. P. Potential for minimal self-replicating systems in a dynamic combinatorial library of equilibrating imines. *Tetrahedron* **73**, 5005-5010 (2017). https://doi.org:10.1016/j.tet.2017.06.045
66 Adamski, P. *et al.* From self-replication to replicator systems en route to de novo life. *Nat. Rev. Chem.* **4**, 386-403 (2020). https://doi.org:10.1038/s41570-020-0196-x
67 Walde, P. Surfactant Assemblies and their Various Possible Roles for the Origin(S) of Life. *Orig. Life Evol. Biosph.* **36**, 109-150 (2006). https://doi.org:10.1007/s11084-005-9004-3
68 Luisi, P. L., Walde, P. & Oberholzer, T. Lipid vesicles as possible intermediates in the origin of life. *Current Opinion in Colloid & Interface Science* **4**, 33-39 (1999). https://doi.org:https://doi.org/10.1016/S1359-0294(99)00012-6
69 Monnard, P.-A. & Deamer, D. W. Membrane self-assembly processes: Steps toward the first cellular life. *Anat. Rec.* **268**, 196-207 (2002). https://doi.org:https://doi.org/10.1002/ar.10154
70 Kahana, A., Maslov, S. & Lancet, D. Dynamic lipid aptamers: non-polymeric chemical path to early life. *Chem. Soc. Rev.* **50**, 11741-11746 (2021). https://doi.org:10.1039/D1CS00633A

71 Budin, I., Prywes, N., Zhang, N. & Szostak, Jack W. Chain-Length Heterogeneity Allows for the Assembly of Fatty Acid Vesicles in Dilute Solutions. *Biophys. J.* **107**, 1582-1590 (2014). https://doi.org:https://doi.org/10.1016/j.bpj.2014.07.067

72 Jordan, S. F. *et al.* Promotion of protocell self-assembly from mixed amphiphiles at the origin of life. *Nat. Ecol. Evol.* **3**, 1705-1714 (2019). https://doi.org:10.1038/s41559-019-1015-y

73 Maurer, S. E. D., D. W.; Boncella, J. M.; Monnard, P. A. Chemical Evolution of Amphiphiles: Glycerol Monoacyl Derivatives Stabilize Plausible Prebiotic Membranes. *Astrobiology* **9**, 979-987 (2009). https://doi.org:10.1089/ast.2009.0384

74 Bell, T. N., Feng, K., Calvin, G., Van Winkle, D. H. & Lenhert, S. Organic Composomes as Supramolecular Aptamers. *ACS Omega* **5**, 27393-27400 (2020). https://doi.org:10.1021/acsomega.0c03799

75 Dingjan, T. & Futerman, A. H. The fine-tuning of cell membrane lipid bilayers accentuates their compositional complexity. *BioEssays* **43**, 2100021 (2021). https://doi.org:https://doi.org/10.1002/bies.202100021

76 Walde, P., Umakoshi, H., Stano, P. & Mavelli, F. Emergent properties arising from the assembly of amphiphiles. Artificial vesicle membranes as reaction promoters and regulators. *Chem. Commun.* **50**, 10177-10197 (2014). https://doi.org:10.1039/C4CC02812K

77 Maturana, H. R. & Varela, F. J. *Autopoiesis and cognition: the realization of the living*. (D. Reidel Pub. Co., 1980).

78 Bachmann, P. A., Walde, P., Luisi, P. L. & Lang, J. Self-replicating reverse micelles and chemical autopoiesis. *J. Am. Chem. Soc.* **112**, 8200-8201 (1990). https://doi.org:10.1021/ja00178a073

79 Fleischaker, G. R. Origins of life: An operational definition. *Orig. Life Evol. Biosph.* **20**, 127-137 (1990). https://doi.org:10.1007/BF01808273

80 Dzieciol, A. J. & Mann, S. Designs for life: protocell models in the laboratory. *Chem. Soc. Rev.* **41**, 79-85 (2012). https://doi.org:10.1039/c1cs15211d

81 Luisi, P. L. *The Emergence of Life: From Chemical Origins to Synthetic Biology*. (Cambridge University Press, 2006).

82 Luisi, P. L. & Varela, F. J. Self-replicating micelles — A chemical version of a minimal autopoietic system. *Orig. Life Evol. Biosph.* **19**, 633-643 (1989). https://doi.org:10.1007/BF01808123

83 Bachmann, P. A., Walde, P., Luisi, P. L. & Lang, J. Self-replicating micelles: aqueous micelles and enzymatically driven reactions in reverse micelles. *J. Am. Chem. Soc.* **113**, 8204-8209 (1991). https://doi.org:10.1021/ja00022a002

84 Bachmann, P. A., Luisi, P. L. & Lang, J. Autocatalytic self-replicating micelles as models for prebiotic structures. *Nature* **357**, 57-59 (1992). https://doi.org:10.1038/357057a0

85 Walde, P., Wick, R., Fresta, M., Mangone, A. & Luisi, P. L. Autopoietic Self-Reproduction of Fatty Acid Vesicles. *J. Am. Chem. Soc.* **116**, 11649-11654 (1994). https://doi.org:10.1021/ja00105a004

86 Wick, R., Walde, P. & Luisi, P. L. Light microscopic investigations of the autocatalytic self-reproduction of giant vesicles. *J. Am. Chem. Soc.* **117**, 1435-1436 (1995). https://doi.org:10.1021/ja00109a031

87 Kust, P. R. & Rathman, J. F. Synthesis of Surfactants by Micellar Autocatalysis: N,N-Dimethyldodecylamine N-Oxide. *Langmuir* **11**, 3007-3012 (1995). https://doi.org:10.1021/la00008a026

88 Bissette, A. J. & Fletcher, S. P. Novel applications of physical autocatalysis. *Orig. Life Evol. Biosph.* **45**, 21-30 (2015). https://doi.org:10.1007/s11084-015-9404-y

89 Takakura, K., Toyota, T. & Sugawara, T. A Novel System of Self-Reproducing Giant Vesicles. *J. Am. Chem. Soc.* **125**, 8134-8140 (2003). https://doi.org:10.1021/ja029379a

90 Kurihara, K. *et al.* Self-reproduction of supramolecular giant vesicles combined with the amplification of encapsulated DNA. *Nat. Chem.* **3**, 775-781 (2011). https://doi.org:10.1038/nchem.1127

91 Hardy, M. D. *et al.* Self-reproducing catalyst drives repeated phospholipid synthesis and membrane growth. *Proc. Natl Acad. Sci.* **112**, 8187-8192 (2015). https://doi.org:doi:10.1073/pnas.1506704112

92 Budin, I. & Devaraj, N. K. Membrane Assembly Driven by a Biomimetic Coupling Reaction. *J. Am. Chem. Soc.* **134**, 751-753 (2012). https://doi.org:10.1021/ja2076873
93 Post, E. A. J., Bissette, A. J. & Fletcher, S. P. Self-reproducing micelles coupled to a secondary catalyst. *Chem. Commun.* **54**, 8777-8780 (2018). https://doi.org:10.1039/c8cc02136h
94 Post, E. A. J. & Fletcher, S. P. Controlling the Kinetics of Self-Reproducing Micelles by Catalyst Compartmentalization in a Biphasic System. *J. Org. Chem.* **84**, 2741-2755 (2019). https://doi.org:10.1021/acs.joc.8b03149
95 Priest, L., Peters, J. S. & Kukura, P. Scattering-based Light Microscopy: From Metal Nanoparticles to Single Proteins. *Chem. Rev.* **121**, 11937-11970 (2021). https://doi.org:10.1021/acs.chemrev.1c00271
96 Young, G. & Kukura, P. Interferometric Scattering Microscopy. *Annu. Rev. Phys. Chem.* **70**, 301-322 (2019). https://doi.org:10.1146/annurev-physchem-050317-021247
97 Ortega-Arroyo, J., Bissette, A. J., Kukura, P. & Fletcher, S. P. Visualization of the spontaneous emergence of a complex, dynamic, and autocatalytic system. *Proc. Natl Acad. Sci.* **113**, 11122-11126 (2016). https://doi.org:doi:10.1073/pnas.1602363113
98 Grzybowski, B. A., Fitzner, K., Paczesny, J. & Granick, S. From dynamic self-assembly to networked chemical systems. *Chem. Soc. Rev.* **46**, 5647-5678 (2017). https://doi.org:10.1039/C7CS00089H
99 van Esch, J. H., Klajn, R. & Otto, S. Chemical systems out of equilibrium. *Chem. Soc. Rev.* **46**, 5474-5475 (2017). https://doi.org:10.1039/C7CS90088K
100 Pascal, R., Pross, A. & Sutherland, J. D. Towards an evolutionary theory of the origin of life based on kinetics and thermodynamics. *Open Biol.* **3**, 130156 (2013). https://doi.org:doi:10.1098/rsob.130156
101 Lerch, M. M., Grinthal, A. & Aizenberg, J. Viewpoint: Homeostasis as Inspiration—Toward Interactive Materials. *Adv. Mater.* **32**, 1905554 (2020). https://doi.org:https://doi.org/10.1002/adma.201905554
102 Merindol, R. & Walther, A. Materials learning from life: concepts for active, adaptive and autonomous molecular systems. *Chem. Soc. Rev.* **46**, 5588-5619 (2017). https://doi.org:10.1039/C6CS00738D
103 Boekhoven, J. *et al.* Dissipative Self-Assembly of a Molecular Gelator by Using a Chemical Fuel. *Angew. Chem. Int. Ed.* **49**, 4825-4828 (2010). https://doi.org:https://doi.org/10.1002/anie.201001511
104 De, S. & Klajn, R. Dissipative Self-Assembly Driven by the Consumption of Chemical Fuels. *Adv. Mater.* **30**, 1706750 (2018). https://doi.org:https://doi.org/10.1002/adma.201706750
105 van Rossum, S. A. P., Tena-Solsona, M., van Esch, J. H., Eelkema, R. & Boekhoven, J. Dissipative out-of-equilibrium assembly of man-made supramolecular materials. *Chem. Soc. Rev.* **46**, 5519-5535 (2017). https://doi.org:10.1039/C7CS00246G
106 Ragazzon, G. & Prins, L. J. Energy consumption in chemical fuel-driven self-assembly. *Nat. Nanotechnol.* **13**, 882-889 (2018). https://doi.org:10.1038/s41565-018-0250-8
107 Amano, S., Borsley, S., Leigh, D. A. & Sun, Z. Chemical engines: driving systems away from equilibrium through catalyst reaction cycles. *Nat. Nanotechnol.* **16**, 1057-1067 (2021). https://doi.org:10.1038/s41565-021-00975-4
108 Rieß, B., Grötsch, R. K. & Boekhoven, J. The Design of Dissipative Molecular Assemblies Driven by Chemical Reaction Cycles. *Chem* **6**, 552-578 (2020). https://doi.org:https://doi.org/10.1016/j.chempr.2019.11.008
109 Zepik, H. H., Blöchliger, E. & Luisi, P. L. A Chemical Model of Homeostasis. *Angew. Chem. Int. Ed.* **40**, 199-202 (2001).
110 Colomer, I., Morrow, S. M. & Fletcher, S. P. A transient self-assembling self-replicator. *Nat. Commun.* **9** (2018). https://doi.org:10.1038/s41467-018-04670-2
111 Morrow, S. M., Colomer, I. & Fletcher, S. P. A chemically fuelled self-replicator. *Nat. Commun.* **10**, 1011 (2019). https://doi.org:10.1038/s41467-019-08885-9
112 Afrose, S. P., Ghosh, C. & Das, D. Substrate induced generation of transient self-assembled catalytic systems. *Chem. Rev.* **12**, 14674-14685 (2021). https://doi.org:10.1039/d1sc03492h
113 Lutz, J. F. Can Life Emerge from Synthetic Polymers? *Isr. J. Chem.* **60**, 151-159 (2020).

114 Lebedeva, M. A., Palmieri, E., Kukura, P. & Fletcher, S. P. Emergence and Rearrangement of Dynamic Supramolecular Aggregates Visualized by Interferometric Scattering Microscopy. *ACS Nano* **14**, 11160-11168 (2020). https://doi.org:10.1021/acsnano.0c02414
115 Engwerda, A. H. J. *et al.* Coupled Metabolic Cycles Allow Out-of-Equilibrium Autopoietic Vesicle Replication. *Angew. Chem. Int. Ed.* **59**, 20361-20366 (2020). https://doi.org:10.1002/anie.202007302
116 Colomer, I., Borissov, A. & Fletcher, S. P. Selection from a pool of self-assembling lipid replicators. *Nat. Commun.* **11**, 176 (2020). https://doi.org:10.1038/s41467-019-13903-x
117 Myrgorodska, I., Colomer, I. & Fletcher, S. P. Oligomerization Driven by Phase Separation. *ChemSystChem* **2** (2020). https://doi.org:10.1002/syst.201900059
118 Post, E. A. J. & Fletcher, S. P. Dissipative self-assembly, competition and inhibition in a self-reproducing protocell model. *Chem. Sci.* **11**, 9434-9442 (2020). https://doi.org:10.1039/D0SC02768E
119 Feynman, R. P. in *Engineering and Science* Vol. 22 22-26 (1960).
120 Drexler, K. E. *Engines of creation: the coming era of nanotechnology*. (Doubleday, 1986).
121 Corra, S., Curcio, M., Baroncini, M., Silvi, S. & Credi, A. Photoactivated Artificial Molecular Machines that Can Perform Tasks. *Adv. Mater.* **32**, 1906064 (2020). https://doi.org:https://doi.org/10.1002/adma.201906064
122 van Dijk, L. *et al.* Molecular machines for catalysis. *Nat. Rev. Chem.* **2**, 0117 (2018). https://doi.org:10.1038/s41570-018-0117
123 Lewandowski, B. *et al.* Sequence-Specific Peptide Synthesis by an Artificial Small-Molecule Machine. *Science* **339**, 189-193 (2013). https://doi.org:doi:10.1126/science.1229753
124 Engwerda, A. H. J. & Fletcher, S. P. A molecular assembler that produces polymers. *Nat. Commun.* **11** (2020). https://doi.org:10.1038/s41467-020-17814-0
125 Babu, D. *et al.* Acceleration of lipid reproduction by emergence of microscopic motion. *Nat. Commun.* **12**, 2959 (2021). https://doi.org:10.1038/s41467-021-23022-1
126 Izri, Z., Van Der Linden, M. N., Michelin, S. & Dauchot, O. Self-Propulsion of Pure Water Droplets by Spontaneous Marangoni-Stress-Driven Motion. *Phys. Rev. Lett.* **113** (2014). https://doi.org:10.1103/physrevlett.113.248302
127 Schmitt, M. & Stark, H. Marangoni flow at droplet interfaces: Three-dimensional solution and applications. *Phys. Fluids* **28**, 012106 (2016). https://doi.org:10.1063/1.4939212
128 Schwarz, P. S., Tebcharani, L., Heger, J. E., Müller-Buschbaum, P. & Boekhoven, J. Chemically fueled materials with a self-immolative mechanism: transient materials with a fast on/off response. *Chem. Sci.* **12**, 9969-9976 (2021). https://doi.org:10.1039/d1sc02561a
129 Rieß, B. *et al.* Dissipative assemblies that inhibit their deactivation. *Soft Matter* **14**, 4852-4859 (2018). https://doi.org:10.1039/C8SM00822A
130 Tena-Solsona, M. *et al.* Non-equilibrium dissipative supramolecular materials with a tunable lifetime. *Nat. Commun.* **8**, 15895 (2017). https://doi.org:10.1038/ncomms15895
131 Wanzke, C., Tena-Solsona, M., Rieß, B., Tebcharani, L. & Boekhoven, J. Active droplets in a hydrogel release drugs with a constant and tunable rate. *Mater. Horiz.* **7**, 1397-1403 (2020). https://doi.org:10.1039/C9MH01822K

Statement of Authorship for joint/multi-authored papers for PGR thesis

To appear at the end of each thesis chapter submitted as an article/paper

The statement shall describe the candidate's and co-authors' independent research contributions in the thesis publications. For each publication there should exist a complete statement that is to be filled out and signed by the candidate and supervisor **(only required where there isn't already a statement of contribution within the paper itself).**

Title of Paper	(Self-)reproducing lipid systems: from autocatalysis to survival of the fittest
Publication Status	~~Published~~ ☑ Accepted for Publication ~~Submitted for Publication~~ ~~Unsubmitted work written in a manuscript style~~
Publication Details	Michael G. Howlett and Stephen P. Fletcher. n/a – in press with Nature Reviews Chemistry (no DOI available at time of submission)

Student Confirmation

Student Name:	Michael Howlett		
Contribution to the Paper	Writing original draft and editing of manuscript (review). Co-author (S. Fletcher) also contributed to writing the manuscript.		
Signature		Date	14 / 04 / 2023

Supervisor Confirmation

By signing the Statement of Authorship, you are certifying that the candidate made a substantial contribution to the publication, and that the description described above is accurate.

Supervisor name and title: Prof. Stephen Fletcher			
Supervisor comments			
Signature		Date	

This completed form should be included in the thesis, at the end of the relevant chapter.

Chapter 2

Competition Between Self-Reproducing Lipids

Chapter 2

Competition Between Self-Reproducing Lipids

The work in this chapter was undertaken in collaboration with Robert Scanes and was published in JACS Au in 2021: 'Selection Between Competing Self-reproducing Lipids: Succession and Dynamic Activation'.

2.1 Introduction

While evolution from primitive cells to current organisms is generally well understood, the pathway from small molecules to functional cell-like systems is still unresolved. Our prebiotic origins are therefore the subject of much ongoing systems chemistry research. One emerging approach is to examine kinetically controlled autocatalytic reactions in the hopes of learning how life-like properties may have developed in prebiotic scenarios. Further to this, gaining insight into the origins of biological complexity can inform how to construct new responsive, functional synthetic systems.

It is expected that early chemical evolution involved a diverse pool of molecules undergoing various chemical adaptation, replication and selection processes before reaching familiar biological assemblies.[1] Early chemical species which behave in a life-like way need energy and raw materials to sustain their structures, yet these resources are finite and so competition between different structures is expected. Understanding how selection may arise in this scenario is key to ongoing research in dynamic systems, synthetic protocells and replicator networks.[2-4] Even so, little is known about what selection mechanisms are available to simple replicating species competing for resources. Progress has been made regarding plausible routes to building blocks for living cells[2,5-7] but questions remain about how dominant self-replicating motifs can emerge from prebiotic beginnings.[8,9]

Species that can replicate possess clear advantages over those which cannot and are relevant to theories of chemical evolution. Inspired by nature's functional biopolymers and the "RNA world" hypothesis,[6,10,11] template based molecular replication has long been a major feature of prebiotic chemistry research. For example, template replicators based upon nucleotides,[12] fibre stacking,[13] Diels-Alder[14] and dipolar cycloaddition chemistry[15] have all been reported. In contrast, self-reproducing surfactants possess their own unique abilities and selection rules, in line with the "lipid world" theory.[16,17] Surfactants can accelerate their own formation by forming aggregates which aid reaction between their phase separated precursors, in a process termed physical autocatalysis.[18-21] It's also worth pointing out that catalytic species that can enhance the mixing of organic and aqueous phases would also allow such species access to a wider pool of resources, providing a competitive advantage. Importantly, where multiple self-reproducing species are present, surfactant production can result in a global cross-catalytic effect. Complex systems of this type can lead to ill-defined scenarios where the replication effects are tied to the system as a whole, rather than individual self-serving species.

Selection between species is important in models of the development of life. Past studies into template replicator selection have typically relied upon competing auto- and cross-catalytic processes, providing valuable insight into the interplay between species.[13,22-25] However, by virtue of their stability, these replicators primarily exist close to thermodynamic equilibrium – the domain of inanimate materials.[26,27] Recognising life as an inherently dissipative state has prompted the development of metastable systems to uncover more life-like phenomena (*e.g.* Scheme 1a).[28-32]

Selection in metastable systems has been reported in a few cases and can arise from factors such as precursor solubility under heterogeneous conditions,[33] selective degradation,[34-36] rate of assembly[37] and product compartmentalisation.[38] These cases highlight the breadth of potential selection mechanisms available to life-like systems. Further selection modes await discovery and could shed light on how chemical selection may serve as a basis for early biological evolution. For example, it

seems plausible that certain mixtures may have functions not available to their isolated components.[39-41]

Previous work by Morrow et al. described a metastable self-reproducer formed through thiol-disulfide exchange.[31] This established a surfactant-forming reaction between a disulfide (**1a**) and an alkyl thiol (**2a**) to give a surfactant that self-reproduces by physical autocatalysis (**3aa**, see Section 1.2.1).

2.2 Aims

The aim of this work is to explore competition between self-reproducing lipids. This builds upon the work of Morrow et al. and uses thiol-disulfide chemistry under biphasic conditions. Mixtures of different self-reproducing lipids may create new behaviour that's not available to single species in isolation. When different precursors compete for reactants (*e.g.* thiols and disulfides) they could interact with each other or be affected by the products of their reactions. It is expected that using a more compositionally diverse mixture will allow for interesting, emergent effects to be observed. For example, the lipid species are metastable and can be formed and broken down continuously. Due to this constant turnover, we believed we might observe succession analogous to that seen in ecological systems of the natural world.

2.3 Results and Discussion

2.3.1 System overview

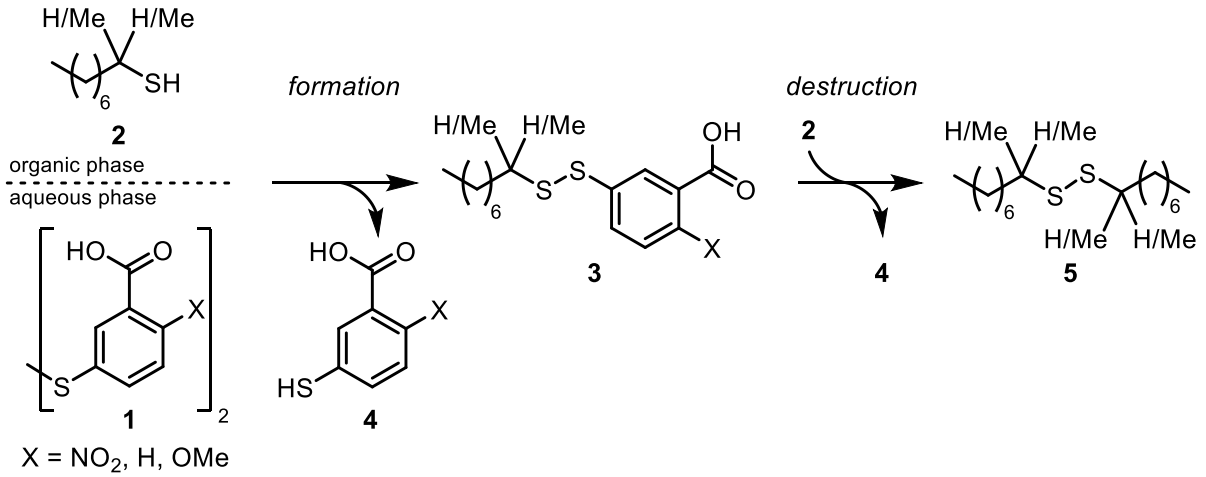

Figure 2.1: Two sequential reactions form and destroy the self-reproducing surfactants. Formation: hydrophilic disulfide **1** reacts with phase separated thiol **2** to produce lipid **3**. **4** is the leaving group in this reaction. Destruction: **3** reacts with another equivalent of **2** and breaks down into thermodynamic products **4** and **5**. **5** represents the generic corresponding dialkyl disulfide product(s) formed from parent thiol(s). Surfactant **3** helps the reactants mix better, accelerating its own formation autocatalytically. Disulfides with different electronic properties (**1a-c**) and thiols with different steric properties (**2a-c**) are used. Typical conditions: **1** (25 mM in pH 8.0 HEPES buffer) + **2** (8.0 equiv.) stirred at 100 rpm at room temperature. See Experimental section 7.2.3 for details.

A system of competing lipid products was envisaged, formed from reaction between different hydrophilic disulfide (**1**) and hydrophobic thiol (**2**) building blocks (see Figure 2.1). Thiol-disulfide exchange reactions give rise to both the formation and destruction of each surfactant, determining their lifetime. When electrophilic disulfide **1** is attacked by phase separated alkyl thiol **2** it gives surfactant **3** and byproduct **4**. Next, a second equivalent of thiol **2** reacts with **3**, depleting the lipid population and giving products **4** and **5** (see Figure 2.1). Consistent with our prior work by Morrow et al., this surfactant-forming process shows autocatalytic reaction kinetics due to the interfacial reaction steps involved.[31] Three disulfides **1a-c** were selected as the electrophilic partner in these reactions with differing properties to affect their reaction rate in thiol-disulfide exchange. Varying the 4-position substituent on the disulfides dramatically changes their reaction rate, with X = NO_2 (**1a**) providing the best aromatic leaving group in thiol-disulfide exchange and X = OMe (**1c**) resulting in a relatively poor leaving group. Three alkyl thiols with different structural properties were also chosen: a primary thiol (**2a**), a secondary thiol (**2b)** and the most sterically hindered, a

tertiary thiol (**2c**) (Figure 2.2). These thiols react with disulfides at distinctly different rates, allowing for different kinetic behaviour when competing. When reacted, these precursors can give up to nine hetero-disulfide surfactants (**3aa-cc**, see Figure 2.3 for full structures).

The thiol-disulfide reactions of interest were set up analogously to previously reported[32] with the disulfides dissolved in an aqueous buffer (pH 8.0 HEPES), the hydrophobic thiol layered on top and the two phases stirred at a specific speed (100 rpm). To monitor the progress of the reactions and gain information on the composition of the mixture, aliquots were manually removed from the lower aqueous layer by microsyringe. These aliquots were then directly quenched in a concentrated maleimide solution to prevent further thiol-disulfide reactions and the composition of the samples analysed by UPLC. The choice of these conditions allowed for good solubility of **1** and suitable reaction timescales for convenient kinetic monitoring. See Experimental Section 7.2.3 for details.

2.3.2 Reactivity trends established in non-competition reactions

We performed nine independent reactions, combining each disulfide **1a-c** with each nucleophilic thiol **2a-c** in turn. Increasing the steric hindrance of the alkyl thiol used (and therefore also the stability of surfactant **3**) resulted in lower formation and destruction rates, *i.e.* decreased reactivity. Lower reactivity was also seen when using more electron rich aromatic disulfides **2b-c**. The reactivity patterns from these combinations are summarized in Figure 2.2.

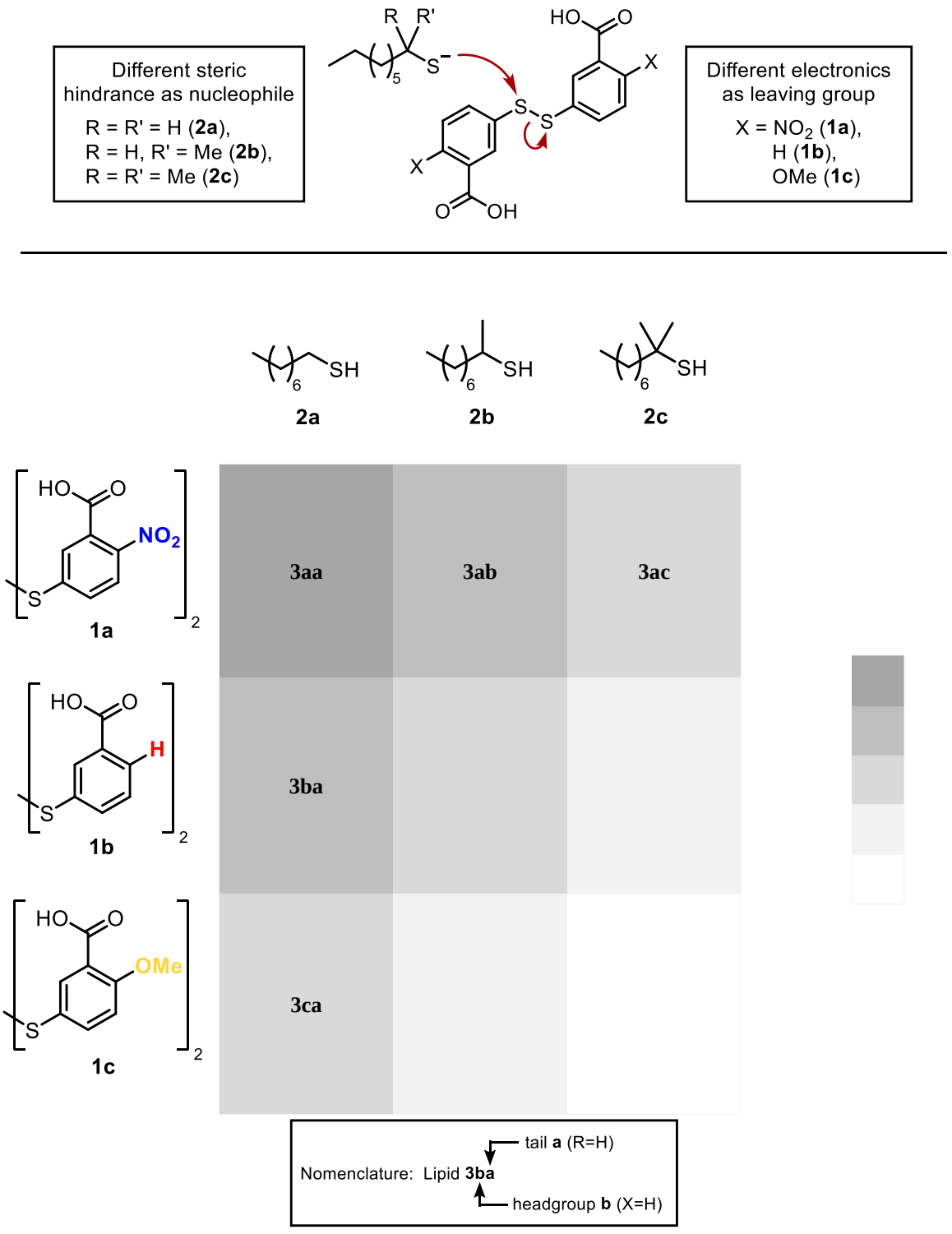

Figure 2.2: Reactivity trends for surfactant precursors in thiol-disulfide exchange. Three surfactant series with various headgroups (**a**, **b** and **c**) and hydrophobic tails are accessible. The surfactant products **3** are named according to the following example: **3ba** = headgroup b + tail a. The relative reactivities of the components as indicated by the colour scale are intended only as a guide. Data supporting these trends may be found in Figure 2.3.

Inspecting the kinetic profiles obtained in the non-competition control experiments in Figure 2.3, the magnitude of the reactivity differences can be seen. Use of disulfide **1a** always results in

significant concentrations of the surfactant, regardless of the hindrance of the thiol used. However, the maximum surfactant concentration and point at which it is reached during the 8 hour monitoring period is sensitive to thiol nucleophilicity. Surfactants derived from disulfide **1b** exist at only a very low concentrations as these systems do not have a rapid formation reaction or sufficient kinetic stability to persist for long. In a competition scenario, this middle ground, in terms of kinetic behaviour, may not be favourable for species like this as there is no specific advantage over other species. Surfactants derived from **1c** have some similarities to those formed from **1b** due to their lower reactivity with **2**. However, when using the most reactive thiol **2a**, surfactant **3ca** is gradually formed in measurable amounts and it experiences steady growth due to possessing relatively high resistance to destruction.

Remarkably, dynamic light scattering (DLS) of the surfactants highlighted a further trend associated with their electronic properties. While electron poor headgroup **a** gives rise to micellar structures, surfactants in series **b** or **c** possess size distributions consistent with vesicles (see Experimental section 7.2.5, Figures S15-23). This difference is possibly due to the relative acidity of the carboxylic acid groups on each headgroup. This would strongly affect the hydrogen bonding between aggregated surfactant monomers and alter the charge density and headgroup repulsion, influencing the packing of monomers.[42] This phenomenon is observed with oleic acid, where at pH >10.2 micelles form, whereas below this value vesicles are found.[43]

Disulfide:
1a, **1b** or **1c**
+
Thiol:
2a, **2b** or **2c**

Non-competition

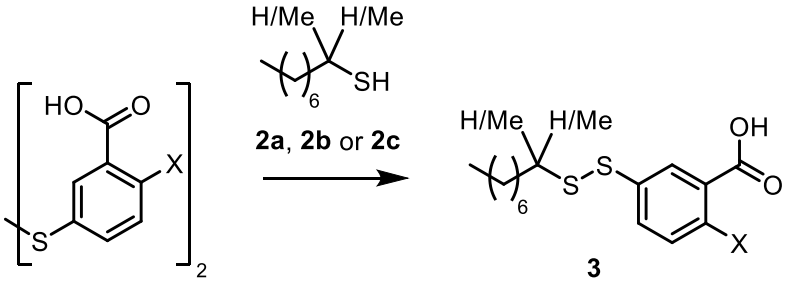

Either:
X = NO_2 (**1a**), H (**1b**), OMe (**1c**)

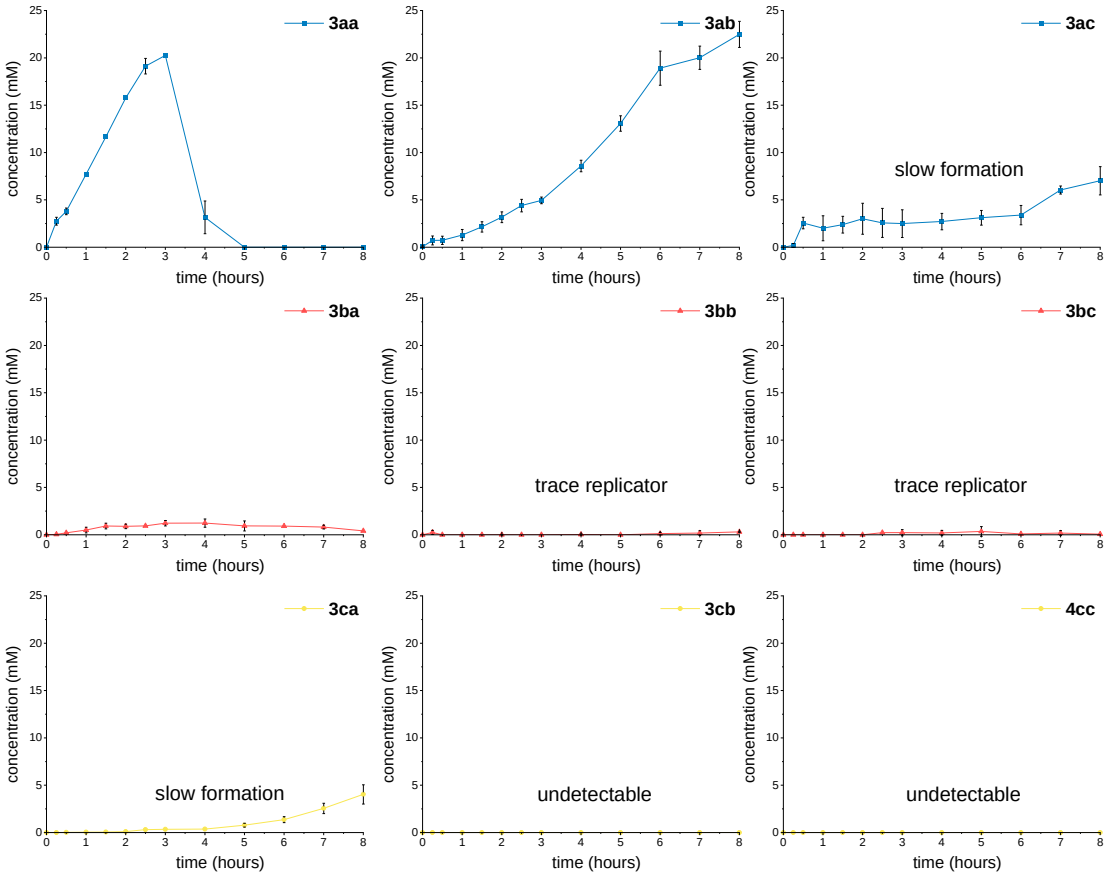

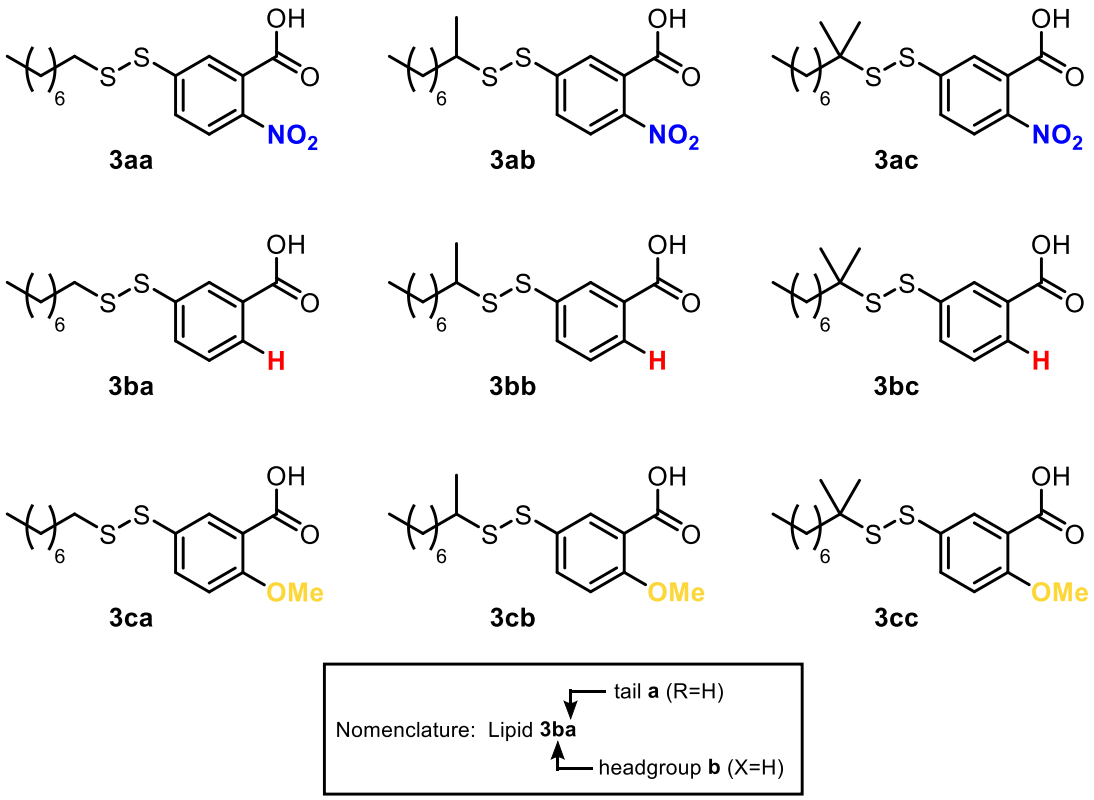

Figure 2.3: Summary of non-competition experiments for all lipids **3** showing the relative formation and destruction characteristics (i.e. relative reactivity in biphasic thiol-disulfide exchange) for each thiol (**1**) and disulfide (**2**) pair in turn. HEPES buffer (pH 8.0), r.t., 100 rpm, 8.0 eq. thiol (**1a**, **1b** or **1c**) n = 3, error bars (where visible) represent the standard deviation.

2.3.3 Species succession by intrinsic structural factors

We then examined systems where multiple competing surfactants could be produced in the same reaction. Beginning with a mixture of disulfide **1a** and thiols **2a-c** the influence of steric effects on surfactant populations was examined.

Monitoring the reactions over time revealed a clear succession pattern where the dominant lipid product changes over time (Figure 2.4). This can be understood based on thiol nucleophilicity and the relative steric hindrance of **3aa, 3ba** and **3ca**. **3aa** is the fastest to form and shortest lived (pioneer species), followed by **3ab** (follower species) and then **3ac**, which has relatively high kinetic stability under the reaction conditions (mature species). Furthermore, as the amount of surfactant **3aa** increases in the system, **3ab** and **3ac** benefit from a cross-catalytic effect (increased solubilisation of thiols) and experience population growth. Hindered species **3ac** has a sufficiently

slow destruction step to enable persistence under these conditions and is the dominant species at long reaction times.

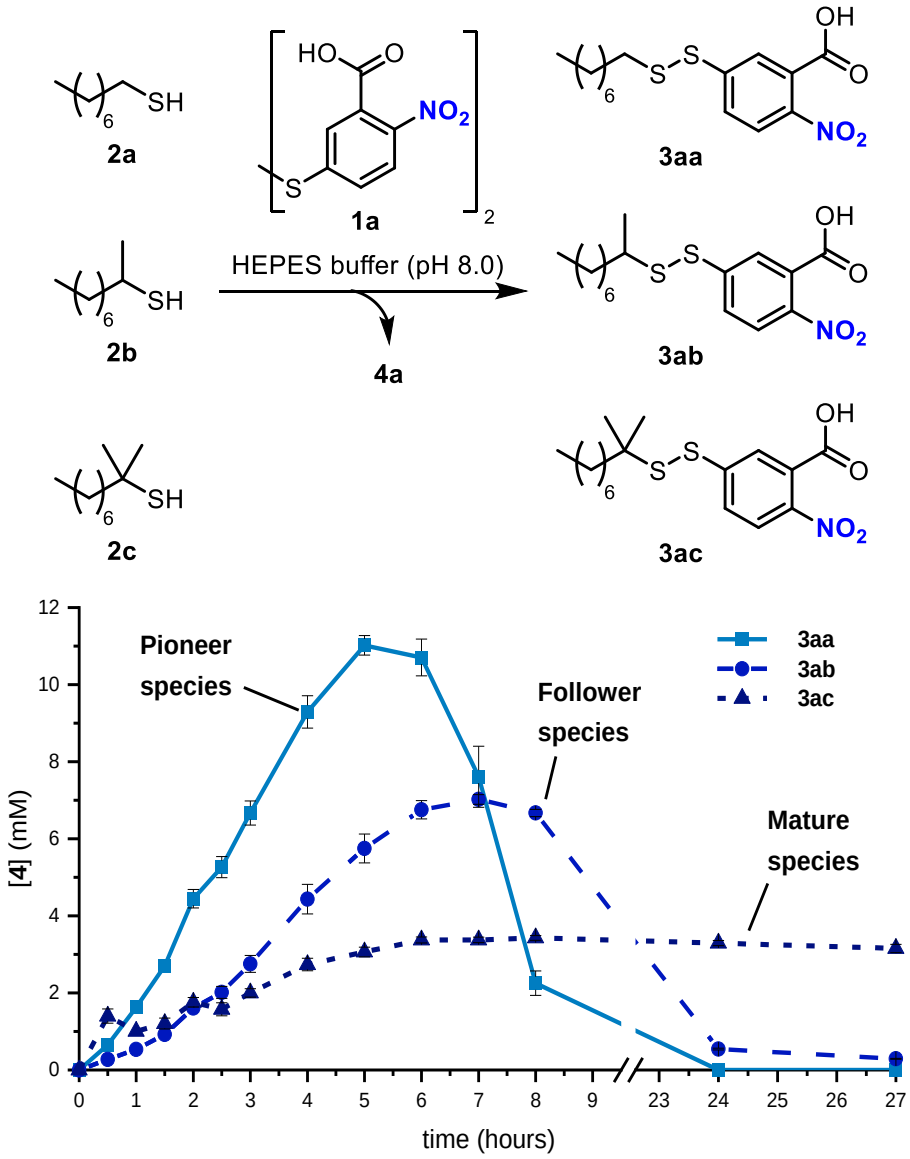

Figure 2.4: Competition between sterically differentiated precursors leads to species succession in time. Destruction step with concomitant formation of product **5** not shown for clarity. n = 3, error bars (where visible) represent the standard deviation.

Ultimately, all metastable surfactants tend towards degrading into thermodynamic products **4** and **5**. The chemical succession shown in Figure 2.4 is directly derived from the intrinsic structural properties of precursors **2a-c** which is also translated into the stability of surfactants **3aa**, **3ab** and **3ac**.

2.3.4 Unexpected selection effects with increased compositional complexity

Next, we examined combinations of disulfide electrophiles **1a-c**, which have different electronic properties. As shown in Figure 2.5, thiol **2a** was reacted with mixtures of disulfides **1a-c**, to give multiple products (**3aa**, **3ba**, **3ca**) in each reaction. First, pairs of disulfides were tested to examine competition between two electrophiles (**1a** + **1b**, Figure 2.6a and **1a** + **1c**, Figure 2.6b). The relative proportion of each surfactant was found to change over time. Interestingly, competing products initially formed at similar rates, despite large rate differences observed when formed in isolation (see Figure 2.6).

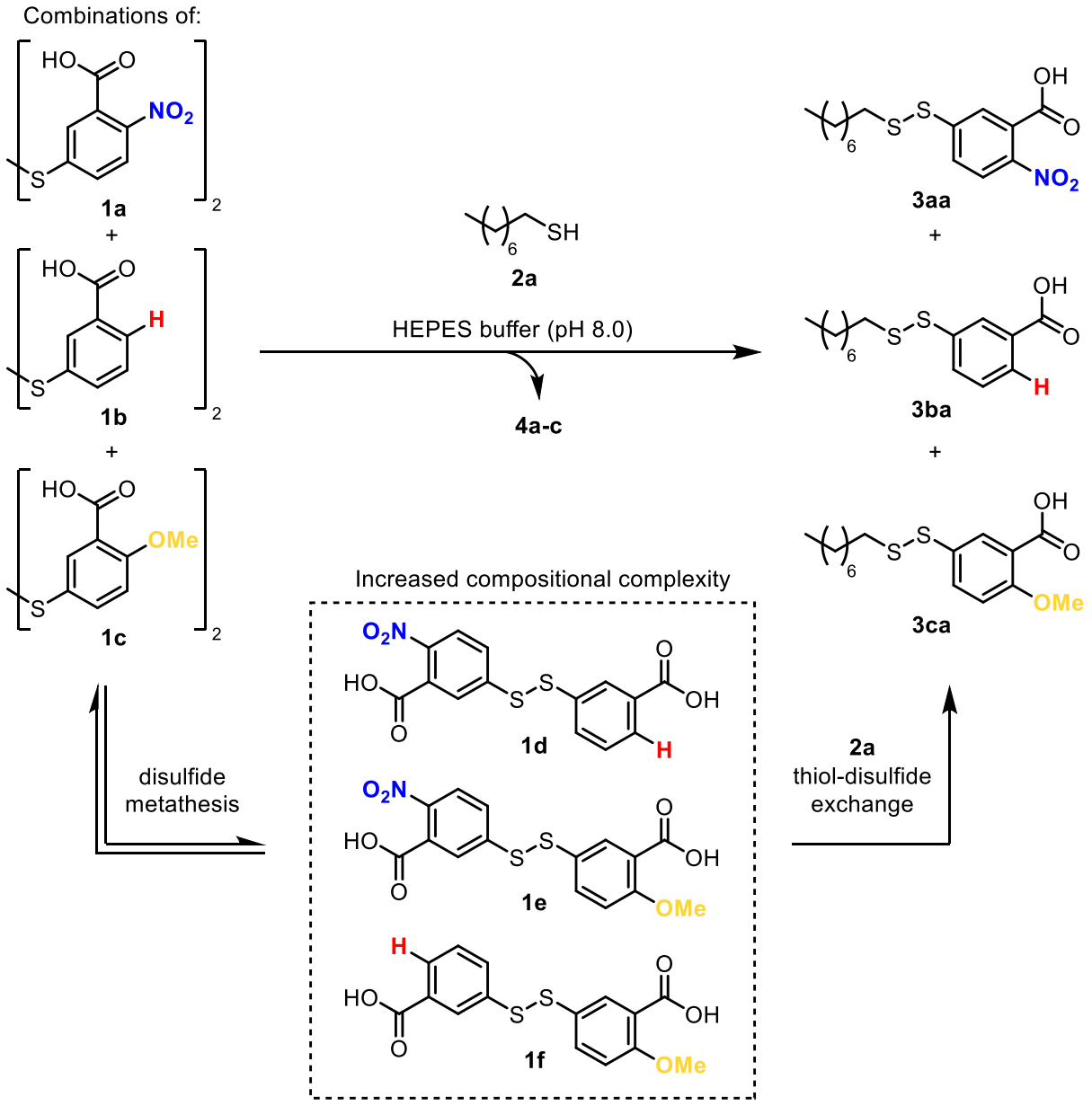

Figure 2.5: Competition experiments using mixtures of disulfides **1** to react with **2** gives three surfactant products

3aa-ca. The presence of multiple disulfide building blocks allows for a fast disulfide metathesis process that changes the selectivity pattern when forming **3**. New intermediate hetero-disulfides **1d-f** are accessed which can also undergo thiol-disulfide exchange. This means the mixture complexity has increased, and more combinations of reaction partners are available. See Figure 2.6 for kinetic data of the corresponding experiments.

When disulfide **1a** and thiol **2a** react in isolation (non-competition), surfactant **3aa** reaches concentrations up to 20 mM (Figure 2.3). However, when competing with **3ba**, the peak concentration of **3aa** is greatly diminished (~4 mM), whilst **3ba** benefits and forms faster than in non-competition experiments (dashed vs solid lines, Figure 2.6a). In this competition experiment, **3ba** achieves ~10x the maximum concentration seen in the absence of disulfide **1a**.

Competition between surfactants **3aa** and **3ca** also shows lower [**3aa**] than in isolation (*ca.* 5 mM) and **3ca** achieves near complete conversion within 8 hours, despite being the product of the least electrophilic precursor **1c** (Figure 2.6b). When all three surfactants **3aa**, **3ba** and **3ca** are being formed and destroyed together, the system displays selection over time (Figure 2.6c). As before, **3aa** degrades fastest, decreasing in concentration after peaking at ~5 hours. **3ba** and **3ba** initially perform comparably to one another with **3ac** (the least electrophilic disulfide of the two) eventually becoming slightly dominant at long reaction times.

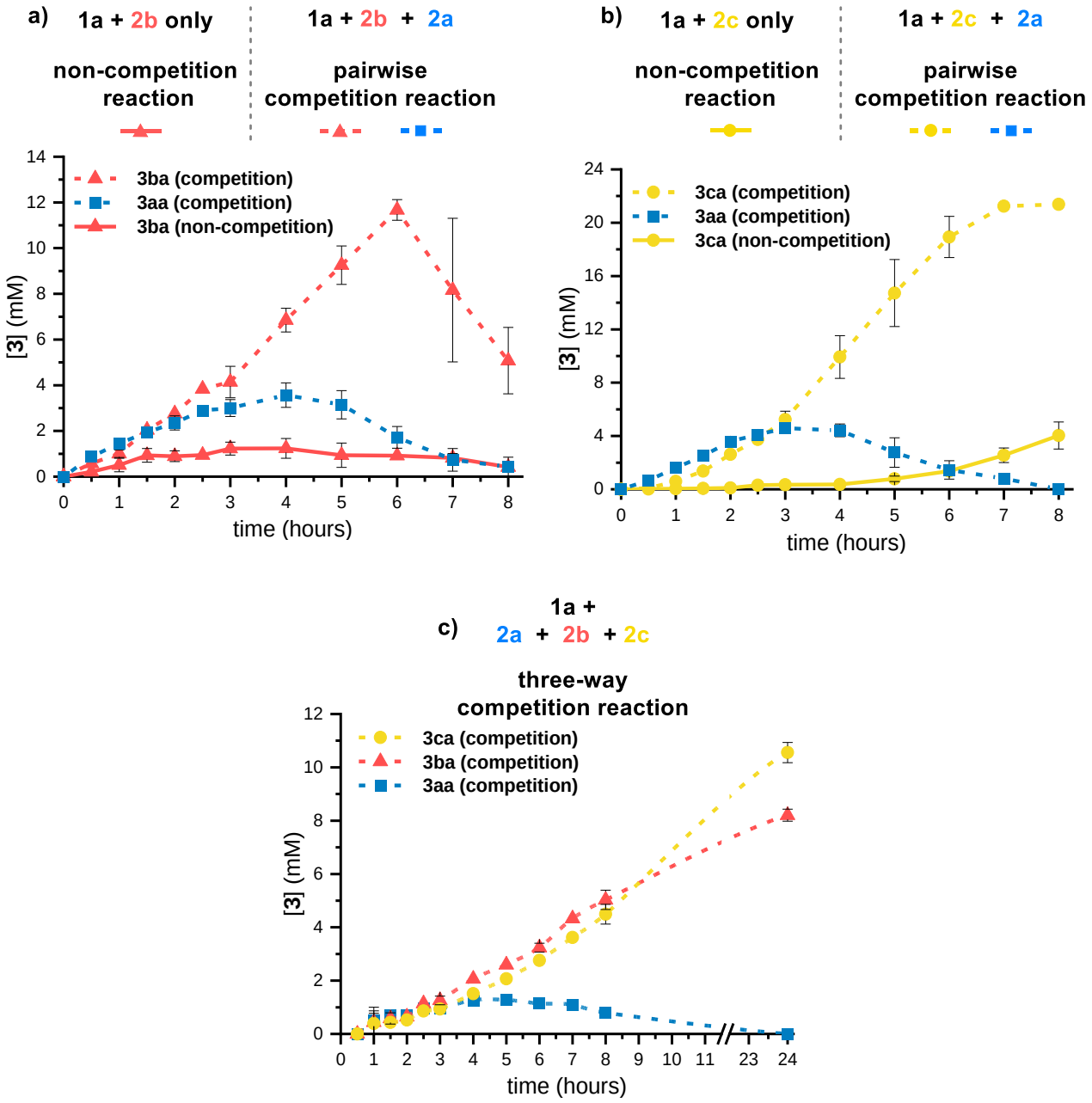

Figure 2.6: Competition between electronically differentiated precursors leads to surfactant selection over time by an emergent mechanism. a Overlaid reactions of thiol **2a** with precursor **1b** alone (non-competition) and with a mixture of **1a** and **1b** (competition). b Overlaid reactions of thiol **2a** with precursor **1c** alone (non-competition) and with a mixture of **1a** and **1c** (competition). c three-way competition experiment between thiol **2a** and precursors **1a**, **1b** and **1c**. n = 3, error bars (where visible) represent the standard deviation. See Experimental section 7.2.3 for details

These competition experiments show that the formation of **3ba** and **3ca** is unexpectedly enhanced in the presence of additional species. This indicates the emergence of secondary selection factors and the benefits of increased mixture complexity for certain self-reproducing species. The rationale for these effects is described below.

2.3.5 A dynamic selection mechanism through metathesis

The kinetic trends of the competition reactions involving surfactants **3aa**, **3ba** and **3ca** were initially unexpected as disulfides **1b** and **1c** are ordinarily less reactive than **1a** and so should not compete well for reactant **2a**. Analysis of reaction UPLC data suggested the presence of new major species and led to the discovery of an underlying metathesis between homo-disulfides **1a-c.** This fast exchange was shown to give three new hetero-disulfides **1d-f** (Figure 2.5).

Figure 2.7 shows the reaction pathways available to disulfides **1a**, **1c** and their metathesis product **1e**. All three disulfides (**1a**, **1c** and **1e**) can react with thiol **2a** directly to give surfactants **3aa**, **3ca** or both, respectively. The relative leaving group ability of the headgroups (**4**) causes any disulfides bearing electron deficient headgroup **a** (X = NO_2) to be consumed the fastest, regardless of the product formed. This means that **1a** and **1e** are of similar reactivity and are both more reactive than **1c**.

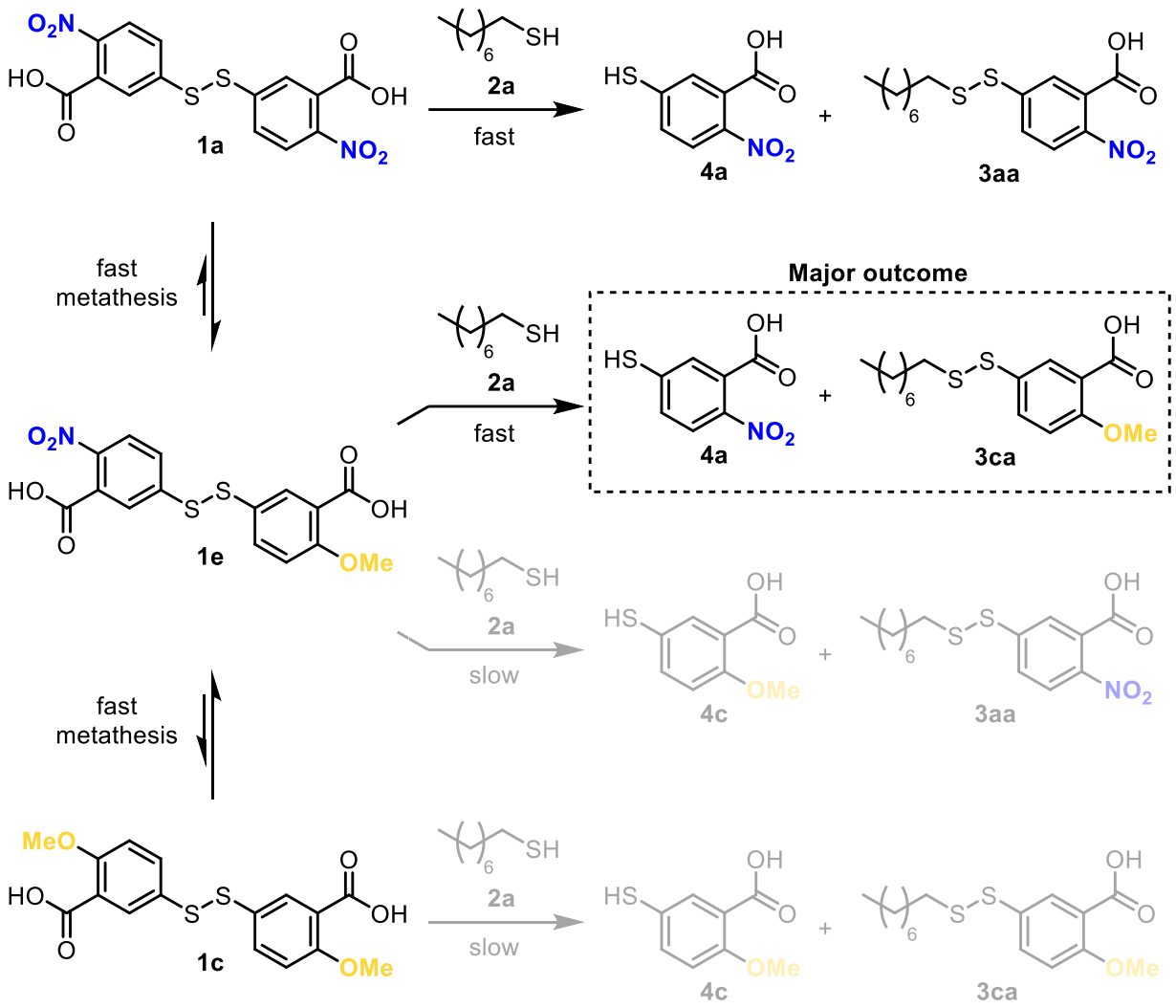

Figure 2.7: Reaction pathways in a competition reaction. Fast disulfide metathesis between **1a** and **1c** produces **1e** and gives access to the major route to **3ac**.

Kinetic data showing the consumption of disulfides **1** show that hetero-disulfide **1e** is initially present at a high concentration and undergoes fast consumption from the outset (Figure 2.8). When **1a** becomes depleted the less reactive **1c** then directly contributes to product formation by reaction with **2a**. This means there is a fast route with an abundant starting material (**1e**) as well as a slower, direct route to forming **3ca**. Overall, this causes the production of electron-rich surfactants via hetero-disulfides to be the dominant pathway in a competition setting, contrasting to the outcome in isolation.

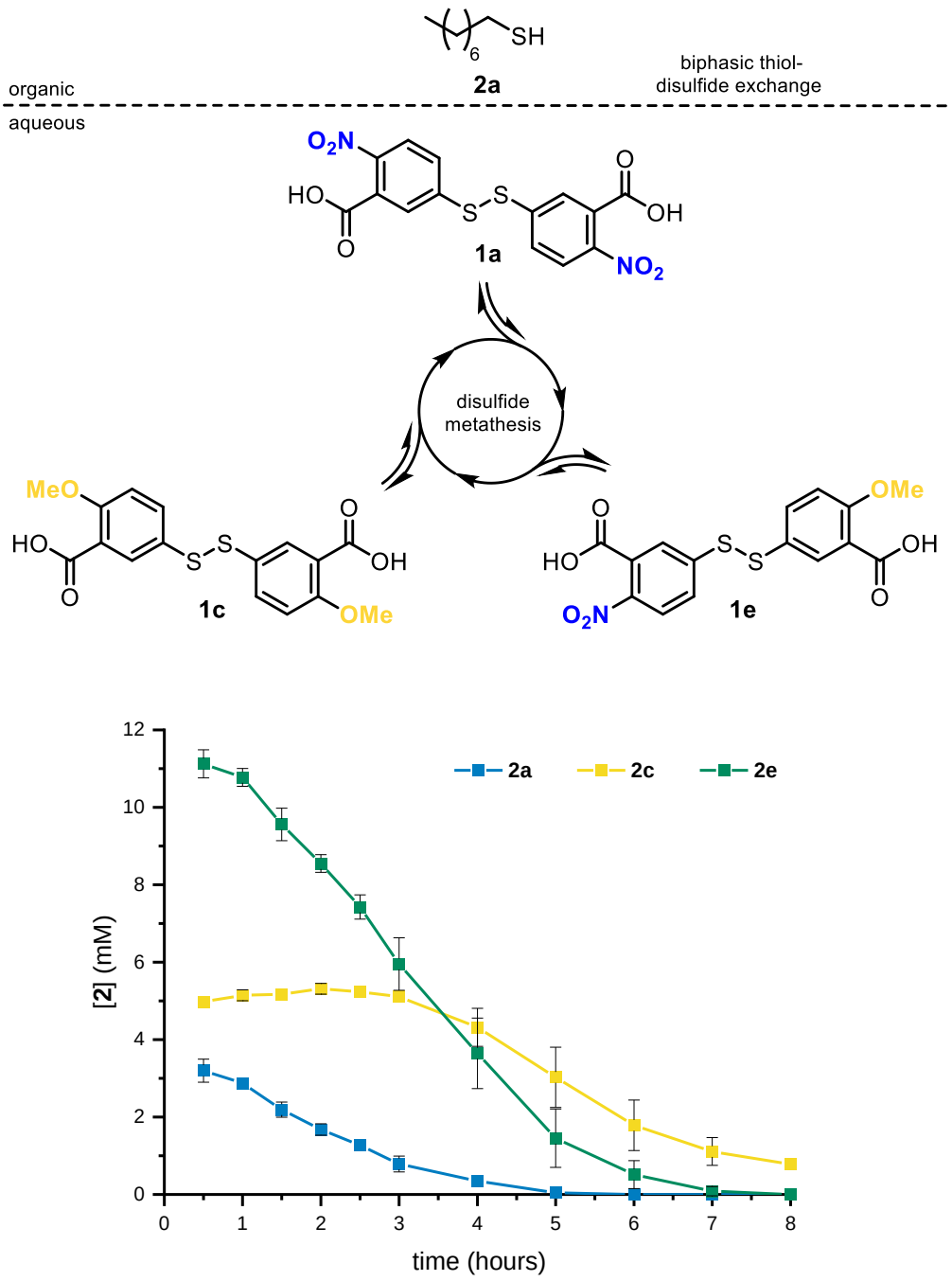

Figure 2.8: Disulfide consumption in a competition reaction between **1a** and **1c** for thiol **2a**. [4aa] and [4ac] data may be found in Scheme 4b. n = 3, error bars (where visible) represent the standard deviation

Hetero-disulfides **1d** and **1e** may be viewed as activated forms of parent disulfides **1b** and **1c** and their presence allows rationalization of the kinetics and selectivity seen in competition experiments. For example, the very similar initial rates of **3aa**, **3ba** and **3ca** formation seen in Figure 2.6 is due to a common leaving group (**4a**) released from the most reactive disulfides **1a**, **1d** and **1e**. At longer

times, the succession patterns in Figure 2.6 show that **3ca** is the most kinetically stable surfactant, as destruction is still governed by intrinsic electronic trends.

2.3.6 Dynamic covalent activation

The disulfide metathesis described in this chapter is an example of dynamic covalent chemistry. Dynamic covalent reactions have been widely studied in drug discovery and sensing,[44-47] self-healing materials,[48,49] catalyst discovery[50,51] and synthesis from dynamic mixtures.[52] Exchangeable precursors have been studied in a self-replication setting, but with selectivity guided by auto- and cross-catalytic effects, rather than activation from dynamic exchange.[53,54] The intermediate hetero-disulfides **1d** and **1e** described above promote the formation of products which are otherwise difficult to form and may be considered to take part in an 'activating metathesis'. Through dynamic covalent substrate interactions, a particular reaction pathway is enabled which, to the best of our knowledge, is a unique selection mechanism for chemical replicators.

More broadly, *dynamic covalent activation* may facilitate the formation of otherwise inaccessible small molecules and supramolecular assemblies. Activation by stepwise covalent modification, such as transformation of a hydroxyl to a leaving group or relay ring-closing metathesis,[55] relies upon discrete, irreversible chemical steps to access desired product(s) (Figure 2.9a). Many catalytic activation strategies, *e.g.* Lewis acid or transition metal catalysis, produce intermediates which undergo mechanistically different reactions from the unactivated transformation (Figure 2.9b). In contrast, dynamic covalent activation, elevates leaving group ability *in situ* through dynamic covalent reactions and requires no functional group interconversion or catalyst association. For example, Figure 2.9c shows how product $\mathbf{P_B}$ may be accessed via intermediate **B′** on a pathway qualitatively similar to the unactivated route.

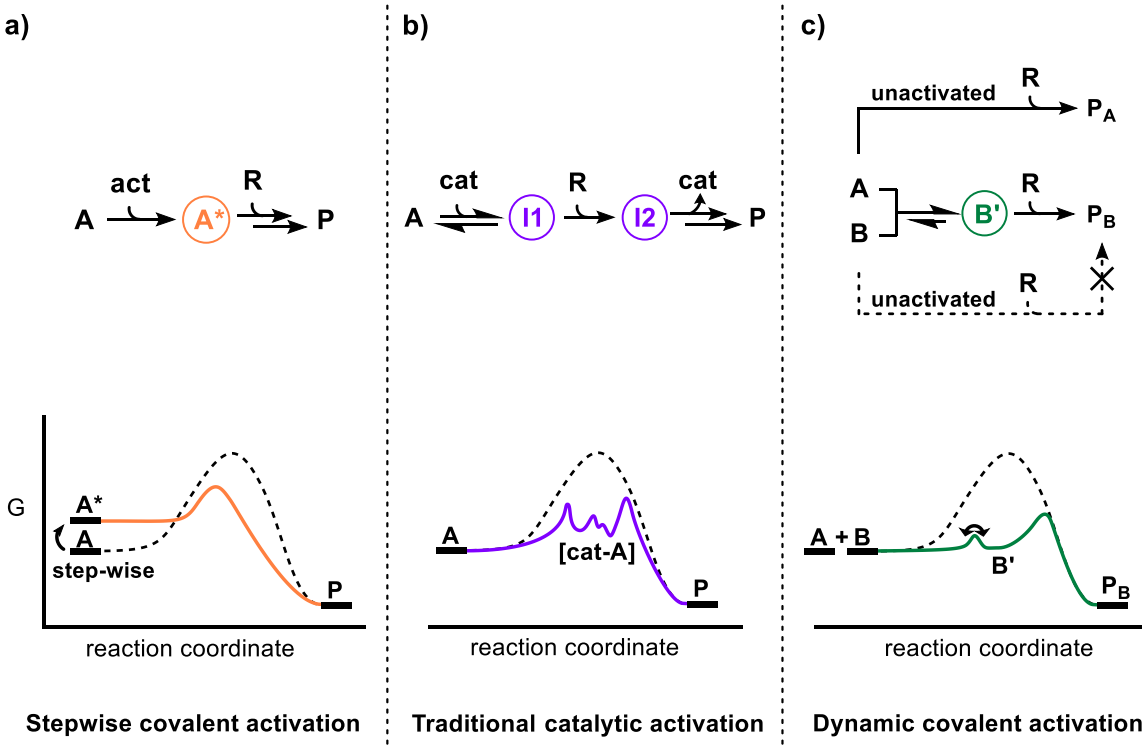

Figure 2.9. Comparison of synthetic activation strategies and illustrative energy landscapes. a stepwise covalent activation e.g. leaving group enhancement, relay ring closing metathesis (RRCM) b Traditional catalytic activation e.g. Lewis acid catalysis, transition metal coordination. c Dynamic covalent activation e.g. disulfide metathesis. act = activating reagent, R = generic reagent, cat = catalyst, P = product

2.4 Conclusions

We have found two mechanisms that can give rise to selection in systems of competing self-reproducing lipids. Firstly, selection arises from differing chemical properties of the self-reproducing species themselves and their direct precursors. Here the more sterically hindered surfactants form slower but are longer lived. A pattern reminiscent of ecological succession involving pioneer, follower and mature species was observed.[56]

A second, more intriguing mechanism arises from network effects when precursors can inter-react. We demonstrate an unexpected but clear effect where, contrary to first expectations, the lipid products derived from less electrophilic disulfides experience preferential formation and are the dominant species in a competing mixture. This is due to dynamic covalent reactions that activate precursors, unlocking an alternative, favoured pathway for the formation reaction. In effect, lipid **3c** was able to bypass its originally poor 'fitness' as an autocatalyst (*i.e.* slow formation rate) by

using material from competing lipids' precursors (*i.e.* **1a**), in a parasite-like mechanism to gain advantage.

The selectivity and non-intuitive reaction outcomes observed are a powerful demonstration of emergent selection at the systems level and highlights how little is actually known about complex (lipid) reaction systems. As referred to in Chapter 1, many synthetic systems which involve diverse components and non-trivial kinetics can be a challenge to analyse, complicating the realisation of interesting complex systems such as the one described here.

Notably, the originally intended degree of compositional complexity (*i.e.* multiple disulfide precursors), led to a process where the species diversity can increase further. The availability of chemical mechanisms to do this may provide support to prebiotic scenarios with only low-moderate levels of diversity in the chemical species, as this diversity might expand unexpectedly and produce highly complex mixtures with lots of available reactions and feedback processes.

Overall, this work suggests that increased species diversity can unlock new pathways in evolving systems and can provide unexpected competitive advantages for specific species. Additionally, it uncovered a dynamic activation mechanism that may be strategically useful in small molecule and supramolecular synthesis.[57,58]

References

1 Luisi, P. L. *The Emergence of Life: From Chemical Origins to Synthetic Biology*. (Cambridge University Press, 2006).

2 Wagner, A. J. & Blackmond, D. G. The Future of Prebiotic Chemistry. *ACS Central Science* **2**, 775-777 (2016). https://doi.org:10.1021/acscentsci.6b00336

3 Pross, A. & Pascal, R. The origin of life: what we know, what we can know and what we will never know. *Open Biology* **3**, 120190 (2013). https://doi.org:doi:10.1098/rsob.120190

4 Mann, S. The Origins of Life: Old Problems, New Chemistries. *Angew. Chem. Int. Ed.* **52**, 155-162 (2013). https://doi.org:https://doi.org/10.1002/anie.201204968

5 Islam, S., Bučar, D.-K. & Powner, M. W. Prebiotic selection and assembly of proteinogenic amino acids and natural nucleotides from complex mixtures. *Nature Chemistry* **9**, 584-589 (2017). https://doi.org:10.1038/nchem.2703

6 Powner, M. W., Gerland, B. & Sutherland, J. D. Synthesis of activated pyrimidine ribonucleotides in prebiotically plausible conditions. *Nature* **459**, 239-242 (2009). https://doi.org:10.1038/nature08013

7 Patel, B. H., Percivalle, C., Ritson, D. J., Duffy, C. D. & Sutherland, J. D. Common origins of RNA, protein and lipid precursors in a cyanosulfidic protometabolism. *Nat. Chem.* **7**, 301-307 (2015). https://doi.org:10.1038/nchem.2202
8 Duim, H. & Otto, S. Towards open-ended evolution in self-replicating molecular systems. *Beilstein Journal of Organic Chemistry* **13**, 1189-1203 (2017). https://doi.org:10.3762/bjoc.13.118
9 Danger, G., d'Hendecourt, L. L. S. & Pascal, R. On the conditions for mimicking natural selection in chemical systems. *Nature Reviews Chemistry* **4**, 102-109 (2020). https://doi.org:10.1038/s41570-019-0155-6
10 Robertson, M. P. & Joyce, G. F. The Origins of the RNA World. *Cold Spring Harb. Perspect. Biol.* **4** (2012). https://doi.org:10.1101/cshperspect.a003608
11 Gilbert, W. Origin of life: The RNA world. *Nature* **319**, 618-618 (1986). https://doi.org:10.1038/319618a0
12 von Kiedrowski, G. A Self-Replicating Hexadeoxynucleotide. *Angew. Chem. Int. Ed.* **25**, 932-935 (1986). https://doi.org:https://doi.org/10.1002/anie.198609322
13 Carnall, J. M. A. *et al.* Mechanosensitive Self-Replication Driven by Self-Organization. *Science* **327**, 1502-1506 (2010). https://doi.org:doi:10.1126/science.1182767
14 Wang, B. & O. Sutherland, I. Self-replication in a Diels–Alder reaction. *Chem. Commun.*, 1495-1496 (1997). https://doi.org:10.1039/A701573I
15 Kassianidis, E. & Philp, D. Design and Implementation of a Highly Selective Minimal Self-Replicating System. *Angew. Chem. Int. Ed.* **45**, 6344-6348 (2006). https://doi.org:https://doi.org/10.1002/anie.200601845
16 Segré, D., Ben-Eli, D., Deamer, D. W. & Lancet, D. The Lipid World. *Orig. Life Evol. Biosph.* **31**, 119-145 (2001). https://doi.org:10.1023/A:1006746807104
17 Lancet, D., Zidovetzki, R. & Markovitch, O. Systems protobiology: origin of life in lipid catalytic networks. *Journal of The Royal Society Interface* **15**, 20180159 (2018). https://doi.org:doi:10.1098/rsif.2018.0159
18 Bissette, A. J. & Fletcher, S. P. Mechanisms of Autocatalysis. *Angew. Chem. Int. Ed.* **52**, 12800-12826 (2013). https://doi.org:10.1002/anie.201303822
19 Kust, P. R. & Rathman, J. F. Synthesis of Surfactants by Micellar Autocatalysis: N,N-Dimethyldodecylamine N-Oxide. *Langmuir* **11**, 3007-3012 (1995). https://doi.org:10.1021/la00008a026
20 Bachmann, P. A., Luisi, P. L. & Lang, J. Autocatalytic self-replicating micelles as models for prebiotic structures. *Nature* **357**, 57-59 (1992). https://doi.org:10.1038/357057a0
21 Bissette, A. J., Odell, B. & Fletcher, S. P. Physical autocatalysis driven by a bond-forming thiol–ene reaction. *Nat. Commun.* **5**, 4607 (2014). https://doi.org:10.1038/ncomms5607
22 Kosikova, T. & Philp, D. Exploring the emergence of complexity using synthetic replicators. *Chem. Soc. Rev.* **46**, 7274-7305 (2017). https://doi.org:10.1039/C7CS00123A
23 Sievers, D. & von Kiedrowski, G. Self-Replication of Hexadeoxynucleotide Analogues: Autocatalysis versus Cross-Catalysis. *Chemistry – A European Journal* **4**, 629-641 (1998). https://doi.org:https://doi.org/10.1002/(SICI)1521-3765(19980416)4:4<629::AID-CHEM629>3.0.CO;2-0
24 Kosikova, T. & Philp, D. A Critical Cross-Catalytic Relationship Determines the Outcome of Competition in a Replicator Network. *Journal of the American Chemical Society* **139**, 12579-12590 (2017). https://doi.org:10.1021/jacs.7b06270
25 Sevim, İ., Pankau, W. M. & von Kiedrowski, G. Re-Evaluation of a Fulvene-Based Self-Replicating Diels–Alder Reaction System. *Chemistry – A European Journal* **26**, 9032-9035 (2020). https://doi.org:https://doi.org/10.1002/chem.201905594
26 Pross, A. & Khodorkovsky, V. Extending the concept of kinetic stability: toward a paradigm for life. *J. Phys. Org. Chem.* **17**, 312-316 (2004). https://doi.org:https://doi.org/10.1002/poc.729
27 Pross, A. On the Emergence of Biological Complexity: Life as a Kinetic State of Matter. *Origins of Life and Evolution of Biospheres* **35**, 151-166 (2005). https://doi.org:10.1007/s11084-005-5272-1

28 Boekhoven, J., Hendriksen, W. E., Koper, G. J. M., Eelkema, R. & van Esch, J. H. Transient assembly of active materials fueled by a chemical reaction. *Science* **349**, 1075-1079 (2015). https://doi.org:doi:10.1126/science.aac6103

29 Maiti, S., Fortunati, I., Ferrante, C., Scrimin, P. & Prins, L. J. Dissipative self-assembly of vesicular nanoreactors. *Nature Chemistry* **8**, 725-731 (2016). https://doi.org:10.1038/nchem.2511

30 Colomer, I., Morrow, S. M. & Fletcher, S. P. A transient self-assembling self-replicator. *Nat. Commun.* **9** (2018). https://doi.org:10.1038/s41467-018-04670-2

31 Morrow, S. M., Colomer, I. & Fletcher, S. P. A chemically fuelled self-replicator. *Nat. Commun.* **10**, 1011 (2019). https://doi.org:10.1038/s41467-019-08885-9

32 Mattia, E. & Otto, S. Supramolecular systems chemistry. *Nature Nanotechnology* **10**, 111-119 (2015). https://doi.org:10.1038/nnano.2014.337

33 Colomer, I., Borissov, A. & Fletcher, S. P. Selection from a pool of self-assembling lipid replicators. *Nat. Commun.* **11**, 176 (2020). https://doi.org:10.1038/s41467-019-13903-x

34 Bonfio, C. *et al.* Length-Selective Synthesis of Acylglycerol-Phosphates through Energy-Dissipative Cycling. *J. Am. Chem. Soc.* **141**, 3934-3939 (2019). https://doi.org:10.1021/jacs.8b12331

35 Post, E. A. J. & Fletcher, S. P. Dissipative self-assembly, competition and inhibition in a self-reproducing protocell model. *Chem. Sci.* **11**, 9434-9442 (2020). https://doi.org:10.1039/D0SC02768E

36 Yang, S. *et al.* Chemical Fueling Enables Molecular Complexification of Self-Replicators. *Angew. Chem. Int. Ed.* **60**, 11344-11349 (2021). https://doi.org:https://doi.org/10.1002/anie.202016196

37 Leira-Iglesias, J., Sorrenti, A., Sato, A., Dunne, P. A. & Hermans, T. M. Supramolecular pathway selection of perylenediimides mediated by chemical fuels. *Chem. Commun.* **52**, 9009-9012 (2016). https://doi.org:10.1039/C6CC01192F

38 Tena-Solsona, M., Wanzke, C., Riess, B., Bausch, A. R. & Boekhoven, J. Self-selection of dissipative assemblies driven by primitive chemical reaction networks. *Nat. Commun.* **9**, 2044 (2018). https://doi.org:10.1038/s41467-018-04488-y

39 Ruiz-Mirazo, K., Briones, C. & De La Escosura, A. Prebiotic Systems Chemistry: New Perspectives for the Origins of Life. *Chem. Rev.* **114**, 285-366 (2014). https://doi.org:10.1021/cr2004844

40 Cafferty, B. J. *et al.* Robustness, Entrainment, and Hybridization in Dissipative Molecular Networks, and the Origin of Life. *J. Am. Chem. Soc.* **141**, 8289-8295 (2019). https://doi.org:10.1021/jacs.9b02554

41 Bandela, A. K. *et al.* Primitive selection of the fittest emerging through functional synergy in nucleopeptide networks. *Proc. Natl Acad. Sci.* **118**, e2015285118 (2021). https://doi.org:10.1073/pnas.2015285118

42 Okur, H. I., Tarun, O. B. & Roke, S. Chemistry of Lipid Membranes from Models to Living Systems: A Perspective of Hydration, Surface Potential, Curvature, Confinement and Heterogeneity. *Journal of the American Chemical Society* **141**, 12168-12181 (2019). https://doi.org:10.1021/jacs.9b02820

43 Peterlin, P., Arrigler, V., Kogej, K., Svetina, S. & Walde, P. Growth and shape transformations of giant phospholipid vesicles upon interaction with an aqueous oleic acid suspension. *Chem. Phys. Lipids* **159**, 67-76 (2009). https://doi.org:https://doi.org/10.1016/j.chemphyslip.2009.03.005

44 Black, S. P., Sanders, J. K. M. & Stefankiewicz, A. R. Disulfide exchange: exposing supramolecular reactivity through dynamic covalent chemistry. *Chem. Soc. Rev.* **43**, 1861-1872 (2014). https://doi.org:10.1039/C3CS60326A

45 Li, J., Nowak, P. & Otto, S. Dynamic Combinatorial Libraries: From Exploring Molecular Recognition to Systems Chemistry. *Journal of the American Chemical Society* **135**, 9222-9239 (2013). https://doi.org:10.1021/ja402586c

46 Jin, Y., Yu, C., Denman, R. J. & Zhang, W. Recent advances in dynamic covalent chemistry. *Chem. Soc. Rev.* **42**, 6634-6654 (2013). https://doi.org:10.1039/C3CS60044K

47 Frei, P., Hevey, R. & Ernst, B. Dynamic Combinatorial Chemistry: A New Methodology Comes of Age. *Chemistry – A European Journal* **25**, 60-73 (2019). https://doi.org:https://doi.org/10.1002/chem.201803365

48 Imato, K. *et al.* Repeatable mechanochemical activation of dynamic covalent bonds in thermoplastic elastomers. *Chem. Commun.* **52**, 10482-10485 (2016). https://doi.org:10.1039/C6CC04767J

49 Commins, P., Al-Handawi, M. B., Karothu, D. P., Raj, G. & Naumov, P. Efficiently self-healing boronic ester crystals. *Chemical Science* **11**, 2606-2613 (2020). https://doi.org:10.1039/C9SC05640H

50 Gasparini, G., Dal Molin, M. & Prins, L. J. Dynamic Approaches towards Catalyst Discovery. *Eur. J. Org. Chem.* **2010**, 2429-2440 (2010). https://doi.org:https://doi.org/10.1002/ejoc.200901338

51 Schaufelberger, F. & Ramström, O. Dynamic Covalent Organocatalysts Discovered from Catalytic Systems through Rapid Deconvolution Screening. *Chemistry – A European Journal* **21**, 12735-12740 (2015). https://doi.org:https://doi.org/10.1002/chem.201502088

52 Puangsamlee, T. & Miljanić, O. Š. Three-Way Chemoselectivity Switching through Coupled Equilibria. *Org. Lett.* **22**, 5900-5904 (2020). https://doi.org:10.1021/acs.orglett.0c02003

53 Sadownik, J. W. & Philp, D. A Simple Synthetic Replicator Amplifies Itself from a Dynamic Reagent Pool. *Angew. Chem. Int. Ed.* **47**, 9965-9970 (2008). https://doi.org:https://doi.org/10.1002/anie.200804223

54 Altay, Y., Altay, M. & Otto, S. Existing Self-Replicators Can Direct the Emergence of New Ones. *Chemistry – A European Journal* **24**, 11911-11915 (2018). https://doi.org:https://doi.org/10.1002/chem.201803027

55 Hoye, T. R., Jeffrey, C. S., Tennakoon, M. A., Wang, J. & Zhao, H. Relay Ring-Closing Metathesis (RRCM): A Strategy for Directing Metal Movement Throughout Olefin Metathesis Sequences. *Journal of the American Chemical Society* **126**, 10210-10211 (2004). https://doi.org:10.1021/ja046385t

56 Odum, E. P. The Strategy of Ecosystem Development. *Science* **164**, 262-270 (1969). https://doi.org:doi:10.1126/science.164.3877.262

57 Schnitzer, T. & Vantomme, G. Synthesis of Complex Molecular Systems—The Foreseen Role of Organic Chemists. *ACS Central Science* **6**, 2060-2070 (2020). https://doi.org:10.1021/acscentsci.0c00974

58 Vantomme, G. & Meijer, E. W. The construction of supramolecular systems. *Science* **363**, 1396-1397 (2019). https://doi.org:doi:10.1126/science.aav4677

Statement of Authorship for joint/multi-authored papers for PGR thesis

To appear at the end of each thesis chapter submitted as an article/paper

The statement shall describe the candidate's and co-authors' independent research contributions in the thesis publications. For each publication there should exist a complete statement that is to be filled out and signed by the candidate and supervisor **(only required where there isn't already a statement of contribution within the paper itself).**

Title of Paper	Selection between competing self-reproducing lipids: succession and dynamic activation
Publication Status	☑Published ~~Accepted for Publication~~ ~~Submitted for Publication~~ ~~Unsubmitted work written in a manuscript style~~
Publication Details	Michael G. Howlett, Robert J. H. Scanes, and Stephen P. Fletcher JACS Au 2021 1 (9), 1355-1361 DOI: 10.1021/jacsau.1c00138

Student Confirmation

Student Name:	Michael Howlett		
Contribution to the Paper	Performed experiments and analysed data. Wrote and edited the manuscript. Co-author (R. Scanes) also performed experiments and took part in data analysis. Co-author (S. Fletcher) supervised the project and contributed to data analysis and manuscript writing.		
Signature 		Date	14 / 04 / 2023

Supervisor Confirmation

By signing the Statement of Authorship, you are certifying that the candidate made a substantial contribution to the publication, and that the description described above is accurate.

Supervisor name and title: Prof. Stephen Fletcher		
Supervisor comments 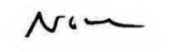		
Signature 	Date	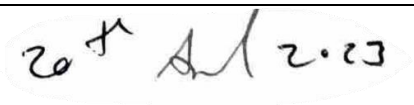

This completed form should be included in the thesis, at the end of the relevant chapter.

Chapter 3

A Supramolecular Chemical Oscillator

Chapter 3

A Supramolecular Chemical Oscillator

The work in this chapter was undertaken in joint collaboration with Antonius Engwerda and was published in Nature Chemistry, 2022: 'An Autonomously Oscillating Supramolecular Self-replicator'.

3.1 Introduction

While evolution from primitive cells to current organisms is generally well understood, the pathway from small molecules to functional cell-like systems is almost completely unresolved. One emerging approach is to examine out-of-equilibrium systems to learn how chemical systems may have developed life-like properties in prebiotic scenarios. Further to this, gaining insight into how systems of biological complexity originated can inform how to construct new responsive synthetic systems which may have practical use.

3.1.1 Oscillations in the natural world

Oscillating systems are seen at various length scales in the natural world. Oscillations are inherent to cellular level functions such as respiration and hormone secretion. At the other end of the spectrum, oscillations are also readily observable in some climate cycles and the dynamics of species populations.[1-5] Because they exist in different alternating states, oscillations can drive numerous functions in biology and, in fact, many processes we take for granted such as our circulatory system and sleep cycle arise from complex oscillators.

3.1.2 Requirements and rationale for designing oscillators

Oscillations involve the periodic fluctuation between two or more distinct states. Oscillators tend to have unique feedback mechanisms, making them generally difficult to understand, and even more difficult to design. To observe oscillatory behaviour in chemical systems, several criteria need to

be met. The states need to be metastable, *i.e.* away from thermodynamic minima, and the system must be sustained out-of-equilibrium, which can be achieved by consuming a fuel.[6,7] Oscillations also require non-linear kinetics to escape a steady state, which emerge from positive and/or negative feedback processes such as autocatalysis.[8]

The design and realisation of supramolecular replicators capable of sustained oscillations would be a major step towards creating systems with life-like complexity, especially as all known life forms operate beyond the molecular scale. This view is also expressed by other researchers in the field who believe that novel oscillators are a vital research objective.[9]

> *"…the chemistry community is still looking for the first example of chemical oscillators driven by efficient (self-)replication of synthetic supramolecular complexes. Once produced, these replicators will represent the 'intermediate' stage in chemical evolution, in between the prebiotic oscillators made of small molecules and cellular biochemical machines."*
>
> *Nature Chem.* ***11***, 681-683 *(2019)*

It would also give insight into how complex systems could emerge, evolve and exhibit robust lifecycles. The design of supramolecular systems exhibiting opposing feedback processes, which also incorporate non-linear kinetics, is challenging and the few reported examples of oscillations in supramolecular systems quickly cease over time.[10-12] Molecular events such as the construction of bonds, often occur on different time scales than processes occurring at greater length scales (such as the self-assembly of compartments, interfacial events and mass transport). Coupling molecular and supramolecular feedback processes to form a sustained supramolecular oscillator would potentially unlock an important stepping stone on the path to new biomimetic machinery.[9]

3.1.3 Synthetic oscillators

Scientists have long been intrigued by oscillating reactions[6,13-16] and there is substantial interest in using oscillators to drive functional out-of-equilibrium systems.[10,17-20] Synthetic oscillating systems exhibit complexity not found in traditional reactions as they require feedback processes and the capacity to persist in unstable states[6,21] making them challenging to design.

The most prominent chemical oscillators are based on inorganic redox reactions, for example the Belousov-Zhabotinsky (BZ) and Briggs-Rauscher reactions.[13,14,22] A complex, and not fully understood,[23] sequence of steps allows these inorganic systems to produce fascinating visual effects which can be used in chemistry demonstrations and coupled to other systems.[24-32] In these systems, oscillations are the result of mixing reactive precursors which then undergo reactions, including autocatalytic events, as the system tends towards thermodynamic equilibrium. Recently, a series of new oscillators has been developed, significantly expanding the chemistry of oscillating systems.[10,17,18,20,33-35] The operation of many oscillators requires continuous addition and removal of material to maintain oscillations, potentially complicating advanced applications,[8] and many systems only effectively operate within a narrow window of suitable conditions. This calls for new designs for oscillating systems with greater flexibility over their operation and which aren't reliant on continuously-stirred tank reactors (CSTR). Impressive examples of synthetic oscillators from the Huck, Whitesides and Hermans groups each have a unique mode of operation and present design principles for future oscillators. These systems are highly sophisticated and are described in brief below.

In 2015, Semenov and coworkers in the Huck group reported a biochemical reaction network centred around the trypsin enzyme (Tr) (see Figure 3.1a). Trypsin can convert its precursor trypsinogen (Tg) into trypsin, resulting in autocatalytic feedback. Trypsin also takes part in a two step inhibition process (aided by aminopeptidase M), unmasking an inhibitor of itself and providing delayed negative feedback. By continuously supplying all of the components of this network in a flow reactor (and removing waste), the concentration of Tr shows robust oscillations in time. Soon after, Semenov and coworkers in the Whitesides group created a somewhat related oscillator using small organic molecules to produce autocatalytic and inhibitory effects in a CSTR (Figure 3.1b). This system uses simple thiol-containing molecules to provide the necessary reaction steps for the concentration of thiol (RSH) to oscillate in time. This system also depends upon a flow reactor to wash out the waste and continuously recharge the reagents.

A distinct example comes from the Hermans group, reported in 2018. Using a redox active perylene diimide (PDI) monomer which can cooperatively self-assemble into fibres, they showed that adding a reductant ($Na_2S_2O_4$) at different flow rates could induce a steady state (SS) or oscillations (OSC) in the amount of the PDI material (Figure 3.1c).

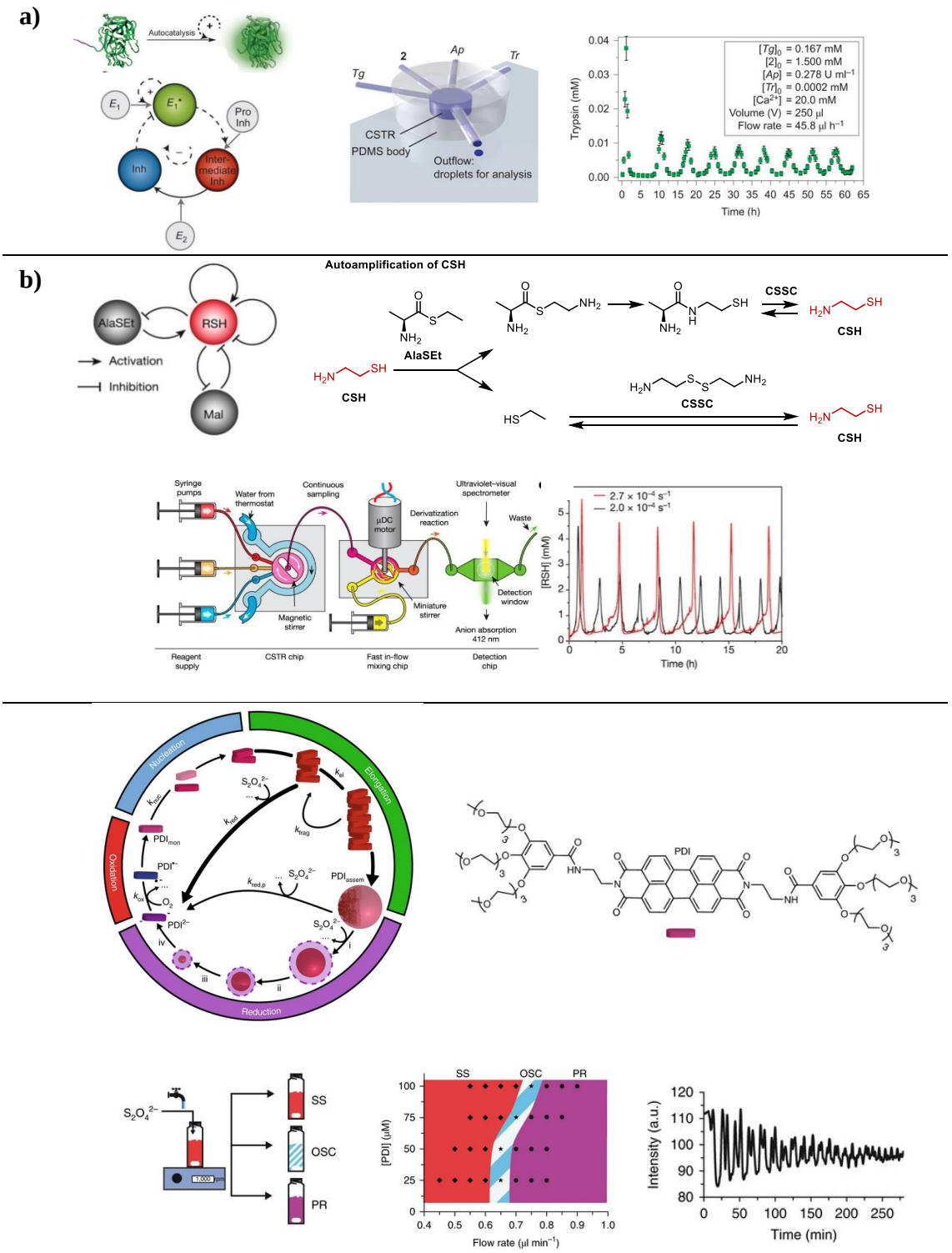

Figure 3.1: Selected synthetic oscillators built from (bio)chemical reaction networks. a) Enzymatic oscillator within a CSTR which is based on the autocatalytic formation of trypsin (Tr) and a time-delayed negative feedback loop;[17] b) Network of small organic molecules within a CSTR where cysteamine (CSH) forms autocatalytically and is inhibited by electrophiles to give positive and negative feedback;[18] c) Cooperative polymerisation of perylene diimide (PDI) monomers and non-linear fragmentation of the fibres upon reduction by $Na_2S_2O_4$ generates dampened oscillations in the self-assembly of PDI. SS = steady state, OSC = oscillations, PR = precipitation.[10] Adapted from Semenov et al. and Leira-Iglesias et al.[10,17,18]

3.2 Aims

The aim of this project is the realisation and development of a working chemical oscillator based upon the principles of physical autocatalysis and the thiol-disulfide chemistry used within the Fletcher group. The main objectives were to investigate if (reproducible) oscillations in the concentrations of reaction species can be achieved; to determine the factors affecting the sensitivity and output of the oscillations and to understand the underlying mechanism of the oscillating system.

3.3 Results and Discussion

3.3.1 System overview

The chemistry underpinning this chapter is the same as introduced in Chapter 2. Components **1** and **2** react together by thiol-disulfide exchange to give a metastable surfactant **3** which can self-assemble and also break down in a second step (Figure 3.2). Micelles composed of **3** are capable of encapsulating reagents. This brings the reagents close together, catalysing both the formation and breakdown of the compartment's own building blocks **3** (see physical autocatalysis in Chapter 1, Figure 1.3).

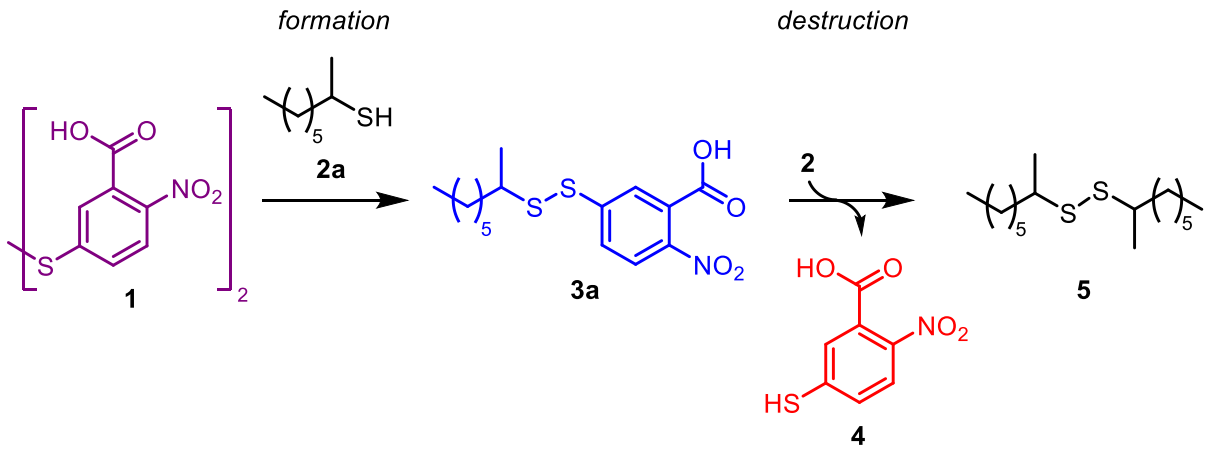

Figure 3.2: Two sequential reactions form and destroy the self-reproducing surfactants. Formation: hydrophilic disulfide 1 reacts with phase separated thiol **2a** to produce lipid **3a**. **4** is the leaving group in this reaction. Destruction: **3a** reacts with another equivalent of **2** and breaks down into thermodynamic products **4** and **5**. Typical conditions: **1** (25 mM in pH 9.0 TRIS buffer) + **2** (8 equiv.) stirred at 800 rpm at room temperature. See Experimental section 7.3.3 for details.

In doing so, these supramolecular structures induce both positive feedback (autocatalytic formation) and negative feedback (destruction cascade) in the reaction network. In contrast to Chapter 2, by-

product **4** is recycled back to **1** in this system using a chemical oxidant that is continuously added by syringe pump (Figure 3.3). This maintains the system out-of-equilibrium, allowing the continuous formation of **3**. This system is related to one previously described by Morrow et al. in which chemical fuelling gave a steady state concentration of metastable **3** (Chapter 1, Figure 1.19).[36]

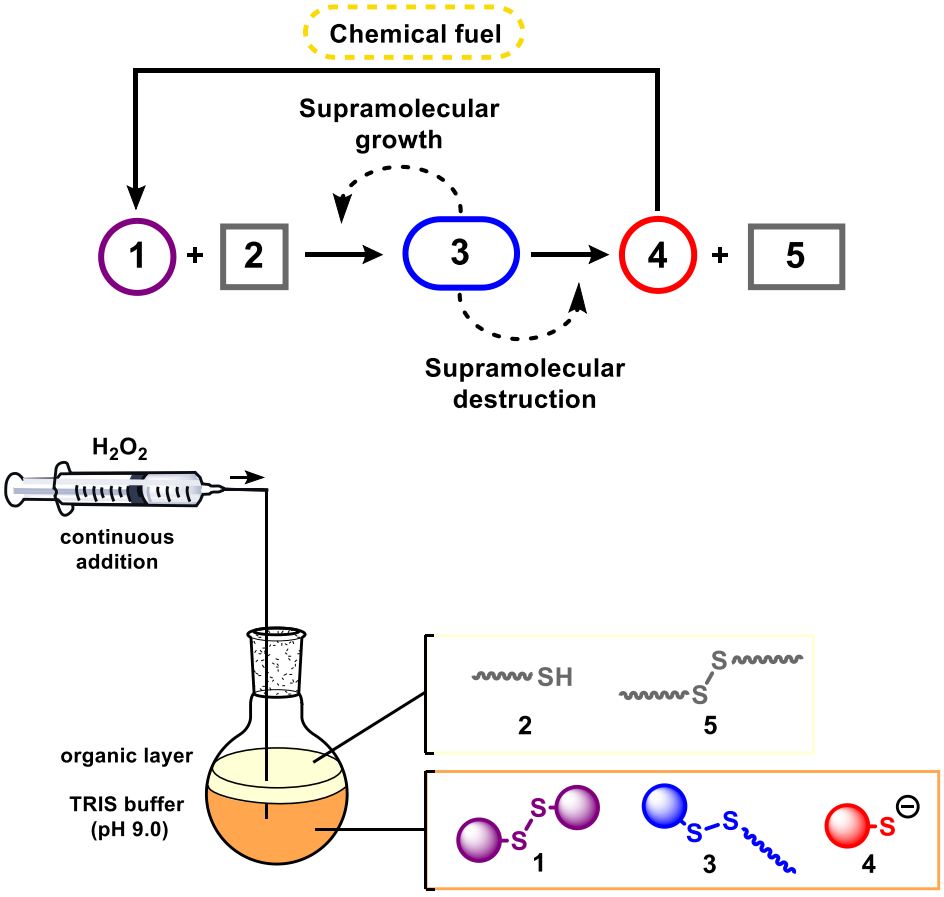

Figure 3.3: Schematic overview of the reaction network and biphasic setup which underpins the oscillator. Surfactant **3** is formed from **1** and **2** and accelerates their mixing (feedback on micelle growth). Destruction of **3** by **2** is also accelerated by greater [**3**], leading to breakdown of the micelles (feedback on micelle destruction). Waste product **4** is continuously recycled using a chemical fuel (H_2O_2), keeping the system operating out-of-equilibrium.

3.3.2 Initial experiments and optimisation

We discovered that altering the reaction parameters in Morrow et al.'s system gave access to a new kinetic regime where it could break out of the steady state and produce oscillations in [**3**]. An early, unoptimised example of this can be seen in Figure 3.4.

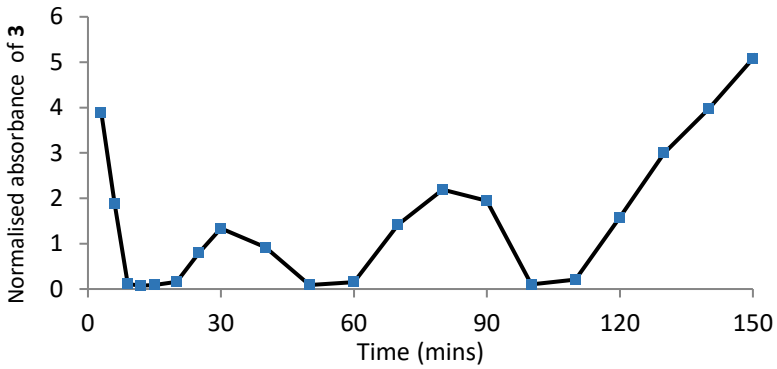

Figure 3.4: Early example of oscillations in the concentration of **3c** after modifying the conditions of Morrow et al. For details see the Experimental section 7.3.3

To produce oscillations in this system we increased the rate of **3** formation and destruction by increasing the stirring rate and the pH of the aqueous buffer. Increasing the stirring rate (from 100 to 800 rpm) enhances mixing between the aqueous and apolar layers. Under these conditions an emulsion is observed, which increases the availability of **2** in the aqueous layer, accelerating both the formation and destruction processes. Increasing the supply of H_2O_2 fuel to the reaction was also key to seeing oscillations as it allowed higher concentrations of **1** (and therefore faster **3** formation). Combined, these changes can result in oscillations in the concentration of **3a**, as illustrated in Figure 3.5.

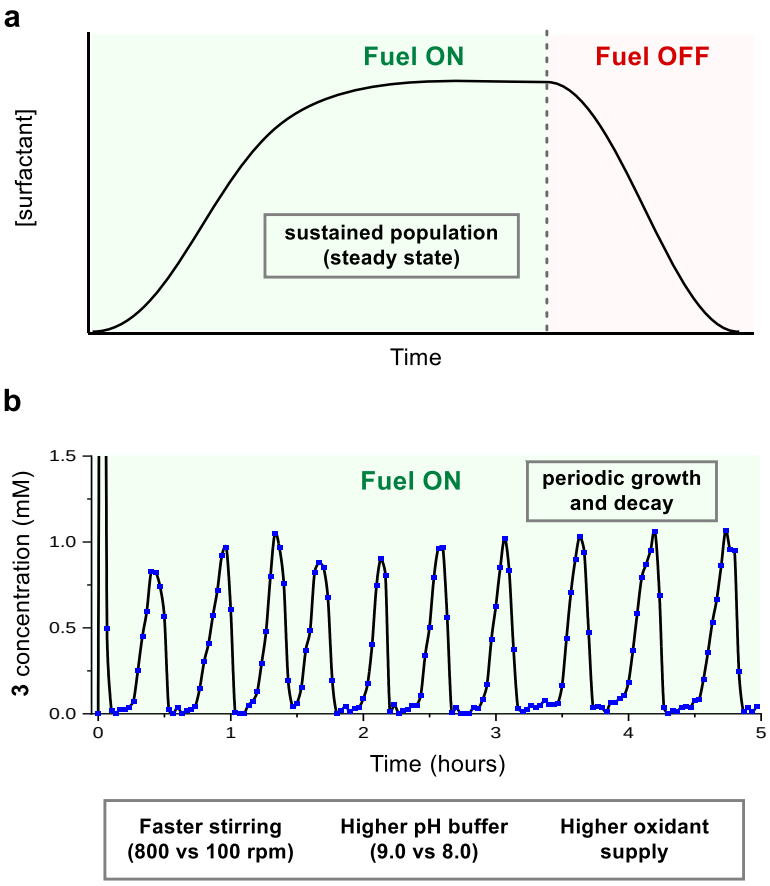

Figure 3.5: Comparison of kinetic output from a) Morrow et al.'s prior fuelled system and b) this work which shows oscillations when the formation and destruction of **3a** is accelerated. Note: the oscillations shown are an optimised example. For details see the Experimental section 7.3.3

In this chapter the main thiol used is 2-octanethiol (**2a**), although the reactivity was found to be very general. The thiol used in preliminary work (1-octanethiol, **2c**) is capable of producing oscillations but has a less reproducible output than **2a**. Using this thiol, sharp oscillations were obtained, that could not be tuned to a high extent and required high frequency kinetic monitoring (see Figure 3.6). By switching to secondary thiols **2a** or **2b**, a much higher degree of control could be obtained over the appearance (period, amplitude) of the oscillations. Replacing thiol **2a** by the more hydrophobic **2b** decreases the interfacial availability of the thiol, which effects the various reaction rates in the reaction cycle. When switching between thiols, a decrease in reactivity can be compensated for with increased or decreased stirring to maintain oscillations. Alternatively, in our optimised system, the thiol-disulfide exchange reactions are accelerated by 4-dimethylaminopyridine (DMAP),[37] and changing the amount of DMAP can be used to increase the rate of destruction and formation steps.

Notably, DMAP is not essential to observe oscillations as shown by experiments in the absence of DMAP that also oscillate (see Experimental section 7.2.4, Figure S25). Overall, thiols of differing hydrophobicity and steric properties can all take part in our oscillating system and it's a matter of controlling the resulting kinetics with the reaction parameters.

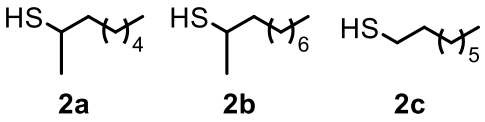

2a **2b** **2c**

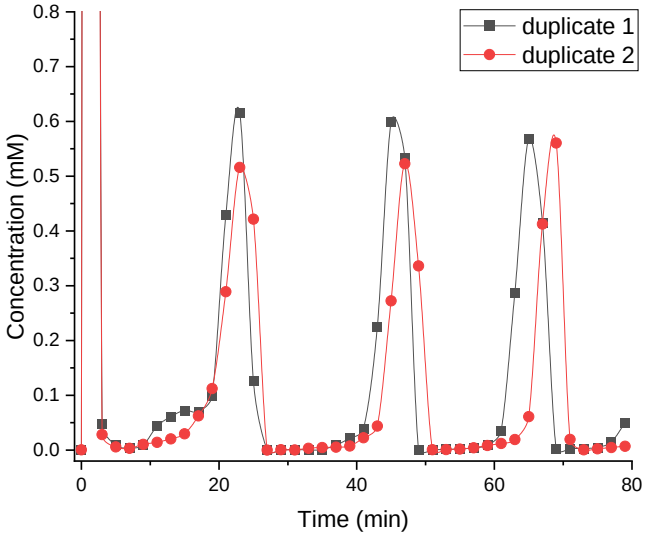

Figure 3.6: Reaction profile of duplicate oscillation experiments using primary thiol **2c**. These oscillations tend to be sharper and the control over their appearance is more challenging, compared to thiols **2a** and **2b**. Compared to when using **2a**, the conditions have been modified to compensate for the higher reactivity of **2c** (stirring rate = 700 rpm, no DMAP). For details see the Experimental section 7.3.3

3.3.3 Mechanistic descriptions of the system

Figure 3.7a shows how compounds **1-5** are involved in the chemically fuelled reaction cycle which generates oscillations. Changes in the concentration of **3b** are strongly coupled to the concentrations of **1** and **4** – as expected to maintain mass balance (Figure 3.7b). The concentration profiles of compounds **1** (Figure 3.7b, bottom) and **3b** (Figure 3.7b, middle) are similar but differ slightly in peak shape and the concentration maximum of **1** consistently precedes that of **3b**. The concentration of **4** is inversely correlated with **3b** (Figure 3.7b, top), so the concentration of **4** peaks as [**3b**] is at

a minimum. The concentration of **2** in the aqueous layer was also expected to oscillate in time due to increased [**3b**] taking up the apolar thiol and creating a stabilised emulsion. This is a temporary state and in the absence of **3**, thiol **2** gradually returns to the apolar layer.

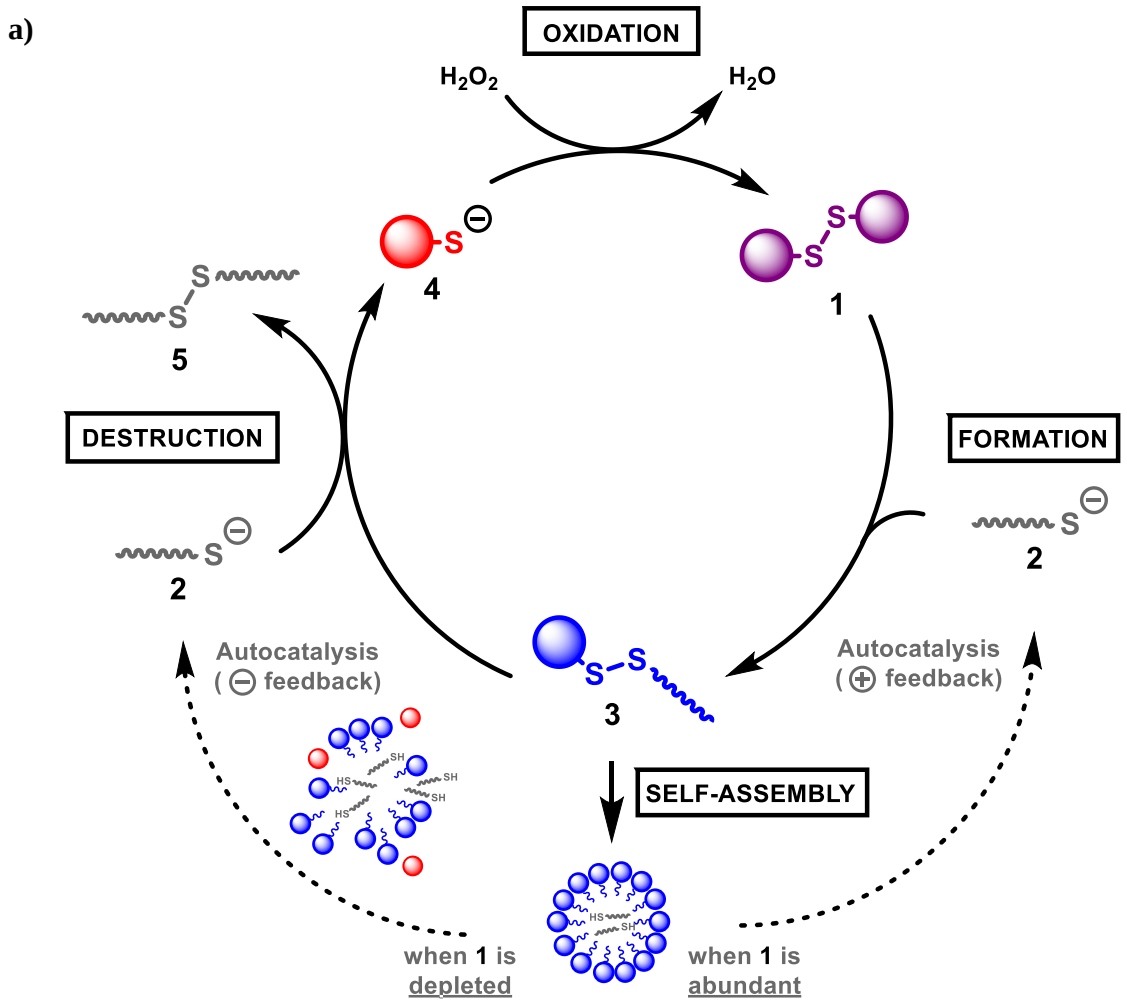

Figure 3.7: a) Reaction cycle for the fuelled thiol-disulfide system. Formation: interfacial reaction which experiences physical autocatalysis; Self-assembly: surfactant **3** forms micelles which uptake hydrophobic thiol **2** into the aqueous layer (physical autocatalysis); Destruction: interfacial / micelle-surface reaction which breaks down the micelles subcomponents (3); Oxidation: crucial step to close the cycle and regenerate **1**, maintaining the

system out-of-equilibrium. b) Reaction kinetics showing the concentrations of **1**, **3b** and **4** each oscillating in time. Concentrations were obtained by analysis of reaction aliquots by UPLC. See Experimental section 7.3.3 for details

Whilst the individual steps to the reaction network are reasonably intuitive and involve interactions between known nucleophiles, electrophiles and an oxidant, there are important mechanistic subtleties to note. For example, the role of byproducts, any supramolecular considerations and how the system avoids a steady state. Figure 3.7 shows how these elementary steps connect into a reaction cycle which is closed by the oxidation of **4** to **1** but does not show obvious causes of oscillations. As previously highlighted, oscillating systems rely on feedback processes to move between different states or stages periodically. The oscillator described in this chapter is entirely unique but efforts to rationalise its operation on a molecular and supramolecular basis are illustrated below.

The oscillations in the concentration of **3** can be broadly viewed as a sequence of five different stages **i.-v.** which describe a full growth-decay 'pulse' (Figure 3.8). The repeated growth and decay of micelles as the oscillations passed through these stages was also clearly visible at the supramolecular level by iSCAT microscopy (see section 3.3.4, and 1.2.3 for background).

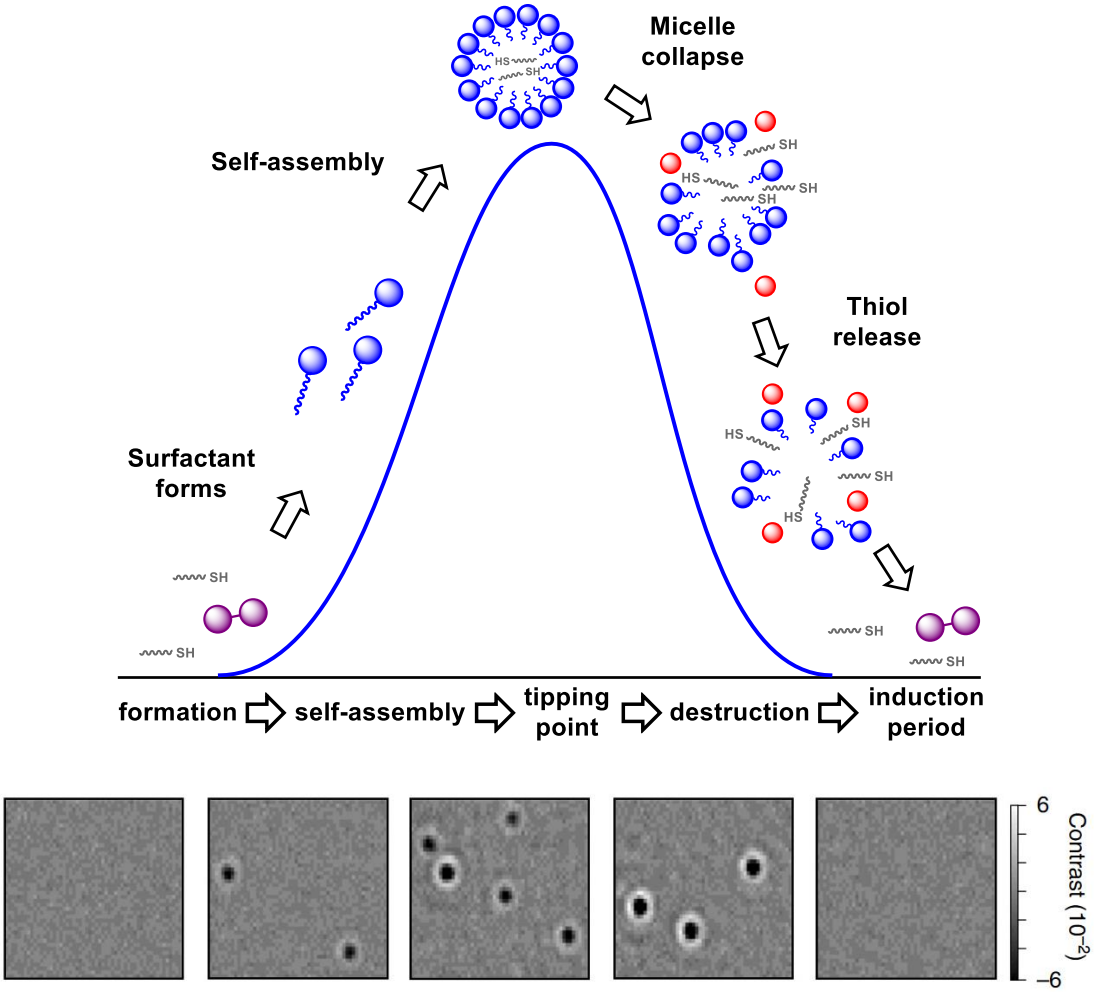

Figure 3.8: Five stages of a growth-decay cycle or 'pulse'. Formation of the subcomponent **3** drives micelle growth at the beginning, before destruction of **3** becomes the dominant process after the peak apex. This trend is also reflected by the real-time microscopy studies conducted on the reaction which show growth and decay. Note: contrast is an indirect measure of particle size (see iSCAT section 1.2.3 for background)

i. formation: the interfacial reaction between a solution of hydrophilic **1** and phase separated **2** is initially limited by the transfer of **2** into the aqueous layer. **ii. self-assembly**: dynamic light scattering (DLS) and cryo-EM measurements reveal that the product **3** can self-assemble into micelles (see Figures S26, Experimental section 7.2.5). As the concentration of **3** increases, micelles of **3** are formed which help solubilize **2** and speeds up **3** formation. This autocatalytic process[38-40] provides positive feedback and results in an exponential increase in micelles. Next, the concentration of **3** increases linearly while the micelles continue to form, likely taking up and stabilizing microdroplets of thiol **2**. Here, the increase in [**3**] is roughly equal to the amount of oxidant fed to the system, which at that point is the limiting factor.

iii. tipping point: large quantities of **2** are now in the aqueous layer because of the fast stirring and the presence of micelles. The maximum [**3**] is approached as compound **1** becomes increasingly depleted, due to the oxidant supply no longer keeping up with the increasing amount of solubilised thiol (which is constantly consuming **1**). **iv. destruction:** as a result of the excess thiol, a breakdown reaction between **2** and **3** dominates, depleting the micelle's building blocks. Key to oscillatory behaviour is a second, counteracting non-linear process, which we propose is provided by the breakdown of the micelles. As the system becomes starved of **1** due to limited oxidant supply, **2** can increasingly react with **3** instead. The destruction of molecular **3** causes the micelles of **3** to break down. As these micelles solubilise **2** in their interior, any **2** that was in the interfacial or aqueous layer becomes released and/or destabilized and engages in the further destruction of molecular **3** and its micellar compartments, propagating the breakdown. **v. induction period:** After the complete consumption of **3**, any excess of aqueous thiol either returns to the apolar layer over time or reacts with regenerated **1**, as the addition of fuel continues. This restores the system to its original conditions, allowing the next pulse to begin.

3.3.4 Supramolecular investigations by iSCAT

While the molecular concentration of **3** shows a clear oscillating pattern, characterizing the real time dynamics of supramolecular architectures requires different techniques with high spatiotemporal resolution. To study the self-assembled micelles of **3** (measuring *ca.* 8-10 nm in diameter by DLS) we turned to interferometric scattering microscopy (iSCAT). iSCAT measures changes to the scattering properties of the glass-water interface caused by the binding of nanoparticles to a microscope slide. This is visualised as a change in contrast for each particle binding event, enabling quantification of the number of particles for a given time interval.[41-43] Samples from active reactions can be diluted and visualised label-free on the microscope, with minimal disruption to the sample. Compared to DLS, iSCAT analysis can produce highly detailed histograms which show the distribution of sizes within a given population of particles. Figure 3.9 below shows the distribution of contrast value (as a proxy for micelle size) obtained from a sample

of **3a** taken from a standard oscillating reaction. As can be seen, **3a** produces a highly polydisperse mixture of aggregates.

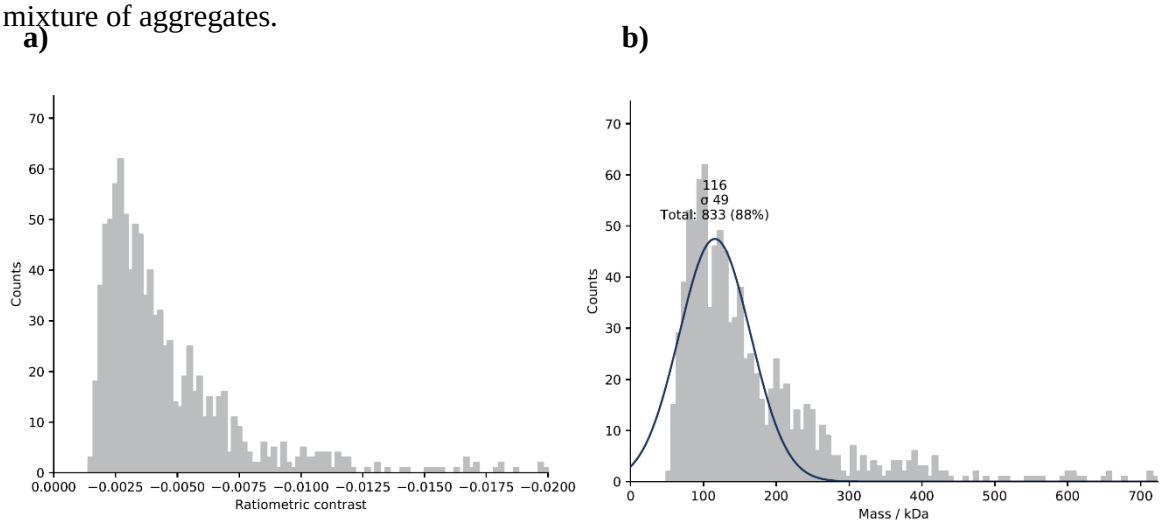

Figure 3.9: iSCAT measurement on aggregates of **3a** formed in a standard oscillating reaction between **1** and **2a** at pH 9.0. a) Ratiometric contrast distribution. b) using the calibration curve of Figure S26, Experimental section 7.2.5, the contrast can be converted to give the average mass (in kDa) of the aggregates.

Monitoring an oscillating reaction simultaneously with iSCAT and UPLC, we found the number of micellar particles closely correlates to the trends in molecular concentration of **3**. The micelle count experiences rapid increases and decay that produces clear oscillations over time in phase with the building block (Figure 3.10a). This synchronicity between the molecular and supramolecular entities supports the role of the self-assembly in the feedback mechanisms as the oscillations are identifiable at both length scales.

We found that the biphasic reaction between **1** and **2a** yields oscillations even at conditions where the measured critical micelle concentration (CMC) of pure **3a** in buffer was never reached (**3a** CMC = 1.56 mM). It should be noted that the CMC was determined using ring tensiometry at 20°C, while all oscillation experiments were carried out at 40°C. While the CMC can be significantly temperature dependent,[44] our experimental set-up didn't allow us to investigate this effect for our compounds. To show that aggregation of **3a** still occurs under biphasic conditions at concentrations below the measured CMC, a second type of experiment was followed using iSCAT. In this experiment, the maximum concentration of **3** is approximately half the CMC, yet (micellar) particles are clearly forming repeatedly and are quantified by iSCAT (Figure 3.10b).

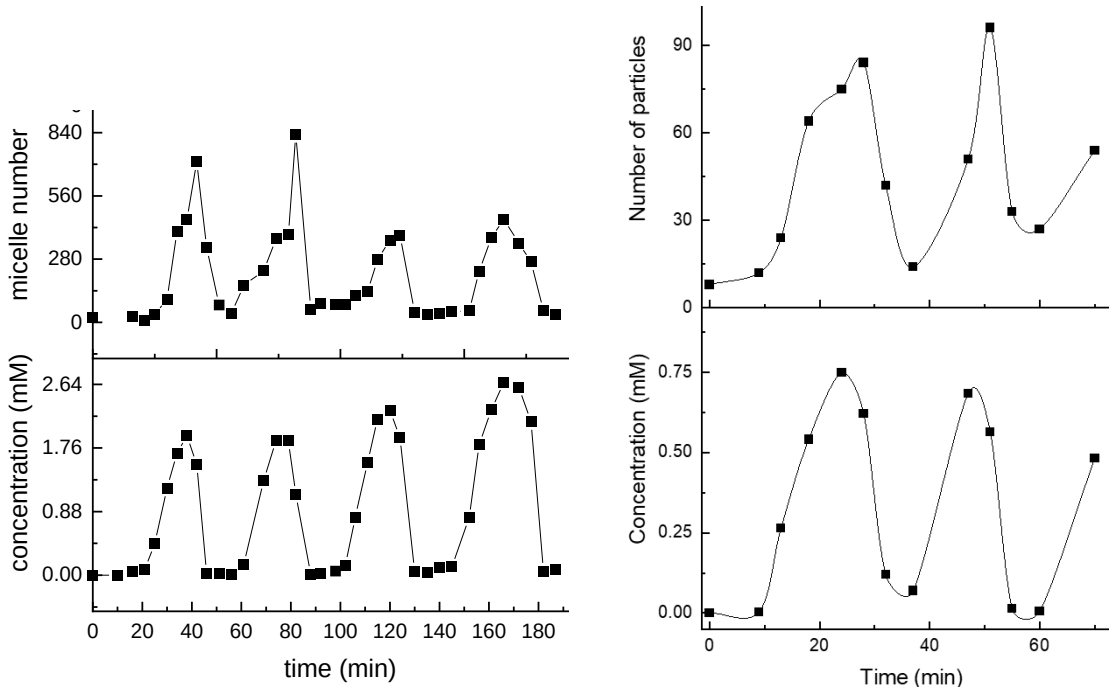

Figure 3.10: iSCAT monitoring of active oscillating reactions showing the concentration of **3a** and the number of particles formed during the biphasic reaction between **1** and **2** in TRIS buffer (pH 9.0). a) oscillating reaction where [**3a**] can exceed the CMC, b) oscillating reaction where [**3a**] does not approach the CMC yet micelles are seen

3.3.5 Mechanistic investigations

Being able to observe the oscillations at the supramolecular scale with iSCAT supports the relevance of the micelles in this specific oscillating mechanism but it does not directly inform on other important features. For this, different properties and requirements of the oscillator were examined in control experiments, as detailed below.

Interrupted oxidant supply experiment: the oscillating system requires a constant driving force away from equilibrium to operate. To demonstrate the importance of this and understand its impact on the kinetics an oscillating experiment with interrupted fuel supply (H_2O_2) was performed (Figure 3.11). After seeing regular oscillations in the first two hours of the experiment, the pump supplying H_2O_2 was switched off for precisely two hours. Consistent with the described reaction cycle and mechanism, temporarily removing the oxidation step prevented oscillations. Once oxidant supply was resumed the oscillations immediately resumed (Figure 3.11). This clearly shows the addition of hydrogen peroxide as a chemical fuel is essential to obtaining oscillations. Furthermore, this

experiment showed that the reaction components could lay dormant and be activated again by the presence of chemical fuel.

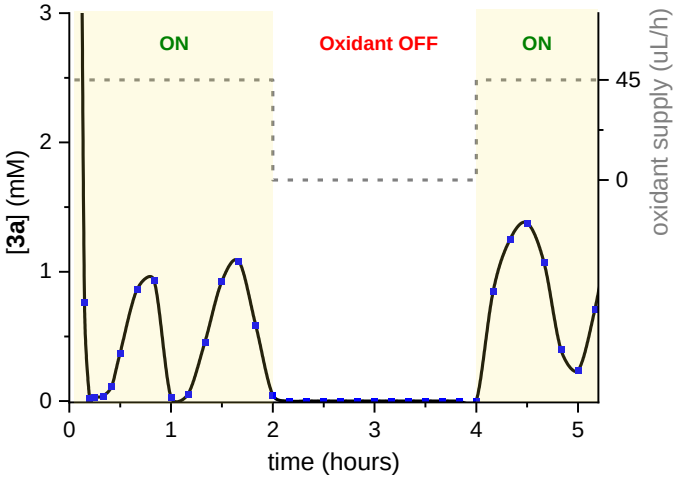

Figure 3.11: Interrupted oxidant supply oscillation experiment. When the oxidant supply is temporarily paused during an oscillation experiment, the oscillations no longer occur. This shows the addition of chemical fuel is essential to obtaining oscillations.

Seeding experiments and transient aggregation: the self-assembly and destruction of **3** are key features of our proposed mechanism for oscillations in that both processes initiate non-linear feedback and that the breakdown enables the system to reset after each pulse. We performed control experiments using chemically stable surfactants to test the effect of always having micelles present, independent of the changing concentration of (metastable) **3**.

We found that adding micelle-forming sodium dodecyl sulfate (SDS) or a sulfide analogue of **3** (compound **6**) completely removed the oscillations (Figure 3.12). This effect of SDS both above and below its reported CMC (8.7 mM)[45] and of **6** above its measured CMC (1.8 mM, Experimental section 7.2.5) highlights the importance of chemically metastable species and the sensitivity of the system. As the structure of stable surfactant **6** is so similar to species **3a** this strongly suggests that it is the metastable properties of surfactant **3a** which are essential to enable oscillations.

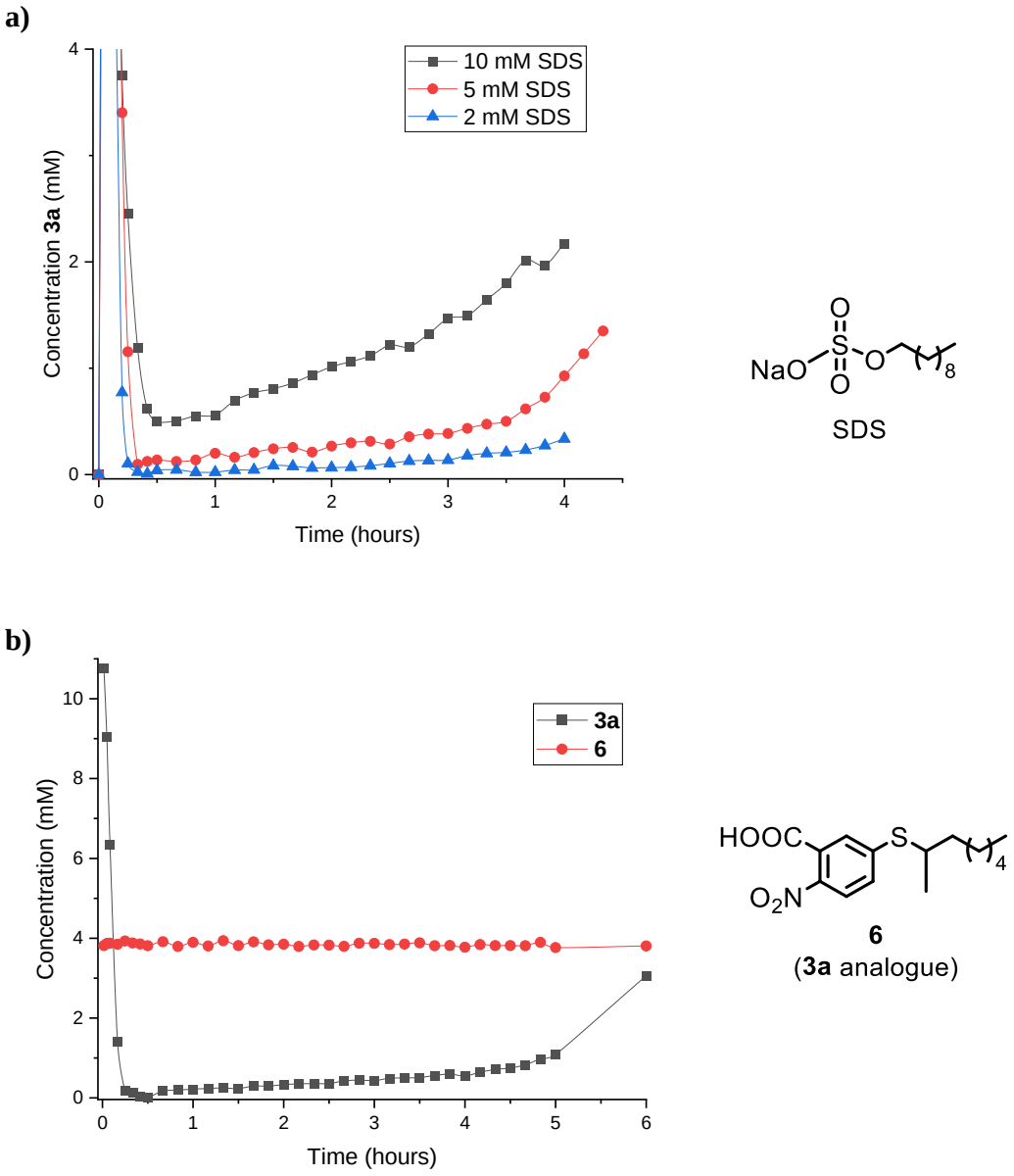

Figure 3.12: Reaction profiles for oscillation experiments involving **1**, **2a** seeded with a) 2, 5 or 10 mM sodium dodecyl sulfate (SDS) and b) 4 mM of stable sulfide surfactant **6**. In the presence of SDS or **6**, micelles are present throughout the experiment, which removes the oscillations. This shows the importance of transient aggregation to the oscillatory behaviour.

Monitoring oscillations in [2]: based on the ability of micelles to solubilise thiol we expected the concentration of thiol **2a** in the aqueous layer to also oscillate over time alongside [**3a**]. By quenching aliquots of the oscillating reaction using maleimide, we were able to follow the concentration of the UV-visible maleimide adduct of this thiol. We found that the concentration trends for **2a** in the aqueous layer consistently matches that of surfactant **3a** during oscillating reactions (representative example: Figure 3.13). The degree to which [**2a**] and [**3a**] synchronised

sometimes varied between different experiments, occasionally showing only a weak relation between the two profiles. This is likely due to a combination of experimental sensitivity (*i.e.* identical experiments with high variability) and different dominant factors under different reaction conditions (*e.g.* reactions with very high concentrations of surfactant **3** or high stirring rates, which may control the solubilisation of the thiol to a greater or lesser extent than other conditions).

Confirming that the thiol concentration oscillates during oscillating experiments strengthens a key relationship in the reaction network. As has been mentioned, the micelles form and are destroyed by the action of thiol **2** and the aqueous concentration of **2** responds to the amount of micelles. This sets up feedback between these species which is central to the origin of the oscillations. It is suspected that the different speed of processes at the supra-, meso- and macroscopic scales, such as the transient sequestration and phase separation of the thiol, could be a key factor in the phenomena seen.

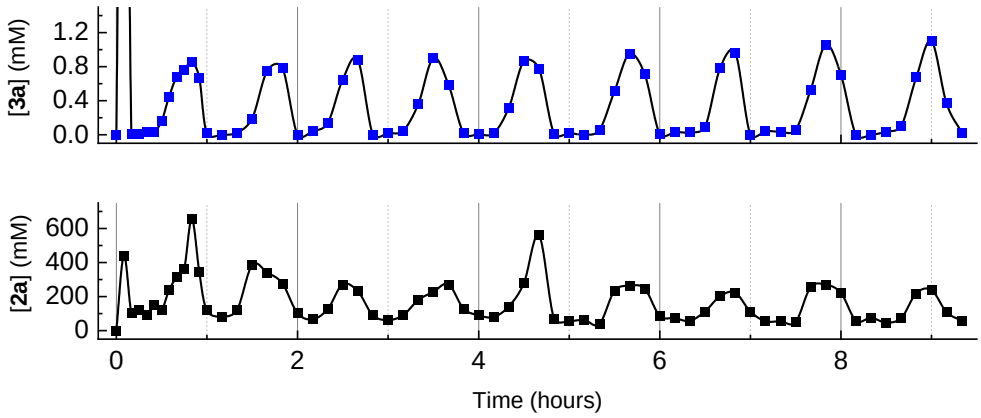

Figure 3.13: Oscillations in the concentration of aqueous thiol **2a**. The concentration of thiol **2a** (black) in the aqueous phase matches oscillations in the concentration of surfactant **3a** (blue).

Effect of waste product 5: we noticed that in all of our oscillating reactions the peak concentration of **3** increased over time and the peaks became broader compared to the start of the experiments. This signalled that some property of the reaction mixture was gradually changing over time. We hypothesized that this amplitude and period 'drift' was caused by the formation of dialkyl disulfide **5**, which competes with thiols **3** for uptake into the micelles.

To test this hypothesis, the standard oscillation experiment was repeated in the presence of 90 µL dialkyl disulfide **5** from the outset. This resulted in broad oscillations from the start of the experiment (Figure 3.14), confirming the expected influence of this waste product.

We also supported this theory by monitoring the impact of **5** on the formation and destruction rates of **3** in controls. In these experiments, 67% of the starting thiol **2a** was replaced with alkyldisulfide **5**, which resulted in a significantly slower formation rate compared to **2a** alone (Figure 3.14). The same was done to examine **3a** destruction rate using preformed **3a**, which resulted in a significantly slower destruction rate (Figure 3.14). To show that the lower destruction rate was not just due to the reduced amount of thiol (5 equivalents vs. 15 equivalents wrt **3a**), experiments with only 33% of the thiol (5 equivalents), but without any alkyldisulfide **5** were performed. Only a minor decrease in destruction rate was observed here, showing that it is not simply the reduced quantity of **3** that causes the oscillations to increase in period and amplitude over time but is related to the presence of **5**.

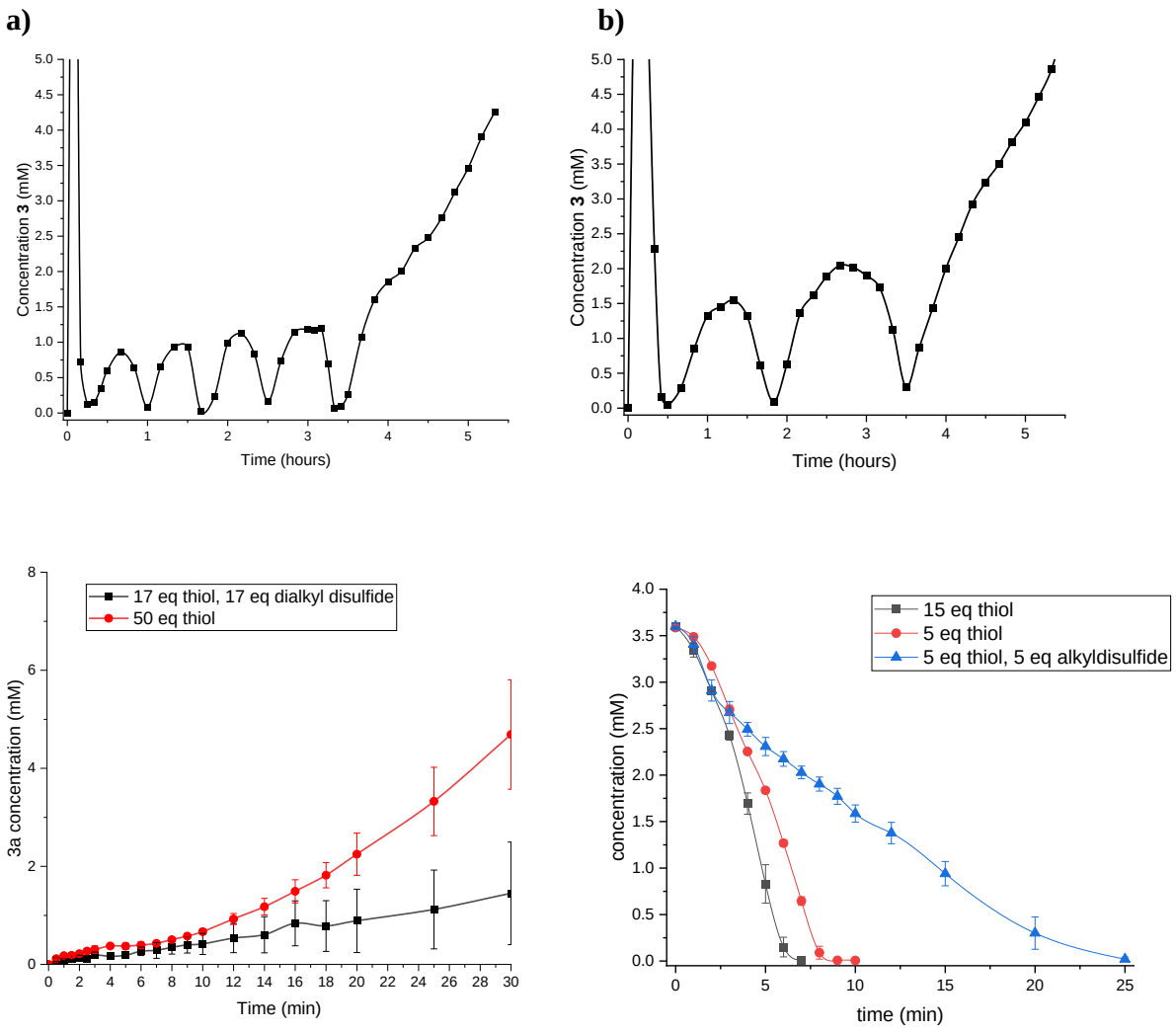

Figure 3.14: Effect of dialkyl disulfide **5** on the oscillations. a) standard oscillation experiment where [**3a**] oscillates over time until thiol **2a** starts to be consumed. The period and amplitude of the peaks increases during the experiment; b) standard oscillation experiment seeded with **5** (90 µL), causing the peaks to have a larger amplitude and period from the outset; c) Formation control which shows that **3a** formation is significantly decreased in the presence of **5**; d) Destruction control which shows the presence of **5** is responsible for decreased **3a** destruction rate. Control experiments were performed in triplicate and error bars represent the standard deviation.

Autocatalytic destruction controls: the autocatalytic nature of the destruction, where the decay of some micelles accelerates the breakdown of others, is key to our hypothesis for the mechanism of the oscillations. We sought ways to investigate this process in more detail. This is challenging for a system which involves unstable non-equilibrium states and non-linear kinetics as altering the system may not give realistic conclusions or reliable data. Nonetheless, we designed experiments which could inform on the oscillations with as little disturbance as possible.

Our current hypothesis regarding the micellar destruction in the oscillations assumes that the release of previously encapsulated alkylthiol by decaying micelles results in the destruction of remaining, intact micelles. To test this hypothesis, we added decaying micelles (*i.e.* an aliquot from an oscillating reaction that has passed the tipping point) into a separate reaction that was still in the linear growth regime (see Figure 3.15). To achieve this, the general oscillation experiment was adapted so as to display longer periods. This was achieved by increasing the oxidant flow (120 μL/h) and the amount of DMAP while decreasing the stirring rate (to 400 rpm). Approximately half an hour after this experiment (experiment **A**) was started, an identical experiment (experiment **B**) was started, ensuring a phase difference between the oscillations of these two experiments. The oscillations of experiment **A** consequently preceded those of experiment **B**. After approximately 2.5 hours, when the concentration of **3a** in experiment **A** started to decline rapidly, 1 mL of this solution was transferred to experiment **B** for which the concentration of **3a** at that point was still increasing. This resulted in the immediate, premature decrease of [**3**]. Being able to seed the breakdown step in this way supports the idea that this this an autocatalytic process.[40] This breakdown cascade causes the micelles to rapidly disappear from the system in a delayed, non-linear fashion as is required to obtain oscillations.

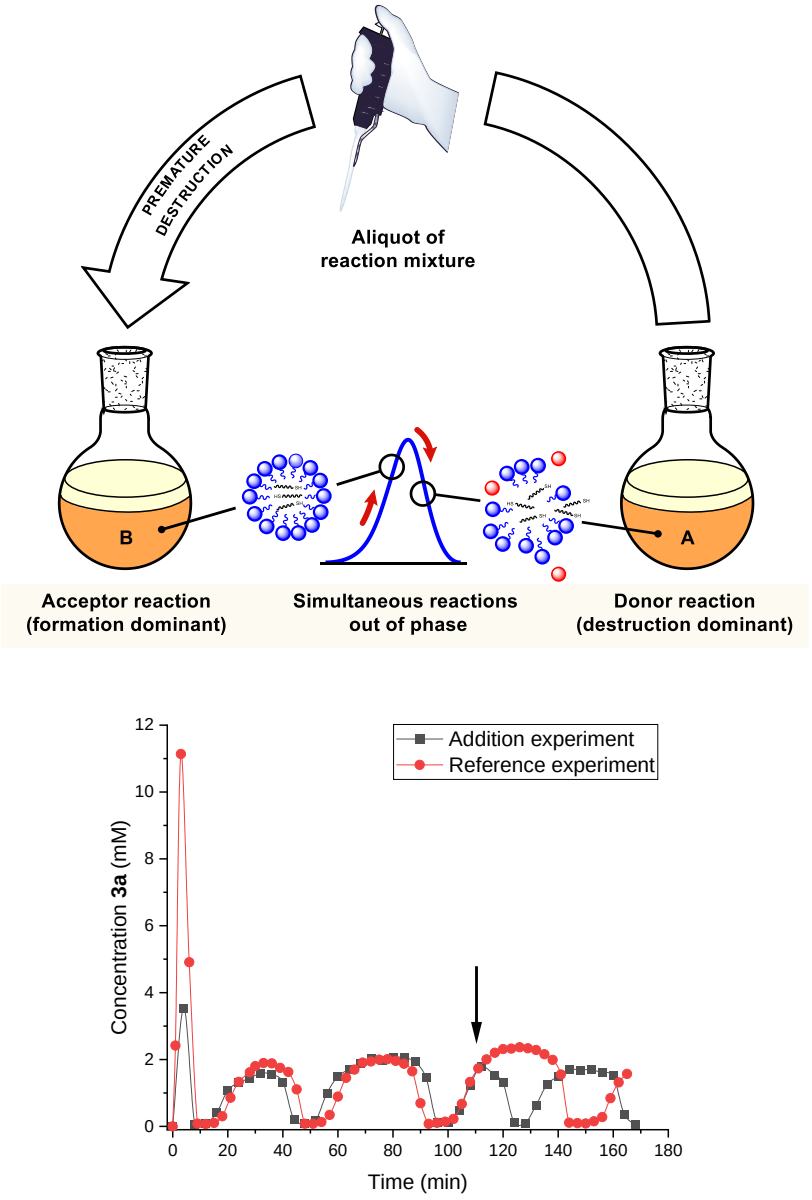

Figure 3.15: Control experiment to show that micelle decay occurs autocatalytically. Seeding an oscillating reaction (acceptor Experiment **B**, black curve) with decaying micelles from a duplicate (donor, Experiment **A**) results in the immediate decline in the concentration of surfactant (black arrow). The red curve shows oscillations for an identical, undisturbed reaction.

Although the oscillations may be initially understood as a sequence of five stages, some destruction of species **3** is expected throughout. Since surfactant destruction and formation could potentially occur simultaneously in these experiments, it is difficult to disentangle the exact rates of these two processes. To quantify the rate of destruction at different stages of the oscillation we designed an experiment featuring two metastable surfactants. Surfactant **3b** is formed in the usual way *in situ*, from the reaction between **1** and thiol **2b**, and **1** is regenerated via the continuous addition of

hydrogen peroxide. This results in oscillations in [**3b**] as seen in Figure 3.16. After the first full oscillation was completed, continuous addition of the second surfactant (**3a**) was started. Since the amount of **3a** supplied to the system is relatively small compared to the oxidant supply, **3b** remains the dominant surfactant species, and the appearance of its oscillations is not perturbed. For compound **3a**, the formation process (via physical autocatalysis) does not occur, so the destruction rate is the difference between the **3a** addition rate and measured concentration. Since the addition rate was exactly known, and the concentration of **3a** could be measured using UPLC, this allowed us to calculate the destruction rate over time (Figures 3.16a-c).

These results show that destruction is taking place throughout most stages of the oscillations and in fact that a plot of destruction rate in time shows an oscillating pattern itself. It also shows a clear correlation between the destruction rate and the presence of **1**: when the concentration of **1** is high, destruction is slow and when [**1**] decreases, the rate of destruction goes up. This supports the hypothesis that the destruction step is hampered by the availability of **1**.

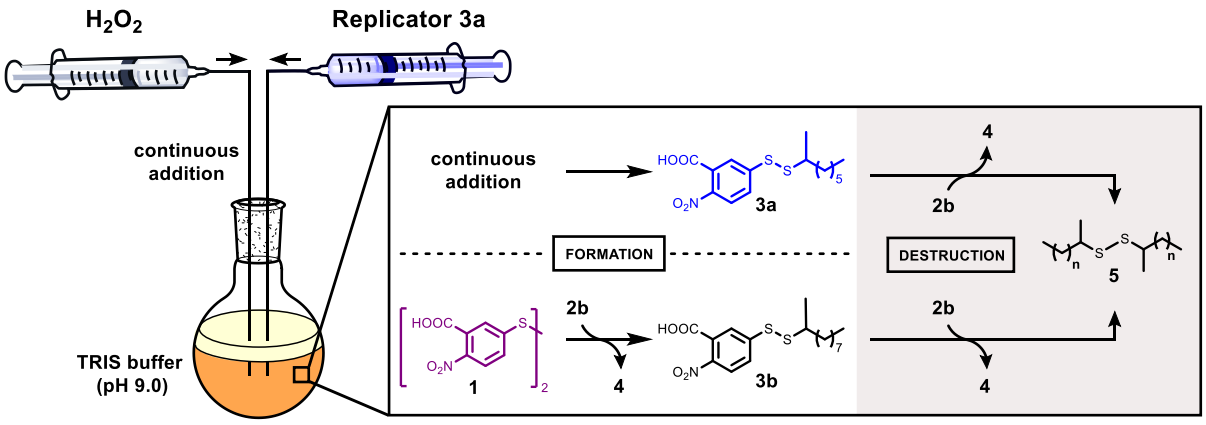

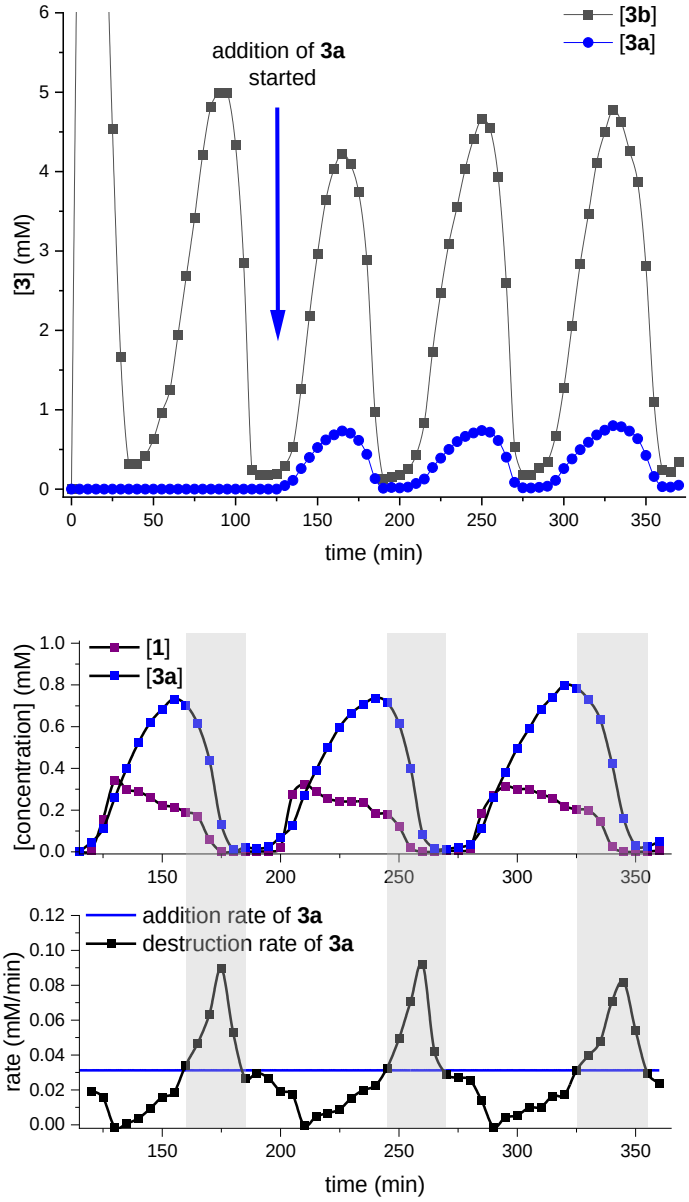

Figure 3.16: Deconvoluting destruction rate in an oscillating reaction. a) Surfactant **3b** is formed through the biphasic reaction between compounds **1** and **2b**, while surfactant **3a** is continuously supplied to the system; b) the concentration of both surfactants oscillates in time; c) the destruction of both surfactants via the reaction with thiol **2b** results in changes to the concentration of **3a-b** which can be analysed by UPLC. As the addition rate of surfactant **3a** is constant, the **3a** destruction rate is found by calculating the difference between the expected and measured concentration of **3a**. Shaded areas indicate the time periods where the rate of destruction exceeds formation.

An updated mechanistic description of the oscillations: The mechanistic experiments and kinetic data in this section support the importance of a continuous supply of chemical energy, metastable surfactants and the transient uptake of thiol **2** within micelles. The micelle destruction process in this system is clearly key to the oscillator but is especially difficult to investigate due to dynamic

and supramolecular features. In particular, the experiments in Figures 3.15 and 3.16 above have shed some light on the way the destruction events take place and enable a better mechanistic understanding. Based upon all of the experiments discussed, Figure 3.17 below presents a qualitative overview of how the formation and destruction events evolve over time during the oscillations. This is intended to be a refinement of the distinct stages of the oscillations discussed above but will not address all mechanistic aspects.

The oscillations begin with the rate of **3** formation exceeding the destruction rate, although both processes occur and benefit from physical autocatalysis and accelerate. At this stage the phase separated thiol is the limiting reagent. As [**3**] grows the thiol continues to be emulsified into the aqueous layer leading to **1** becoming the limiting reagent for the formation of **3**. The amount of emulsified thiol is relatively high and formation and destruction both occur rapidly, depleting **1** faster than it can be replenished by the oxidant supply. Critically, as **1** formation relies upon the addition of oxidant at a fixed rate, it has a maximum production rate set by the syringe pump (see grey dashed line, Figure 3.17). This ceiling to **1** and **3** formation enables the growing destruction rate to surpass formation, leading to net breakdown of micelles. The net destruction of micelles causes two main changes in the system: encapsulated thiol is released into the aqueous phase where it can accelerate the depletion of **1** and **3**, and as surfactant concentration rapidly falls the thiol begins to gradually phase separate (although this is slow relative to the molecular reaction events). At this point in the pulse, the destruction process remains faster than formation and there remains an abundance of thiol **2** in the aqueous phase to suppress the concentrations of **1** and **3**. Once [**3**] is depleted there is a delay in **1** and **3** formation restarting, due to the remaining emulsified **2** which must either phase separate or be converted (via **3**) to **5** by the continued supply of oxidant. This is the sequence of events which, at this time, are thought to be key to the operation of this biphasic oscillator.

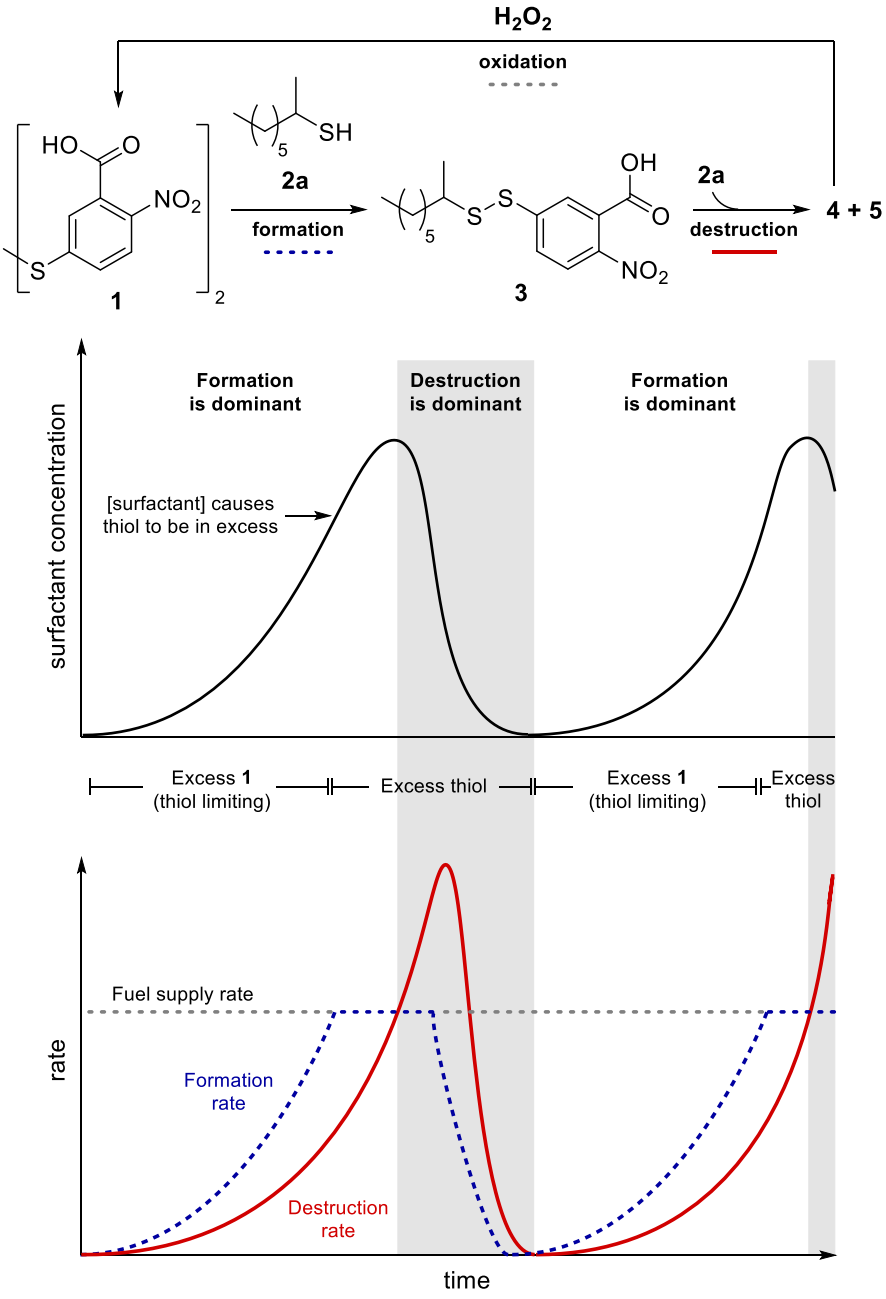

Figure 3.17: A refinement of the oscillation mechanism, focussing on how the formation and destruction rates evolve over time. Shaded areas indicate the time periods where the rate of destruction exceeds formation

3.3.6 Control of the oscillations

The system is highly tuneable by varying the destruction rate of **3** and the oxidation of **4**. Increasing the amount of DMAP increases the destruction of **3** and causes the tipping point (when destruction overtakes formation) to occur earlier, thereby decreasing the period (lifetime of the micelles) and the amplitude (maximum concentration of **3**) (Figure 3.18a). Increasing the rate of oxidant supply reduces the period of the oscillations and increases their amplitude: more oxidant results in faster

amphiphile formation as limiting **1** is produced faster – increasing the slope and peak amplitude (Figure 3.18b). Increased uptake of **2** due to the higher micelle concentrations also accelerates the autocatalytic formation process such that the tipping point (where oxidation can no longer keep up with thiol uptake) is reached faster, reducing the overall lifetime of the micelles. The system shows remarkable responsiveness to changes in oxidation rate within an experiment, allowing the amplitude and period of the oscillations to be controlled in a predictable and reversible way (Figure 3.19a). The ways in which this oscillator can respond *in situ* to changes to reaction variables will be further discussed in Chapter 4.

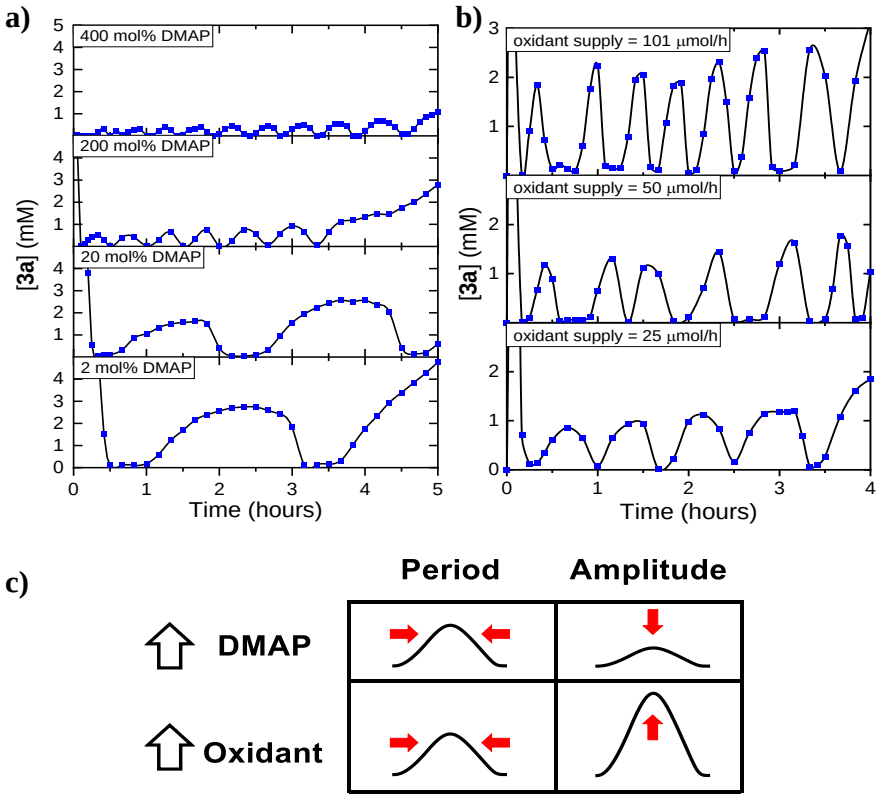

Figure 3.18: Controlling the oscillations. a) the effect of DMAP concentration on the period and amplitude of the oscillations. Percentages are given relative to the amount of compound **1** at the start of the experiment b) the effect of the oxidant supply on the oscillations. c) overall effect of changes in the DMAP concentration and oxidant supply on the appearance of the oscillations

The perpetuation of oscillations is only limited by the amount of available thiol (**2**) and continuous oxidant supply. By supplying the system with a large excess of **2**, oscillations can be sustained,

without dampening, for several days (Figure 3.19b). The production of waste product **5** clearly changes the amplitude and period of the oscillations over the course of days (as discussed above), but changes on the timescale of several hours are negligible and reproducible peaks are obtained.

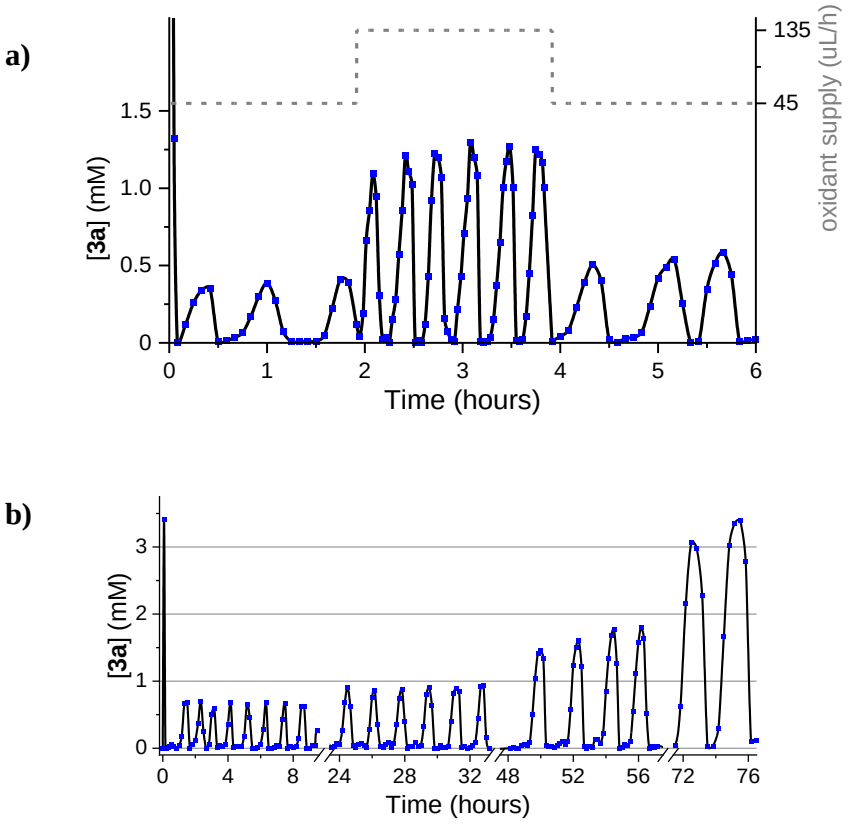

Figure 3.19: a) the period and amplitude of these oscillations can be reversibly altered during an experiment by changing the oxidant flow over time, b) by increasing the amount of thiol **2** to 111 eq., the oscillations can be sustained for several days. During this time, the oscillations increase in period and amplitude, which can be attributed to the continuous formation of waste-product **5**

3.4 Conclusions and outlook

Despite the interest in out-of-equilibrium systems, examples of oscillating reactions remain rare. Previous chemical reactions showing sustained oscillations have focussed on molecular scale processes for small molecule organic[18] and biochemical systems[17] and it is typical that flow reactors drive the phenomenon. Our system of supramolecular self-replicators is uniquely capable of autonomous oscillations (i.e. it does not require coupling to an external reaction) in a small molecular network. Moreover, it is the self-assembly that drives the oscillations, rather than supramolecular events just being a secondary phenomenon. The differing timescales of the

molecular and greater length-scale events (supramolecular assembly, mass transport and phase behaviour) are critical in this work in order to produce oscillations. Hence, it may even be possible to design future systems with an intrinsic delay process, based upon this principle.

This chemical oscillator driven by self-replication of primitive compartmentalized structures, or protocells,[46,47] may be relevant to understanding how living systems can emerge from simpler chemistry. For instance, it has been proposed that a key step in chemical evolution is to go from prebiotic chemical oscillators towards complex, living cells.[9] Further, transient phase behaviour like that encountered in this system is now thought to mediate many important biological mechanisms, e.g. protein coacervates and localisation of cell machinery.[48-51] The reaction network of this system displays controlled and sustained oscillations in the concentrations of all key species. Reminiscent of apoptosis (programmed cell death) in real cells,[52] a dramatic self-destructive process controls the lifetime and population of the self-assembled structures. These experiments show how protocell-like structures can form spontaneously, repeatedly, and robustly while responding to changes in their environment. This adaptability of the system may be used to allow control over its environment[53-55] and in Chapter 5 we will show how oscillations can be coupled to additional processes to control the location and concentration of other compounds. Substantial work has been put into understanding how this oscillator operates and further mechanistic investigation may inform on the generality of its mode of action and what other functions it may perform.

References

1 Goldbeter, A. *Biochemical Oscillations and Cellular Rhythms*. (Cambridge University Press: Cambridge, U.K., 1996).

2 Cao, Y. X. L., Lopatkin, A. & You, L. C. Elements of biological oscillations in time and space. *Nat. Struct. Mol. Biol.* **23**, 1030-1034 (2016). https://doi.org:10.1038/nsmb.3320

3 Ruiz-Mirazo, K., Briones, C. & De La Escosura, A. Prebiotic Systems Chemistry: New Perspectives for the Origins of Life. *Chem. Rev.* **114**, 285-366 (2014). https://doi.org:10.1021/cr2004844

4 Lotka, A. J. Undamped oscillations derived from the law of mass action. *J. Am. Chem. Soc.* **42**, 1595-1599 (1920). https://doi.org:10.1021/ja01453a010

5 Volterra, V. Fluctuations in the abundance of a species considered mathematically. *Nature* **118**, 558-560 (1926). https://doi.org:10.1038/118558a0

6 Epstein, I. R. & Showalter, K. Nonlinear Chemical Dynamics: Oscillations, Patterns, and Chaos. *J. Phys. Chem. A* **100**, 13132-13147 (1996). https://doi.org:10.1021/jp953547m

7 van Rossum, S. A. P., Tena-Solsona, M., van Esch, J. H., Eelkema, R. & Boekhoven, J. Dissipative out-of-equilibrium assembly of man-made supramolecular materials. *Chem. Soc. Rev.* **46**, 5519-5535 (2017). https://doi.org:10.1039/C7CS00246G
8 Ashkenasy, G., Hermans, T. M., Otto, S. & Taylor, A. F. Systems chemistry. *Chem. Soc. Rev.* **46**, 2543-2554 (2017). https://doi.org:10.1039/C7CS00117G
9 Wagner, N. & Ashkenasy, G. Rhythm before life. *Nat. Chem.* **11**, 681-683 (2019). https://doi.org:10.1038/s41557-019-0301-2
10 Leira-Iglesias, J., Tassoni, A., Adachi, T., Stich, M. & Hermans, T. M. Oscillations, travelling fronts and patterns in a supramolecular system. *Nat. Nanotechnol.* **13**, 1021-1027 (2018). https://doi.org:10.1038/s41565-018-0270-4
11 Green, L. N. *et al.* Autonomous dynamic control of DNA nanostructure self-assembly. *Nat. Chem.* **11**, 510-520 (2019). https://doi.org:10.1038/s41557-019-0251-8
12 Srinivas, N., Parkin, J., Seelig, G., Winfree, E. & Soloveiehile, D. Enzyme-free nucleic acid dynamical systems. *Science* **358** (2017). https://doi.org:10.1126/science.aal2052
13 Belousov, B. P. A periodic reaction and its mechanism. *Sb. Ref. Radiats. Med.* **145** (1958).
14 Briggs, T. S. & Rauscher, W. C. An oscillating iodine clock. *J. Chem. Educ.* **50**, 496 (1973). https://doi.org:10.1021/ed050p496
15 Bray, W. C. A periodic reaction in homogeneous solution and its relation to catalysis. *J. Am. Chem. Soc.* **43**, 1262-1267 (1921). https://doi.org:10.1021/ja01439a007
16 Rabai, G., Orban, M. & Epstein, I. R. Design of pH-regulated oscillators. *Acc. Chem. Res.* **23**, 258-263 (1990). https://doi.org:10.1021/ar00176a004
17 Semenov, S. N. *et al.* Rational design of functional and tunable oscillating enzymatic networks. *Nat. Chem.* **7**, 160-165 (2015). https://doi.org:10.1038/nchem.2142
18 Semenov, S. N. *et al.* Autocatalytic, bistable, oscillatory networks of biologically relevant organic reactions. *Nature* **537**, 656-660 (2016). https://doi.org:10.1038/nature19776
19 Lagzi, I., Kowalczyk, B., Wang, D. & Grzybowski, B. A. Nanoparticle Oscillations and Fronts. *Angew. Chem. Int. Ed.* **49**, 8616-8619 (2010). https://doi.org:https://doi.org/10.1002/anie.201004231
20 Howlett, M. G., Engwerda, A. H. J., Scanes, R. J. H. & Fletcher, S. P. An autonomously oscillating supramolecular self-replicator. *Nat. Chem.* **14**, 805-810 (2022). https://doi.org:10.1038/s41557-022-00949-6
21 Goldbeter, A. Dissipative structures in biological systems: bistability, oscillations, spatial patterns and waves. *Philosophical Transactions of the Royal Society a-Mathematical Physical and Engineering Sciences* **376** (2018). https://doi.org:10.1098/rsta.2017.0376
22 Zhabotinsky, A. M. Periodic course of the oxidation of malonic acid in solution. *Biofizika* **9**, 306-311 (1964).
23 Gyorgyi, L., Turanyi, T. & Field, R. J. Mechanistic details of the oscillatory Belousov-Zhabotinskii reaction. *J. Phys. Chem. A* **94**, 7162-7170 (1990). https://doi.org:10.1021/j100381a039
24 Epstein, I. R. Coupled chemical oscillators and emergent system properties. *Chem. Commun.* **50**, 10758-10767 (2014). https://doi.org:10.1039/C4CC00290C
25 Isakova, A. & Novakovic, K. Oscillatory chemical reactions in the quest for rhythmic motion of smart materials. *Eur. Polym. J.* **95**, 430-439 (2017). https://doi.org:https://doi.org/10.1016/j.eurpolymj.2017.08.033
26 Grinthal, A. & Aizenberg, J. Adaptive all the way down: Building responsive materials from hierarchies of chemomechanical feedback. *Chem. Soc. Rev.* **42**, 7072-7085 (2013). https://doi.org:10.1039/C3CS60045A
27 Gizynski, K. & Gorecki, J. Chemical memory with states coded in light controlled oscillations of interacting Belousov–Zhabotinsky droplets. *Physical Chemistry Chemical Physics* **19**, 6519-6531 (2017). https://doi.org:10.1039/C6CP07492H
28 Parrilla-Gutierrez, J. M. *et al.* A programmable chemical computer with memory and pattern recognition. *Nat. Commun.* **11**, 1442 (2020). https://doi.org:10.1038/s41467-020-15190-3
29 Dueñas-Díez, M. & Pérez-Mercader, J. How Chemistry Computes: Language Recognition by Non-Biochemical Chemical Automata. From Finite Automata to Turing Machines. *iScience* **19**, 514-526 (2019). https://doi.org:10.1016/j.isci.2019.08.007

30 Draper, T. C., Dueñas-Díez, M. & Pérez-Mercader, J. Exploring the symbol processing 'time interval' parametric constraint in a Belousov–Zhabotinsky operated chemical Turing machine. *RSC Advances* **11**, 23151-23160 (2021). https://doi.org:10.1039/D1RA03856G
31 Dueñas-Díez, M. & Pérez-Mercader, J. Native Chemical Computation. A Generic Application of Oscillating Chemistry Illustrated With the Belousov-Zhabotinsky Reaction. A Review. *Frontiers in Chemistry* **9** (2021). https://doi.org:10.3389/fchem.2021.611120
32 Bastakoti, B. P. & Perez-Mercader, J. Facile One-Pot Synthesis of Functional Giant Polymeric Vesicles Controlled by Oscillatory Chemistry. *Angew. Chem. Int. Ed.* **56**, 12086-12091 (2017). https://doi.org:https://doi.org/10.1002/anie.201703816
33 Cafferty, B. J. *et al.* Robustness, Entrainment, and Hybridization in Dissipative Molecular Networks, and the Origin of Life. *J. Am. Chem. Soc.* **141**, 8289-8295 (2019). https://doi.org:10.1021/jacs.9b02554
34 Sharko, A., Livitz, D., De Piccoli, S., Bishop, K. J. M. & Hermans, T. M. Insights into Chemically Fueled Supramolecular Polymers. *Chem. Rev.* **122**, 11759-11777 (2022). https://doi.org:10.1021/acs.chemrev.1c00958
35 Novichkov, A. I. *et al.* Autocatalytic and oscillatory reaction networks that form guanidines and products of their cyclization. *Nat. Commun.* **12**, 2994 (2021). https://doi.org:10.1038/s41467-021-23206-9
36 Morrow, S. M., Colomer, I. & Fletcher, S. P. A chemically fuelled self-replicator. *Nat. Commun.* **10**, 1011 (2019). https://doi.org:10.1038/s41467-019-08885-9
37 Engwerda, A. H. J. *et al.* Coupled Metabolic Cycles Allow Out-of-Equilibrium Autopoietic Vesicle Replication. *Angew. Chem. Int. Ed.* **59**, 20361-20366 (2020). https://doi.org:10.1002/anie.202007302
38 Bachmann, P. A., Luisi, P. L. & Lang, J. Autocatalytic self-replicating micelles as models for prebiotic structures. *Nature* **357**, 57-59 (1992). https://doi.org:10.1038/357057a0
39 Morrow, S. M., Colomer, I. & Fletcher, S. P. A chemically fuelled self-replicator. *Nat. Commun.* **10**, 1011 (2019). https://doi.org:10.1038/s41467-019-08885-9
40 Bissette, A. J. & Fletcher, S. P. Mechanisms of Autocatalysis. *Angew. Chem. Int. Ed.* **52**, 12800-12826 (2013). https://doi.org:10.1002/anie.201303822
41 Kukura, P. *et al.* High-speed nanoscopic tracking of the position and orientation of a single virus. *Nat. Methods* **6**, 923-U985 (2009). https://doi.org:10.1038/nmeth.1395
42 Lebedeva, M. A., Palmieri, E., Kukura, P. & Fletcher, S. P. Emergence and Rearrangement of Dynamic Supramolecular Aggregates Visualized by Interferometric Scattering Microscopy. *ACS Nano* **14**, 11160-11168 (2020). https://doi.org:10.1021/acsnano.0c02414
43 Young, G. *et al.* Quantitative mass imaging of single biological macromolecules. *Science* **360**, 423-427 (2018). https://doi.org:10.1126/science.aar5839
44 Khoshnood, A., Lukanov, B. & Firoozabadi, A. Temperature Effect on Micelle Formation: Molecular Thermodynamic Model Revisited. *Langmuir* **32**, 2175-2183 (2016). https://doi.org:10.1021/acs.langmuir.6b00039
45 Marcolongo, J. P. & Mirenda, M. Thermodynamics of Sodium Dodecyl Sulfate (SDS) Micellization: An Undergraduate Laboratory Experiment. *J. Chem. Educ.* **88**, 629-633 (2011). https://doi.org:10.1021/ed900019u
46 Szostak, J. W., Bartel, D. P. & Luisi, P. L. Synthesizing life. *Nature* **409**, 387-390 (2001). https://doi.org:10.1038/35053176
47 Dzieciol, A. J. & Mann, S. Designs for life: protocell models in the laboratory. *Chem. Soc. Rev.* **41**, 79-85 (2012). https://doi.org:10.1039/c1cs15211d
48 Plys, A. J. & Kingston, R. E. Dynamic condensates activate transcription Transcriptional components exhibit transient phase separation to drive gene activation. *Science* **361**, 329-330 (2018). https://doi.org:10.1126/science.aau4795
49 Altenburg, W. J. *et al.* Programmed spatial organization of biomacromolecules into discrete, coacervate-based protocells. *Nat. Commun.* **11** (2020). https://doi.org:10.1038/s41467-020-20124-0
50 Sabari, B. R. *et al.* Coactivator condensation at super-enhancers links phase separation and gene control. *Science* **361** (2018). https://doi.org:10.1126/science.aar3958

51 Boeynaems, S. *et al*. Protein Phase Separation: A New Phase in Cell Biology. *Trends Cell Biol.* **28**, 420-435 (2018). https://doi.org:10.1016/j.tcb.2018.02.004
52 Taylor, R. C., Cullen, S. P. & Martin, S. J. Apoptosis: controlled demolition at the cellular level. *Nat. Rev. Mol. Cell Biol.* **9**, 231-241 (2008). https://doi.org:10.1038/nrm2312
53 Grzybowski, B. A. & Huck, W. T. S. The nanotechnology of life-inspired systems. *Nat. Nanotechnol.* **11**, 584-591 (2016). https://doi.org:10.1038/nnano.2016.116
54 He, X. M. *et al*. Synthetic homeostatic materials with chemo-mechano-chemical self-regulation. *Nature* **487**, 214-218 (2012). https://doi.org:10.1038/nature11223
55 Lerch, M. M., Grinthal, A. & Aizenberg, J. Viewpoint: Homeostasis as Inspiration-Toward Interactive Materials. *Adv. Mater.* **32**, 1905554 (2020). https://doi.org:10.1002/adma.201905554

Statement of Authorship for joint/multi-authored papers for PGR thesis

To appear at the end of each thesis chapter submitted as an article/paper

The statement shall describe the candidate's and co-authors' independent research contributions in the thesis publications. For each publication there should exist a complete statement that is to be filled out and signed by the candidate and supervisor **(only required where there isn't already a statement of contribution within the paper itself).**

Title of Paper	An autonomously oscillating supramolecular self-replicator
Publication Status	☑Published ~~Accepted for Publication~~ ~~Submitted for Publication~~ ~~Unsubmitted work written in a manuscript style~~
Publication Details	Michael G. Howlett, Anthonius H. J. Engwerda, Robert J. H. Scanes and Stephen P. Fletcher. Nat. Chem. 14, 805–810 (2022). https://doi.org/10.1038/s41557-022-00949-6

Student Confirmation

Student Name:	Michael Howlett		
Contribution to the Paper	Performed experiments and analysed data. Wrote and edited the manuscript. Co-author (A. Engwerda) also performed experiments, took part in data analysis and writing of the manuscript. Contributed equally to M Howlett. Co-author (R. Scanes) performed preliminary experiments. Co-author (S. Fletcher) supervised the project and contributed to data analysis and manuscript writing.		
Signature 		Date	14 / 04 / 2023

Supervisor Confirmation

By signing the Statement of Authorship, you are certifying that the candidate made a substantial contribution to the publication, and that the description described above is accurate.

Supervisor name and title: Prof. Stephen Fletcher		
Supervisor comments 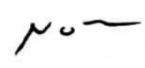		
Signature 	Date	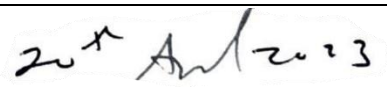

This completed form should be included in the thesis, at the end of the relevant chapter.

Chapter 4

Information transduction via controllable chemical waves

Chapter 4

Information transduction via controllable chemical waves

The work in this chapter was undertaken in collaboration with Anthonius Engwerda.

4.1 Introduction

4.1.1 Communicating information by different means

Society is hugely reliant on the transduction and storage of information. Major advancements in the storage of information have been made over the past century and most information is now stored in magnetic, optical or semiconductor-based technology.[1,2]

The most significant advance for information *transduction* was Hertz's discovery that electromagnetic waves could be generated in the laboratory in 1888. This has had extraordinary practical consequences and much modern communication still uses such waves,[3] for example radio transfers information through space and relies directly on electromagnetic waves being generated and detected. As such, electromagnetic waves are a key technology for transducing information and enable widely used modern communication methods. In nature, cellular systems rely on molecules for data storage and signalling. Genetic information is stored in DNA, whilst signals are transferred *via* messengers such as neurotransmitters, hormones and mRNA, with information often structurally encoded in these molecules.[4,5]

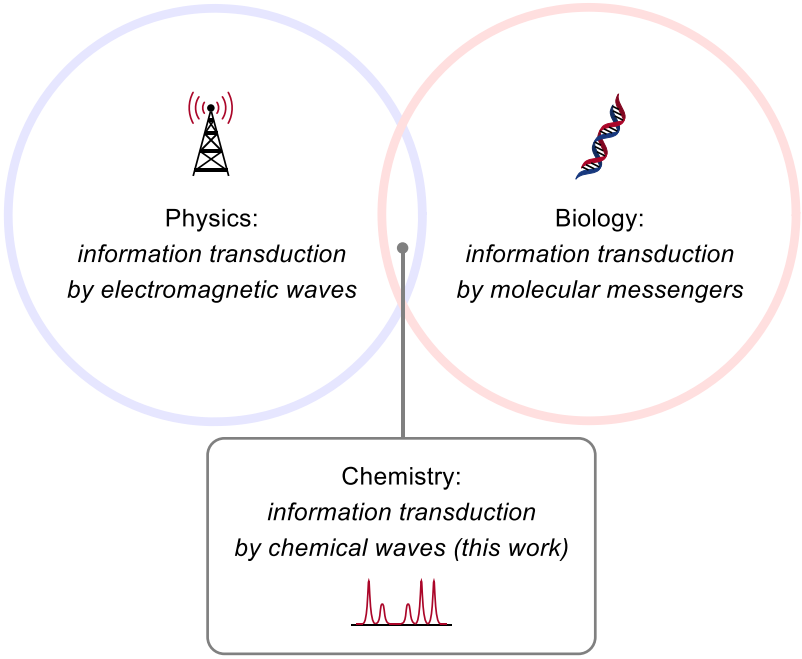

Figure 4.1: Different means of information transduction using principles from physics, chemistry and biology. This work, a new chemical technology, relates to principles of both biology and physics and offers an alternative way to transduce information

Chemical systems which transduce information through waves may enable technologies which interface with the world in new ways and raises the possibility of combining molecular information transfer seen in biology with the programmable waves of physics and engineering (Figure 4.1). Inputs which are transduced into controlled chemical waves could be directly measured as concentration or by engaging in further processes to obtain a readout (Figure 4.2a). Besides signalling or informational applications, demonstrating control over the output of reaction networks may allow the development of new systems of increased complexity and novel functions.

4.1.2 Oscillators for information transduction

A chemical oscillator is a logical starting point for transducing information for several reasons. As described in Section 3.1, oscillators are driven systems which, in theory, can switch between states in a sustained repeated pattern. Like electromagnetic waves or pules of neurotransmitters, these properties allow for the representation of information in the way the oscillations propagate and potentially allow for continuous readout or decoding. Because they arise from fairly complex systems which require chemical or physical feedback and a constant source of energy to propagate,

oscillating systems are unusually sensitive compared to traditional reactions. Whilst sometimes a practical drawback, this makes them innately responsive to input variables. Thus far, oscillating chemical systems have not been well explored for the purpose of information transduction and wide ranging control over their output has not been demonstrated, with some of the most sophisticated examples experiencing dampening or operating only in a narrow range of conditions.[6] Additionally, there is intense recent interest in (bio)chemical oscillators but contemporary systems tend to rely heavily on continuously stirred tank reactors (CSTR) to drive the phenomenon.[7,8] This could raise practical limitations to the outputs that can be produced and less constrained oscillators will possibly enable the most interesting applications.

4.2 Aims

The aim of this work is to take advantage of the responsive oscillating system described in Chapter 3 to generate specific waves of chemical concentration that encode information. Through the controlled manipulation of reaction parameters in real time, we propose this oscillator could be a proof of concept for a chemical-based technology for the transduction of information. By exploring the reaction variable space, we will demonstrate how distinct waveforms can be created and by tuning multiple variables more intricate levels of information encoding should be accessible.

4.3 Results and Discussion

4.3.1 System overview

Chapter 3 described a chemically fuelled system capable of sustained oscillations.[9] Uniquely, this system will oscillate as long as fuel is added to the system and sufficient starting materials from the outset. In contrast to some other recent chemical oscillators,[7,8] observing oscillations does not rely on having a fixed composition of starting materials or maintaining reactant concentrations in a flow reactor. The system is centred around thiol-disulfide chemistry in a biphasic reaction as described in Chapters 2 and 3 (Figure 4.2b). Under certain conditions this network of feedback processes shows periodic growth and decline in the concentration of **3** and other molecular species. These

changes in concentrations, or chemical waves, can be used as an output or signal and measured by liquid chromatography.

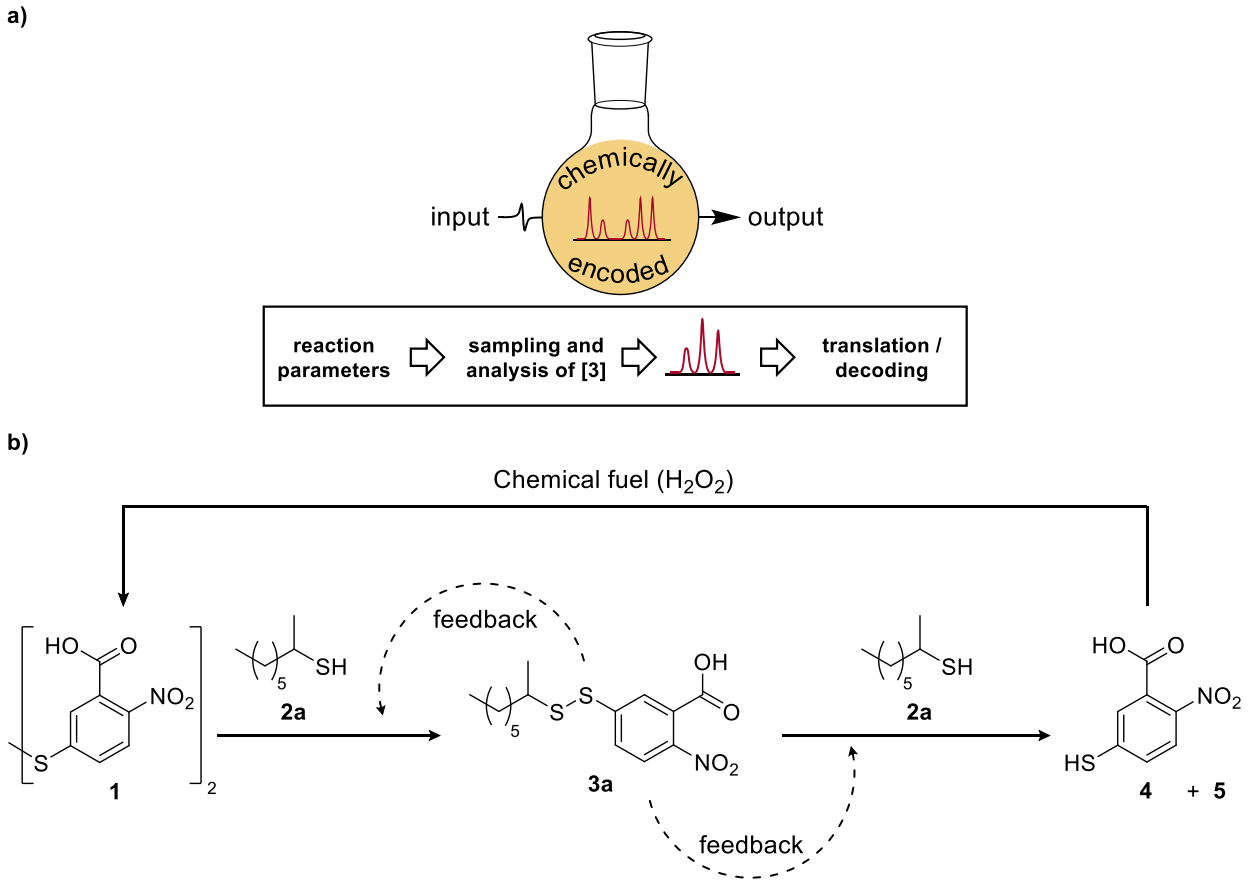

Figure 4.2: The concept of signal transduction via controllable chemical waves where input stimuli are converted into output data. c. The system: a chemically fuelled network which generates highly controllable concentrations of species (see Chapters 2 and 3 for details[9]).

4.3.2 A waveform generator

We reasoned that the ability to tightly control the output of waves would be key to transducing information which could potentially serve as the basis of advanced functional systems, including communication devices. Using the oscillating system described in Chapter 3 as a starting point, we set out to identify variables that would reliably allow us to produce different shapes, amplitudes and frequencies. We found that i) the rate of chemical fuel supply and ii) the rate of stirring, allowed us to modulate the frequency and amplitude as measured by the concentration of **3** (see Figure 4.3).

Disulfide **1** is a limiting reagent in the system whose concentration is itself limited by the continuous H_2O_2 supply. The formation of **3** is strongly dependent on the concentration of **1** and so adding

more H_2O_2 increases both the formation rate of **3** and the maximum concentration of **3**. When **3** is able to reach higher concentrations, more thiol (**2**) is solubilised in the aqueous phase, causing the destruction of **3** to be faster as well. As a result of these increased rates, the period of the peaks is shorter and the system resets sooner (the concentration of **3** tending to zero). Overall, this results in sharper, higher amplitude waves due to the greater supply of H_2O_2 (Figure 4.3a-c).

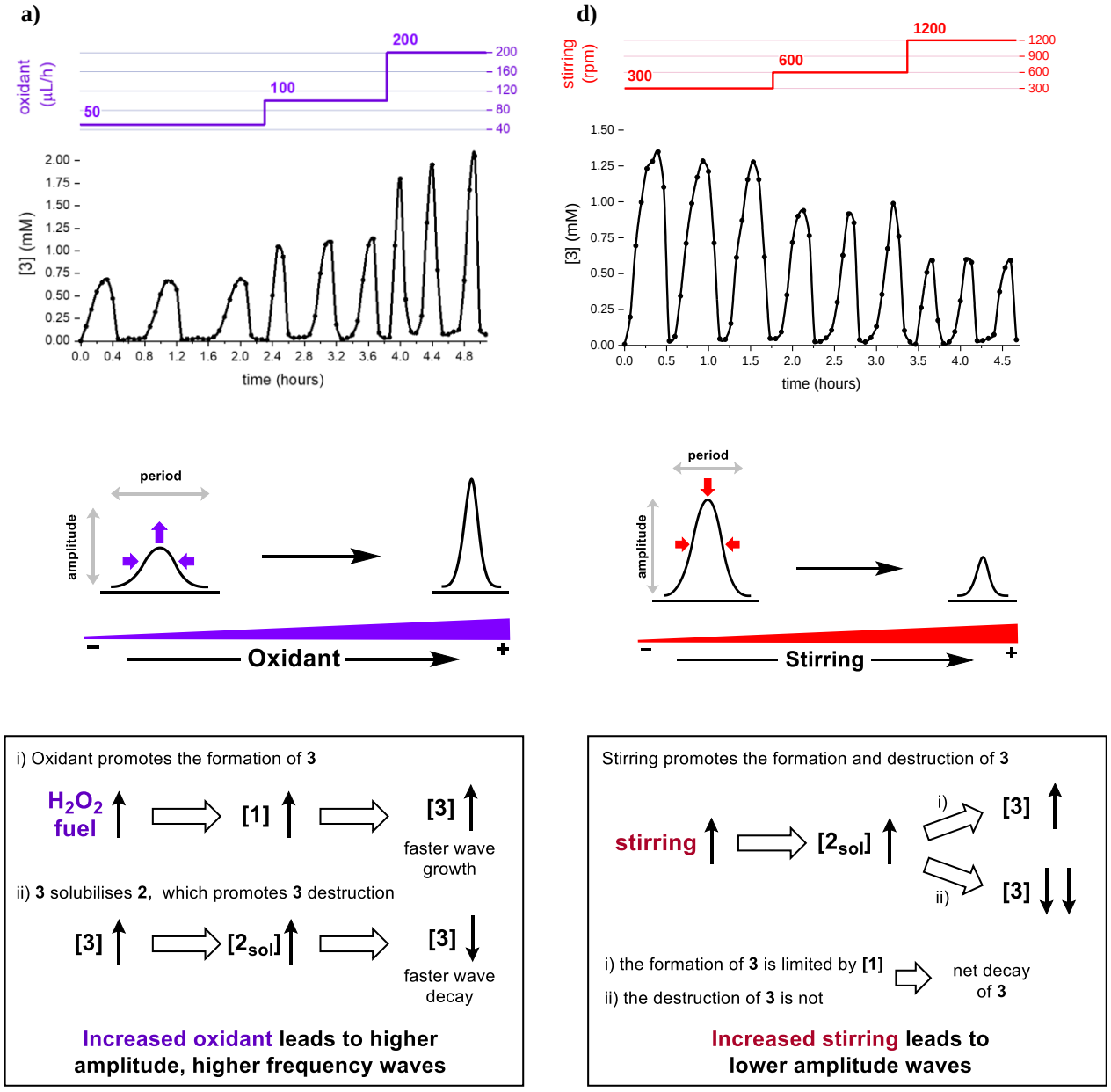

Figure 4.3: Changing input variables allows control over the waveforms in time. a-c) oxidant supply: as the chemical fuel supply is increased, growth in both amplitude and frequency is observed. H_2O_2 (0.56 M) is injected by syringe pump at the indicated rate (50, 100 and 200 µL/h) while stirring at 800 rpm; d-f) stirring rate: faster stirring decreases wave amplitude. Reactions were stirred at the indicated speed (300, 600 and 1200 rpm) while injecting H_2O_2 (0.56 M) at 100 µL/h. Further details may be found in the Experimental Section 7.4.2.

The concentration of **3** is also sensitive to the rate of stirring as stirring mixes the phase separated reactants. The underlying relationship between stirring and concentration is slightly more subtle as there are counteracting effects. Higher rates of stirring give rise to an increase in the interfacial surface area through blending of the layers, resulting in greater exposure of reactants in the aqueous layer to reactant **2**. Consequently, while increased mixing promotes the formation of **3**, it also increases the destruction of **3** because both processes rely on the presence of non-polar **2**. It should be noted that while changes to the stirring rate do affect the rates of both formation and destruction processes, the *maximum* rate of **3** formation is always limited by the rate of H_2O_2 supply. At higher stirring rates, the rate of destruction exceeds the rate of formation at a lower concentration of **3**, and so the apex of the [**3**] pulse is reached sooner (see Figure 3.17, Chapter 3 for an illustration of how the reaction rates evolve over time). Overall, the increased amount of solubilized thiol ($\mathbf{2_{sol}}$) at higher stirring speeds lowers the amplitude of the waves, as **3** destruction becomes a more dominant process (Figure 4.3d-f). It is worth noting that although the waveforms in Figure 4.3d appear sharper with increasing stirring rate, it would not be accurate to say that the frequency of the oscillations increases when adjusting this variable as the increased amounts of $\mathbf{2_{sol}}$ actually increases the lag period between waves, compensating for the sharpening.

To summarise, increasing the oxidant supply from 50 μL/h to 100 μL/h and then 200 μL/h results in distinctly sharper and taller peaks after each change (Figure 4.3a). Conversely, increasing the stirring rate from 300 rpm to 600 rpm and then 1200 rpm produces sharper peaks of lower amplitude (Figure 4.3d). The control achieved over the amplitude and period of individual pulses of molecular concentration means that the system does not simply oscillate but is able to respond to different inputs in order to reversibly access a wide continuum of wave forms of chemical concentration. These waves can be sustained for many hours and altered reversibly *in situ*, allowing real time changes to the output.

4.3.3 Signalling via chemical waves

Being able to control waveforms inspired us to use them to encode data in a way similar to how radio waves operate. As a simple proof of principle of a signalling application, we used Morse code to translate peaks into a meaningful output. Changing one variable (oxidant supply) in a single experiment gives access to two distinct peak types that can be assigned as either a dot (•) or a dash (–), while switching off the syringe pump defines a break. Suppling H_2O_2 at 135 μL/h gives a short waveform (dash –), while 300 μL/h gives taller peaks defined here as a dot (•) (Figure 4.4). Any letter in the alphabet can readily be accessed in this way and sequences of waveforms can be converted into words using a standard Morse code chart.

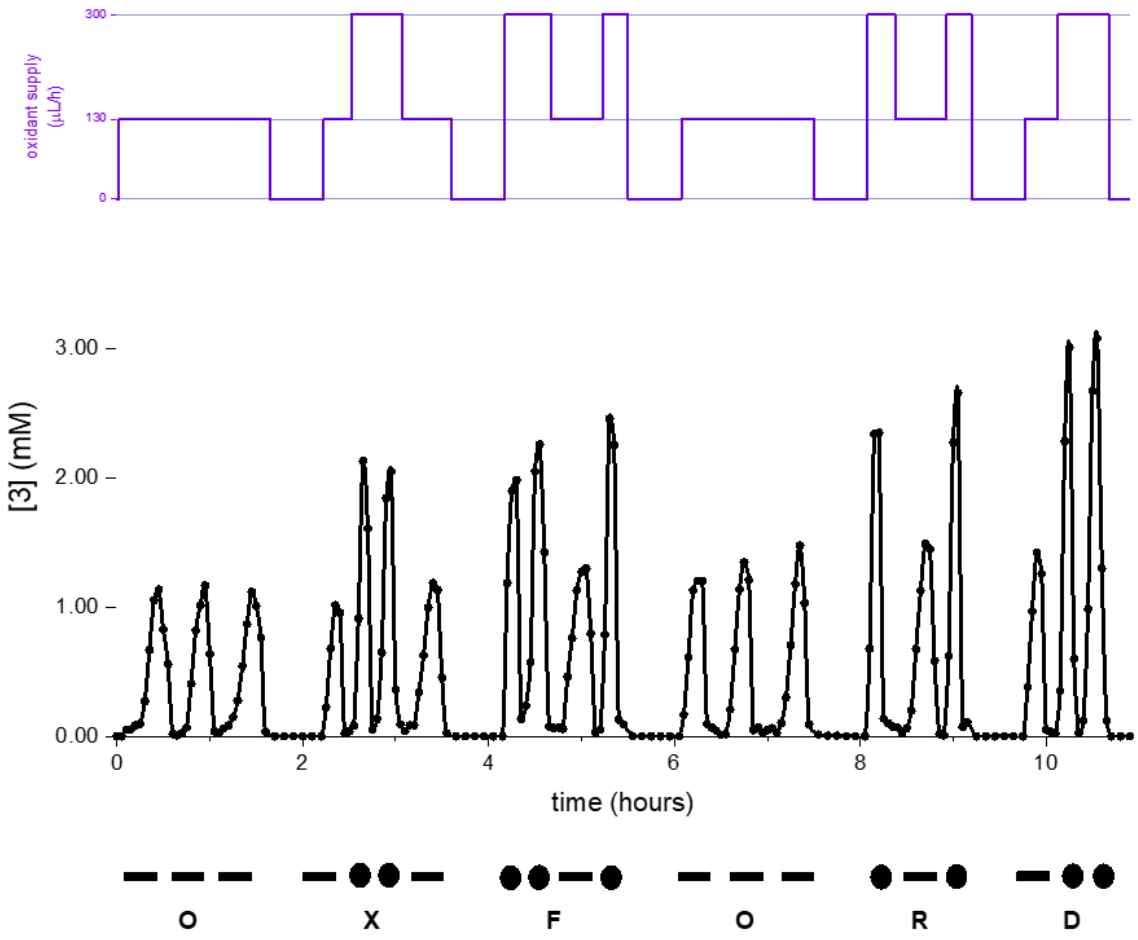

Figure 4.4: Continuous encoding of data in chemical waves in a single experiment. Using chemical fuel supply as the input variable, two distinct waveform outputs can be achieved: a short broad waveform (H_2O_2 supply rate = 135 µL/h, dash –) and a tall, sharp waveform (H_2O_2 supply rate = 300 µL/h, dot •). Translation of the waveforms using Morse code into a word (Oxford) completes the transduction of information via chemical waves.

Theoretically, more peak types that those shown in Figure 4.4 could be accessed by control of oxidant levels (e.g. four different oxidant addition rates could induce peaks of four different shapes). However, waveform control using oxidant addition rate alone is limiting because increasing the oxidant flow increases both the frequency and amplitude of the waves. This hinders modulation of either frequency or amplitude independent of the other. To increase the complexity of the encoded data, and thus the information density of the waves, we considered exploiting more than one experimental variable at a time, to allow independent control over both peak characteristics.

To control both frequency and amplitude, we incorporated the stirring rate as the second input variable. Since increasing the stirring rate impacts the wave output in a different way to the oxidant supply (increased stirring rate decreases amplitude, whereas higher oxidant supply increases both frequency and amplitude), a larger spectrum of frequency and amplitude combinations become feasible. For example, by changing the two inputs simultaneously we have produced four distinct waveforms, each defined by their unique amplitude and period (see Figure 4.5).

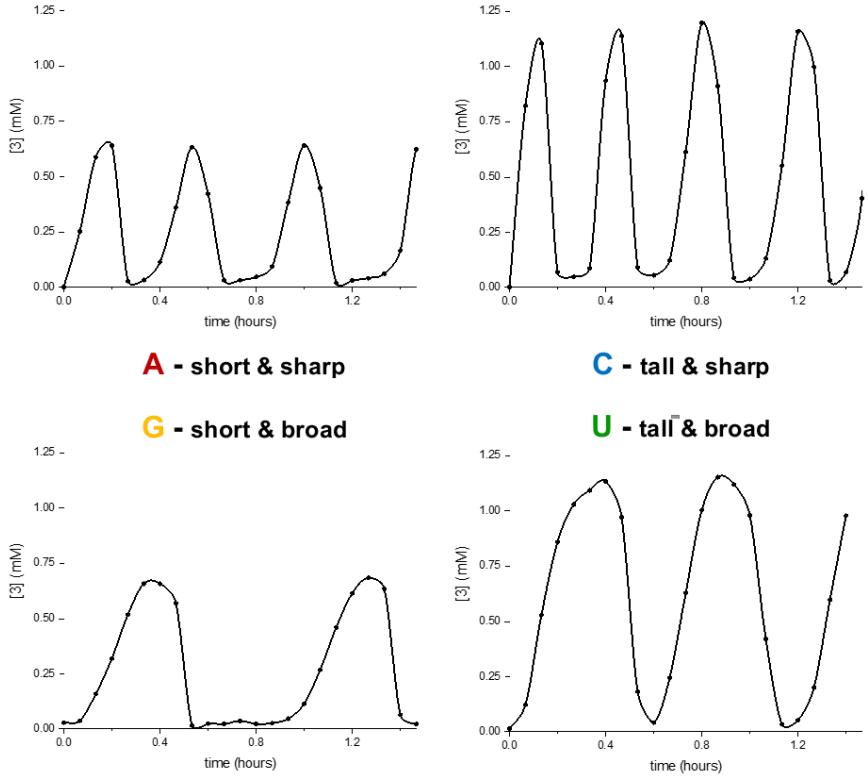

Figure 4.5: Increasing the information density of the chemical waveforms. Exploiting the different effects of the control variables (stirring rate and oxidant supply) on the frequency and amplitude of the waves, increases the accessible output of the chemical waves. Experiments were run according to the general oscillating procedure (see Experimental section 7.4.2) with the following settings for stirring and H_2O_2 supply: A-type waves: 1200 rpm, 90 µL/h; C-type waves: 1200 rpm, 160 µL/h; G-type waves: 600 rpm, 50 µL/h and U-type waves: 300 rpm, 80 µL/h.

The ability of our system to form and destroy molecular species in a controlled manner is reminiscent of biological systems, where the presence of signalling molecules (such as hormones) is tightly controlled in time. Biological systems expend great amounts of energy to build and sustain these communications infrastructures, allowing them to be adaptable, responsive to external stimuli and capable of amplifying signals biochemically. Emulating a biological language this time, each

waveform can be assigned a nucleobase: adenosine (**A**), cytosine (**C**), guanine (**G**) or uracil (**U**). **C** and **U** waveforms both have a maximum amplitude ranging 1.0-1.25 mM whilst **A** and **G** waveforms are shorter with an amplitude consistently in the range 0.50-0.75 mM. Each pair of peaks is further divided into a broad peak type and a sharp peak type, overall giving four identifiable outputs (Figure 4.5).

With these four waveforms optimized it was then possible to assemble a specific sequence of peaks for translation of the genetic lettering into a protein. Inspired by the messenger function of mRNA in cells we created triplets of waveforms (codons) in separate encoding experiments for translation. Each codon is composed of three peaks (nucleobases) and corresponds to a natural amino acid or stop signal, *e.g.* **GGA** = glycine. Taking a string of these codons together we chemically encoded the proteogenic structure of the nonapeptide hormone oxytosin,[10] imitating the transduction of these genetic instructions to a ribosome (Figure 4.6).

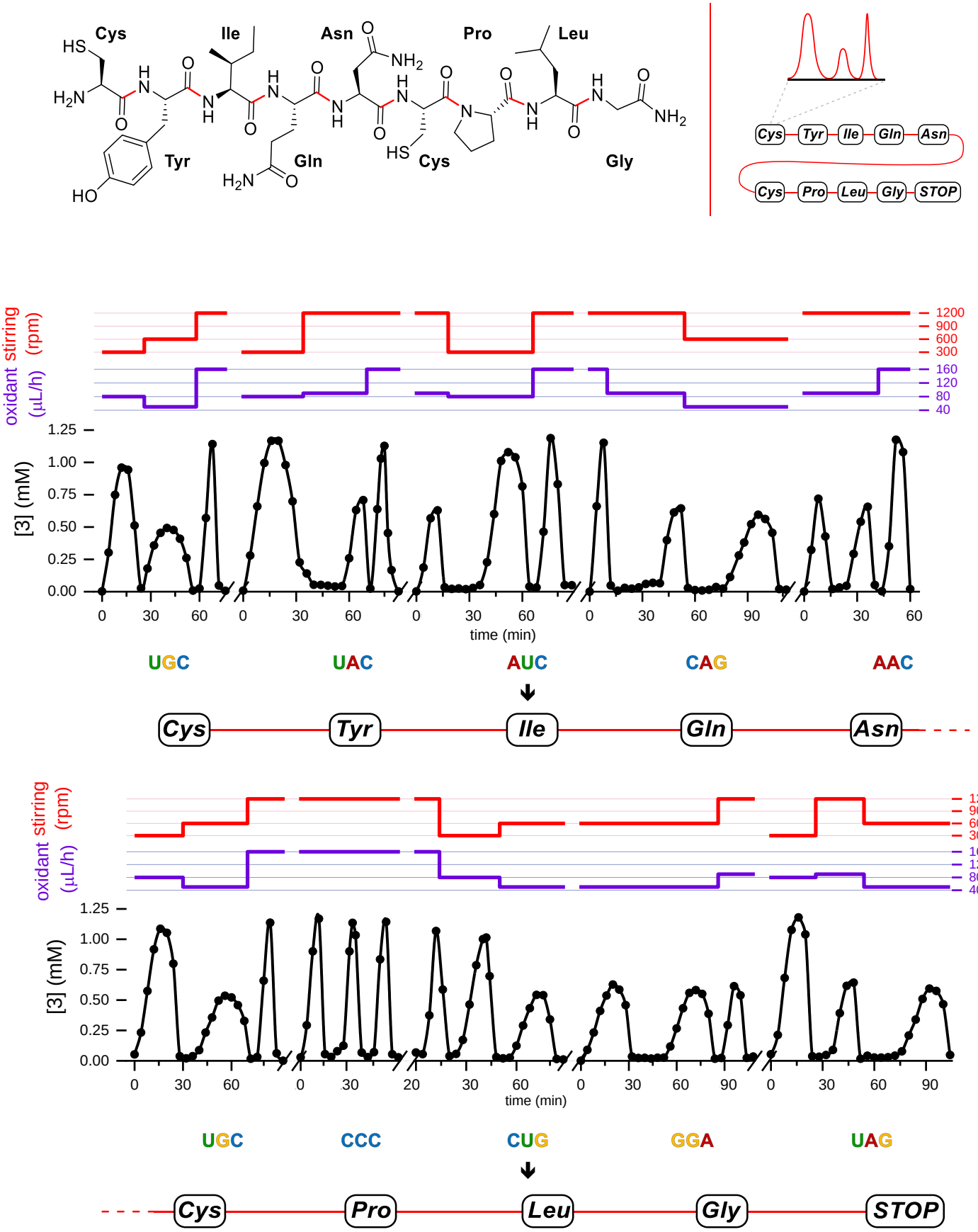

Figure 4.6: The responsiveness of the system to changes in both stirring rate and oxidant supply allows access to discrete wave types (changed amplitude and period) with an assigned meaning. This enables the encoding of amino

acid sequences using four unique outputs, corresponding to the four RNA bases. Using a standard RNA codon table, these chemical waves can be translated to the primary structure of the peptide hormone oxytosin.

2.4 Conclusions

In summary, we present a unique, chemical means of transducing information using a tightly controlled waveform generator that responds to chemical fuel. While previously studied oscillating chemical reactions (most notably the BZ reaction), have allowed distinct functions such as chemical computing[11] and data storage,[12,13] using sequences of chemical waves for data transduction is as yet undemonstrated. By exploiting the underlying processes of a chemical oscillator, we have created a new functional system which can obtain high control over the appearance of waveforms. Setting reaction parameters to different, discrete values results in changes in the frequency and amplitude of these oscillations, bearing close similarities to the use of Fourier transformations for data processing. Changing these reaction parameters during a (single, uninterrupted) reaction modulates the chemical wave sequence in real time, producing waveforms that encode information. The customization and assignment of meaning to these waveforms unlocks the potential to represent many types of data, such as in a computing or biocompatible context. The versatility of our system enables the encoding of interpretable communications (Morse code) and instruction-like outputs (mRNA).

The prevalence and importance of molecular messaging in biological systems makes the modelling of these processes a key objective for anyone trying to build synthetic cells. Here we emulate nature's capacity for signal transduction and in addition, our system displays oscillations across different length scales, whereas most previous oscillating reactions are centred on molecular species only. We believe the chemical nature of this technology has the potential to interface well with, and perhaps be incorporated as components into, emerging informational technologies such as molecular sensing and data storage. This discovery may also inspire new approaches to the bottom-up fabrication of signalling networks in synthetic cells. Further attempts to show bioinspired

functions with our oscillating system are discussed in Chapter 5, where spatial control of molecules with the oscillator is examined.

References

1 Freeman, L. *The History of Data Storage*. 1st edn, (CreateSpace Independent Publishing Platform, 2017).

2 Hilbert, M. & López, P. The World's Technological Capacity to Store, Communicate, and Compute Information. *Science* **332**, 60-65 (2011). https://doi.org:doi:10.1126/science.1200970

3 Mulligan, J. F. Heinrich Hertz and the Development of Physics. *Physics Today* **42**, 50-57 (1989). https://doi.org:10.1063/1.881211

4 Weng, G., Bhalla, U. S. & Iyengar, R. Complexity in Biological Signaling Systems. *Science* **284**, 92-96 (1999). https://doi.org:10.1126/science.284.5411.92

5 Goldbeter, A. Dissipative structures in biological systems: bistability, oscillations, spatial patterns and waves. *Philosophical Transactions of the Royal Society a-Mathematical Physical and Engineering Sciences* **376** (2018). https://doi.org:10.1098/rsta.2017.0376

6 Leira-Iglesias, J., Tassoni, A., Adachi, T., Stich, M. & Hermans, T. M. Oscillations, travelling fronts and patterns in a supramolecular system. *Nat. Nanotechnol.* **13**, 1021-1027 (2018). https://doi.org:10.1038/s41565-018-0270-4

7 Semenov, S. N. *et al.* Autocatalytic, bistable, oscillatory networks of biologically relevant organic reactions. *Nature* **537**, 656-660 (2016). https://doi.org:10.1038/nature19776

8 Semenov, S. N. *et al.* Rational design of functional and tunable oscillating enzymatic networks. *Nat. Chem.* **7**, 160-165 (2015). https://doi.org:10.1038/nchem.2142

9 Howlett, M. G., Engwerda, A. H. J., Scanes, R. J. H. & Fletcher, S. P. An autonomously oscillating supramolecular self-replicator. *Nat. Chem.* **14**, 805-810 (2022). https://doi.org:10.1038/s41557-022-00949-6

10 du Vigneaud, V., Ressler, C. & Trippett, S. The Sequence of Amino Acids in Oxytocin, with a Proposal for the Structure of Oxytosin. *J. Biol. Chem.* **205**, 949-957 (1953). https://doi.org:10.1016/S0021-9258(18)49238-1

11 Parrilla-Gutierrez, J. M. *et al.* A programmable chemical computer with memory and pattern recognition. *Nat. Commun.* **11**, 1442 (2020). https://doi.org:10.1038/s41467-020-15190-3

12 Cafferty, B. J. *et al.* Storage of Information Using Small Organic Molecules. *ACS Cent. Sci.* **5**, 911-916 (2019). https://doi.org:10.1021/acscentsci.9b00210

13 Rutten, M. G. T. A., Vaandrager, F. W., Elemans, J. A. A. W. & Nolte, R. J. M. Encoding information into polymers. *Nat. Rev. Chem.* **2**, 365-381 (2018). https://doi.org:10.1038/s41570-018-0051-5

Statement of Authorship for joint/multi-authored papers for PGR thesis

To appear at the end of each thesis chapter submitted as an article/paper

The statement shall describe the candidate's and co-authors' independent research contributions in the thesis publications. For each publication there should exist a complete statement that is to be filled out and signed by the candidate and supervisor **(only required where there isn't already a statement of contribution within the paper itself).**

Title of Paper	Information transduction via fuel-controlled chemical waves
Publication Status	~~Published~~ ~~Accepted for Publication~~ ☑ Submitted for Publication ~~Unsubmitted work written in manuscript style~~
Publication Details	Michael G. Howlett, Anthonius H. J. Engwerda and Stephen P. Fletcher. n/a

Student Confirmation

Student Name:	Michael Howlett		
Contribution to the Paper	Performed experiments and analysed data. Wrote and edited the manuscript. Co-author (A. Engwerda) also performed experiments, took part in data analysis and writing of the manuscript. Contributed equally to M Howlett. Co-author (S. Fletcher) supervised the project and contributed to data analysis and manuscript writing.		
Signature 		Date	14 / 04 / 2023

Supervisor Confirmation

By signing the Statement of Authorship, you are certifying that the candidate made a substantial contribution to the publication, and that the description described above is accurate.

Supervisor name and title: Prof. Stephen Fletcher		
Supervisor comments 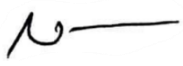		
Signature 	Date	

This completed form should be included in the thesis, at the end of the relevant chapter.

Chapter 5

Oscillation-mediated mass transport

Chapter 5

Oscillation-mediated mass transport

The work in this chapter was undertaken in collaboration with Antonius Engwerda.

5.1 Introduction

5.1.1 Controlled transport of molecules

The controlled movement of molecules is an intensely researched area, approached by those studying molecular machines, lipid membranes, materials chemistry and ion sensing.[1,2] Well known classes of systems capable of directing movement include mechanically threaded molecules,[3-8] transmembrane shuttles[9-12] and intramolecular arm-like transporters.[13,14] Biased or unidirectional movement and performing work against a gradient are prized objectives in this field. Particularly advanced examples of this have been reported by the Leigh and Stoddart groups where macrocycles are pumped onto surface-bound threads.[15,16]

These topics have been well reviewed in recent years and new pumps driven by light, electricity and chemical fuels are frequently being reported.[1,2,17-19] However, the majority of designs continue to incorporate mechanically interlocked molecules such as rotaxanes, although many unique platforms for transport likely exist.

5.1.2 Coupling processes to oscillations

When coupled to other systems, oscillators can control the timing of chemical and physical processes and this is one of the key attractions to designing these complex systems.[20,21] For this reason, oscillators are a potentially good starting point for new designs of transporter as they may be able to control how frequently cargo is delivered. Oscillators also tend to have unique feedback mechanisms and this underlying complexity may lead to ways to achieve biased directionality in transport systems.

Coupling of oscillators to secondary processes can also amplify the oscillations from a molecular effect to one observed at different length scales, for example as seen in the work by Lagzi et al. where a pH oscillator controls the aggregation behaviour of gold nanoparticles.[22]

5.2 Aims

The work in this chapter aims to use the oscillating system described in Chapter 3 to transport molecular cargo on the macroscopic scale. The idea is that micelles will be created in response to chemical fuel (H_2O_2) and will take up hydrophobic molecules into their interior. This molecular cargo can then move with the micellar containers within phases and across interfaces. This makes use of the unique features of our oscillating system, as it produces and relies upon transient supramolecular compartments. In a scenario with multiple immiscible phases, the presence and absence of the micelles (as determined by the oscillator) allows for cargo to periodically move between these phases. This control of the temporal and spatial properties in this system may provide the basis for a number of transport-related functions.

5.3 Results and Discussion

5.3.1 Initial findings: coupling oscillations to the uptake of chemicals

Chapter 3 described how reaction between disulfide **1** and thiol **2** produces surfactant **3** which self-assembles. The resulting supramolecular aggregates solubilise hydrophobic thiol **2** in the aqueous phase. Micelles have a closed hydrophobic interior which can solubilise organic molecules which are not very water soluble (*i.e.* those lacking strong dipoles, charges or hydrogen bonding capabilities). Given their crucial role as nano-compartments that enclose **2**, we envisioned the micelles could also uptake other species during an active oscillating reaction.

To this end, we identified indigo dye as a water-insoluble candidate which may associate with the micelles and provide a convenient visual readout of the effect during a reaction due to its colour. Indigo was added to a solution of **1** in TRIS buffer prior to the beginning of oxidant supply but was not fully soluble in the organic layer (**2**) or aqueous layer (see Experimental section 7.5.1). Once

the oscillating reaction had started the indigo was seen to periodically switch between a phase separated (purple) state and an emulsified (brown) state over time (see Figure 5.1). In the absence of micelles, the solution is orange due to aromatic thiol **4**. By monitoring with UPLC, we could demonstrate that the concentration of **3** and the colour of the reaction are highly correlated (see Figure 5.1). When micelles are formed, indigo is gradually, and transiently, taken into the aqueous layer until the micelles disappear again.

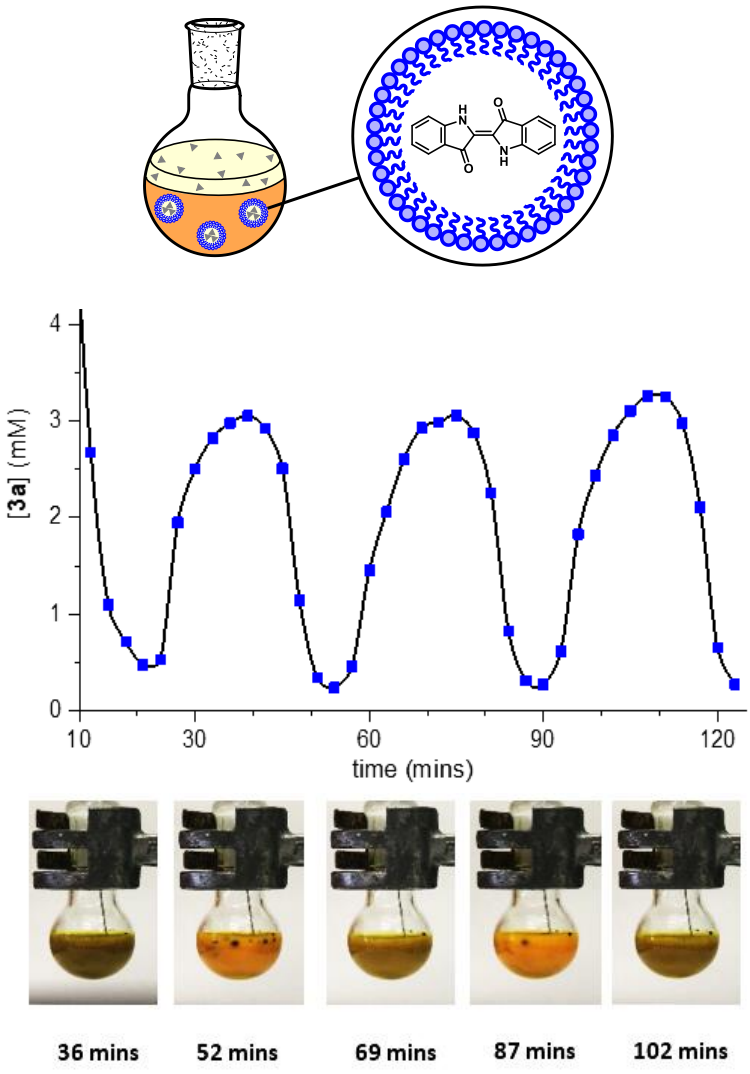

Figure 5.1: Coupling the oscillations to the uptake of chemicals. When surfactant **3** is produced in the oscillator, it solubilises the hydrophobic dye indigo so that it changes the reaction mixture from orange to brown. When the surfactant (and micelles) disappear, the indigo phase-separates, restoring the native orange colour of the reaction. In this way, oscillations in [**3**] are translated into visual oscillations. Details may be found in the Experimental section 7.5.1

This experiment clearly indicated that there was some potential for the micelles to control the location of organic molecules and also the timing of uptake events, regulated by the frequency of the micellar oscillations. This also allowed us to harness the fuelled supramolecular system to give oscillations which are visible on the macroscale, without a separate assay or analysis.

5.3.2 Re-optimisation of the oscillator in a new vessel

Based upon the encouraging observations from including indigo in an oscillating reaction, a new setup for the oscillator was devised. This involved arranging different immiscible phases so that hydrophobic molecules could be transported from an organic phase (LHS, Figure 5.2a), through a central aqueous phase and into a second organic phase (RHS, Figure 5.2a). With the micelles being produced in the central aqueous region, it was hoped that they could encapsulate organic material and, on the basis of a concentration gradient or another source of directionality, would provide the vehicle for mass transport. Just as in the indigo experiment, it was expected that the repeated growth and decay of micelles would cause the transport to be switched on and off in response to the oscillations (see Figure 5.2b).

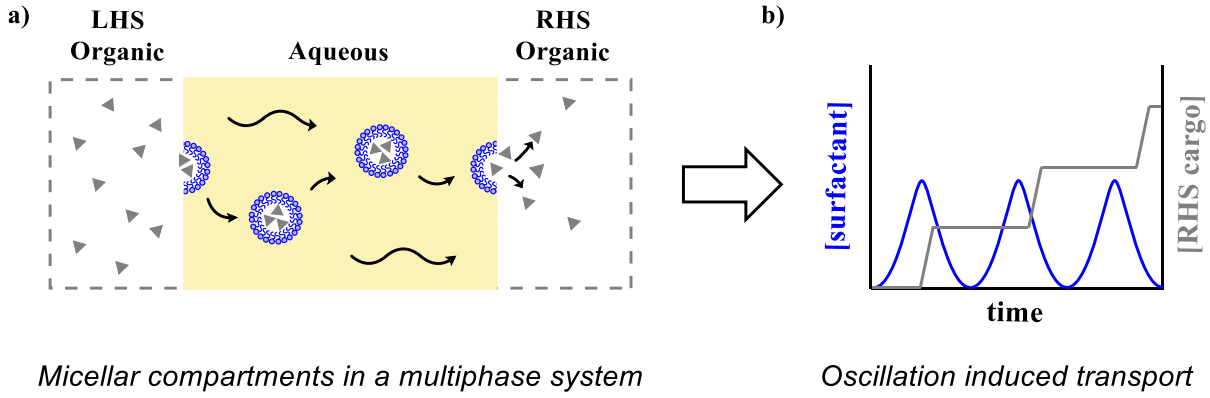

Figure 5.2: a) Micelles provide the vehicle for the transport of organic compounds in a multiphase system; b) Oscillations in the concentration of a transient surfactant will show switchable cargo transport

To create this separation of liquid phases we opted for a U-shaped piece of glassware as pictured in Figure 5.3a. This item is commercially available and manufactured with consistent specification (size, glass thickness) between different units – a factor that can be critical for biphasic reaction kinetics. Furthermore, the dimensions of this U-tube were convenient for us to transplant our

existing (10 mL) round bottom flask method into, as opposed to much larger vessels which might require vast amounts of chemical material or very small vessels where vessel consistency may be more challenging and low reaction volumes would hinder our ability to sample the reactions.

As illustrated in Figure 5.3b, the U-tube shape is ideal for arranging organic solvents which are less dense than water above a central aqueous phase. From left to right, these phases are: a *donating organic layer* of alkyl thiol, aqueous TRIS buffer (0.5 M, pH 9.0) and a *receiving organic layer* of dodecane.

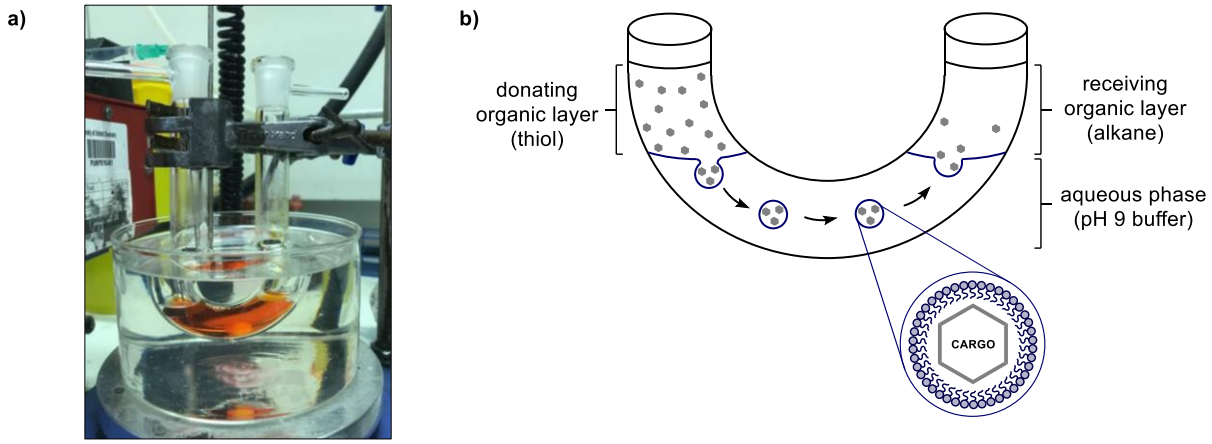

Figure 5.3: The U-tube setup for oscillation-mediated transport. a) The glass U-tube pictured as used for transport experiments, immersed in an oil bath and with a H_2O_2 addition needle into the central aqueous phase; b) A schematic of the three phases used in the U-tube apparatus.

In our biphasic oscillating reaction there are several practical considerations for its setup. These include choosing an appropriate volume and geometry of the flask, how to affect reliable stirring, how to introduce the oxidant flow and how to periodically remove aliquots by microsyringe without disturbance. With a 10 mL round bottom flask these can be addressed quite straightforwardly by prioritising well centred stirring and not impeding the stir bar with H_2O_2 addition or sampling needles. In a U-shaped vessel each of these issues becomes more challenging.

Volumes: the volume of the aqueous buffer must be high enough to separate the two organic phases and to allow needles to reach it for adding H_2O_2 and removing aliquots. However, the larger the aqueous phase, the further the thiol-aqueous phase boundary is from the source of stirring in the aqueous layer, which slows interfacial reactions.

Stirring: one stark contrast with reactions in a round bottom flask is that the organic and aqueous phases in the U-tube cannot be blended together by stirring, as this would make spatial control of molecular cargo impossible – the phases must interact but remain distinct. A further problem with using a U-shaped flask is that without a rounded bottom, the traditional cylindrical and oval stir bars tend to spin chaotically, even at low stirring rates. This meant stirring isn't reproducible and the organic phases are significantly, and randomly, disturbed. We found that using more centrosymmetric disk-like stir bars resolved this problem, albeit providing generally weaker stirring.

Biphasic reaction rate: to account for the gentler stirring required in the U-tube apparatus, we found that using a less hydrophobic thiol (heptanethiol instead of octanethiol) increased the rate of biphasic reaction. Also, for this reason, hindered secondary thiols were avoided and the reactions were run at an elevated temperature of 50 °C. Conveniently, 1-heptanethiol is commercially available and could act as the donating organic layer.

As the points above highlight, transplanting the oscillating reaction from a round bottomed flask to a new vessel requires consideration of several practical parameters and trial and error to optimise the new requirements against each other.

5.3.3 Proof of concept and reproducibility

After exploring the variables described in the previous section, a set of conditions for producing repeatable oscillations in the U-tube was achieved (see Figure 5.4). It was intended that experiments would show 3+ pulses where cargo molecules are transported from the donating layer to the receiving layer. To conveniently follow the transport kinetics in a single session this required oscillations in [**3**] with a short period and total monitoring time of 3-5 hours. Fortunately, the oscillating waves produced in the U-tube are sharp and have a rapid destruction stage, presumably due to the nucleophilic primary thiol and high stirring rates used.

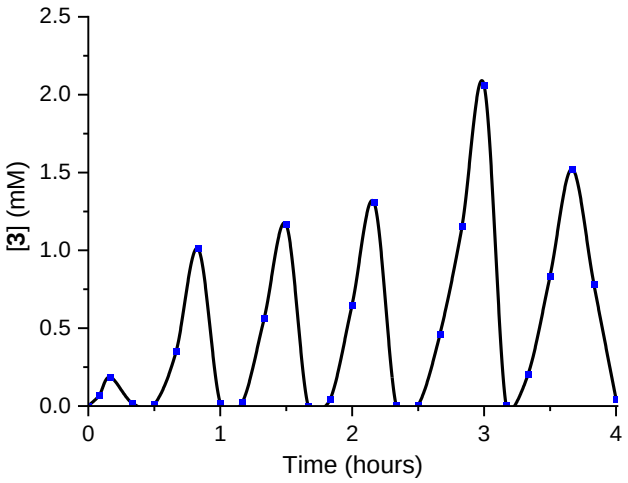

Figure 5.4: Early example of [**3**] oscillations within the U-tube apparatus, following optimisation for the new vessel geometry and constraints. See Experimental section 7.5.1 for details

Figure 5.4 shows the oscillating concentration of surfactant **3** over time within the U-tube setup using 1-heptanethiol as the donating organic layer and n-dodecane as the receiving organic layer. Aside from some minor period and amplitude drift over time caused by dialkyldisulfide **5** (see discussion in Chapter 3) this experiment produces well separated pulses of surfactant with reasonably consistent peak shape.

The same cannot be said for all experiments conducted within the U-tube, in fact, the irreproducibility of the reaction kinetics is a significant drawback of the new conditions and/or the vessel geometry. For example, Figure 5.5 shows three oscillating reactions which were set up identically in the U-tube with the optimised conditions. Despite efforts to control practical aspects of the reactions, there are still large deviations between the kinetics. It is expected that the main sources of this irreproducibility are: i) without the organic and aqueous layers being well mixed, the interfacial processes that the oscillating system relies upon are not as dominant or consistent and ii) the spatial restrictions on the different phases in the U-tube amplifies the sensitivity towards some variables (*e.g.* height above stirring plate, layer disturbances).

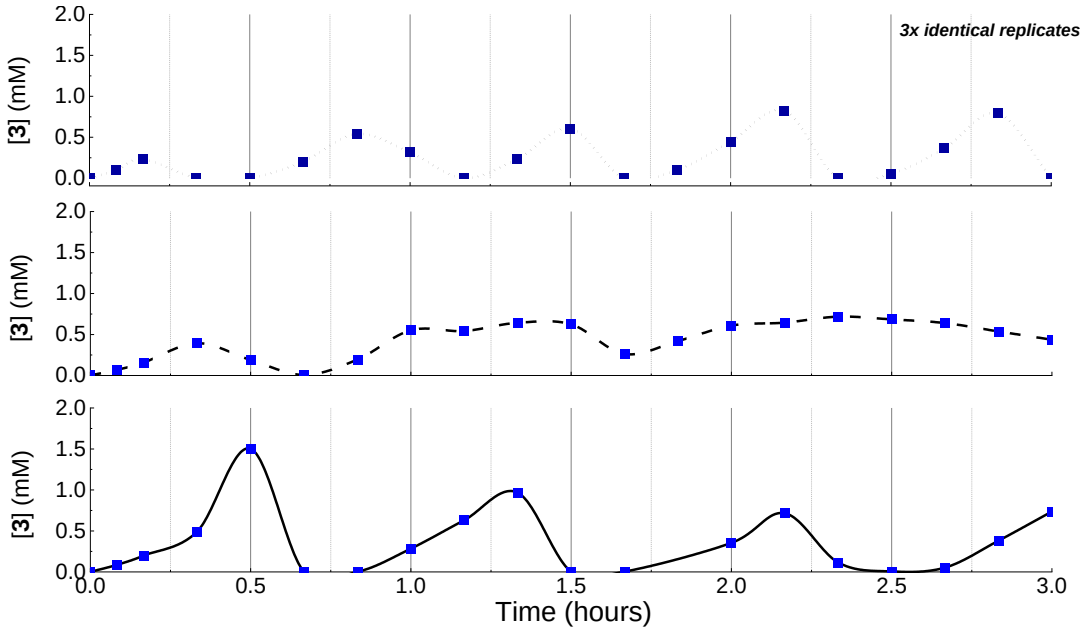

Figure 5.5: Irreproducible kinetics within the U-tube under the same experimental conditions. See Experimental section 7.5.1 for details

Incremental improvements in the reproducibility of the U-tube kinetics were found by: i) ensuring the stirring of the aqueous layer was smooth and optimal before initiating the reaction, ii) having a consistent arrangement of the glassware relative to the stirring plate and iii) by building techniques to minimise layer disturbances during setup and monitoring.

The challenge of obtaining reproducible, quality kinetic data was expected to increase as molecular cargo was introduced into the system as experiments could 'fail' in multiple new ways. To demonstrate oscillation-mediated transport, we were primarily looking to fulfil two conditions: the aqueous oscillations should be reasonably consistent (by UPLC kinetics) and the cargo should undergo controlled transport (by HPLC kinetics). Note: it was necessary to use HPLC for the analysis of the organic layer(s) and solutes as highly non-polar solvents (hexane, THF) were not compatible with the UPLC instrument. With new compounds in the system, it was important to consider the solubility and any undesired reactivity of the cargo. These would potentially cause uncontrolled background transport or could poison the oscillator, for example if stable surfactant-like species were formed.

To first test the concept we opted for coumarin 6 as the molecular cargo. This compound is stable to thiol and alkaline buffer and considerably hydrophobic. These properties, as well as its bright colour, were favourable in our system. Gratifyingly, when the U-tube oscillator was run using a concentrated solution of coumarin 6 in 1-heptanethiol we were able to visually observe transport of the dye (Figure 5.6). This observation was enhanced by irradiation with blue light (445 nm) which revealed that the cargo was delivered in discrete bursts to the receiving organic layer, in response to pulses of surfactant (Figure 5.6, middle photo).

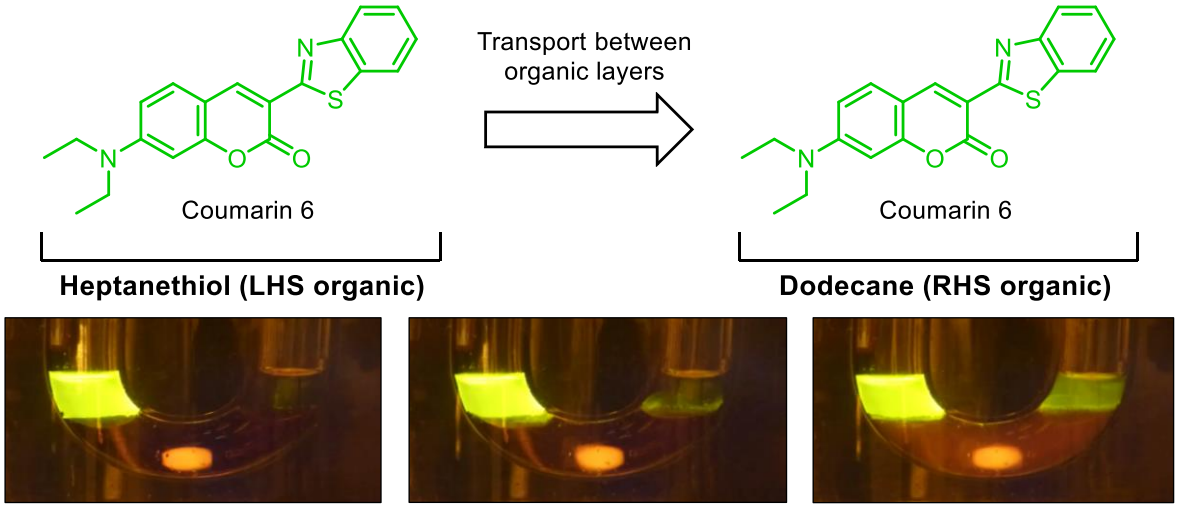

Figure 5.6: Transport of hydrophobic fluorescent dye coumarin 6 within the U-tube. When surfactant **3** was produced, the movement of coumarin 6 from the left hand side (LHS) organic layer to the right hand side (RHS) layer can be clearly seen, illuminated by 445 nm blue light

5.3.3 Transport of hydrophobic cargo

With the successful demonstration of coumarin 6 transport we moved onto selecting other hydrophobic cargo for testing. We were confident that simple hydrocarbons and polyaromatics would be transported readily in the system and therefore focused instead on more interesting molecules with some polar functional groups.

Our search brought us to molecules such as in Figure 5.7 which are recognisable compounds found in biology and that have a significant hydrophobic character. The transport of these compounds was monitored by HPLC analysis of aliquots from the receiving organic layer. Unfortunately, we soon discovered that the success with coumarin 6 was very fortuitous as none of the candidates in Figure

5.7 could be reliably transported within the U-tube. Despite the high carbon content of estrone, estradiol and melatoin, these compounds were too soluble in the aqueous buffer phase and showed significant background transport, uncontrolled by the frequency of the oscillations. Testing of cholecalciferol and β-carotene revealed different issues with our system. Both molecules are highly hydrophobic and could not move between phases without surfactant, however they underwent significant degradation in the presence of thiol **2** or **4**. Aside from depleting the cargo, this also created an emulsion of the organic and aqueous phases, presumably as the breakdown products were surfactant-like. This caused us to avoid transporting compounds with multiple alkenes or electrophilic sites.

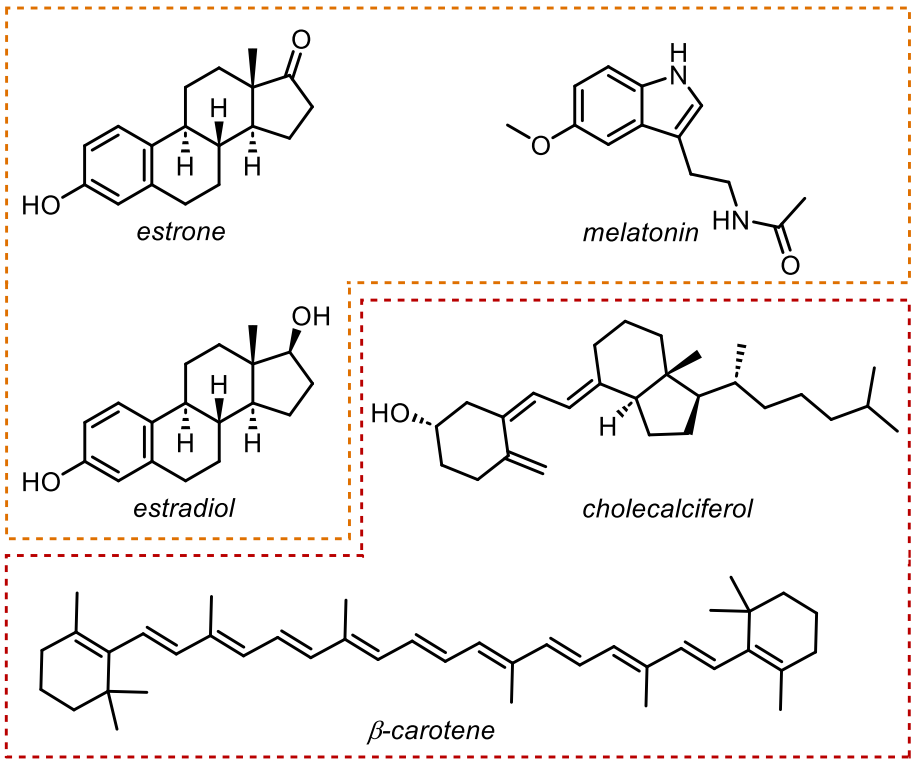

Figure 5.7: Incompatible cargo candidates due to being either too water soluble (orange box) or unstable to the reaction conditions (red box)

Fortunately, with these lessons in mind, we were able to identify several cargo molecules which underwent controlled transport and were compatible with the oscillating system (Figure 5.8). These molecules were largely apolar but a limited number of ketone, hydroxyl and ester functional groups could be tolerated. Analysis of the receiving organic layer revealed that the cargo was delivered in

stepwise portions in sync with the production of surfactant **3** by the oscillating reaction. Interestingly, as the concentration of **3** grows there is not a gradual transport of cargo but instead the portion is delivered only after the surfactant peak is reached and **3** is then experiencing net breakdown. It's possible this is due to a sudden breakdown of micelles at a critical point and release of its contents – a feature of the oscillator that was mechanistically discussed in Chapter 3. Pleasingly, the plateaus in [cargo] between transport events in Figure 5.8 signify that there is not significant background transport without surfactant control.

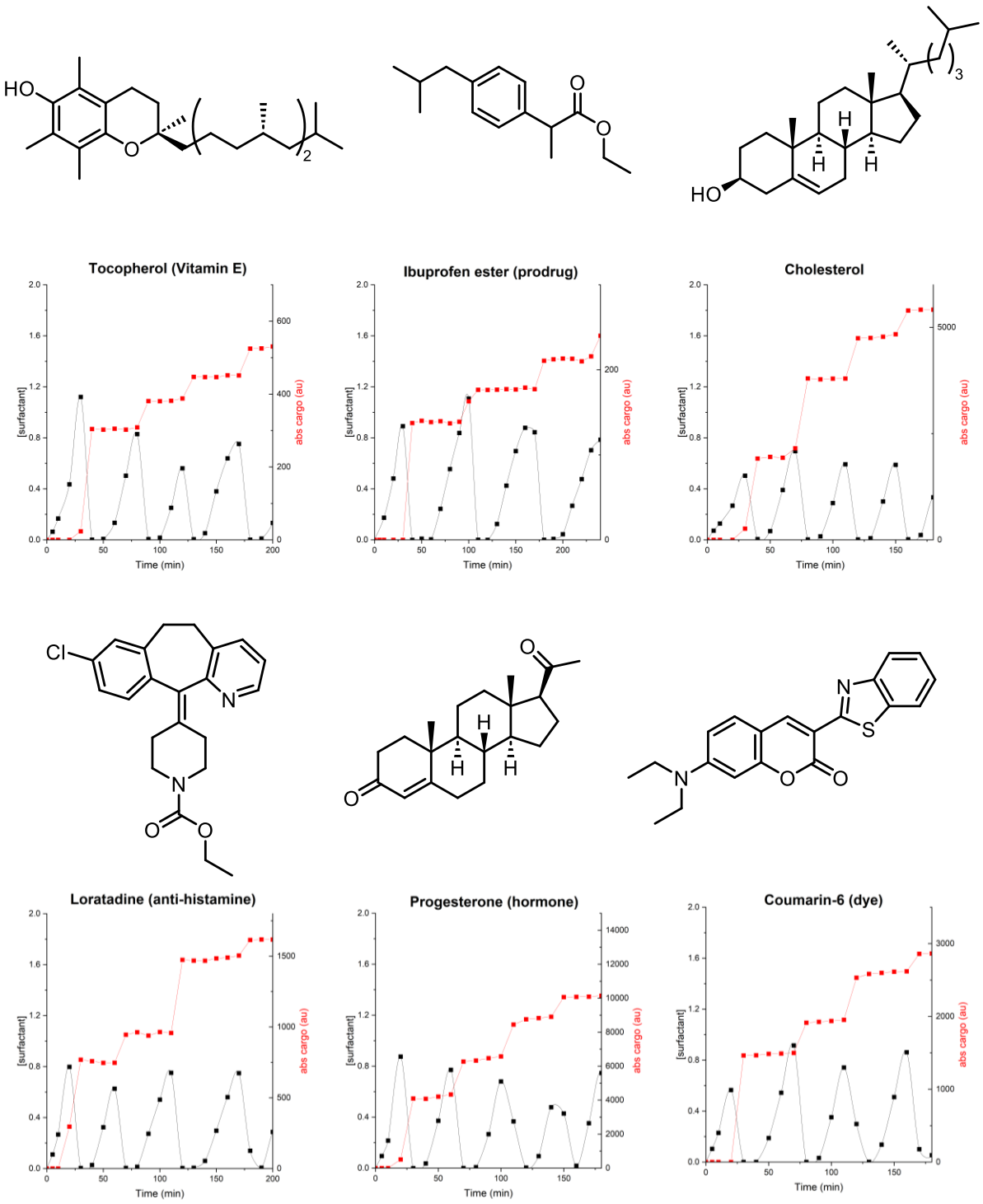

Figure 5.8: Successful cargo molecules which show clear oscillation-controlled transport within the U-tube. All six of these candidates were found to be sufficiently apolar and stable to show stepwise transport from the donating organic layer of the U-tube to the receiving organic layer. Black circles: concentration of surfactant obtained by UPLC analysis. Red squares: amounts of transported cargo in the receiving organic layer, by HPLC analysis. See Experimental section 7.5.1 for details

5.3.4 Transport directionality

Although the transport of the compounds in Figure 5.8 proceeds well and is synchronised to the oscillating surfactant concentration, as was hoped, there remains questions of how this system operates. Specifically, we were interested in the directionality of the transport. For example, the cargo may i) move freely from both organic phases but have *net* transport from LHS to RHS due to the concentration gradient or ii) have a source of directionality, meaning the transport is truly one-way. These two scenarios could appear quite similar in the kinetic data from a regular transport experiment and so a control experiment was devised.

To compare the ability of the cargo to move from the LHS and RHS of the U-tube apparatus, both organic layers were charged with distinct molecules known to transport well. The oscillator was run under the optimised conditions for transport but using a solution of tocopherol/1-heptanethiol in the LHS and coumarin 6/n-dodecane in the RHS (Figure 5.9). This experiment gave a surprising result wherein there was no back-transport of coumarin 6 from the RHS organic layer, as judged visually (with 445 nm illumination) and by HPLC analysis of aliquots. Forward transport of the tocopherol from the LHS thiol layer was seen in this experiment, ruling out a problem with surfactant generation.

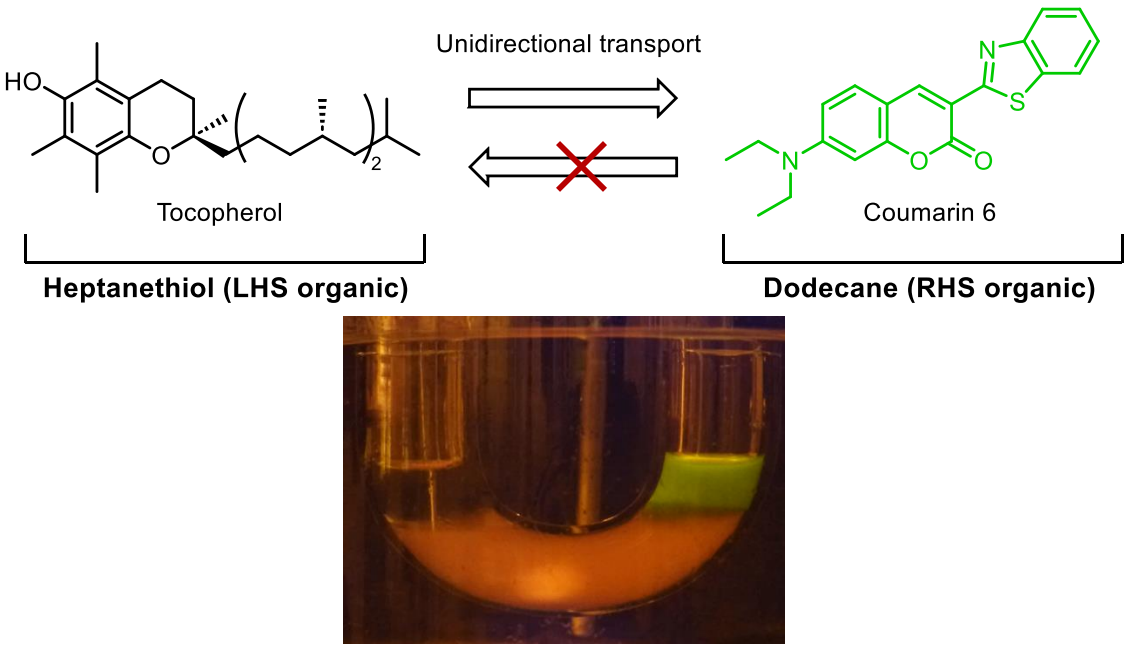

Figure 5.9: Control experiment to test the directionality of transport. Having tocopherol in the LHS layer and coumarin 6 in the RHS layer within the U-tube enabled the comparison of 'forward' and 'backward' transport whilst the oscillator was operating. No backward transport of the coumarin 6 was seen, indicating a strong bias in the direction of transport. See Experimental section 7.5.1 for details

We initially theorised that this unidirectionality may be due to the thiol-buffer interface and H_2O_2 addition needle being on the LHS of the U-tube, facilitating **3** formation near the donating organic layer. This may give rise to preferential growth of micelles on the LHS of the apparatus, where they can then uptake cargo before the micelles break down towards the RHS of the aqueous phase, away from the H_2O_2 source. We tested this theory by repeating the control experiment of Figure 5.9 but replacing compound **4** in the aqueous phase (the precursor to surfactant **3**) with a stable surfactant, SDS. This allowed us to examine whether the formation or metastability of **3** had a role in the directionality of transport. When using SDS we still observed clear unidirectional transport from the donating organic layer (thiol) to the receiving layer (dodecane). This indicated that some property of the experiment that was outside of the oscillating system was responsible for the directionality.

The current hypothesis is that the direction of transport is dictated by the relative polarity of the organic phases, and that the more hydrophobic organic phase will be the receiving layer. This could be because a solvent such as n-dodecane is less able to mix with the aqueous phase than 1-

heptanethiol and therefore cannot interact with micelles efficiently and is less likely to emulsify at the interface. This will be tested with control experiments in due course, for example by varying the organic layer solvents. Repeating the control experiment with SDS in the aqueous phase, but with both organic phases being n-dodecane should provide particularly valuable insight.

5.3.5 Transport-directed reactivity

Having shown that the oscillations in [**3**] can induce transport within the U-tube, we considered more advanced applications of the system. Our next objective was to use the transporter to control when and where reactions happen. This would involve the transport of cargo molecules which were no longer inert but would undergo specific reactions when coming into contact with reagents in the receiving organic phase (Figure 5.10). This would significantly push the complexity of multi-phase, out-of-equilibrium systems and may potentially inspire technology for manipulating liquids.

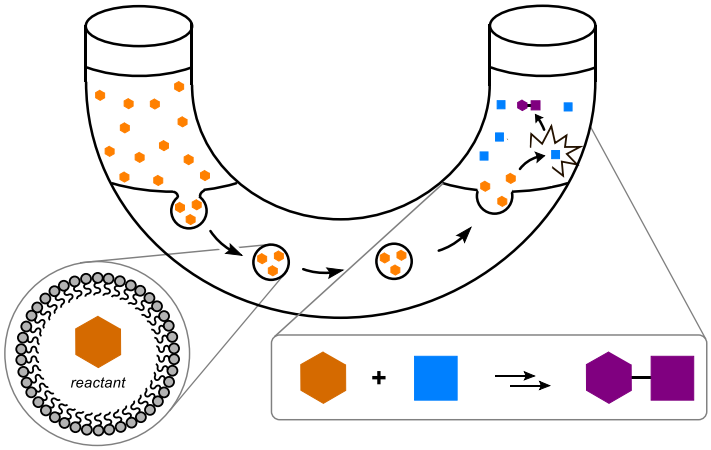

Figure 5.10: Transport-directed reactivity within the U-tube. The oscillating micelles deliver a reagent between the organic phases where it can undergo reaction with components in the receiving layer

This objective has similar challenges to those seen when initially introducing cargo into the oscillating system within the U-tube: new chemical components can have incompatibilities with the oscillator (*i.e.* compounds **1-4**) and may disrupt the phase behaviour in the system. To avoid these issues, both the reactive cargo and its co-reactant in the receiving layer should be chemically orthogonal to thiols, disulfides and tolerant to alkaline solution and the presence of H_2O_2.

Furthermore, the desired transformation should be rapid and free of significant byproducts, to prevent poisoning of the oscillator. A final requirement is that all new reactants and the product should be sufficiently hydrophobic that they don't move freely between the organic and aqueous phases in the U-tube. To satisfy these conditions we looked towards 'click'-type reactions as a starting point for transport-directed reactivity in the U-tube (see Figure 5.11).[23-26]

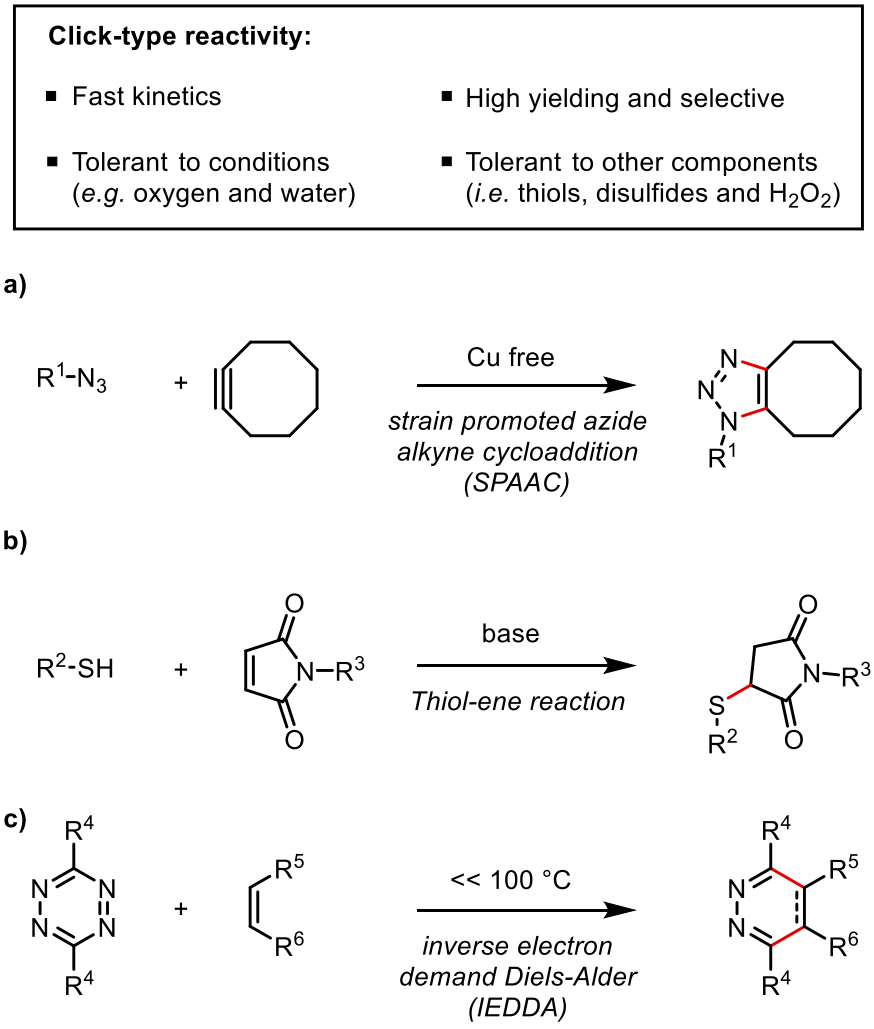

Figure 5.11: Orthogonal reactions which were thought potentially suitable to use in conjunction with the thiol-disulfide chemistry of the oscillator.

Copper catalysed and strain-promoted azide-alkyne cycloadditions (SPAAC) such as in Figure 5.11a are well known rapid, biorthogonal reactions[24] which may meet some of the above criteria for use in the transport experiments. However, SPAAC reactions were seen as a high risk option as both the azide and strained alkyne would need to be custom synthesised in order to be strongly

apolar and were expected to have some undesired reactivity with the electrophilic disulfide and concentrated thiol in the oscillator. We therefore abandoned azide-alkyne cycloadditions and sought other compatible reaction types.

We realised that coumarin 6, which had previously been a convenient component of the oscillator, could readily be synthesised from commercial organic precursors (**6** and **7**) and a piperidine catalyst by Knoevenagel condensation (see Figure 5.12). Mixtures of these precursors with piperidine in organic solvent (*e.g.* MeOH, EtOAc and hexane) quickly formed the bright green coumarin 6 product at room temperature within minutes. Unfortunately, this system ran into problems when attempting to find hydrophobic alternatives to piperidine for use in the U-tube, whilst maintaining the catalytic activity.

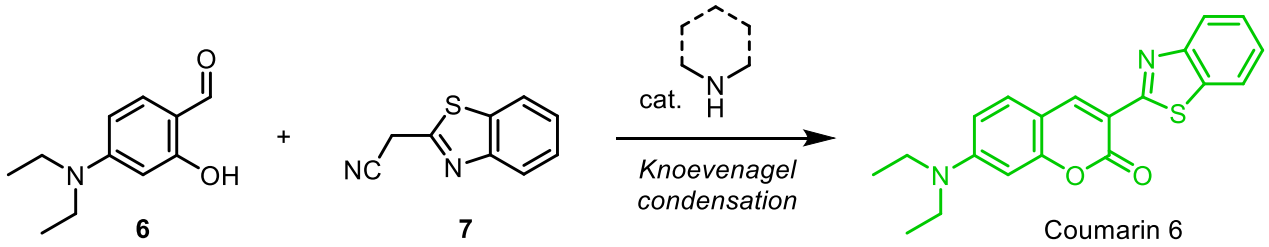

Figure 5.12: Knoevenagel condensation between commercial **7** and **8** to give coumarin 6

Numerous commercial primary, secondary, tertiary amines and anilines were tested as catalysts in the Knoevenagel reaction, a subset of which are shown in Figure 5.13a-d below. This revealed that a nucleophilic, secondary amine was essential for high reactivity (*i.e.* visual coumarin 6 formation within an hour at < 80 °C) and even a single adjacent methyl substituent slowed the condensation markedly. When the most active catalysts (piperidine and perhydroisoquinoline) were tested in the U-tube, these amines caused significant disruption and emulsification of the separated phases and surfactant **3** no longer showed reliable oscillations. It is thought that these polar amines ionised in the aqueous phase and promoted uncontrolled phase transfer.

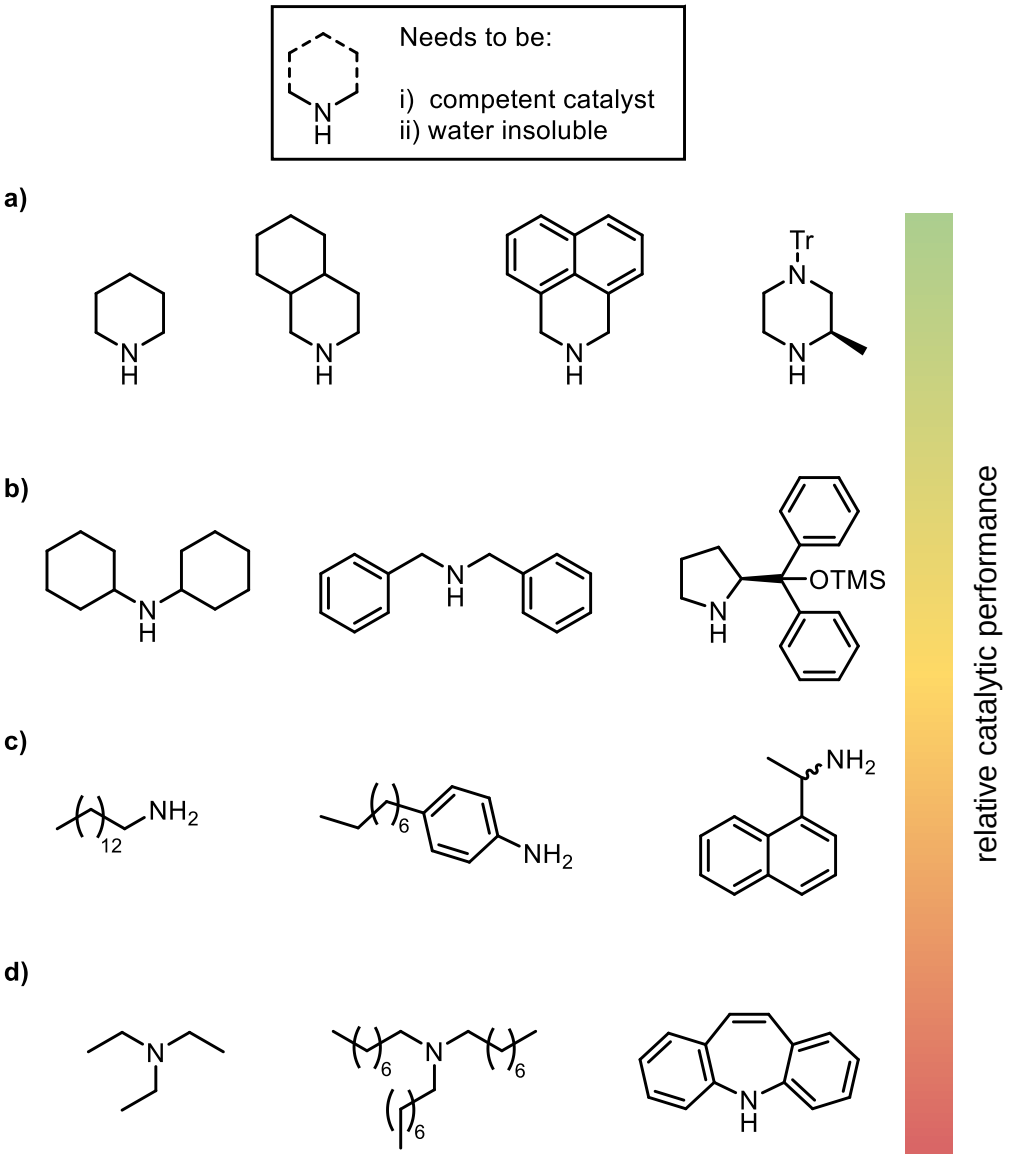

Figure 5.13: Selection of amines tested as catalysts in the Knoevenagel condensation. a) Secondary, unhindered amines were found to be the most active catalysts; b-c) sterically hindered and less nucleophilic amines performed poorly and d) tertiary and aromatic amines were unreactive except under very forcing conditions

Bespoke amine structures such as those in Figure 5.14 were proposed as alternatives to piperidine but their synthesis was considered uncertain and these amines may still have had amphiphilic character if ionised. For this reason, the Knoevenagel condensation approach was abandoned.

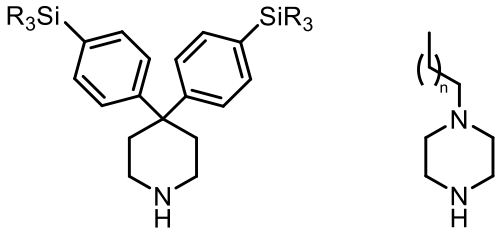

Figure 5.14: Proposed structures for highly hydrophobic, secondary amine catalysts

Inspired by our own use of maleimide to quench thiols when taking reaction aliquots for kinetic analysis, we next turned to the thiol-ene reaction shown in Figure 5.15. This approach would allow us to use the 1-heptanethiol already present in the oscillator as one of the reactants, negating some orthogonality issues. This thiol-ene reaction worked well in organic solvents (MeOH, DCM, EtOAc, hexane) in the presence of stoichiometric Et_3N, however when attempted in n-dodecane stirring over the alkaline TRIS buffer (without base), the thiol addition was sluggish and could not reach completion even at elevated temperatures.

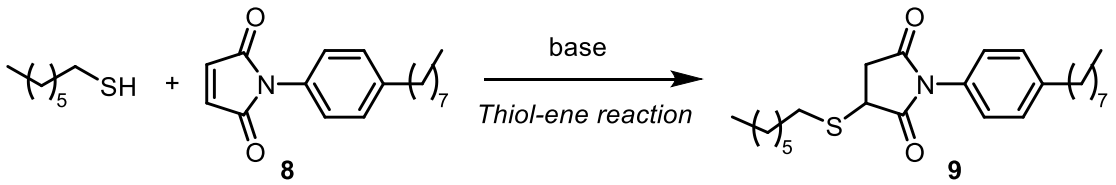

Figure 5.15: Thiol-ene reaction between 1-heptanethiol and maleimide **8** for use within the U-tube apparatus as a proof of concept of transport-directed reactivity

To solve this issue, it was necessary to introduce a catalytic or stoichiometric base into the organic receiving layer. However, it was important to avoid the earlier issues encountered with ionisable, water soluble amines in the Knoevenagel condensation. Fortunately, this time the thiol-ene reaction did not require a secondary amine and could be catalysed with n-trioctylamine. The thiol-ene reaction was taken forward to test within the U-tube apparatus, under the standard conditions for producing oscillating [**3**]. With 1-heptanethiol as the donating organic layer and a concentrated solution of maleimide substrate **8** and trioctylamine in n-dodecane as the receiving layer, it was possible to initiate the synthesis of succinimide **9** by oscillation mediated transport (Figure 5.16).

As shown in the kinetic data, the maleimide substrate **8** (grey line) is consumed in discrete steps and this is coupled with growth in the amount of succinimide **9** (purple line) measured in the dodecane by HPLC. This reactivity is synchronised with surfactant **3** production in the aqueous phase and plateaus in the kinetic data show there is negligible uncontrolled reactivity and that the thiol-ene reaction is rapid under the U-tube conditions.

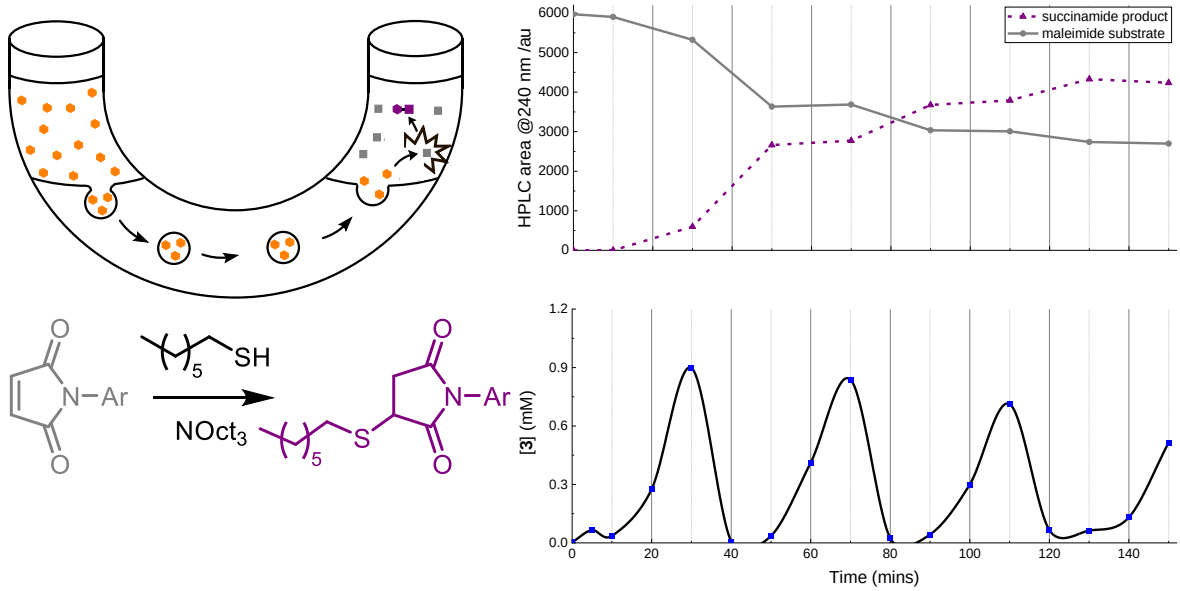

Figure 5.16: Proof of concept of transport-directed reactivity using a thiol-ene reaction. Oscillations in the concentration of surfactant **3** causes 1-heptanethiol to be periodically transported to the receiving organic layer which contained maleimide **8** and trioctylamine. The thiol-ene reaction is sufficiently fast to show stepwise growth of product **9**, explicitly linking transport of the thiol to reaction progress. See Experimental section 7.5.1 for details. Ar = 4-octylphenyl

This example was a satisfying proof of concept for transport-directed synthesis. Investigations into other reactions which could be orthogonal to the oscillator, such as inverse electron demand Diels-Alder reactions (IEDDA)[26] are ongoing (Figure 5.17).

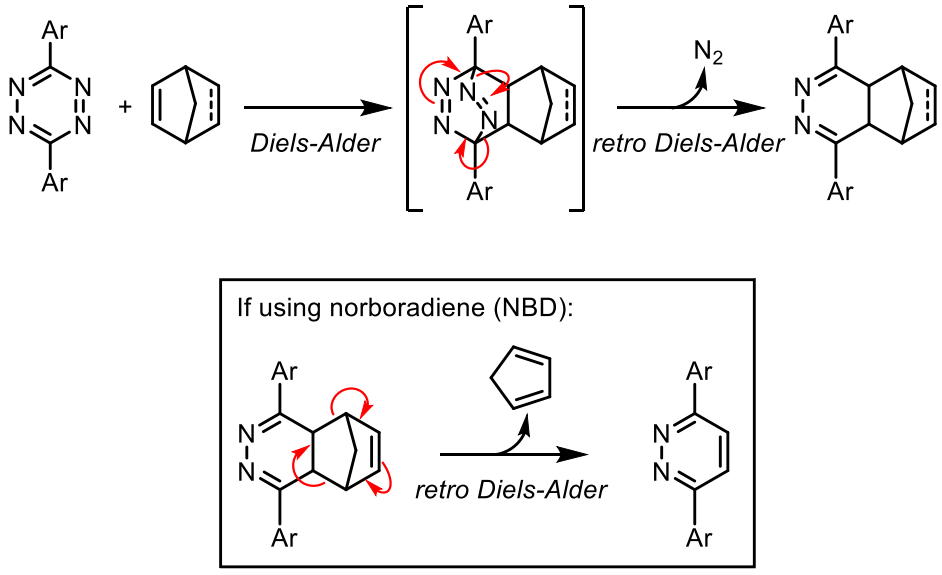

Figure 5.17: Inverse electron demand Diels-Alder reactions as a potential orthogonal reaction to demonstrate transport-directed reactivity. Reaction between an electron poor tetrazine and strained alkene could be viable (hydrophobic) substrates in the U-tube apparatus

5.4 Conclusions

To the best of our knowledge, our oscillating system is unique in being able to influence liquid phase behaviour and thereby promote certain physical processes. This has been demonstrated in this chapter by the simple reversible uptake of indigo dye into an aqueous layer as well as in a multi-liquid phase U-tube apparatus. Transplanting the surfactant oscillator from a round bottomed flask into a new vessel presented reproducibility challenges and various aspects of the reaction required reoptimisation (*e.g.* the stirring regime). The realisation of reliable oscillations in the U-tube provides confidence in the ability to use the system in other settings, such as a cuvette.

Provided the cargo is sufficiently apolar and inert, it is possible for oscillations within the U-tube to mediate time-controlled molecular transport between organic phases. This idea was extended to show transport-directed reactivity, although this generally was met with significant chemical incompatibilities.

It is not yet known what the exact applications of the discoveries in this chapter will be, although chemically driven systems that demonstrate effective spatiotemporal control provide excellent inspiration for future nanotechnology. Long term uses of chemically driven transporters such as this might be precise control over synthetic sequences (Figure 5.18) or the selective separation of chemical mixtures by transient micelles.

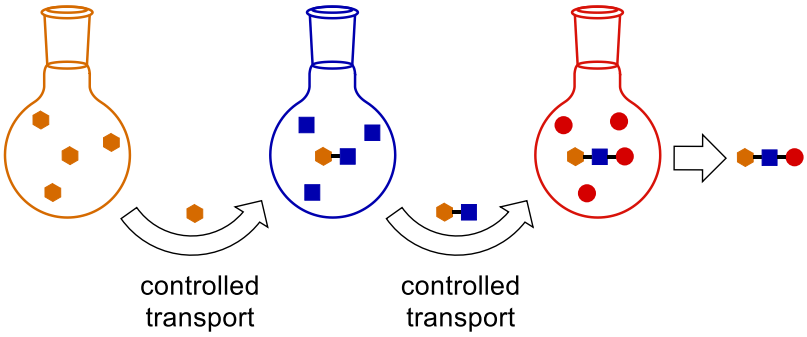

Figure 5.18: Chemical systems which can manipulate liquid phases and thereby control the location and timing of chemical reactivity may present technological opportunities in the future

References

1 Lancia, F., Ryabchun, A. & Katsonis, N. Life-like motion driven by artificial molecular machines. *Nature Reviews Chemistry* **3**, 536-551 (2019). https://doi.org:10.1038/s41570-019-0122-2

2 Aprahamian, I. The Future of Molecular Machines. *ACS Central Science* **6**, 347-358 (2020). https://doi.org:10.1021/acscentsci.0c00064

3 Binks, L., Tian, C., Fielden, S. D. P., Vitorica-Yrezabal, I. J. & Leigh, D. A. Transamidation-Driven Molecular Pumps. *Journal of the American Chemical Society* **144**, 15838-15844 (2022). https://doi.org:10.1021/jacs.2c06807

4 Guo, Q.-H. *et al.* Artificial Molecular Pump Operating in Response to Electricity and Light. *Journal of the American Chemical Society* **142**, 14443-14449 (2020). https://doi.org:10.1021/jacs.0c06663

5 Anelli, P. L., Spencer, N. & Stoddart, J. F. A molecular shuttle. *Journal of the American Chemical Society* **113**, 5131-5133 (1991). https://doi.org:10.1021/ja00013a096

6 Amano, S., Fielden, S. D. P. & Leigh, D. A. A catalysis-driven artificial molecular pump. *Nature* **594**, 529-534 (2021). https://doi.org:10.1038/s41586-021-03575-3

7 Corra, S. *et al.* Artificial Supramolecular Pumps Powered by Light. *Chemistry – A European Journal* **27**, 11076-11083 (2021). https://doi.org:https://doi.org/10.1002/chem.202101163

8 Canton, M. *et al.* Second-Generation Light-Fueled Supramolecular Pump. *Journal of the American Chemical Society* **143**, 10890-10894 (2021). https://doi.org:10.1021/jacs.1c06027

9 Kerckhoffs, A. & Langton, M. J. Reversible photo-control over transmembrane anion transport using visible-light responsive supramolecular carriers. *Chemical Science* **11**, 6325-6331 (2020). https://doi.org:10.1039/d0sc02745f

10 Shinkai, S., Nakaji, T., Ogawa, T., Shigematsu, K. & Manabe, O. Photoresponsive crown ethers. 2. Photocontrol of ion extraction and ion transport by a bis(crown ether) with a butterfly-like motion. *Journal of the American Chemical Society* **103**, 111-115 (1981). https://doi.org:10.1021/ja00391a021

11 Wezenberg, S. J. *et al.* Photomodulation of Transmembrane Transport and Potential by Stiff-Stilbene Based Bis(thio)ureas. *Journal of the American Chemical Society* **144**, 331-338 (2022). https://doi.org:10.1021/jacs.1c10034

12 Langton, M. J., Keymeulen, F., Ciaccia, M., Williams, N. H. & Hunter, C. A. Controlled membrane translocation provides a mechanism for signal transduction and amplification. *Nature Chemistry* **9**, 426-430 (2017). https://doi.org:10.1038/nchem.2678

13 Chen, J., Wezenberg, S. J. & Feringa, B. L. Intramolecular transport of small-molecule cargo in a nanoscale device operated by light. *Chem. Commun.* **52**, 6765-6768 (2016). https://doi.org:10.1039/c6cc02382g

14 Kassem, S. *et al.* Site-to-site peptide transport on a molecular platform using a small-molecule robotic arm. *Chemical Science* **12**, 2065-2070 (2021). https://doi.org:10.1039/d0sc05906d

15 Thomas, D. *et al.* Pumping between phases with a pulsed-fuel molecular ratchet. *Nature Nanotechnology* **17**, 701-707 (2022). https://doi.org:10.1038/s41565-022-01097-1

16 Feng, L. *et al.* Active mechanisorption driven by pumping cassettes. *Science* **374**, 1215-1221 (2021). https://doi.org:doi:10.1126/science.abk1391

17 Corra, S., Curcio, M., Baroncini, M., Silvi, S. & Credi, A. Photoactivated Artificial Molecular Machines that Can Perform Tasks. *Adv. Mater.* **32**, 1906064 (2020). https://doi.org:https://doi.org/10.1002/adma.201906064

18 Feng, Y. *et al.* Molecular Pumps and Motors. *Journal of the American Chemical Society* **143**, 5569-5591 (2021). https://doi.org:10.1021/jacs.0c13388

19 Qiu, Y., Feng, Y., Guo, Q.-H., Astumian, R. D. & Stoddart, J. F. Pumps through the Ages. *Chem* **6**, 1952-1977 (2020). https://doi.org:10.1016/j.chempr.2020.07.009

20 Epstein, I. R. Coupled chemical oscillators and emergent system properties. *Chem. Commun.* **50**, 10758-10767 (2014). https://doi.org:10.1039/C4CC00290C

21 van Esch, J. H., Klajn, R. & Otto, S. Chemical systems out of equilibrium. *Chem. Soc. Rev.* **46**, 5474-5475 (2017). https://doi.org:10.1039/C7CS90088K

22 Lagzi, I., Kowalczyk, B., Wang, D. W. & Grzybowski, B. A. Nanoparticle Oscillations and Fronts. *Angew. Chem. Int. Ed.* **49**, 8616-8619 (2010). https://doi.org:10.1002/anie.201004231

23 Kolb, H. C., Finn, M. G. & Sharpless, K. B. Click Chemistry: Diverse Chemical Function from a Few Good Reactions. *Angew. Chem. Int. Ed.* **40**, 2004-2021 (2001). https://doi.org:https://doi.org/10.1002/1521-3773(20010601)40:11<2004::AID-ANIE2004>3.0.CO;2-5

24 Scinto, S. L. *et al.* Bioorthogonal chemistry. *Nature Reviews Methods Primers* **1**, 30 (2021). https://doi.org:10.1038/s43586-021-00028-z

25 Hoyle, C. E. & Bowman, C. N. Thiol–Ene Click Chemistry. *Angew. Chem. Int. Ed.* **49**, 1540-1573 (2010). https://doi.org:https://doi.org/10.1002/anie.200903924

26 Wu, H. & Devaraj, N. K. Inverse Electron-Demand Diels–Alder Bioorthogonal Reactions. *Top. Curr. Chem.* **374**, 3 (2015). https://doi.org:10.1007/s41061-015-0005-z

Statement of Authorship for joint/multi-authored papers for PGR thesis

To appear at the end of each thesis chapter submitted as an article/paper

The statement shall describe the candidate's and co-authors' independent research contributions in the thesis publications. For each publication there should exist a complete statement that is to be filled out and signed by the candidate and supervisor **(only required where there isn't already a statement of contribution within the paper itself).**

Title of Paper	Oscillation mediated mass transport
Publication Status	~~Published~~ ~~Accepted for Publication~~ ~~Submitted for Publication~~ ☑Unsubmitted work written in manuscript style
Publication Details	Michael G. Howlett, Anthonius H. J. Engwerda and Stephen P. Fletcher. n/a – manuscript in preparation

Student Confirmation

Student Name:	Michael Howlett		
Contribution to the Paper	Performed experiments and analysed data. Writing of manuscript draft (in preparation). Co-author (A. Engwerda) also performed experiments and took part in data analysis. Co-author (S. Fletcher) supervised the project and contributed to data analysis.		
Signature 		Date	14 / 04 / 2023

Supervisor Confirmation

By signing the Statement of Authorship, you are certifying that the candidate made a substantial contribution to the publication, and that the description described above is accurate.

Supervisor name and title: Prof. Stephen Fletcher		
Supervisor comments 		
Signature 	Date	

This completed form should be included in the thesis, at the end of the relevant chapter.

Chapter 6

Conclusions and outlook

Chapter 6

Conclusions and outlook

6.1 Remarks on physical autocatalysis

Given the emergence of complex functionality from manipulating a few simple chemicals in biphasic systems, physical autocatalysis would seem relevant to how life could emerge and also to understanding other interfacial phenomena. It is believed that there is enormous potential in autocatalytic lipids and they will form the basis of many new out-of-equilibrium experimental systems in the future.

However, there are intrinsic practical and technological barriers to such research. One key problem is that biphasic reactions – particularly highly dynamic ones with multiple potential feedback mechanisms – are practically difficult to study. Events take place across different length scales, requiring techniques for measuring molecular and supramolecular and even macroscopic features. As chemical systems become more elaborate, it is important that detailed analytical technologies also advance, in order to uncover the most interesting features of such systems.

6.2 Chapter 2: Competition between self-reproducing lipids

Models of chemical evolution are central to advancing origins of life research. To design more lifelike systems, we must expand our understanding of molecular selection mechanisms. These studies are important not only to trace how the earliest forms of life might have developed, but also so we can build chemical systems from simple parts which might have attractive functions.

In the past, template replicators modelled on RNA have been central to origin of life theories. It is gradually becoming apparent that the emergence of (lipid) compartments, alongside efficient information-containing catalysts, may be vital in prebiotic scenarios.

Chapter 2 describes two selection modes that produce evolving populations of self-reproducing species. This chapter introduced the family of lipids used throughout this thesis and the thiol–disulfide chemistry which drives their formation and destruction. The kinetic stability, or metastability, of the lipids under our reaction conditions is key to modelling changing species populations.

The main limitation of this work was the balance between producing a sufficiently complex system to see trends and relationships between the competing species, whilst practically being able to monitor the concentrations of closely related compounds in time. The use of three thiol precursors and three disulfide precursors gave up to nine (very similar) lipid products for resolution by liquid chromatography and quantification.

In the first case, selection arises from different intrinsic structural properties of the self-reproducing lipids and their direct precursors. This led to succession patterns where the dominant lipid species changed over time, with the more sterically hindered lipids taking longer to form but are longer lived.

A separate, emergent selection mechanism was found when the disulfide precursors of the lipids inter-react. Metathesis between the precursors caused new intermediates and alternative reaction pathways to become accessible in a process we have termed *dynamic activating metathesis*. This altered the reaction network, enabling some lipid products to have a competitive advantage at the expense of others. Unexpectedly, these experiments showed the preferential formation of lipids derived from the less electrophilic disulfides. This work suggests that increased chemical diversity can unlock new pathways in evolving systems and that future prebiotic models which deliberately allow for compositional complexity will reveal unexpected relationships between species, provided the mixtures can be kinetically characterised.

Future work should examine how mixtures of lipids such as these respond to new selection pressures such as harsh ‘environmental’ conditions (*e.g.* exploring reaction parameters such as stirring,

temperature and the presence of additives). A second logical extension of this work would be to examine these same competing disulfide lipids under fuelled out-of-equilibrium conditions, merging this system with the concepts from Morrow et al and Chapter 3 of this thesis.[1,2]

6.3 Chapter 3: A supramolecular chemical oscillator

Oscillations are a phenomenon found throughout nature and are observed at multiple length scales. Synthetic oscillators are inherently challenging to design and operate, yet they are potentially valuable components in biomimetic technology as controllers of other chemical processes.

In Chapter 3, we introduce a unique oscillating system that is entirely synthetic and based upon interactions between small organic molecules. At the core of the system is the autocatalytic formation of surfactants which self-assemble into micelles and are held out-of-equilibrium by a chemical fuel (H_2O_2). We find that the concentrations of species in the reaction network all exhibit sustained oscillations in time and that they are responsive to the supply of chemical fuel.

In contrast to recent prominent (bio)chemical oscillators,[3,4] our system does not rely upon a continuous flow reactor to supply the network components and remove waste, opening up alternative applications. Through super-resolution iSCAT microscopy and control experiments, we determined that the formation and breakdown of the micelle compartments is a key factor in the mechanism of the oscillations. The destruction of the micelles is a critical element of the reaction network and warrants further mechanistic study as this may reveal general design principles for biphasic oscillators. The way in which this phenomenon emerges from a mixture of simple chemicals may be relevant to how living systems build complexity and feedback mechanisms in cells. Additionally, this discovery may serve as a platform for controlling secondary chemical and physical processes, as long as they can be appropriately coupled to the oscillator.

Examples of follow on work that uses the supramolecular oscillator are given in Chapter 4 and 5 but one clear avenue for exploration is the development of analogous oscillators. The thiol-disulfide chemistry underpinning the present oscillator brings with it a number of chemical incompatibilities

and makes applying the system in more ambitious settings challenging. For example, reactive electrophiles and nucleophiles are not tolerated within the oscillator and they can also poison the reaction network (*e.g.* by forming stable surfactants or consuming the chemical fuel). Future designs should aim to emulate the transient surfactants and overall phase behaviour, without the accompanying sensitivity of the system.

6.4 Chapter 4: Information transduction via controllable chemical waves

Waves carrying information are essential to modern society. In Chapter 4, we propose how chemical oscillators may serve as a novel means of transducing information. Using our responsive oscillator introduced in Chapter 3 we show that the frequency and amplitude of the waves (of chemical concentration) can be tightly controlled. Changing reaction parameters such as stirring rate and chemical fuel (H_2O_2) supply *in situ* enables the sequence of waves to be modulated in real time. We use this to represent information in a chemical medium which is then decoded by Morse code and by analogy to amino acid codons. This demonstration may lend inspiration to devices which use chemical oscillators for signalling and sensing applications.

The primary limitation of this work is the way in which the chemical waves are monitored and translated to an output. Currently, the reactions must be manually sampled and the reactant concentrations determined by liquid chromatography. The development of a continuous readout of the oscillations would be transformative and would allow higher throughput exploration of the oscillator's functions. The heterogeneity and sensitivity of the biphasic setup rules out some monitoring methods (IR and NMR) but a spectroscopic technique may be suitable, provided the absorption by the aromatic chromophore in the surfactant can be distinguished from others in the mixture.

6.5 Chapter 5: Oscillation-mediated mass transport

Using the supramolecular oscillator outlined in Chapter 3, Chapter 5 describes the transport of molecular cargo between immiscible liquid phases on the macroscopic scale.

The repeated growth and decay of micellar compartments offers opportunities for mass transport, as we demonstrate via reversible dye uptake. To show transport between separated organic phases, the surfactant-forming reaction was transplanted into a U-tube vessel. After optimisation for the new vessel geometry and stirring regime, oscillations in the surfactant concentration were realised in the U-tube. We were able to show that hydrophobic cargo could be transported from one organic phase to another, mediated by the transient formation of micelles in an aqueous phase. The transport occurred in discrete stages, synchronised to the peaks and troughs of the oscillating surfactant concentration.

An ongoing extension of this work is the control of where and when chemical reactions occur, using the surfactant oscillator in the U-tube. Chapter 5 describes some attempts to find a compatible reaction system to demonstrate this concept. The thiol-disulfide chemistry and the necessary separation of the liquid phases presents significant challenges and efforts were focused on identifying orthogonal chemistries with hydrophobic components. Ultimately, a thiol-ene reaction was coupled to the oscillator and clearly showed transport-directed reactivity. We believe these findings will inspire new biomimetic systems and may unlock nanotechnology systems such as (supra)molecular pumps, where compartment formation is controlled in time and space.

The chemical incompatibility of the thiol-disulfide oscillator presents a significant barrier to further exploration and alternative applications. However, the special ability of this system to periodically switch on and off mass transfer of material between phases is a huge source of future work. Examples include using the oscillator to partition organic reagents and catalysts (in batch as opposed to U-tube) to control the timing of coupled reactions. Additionally, the oscillation-mediated transport within the U-tube may present opportunities for separation of apolar mixtures if selective uptake by the micelles can be realised.

6.6 Ongoing work

6.6.1 Aerobically driven oscillations

Some chemical systems which operate out-of-equilibrium are chemically driven or use a 'fuel' whereas some rely upon the constant supply of reactants and removal of waste in a continuous flow reactor. In our oscillating system introduced in Chapter 3, the supply of H_2O_2 is central to maintaining the system out-of-equilibrium. One thing that distinguishes this system is it does not use a flow reactor and only the oxidant is supplied by syringe pump addition at a constant rate, which could be described as a semi-batch process. This has allowed fine control of the rate of fuelling, which is a mechanistically useful feature and allows modulation of the chemical waves (see Chapter 4). However, being able to separate a chemical oscillator from the continuous addition of reagents may bring new benefits and enable more elaborate applications of the oscillator without this constraint.

Whilst handling the aromatic thiol **4** it was noticed that it readily and cleanly oxidises to disulfide **1** in organic solvent under ambient conditions on the timescale of a few hours (see Figure 6.1). This transformation is greatly accelerated in the presence of an O_2 atmosphere and stalled when **4** was stored under N_2 or argon, strongly implicating an aerobic oxidation. Aerobic oxidations of thiols are known[5-8] and it was thought that, with a catalyst, this could provide the out-of-equilibrium state in our oscillating system without the need for H_2O_2 addition.

Figure 6.1 shows oscillations in a batch system in the absence of any reagent or fuel flow. This was achieved by replacing the typical H_2O_2 supply with a catalytic amount of $CuCl_2$ (10% wrt **4**) and running the reaction open to air. This catalyst accelerates the oxidation of **4** by oxygen dissolved in the TRIS buffer. This is an exciting variation on the original oscillating system and investigations into the important reaction parameters with this new source of oxidant are underway.

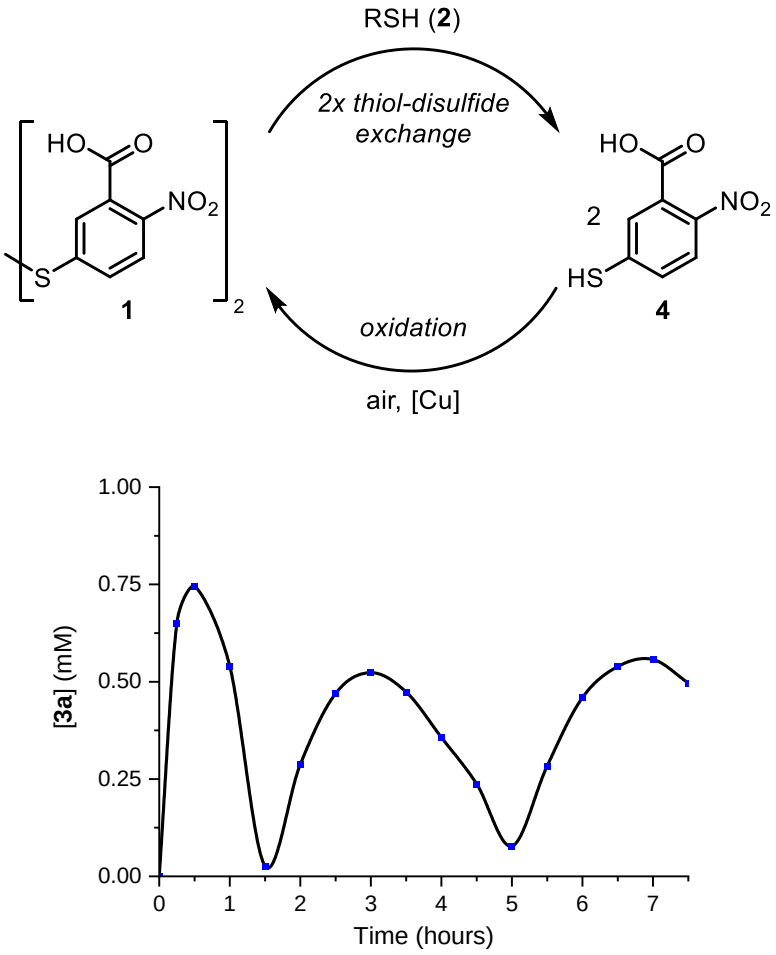

Figure 6.1: A fully batch oscillating reaction, without syringe addition of reagents, is possible using atmospheric oxygen to close the reaction cycle (**4** to **1** oxidation). Conditions: 16 mg 5-mercapto-2-nitrobenzoic acid (**4a**), 200 μL 2-octanethiol and stirred at 500 rpm in 2 mL TRIS (0.5 M, pH 9.0) at 25 °C with 10 mol% $CuCl_2$

6.6.2 Oscillating vesicle populations

Physical autocatalysis provides a general mechanism for molecules to enhance their own formation, provided the product is a molecule which aids mixing of its precursors. Our oscillating system described in Chapter 3 depends upon this principle for its non-linear kinetics and so we expected generality to its behaviour too, as long as metastable surfactants were being used. In Chapter 3 we showed that thiols with different chain lengths and steric hindrance could take part in the reaction network and the concentration of the corresponding surfactants would still oscillate, provided the reaction parameters were adjusted to compensate.

One interesting aspect we did not initially investigate was moving beyond micelle-forming surfactants with the oscillator. Vesicles are of interest in origins of life research as their bilayer and

interior water pool more closely resembles cells. Engwerda et al. and the work from Chapter 2 both reported vesicle-forming surfactants that are formed by thiol-disulfide exchange.[9,10]

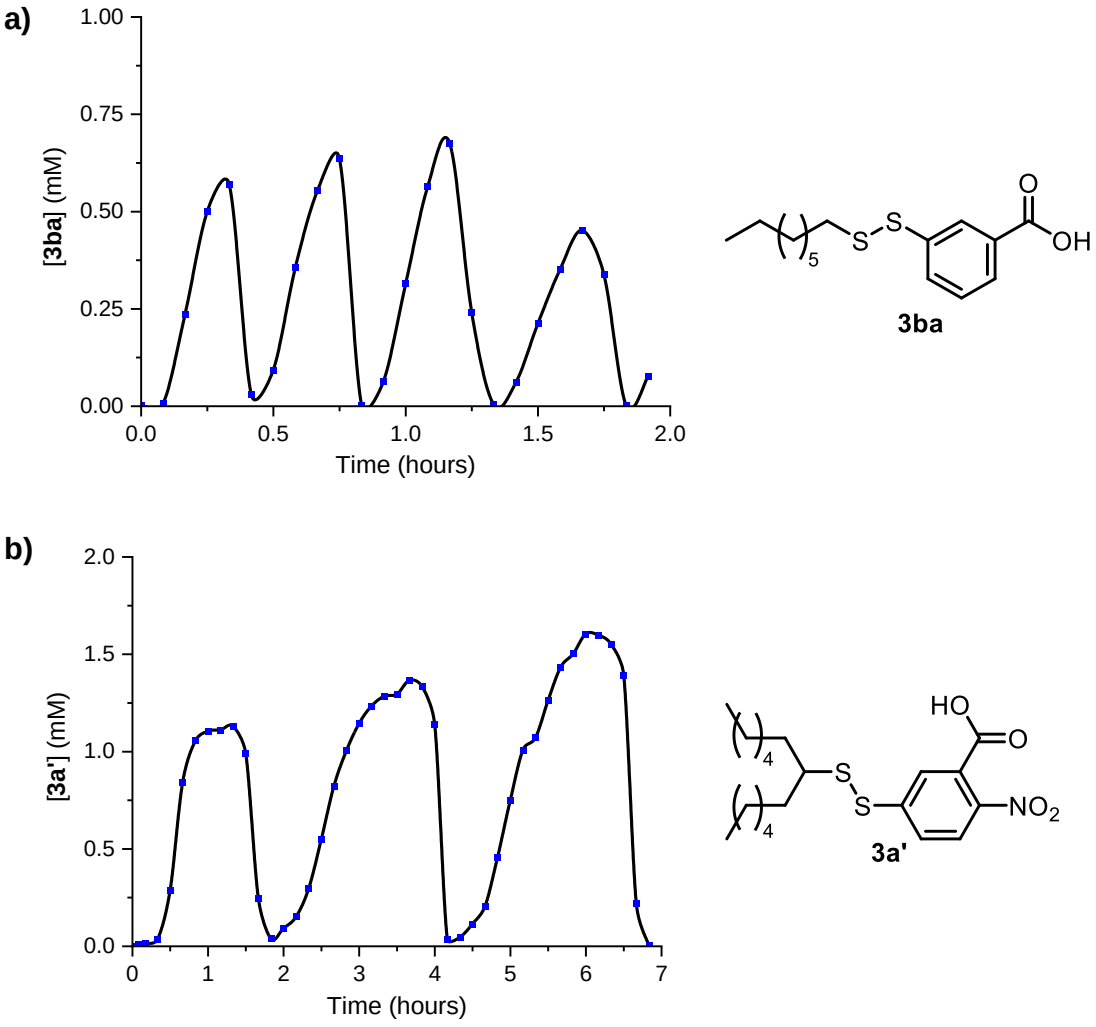

Figure 6.2: The concentration of vesicle-forming surfactants can show oscillations in the presence of nucleophilic catalysts DMAP or DABCO. Conditions: a) 12.2 mg 3,3'-dithiobis(benzoic acid) (**1b**), 60 µL 1-octanethiol, 4.9 mg DMAP stirred at 800 rpm in 4 mL TRIS (0.5 M, pH 9.0) at 40 °C with H_2O_2 addition (25 µL/h, 0.56 M); b) 23 mg 5,5'-dithiobis(2-nitrobenzoic acid) (**1a**), 500 µL 7-tridecanethiol, 100 mg DABCO stirred at 800 rpm in 4 mL TRIS (0.5 M, pH 9.0) at 40 °C with H_2O_2 addition (120 µL/h, 0.50 M)

In the present study, these two compounds were synthesised in biphasic, fuelled reactions and assessed to see if they could exhibit oscillations (see Figure 6.2). Because of their relatively high kinetic stability (due to the poor leaving group ability of the headgroup in **3ba** and steric hindrance confered by the large tail in **3a'**) they initially resisted breakdown in the presence of their respective thiols in alkaline buffer. However, following optimisation and the inclusion of nucleophilic

catalysts DMAP and DABCO, respectively, both surfactants were able to oscillate in time (Figure 6.2). Notably, the oscillations in the concentration of **3a'** have a large period but sharp destruction phase. Additionally, the broad apex of the [**3a'**] curve lends itself towards iSCAT monitoring during the oscillating reaction as each pulse can be sampled multiple times with a high particle (vesicle) count.

Efforts are underway to investigate these vesicle-forming systems on the supramolecular level in real time during oscillations. We anticipate this may reveal interesting trends in the size of the aggregates and perhaps transitions between micelle and vesicle compartments in response to changing concentration of the surfactant monomer. Mimicking the cycling of protocell populations experiencing birth and decay, this could provide an out-of-equilibrium model of evolutionary and competition dynamics.

6.7 Describing future models of life

Self-replicating molecules that act via a template mechanism have the ability, widely believed to be unique, to transfer 'genetic'-type information.[11,12] However, a growing body of work demonstrates advanced roles for lipids, in particular inheritable compositional states, that suggest that purely information based distinctions between different classes of replicators may soon become problematic.[13-15]

Biological entities do not make exact copies of themselves. To understand the transition to living systems we will need chemical models which experience product variation, mutations and emergence. Inevitably, future artificial systems will be capable of exhibiting high levels of selection, information transfer and evolution, and as systems become more advanced it would be desirable to have unambiguous terminology with which to describe systems of increasing complexity. For example, in situations where an autocatalyst can produce numerous different offspring (with or without selection), it is unclear from current usage in the literature if this species is a *self*-replicator,

a *selfish* replicator or an *unselective* replicator. You can add to this the problem of determining *how* structurally related the offspring must be to each other to qualify such terms.

Clearly, there are a number of semantic issues which arise in discussing autocatalytic processes, and in particular the meanings of reproduction and replication which have been considered by chemists and evolutionary biologists.[16-20]. It may be advantageous for someone to describe something as a 'replicator' or 'reproducer' to distinguish a particular phenomenon – though the weight that the semantics are carrying in a particular instance would certainly not be recognized by most readers.

Reproduction has a clear biological meaning which is to generate offspring. But it also has other meanings, including 'to copy' and 'to do something again'. In biology, this process involves the multiplication of a parent's components and then the division of the whole, e.g. mitosis.

Replication also has multiple meanings. Molecular replication means to copy a molecule and when this copy matches the catalyst for this process, self-replication has occurred.[21,22] A preferred usage by some scientists links replication to systems which have been deemed to be information-containing or have molecular recognition capabilities, which would include macromolecules such as RNA and synthetic autocatalysts capable of templating reactions.[22-26]

The concepts of replication and self-replication have a long scientific history, particularly in the context of non-biological machines, and regularly arise in science fiction and popular culture.[27-29] These words are generally used to describe processes where entities multiply without biology or the way that non-living systems somehow mimic biological reproduction. The use of 'replicating' specifically to describe information carrying systems that are capable of making exact copies of themselves is a well-intentioned attempt to redefine and limit the term, but it is problematic because it conflicts with its long-standing general meanings and does not account well for inexact template copying or non-template copying mechanisms which can pass on compositional information

(lipids). Overall, as synthetic systems edge closer to life, clarity on how to describe life-like autocatalytic processes will increase in importance.

All known life forms operate across length scales and are usually bounded structures formed from functional subcomponents. They can contain replicating molecules and are even said to have arisen through the packaging of "old-fashioned replicators" into higher level reproducers during evolutionary transitions.[30] Some autocatalysts directly make structural copies of the parent at the molecular level (*e.g.* template replicators) whereas, others indirectly produce the autocatalyst via subcomponent synthesis and assembly (micelles, vesicles and living cells). We suggest that the 'level' of the copying with respect to level of the autocatalyst (*i.e.* copying of the components or a copy of the whole) could be a key consideration when describing something as a replicator or reproducer. This focus on the copying hierarchy takes a broader view of the autocatalytic process without needing to involve informational or hereditary properties. Synthetic systems which can emulate this hierarchy are innately more complex and closer models of recognisable life – arguably the synthetic examples that are closest to this are self-assembled autocatalysts such as micelles and vesicles.

6.8 Outlook

Lipids are a class of biomolecules which are highly promising as key building blocks of functional and adaptive systems. They can adopt cell-like morphologies which can reproduce. They can adapt to and influence their environment by taking up material and altering surface effects. The dynamic and heterogeneous nature of lipids makes them unique as synthetic building blocks, in contrast to much of synthetic supramolecular chemistry which focuses on producing stable highly ordered structures.

As a potential pathway to producing life-like systems, it is easy to generate impressive complexity with lipids by simply mixing a few components in water. What is more difficult is learning how to control, characterize and harness these systems. Physically autocatalytic systems have progressed

greatly since the original experiments of Luisi and co-workers. In particular, the realisation of kinetically controlled systems has allowed new designs for out-of-equilibrium and competing lipid populations.

In the future, self-reproducing lipids will likely show many more examples of selection and cross-catalytic relationships between molecules than are known right now. These may come from designed systems but many examples will almost certainly emerge unexpectedly from the close observation of lipid-forming mixtures. There is value in periodically returning to known autocatalytic systems with new technological and conceptual assets in hand to seek novel behaviour. Exploring increasingly heterogenous mixtures is challenging, where already the combination of several reaction components can stretch analytical capabilities. However, using diverse structural classes to form autocatalytic lipid aggregates could have two specific advantages: opening new 'reactivity space' and potentially enabling molecular recognition and information transmission between autocatalytic aggregates, an important basis for chemical evolution.

The most interesting lipid systems in this thesis, and those yet to come, involve introducing new conceptual dimensions. For example, coupling of chemical reactions to escape equilibrium, establishing novel feedback and selection mechanisms or developing a better understanding of how phase behaviour can provide control in the time or space domain. A major ambition of the field is the bottom-up realisation of a living system using such design elements but conceptual barriers should not be underestimated – for example, the thermodynamics of functional dissipative systems.

One major, and pressing, requirement in origins of life research is the question of experimentally recognising life and measuring when the threshold for it has been met. A number of reported synthetic systems are now broadly meeting multiple core characteristics of life, such as compartmentalisation and energy consumption. As these artificial systems become more advanced, the probability of a truly living system emerging from a diverse mixture of components increases too. We believe there is therefore a necessity for researchers to soon address the definition of life

as a measurement problem and that developing quantifiable metrics for life may focus the next stage of bottom-up chemistry.

References

1 Morrow, S. M., Colomer, I. & Fletcher, S. P. A chemically fuelled self-replicator. *Nature Communications* **10**, 1011 (2019). https://doi.org:10.1038/s41467-019-08885-9

2 Howlett, M. G., Engwerda, A. H. J., Scanes, R. J. H. & Fletcher, S. P. An autonomously oscillating supramolecular self-replicator. *Nat. Chem.* **14**, 805-810 (2022). https://doi.org:10.1038/s41557-022-00949-6

3 Semenov, S. N. *et al.* Autocatalytic, bistable, oscillatory networks of biologically relevant organic reactions. *Nature* **537**, 656-660 (2016). https://doi.org:10.1038/nature19776

4 Semenov, S. N. *et al.* Rational design of functional and tunable oscillating enzymatic networks. *Nature Chemistry* **7**, 160-165 (2015). https://doi.org:10.1038/nchem.2142

5 Abbasi, M., Nowrouzi, N. & Mousavi, S. Aerobic Oxidation of Thiols and In Situ Generated Thiols to Symmetrical Disulfides (Disulfanes) Catalyzed by Na2S4O6. *ChemistrySelect* **4**, 12227-12231 (2019). https://doi.org:https://doi.org/10.1002/slct.201903099

6 Dong, W.-L., Huang, G.-Y., Li, Z.-M. & Zhao, W.-G. A Convenient Method for the Aerobic Oxidation of Thiols to Disulfides. *Phosphorus, Sulfur, and Silicon and the Related Elements* **184**, 2058-2065 (2009). https://doi.org:10.1080/10426500802418628

7 Rao, T. V., Rao, K. N., Jain, S. L. & Sain, B. Cobalt phthalocyanine mediated aerobic oxidation of thiols: a simple and convenient preparation of disulphides. *Synth. Commun.* **32**, 1151-1157 (2002). https://doi.org:10.1081/SCC-120003604

8 Yang, L. *et al.* TEMPO-Catalyzed Aerobic Oxidative Coupling of Thiols for Metal-Free Formation of S−N/S−S Bonds. *Asian Journal of Organic Chemistry* **6**, 265-268 (2017). https://doi.org:https://doi.org/10.1002/ajoc.201600588

9 Engwerda, A. H. J. *et al.* Coupled Metabolic Cycles Allow Out-of-Equilibrium Autopoietic Vesicle Replication. *Angew. Chem. Int. Ed.* **59**, 20361-20366 (2020). https://doi.org:10.1002/anie.202007302

10 Howlett, M. G., Scanes, R. J. H. & Fletcher, S. P. Selection between Competing Self-Reproducing Lipids: Succession and Dynamic Activation. *JACS Au* **1**, 1355-1361 (2021). https://doi.org:10.1021/jacsau.1c00138

11 Adamski, P. *et al.* From self-replication to replicator systems en route to de novo life. *Nat. Rev. Chem.* **4**, 386-403 (2020). https://doi.org:10.1038/s41570-020-0196-x

12 Orgel, L. E. Molecular replication. *Nature* **358**, 203-209 (1992). https://doi.org:10.1038/358203a0

13 Walde, P., Umakoshi, H., Stano, P. & Mavelli, F. Emergent properties arising from the assembly of amphiphiles. Artificial vesicle membranes as reaction promoters and regulators. *Chem. Commun.* **50**, 10177-10197 (2014). https://doi.org:10.1039/C4CC02812K

14 Kahana, A., Maslov, S. & Lancet, D. Dynamic lipid aptamers: non-polymeric chemical path to early life. *Chem. Soc. Rev.* **50**, 11741-11746 (2021). https://doi.org:10.1039/D1CS00633A

15 Bell, T. N., Feng, K., Calvin, G., Van Winkle, D. H. & Lenhert, S. Organic Composomes as Supramolecular Aptamers. *ACS Omega* **5**, 27393-27400 (2020). https://doi.org:10.1021/acsomega.0c03799

16 Fleischaker, G. R. in *Self-Production of Supramolecular Structures: From Synthetic Structures to Models of Minimal Living Systems* (eds Gail R. Fleischaker, Stefano Colonna, & Pier Luigi Luisi) 33-41 (Springer Netherlands, 1994).

17 Ruiz-Mirazo, K., Umerez, J. & Moreno, A. Enabling conditions for 'open-ended evolution'. *Biol. Philos.* **23**, 67-85 (2008). https://doi.org:10.1007/s10539-007-9076-8

18 Dyson, F. *Origins of Life*. 2 edn, (Cambridge University Press, 1999).

19 Szathmáry, E. The origin of replicators and reproducers. *Philos. Trans. R. Soc. Lond., B, Biol. Sci.* **361**, 1761-1776 (2006). https://doi.org:doi:10.1098/rstb.2006.1912

20 Griesemer, J. The Units of Evolutionary Transition. *Selection* **1**, 67-80 (2001).
21 Wintner, E. A., Conn, M. M. & Rebek, J., Jr. Studies in Molecular Replication. *Acc. Chem. Res.* **27**, 198-203 (1994). https://doi.org:10.1021/ar00043a003
22 Bissette, A. J. & Fletcher, S. P. Mechanisms of Autocatalysis. *Angew. Chem. Int. Ed.* **52**, 12800-12826 (2013). https://doi.org:10.1002/anie.201303822
23 Tjivikua, T., Ballester, P. & Rebek, J. Self-replicating system. *J. Am. Chem. Soc.* **112**, 1249-1250 (1990). https://doi.org:10.1021/ja00159a057
24 Wang, B. & O. Sutherland, I. Self-replication in a Diels–Alder reaction. *Chem. Commun.*, 1495-1496 (1997). https://doi.org:10.1039/A701573I
25 Lee, D. H., Granja, J. R., Martinez, J. A., Severin, K. & Ghadiri, M. R. A self-replicating peptide. *Nature* **382**, 525-528 (1996). https://doi.org:10.1038/382525a0
26 Vidonne, A. & Philp, D. Making Molecules Make Themselves – the Chemistry of Artificial Replicators. *Eur. J. Org. Chem.* **2009**, 593-610 (2009). https://doi.org:10.1002/ejoc.200800827
27 Von Neumann, J. & Burks, A. W. *Theory of self-reproducing automata*. (University of Illinois Press, 1966).
28 Drexler, K. E. *Engines of creation: the coming era of nanotechnology*. (Doubleday, 1986).
29 Moore, E. F. in *Sci. Am.* Vol. 195 118-126 (1956).
30 Szathmáry, E. & Maynard Smith, J. From Replicators to Reproducers: the First Major Transitions Leading to Life. *J. Theor. Biol.* **187**, 555-571 (1997). https://doi.org:https://doi.org/10.1006/jtbi.1996.0389

Chapter 7

Experimental section

Chapter 7

Experimental section

7.1 General experimental

General information

^{1}H NMR and ^{13}C NMR spectra were recorded on a Bruker Avance III HD 400 MHz spectrometer using $CDCl_3$, DMSO-d_6 or acetone-d_6 as solvent. Chemical shifts (δ) are expressed in parts per million (ppm) with respect to residual solvent signals and coupling constants are quoted in hertz (Hz). Multiplets are described as s (singlet), d (doublet), t (triplet), q (quartet), p (pentet), sextet and m (multiplet). Melting points were recorded using purified samples on a Leica Galen III microscope in conjunction with a heated-stage and Testo 720 thermocouple. High-resolution mass spectra were recorded on a Thermo Exactive Orbitrap mass spectrometer equipped with a Waters Acquity LC system under conditions of electrospray ionization (ESI) by the internal service within the Department of Chemistry. Reagents were obtained from commercial sources where indicated and were used directly as supplied. All aqueous samples, standard solutions and buffers used ultrapure Milli-Q water and/or HPLC grade organic solvents. TLC analyses were performed using Merck Kiesegel 60 F_{254} 0.25 mm precoated silica plates and preparative TLC performed using 200 x 200 mm 60 Å Analtech precoated glass backed plates.

Buffer preparation

Buffer solutions were prepared by dissolving the required mass of 2-amino-2-(hydroxymethyl)-1,3-propanediol (TRIS) or 4-(2-hydroxyethyl)-1-piperazineethanesulfonic acid (HEPES) in approximately 90% of the final volume Milli-Q water. The pH and volume were adjusted by addition of an aqueous solution of potassium hydroxide or hydrogen chloride, as measured with a Jenway 3510 benchtop pH meter. The final pH of the buffer was measured at room temperature, after stirring and equilibration of the solution, to an accuracy of ± 0.01 pH units. Buffer solutions were regularly prepared fresh and stored out of direct light. For all

kinetics reactions in Chapters 3-6 the buffer included an internal standard (3-methyl-2-nitrobenzoic acid, 4 mM) which was used in the processing of concentration data.

UPLC analysis of reaction samples

To monitor the kinetics of reactions, the concentration of UV active components of the reaction was monitored using a Waters Acquity ultra performance liquid chromatography (UPLC) H-Class system with photodiode array (PDA) detector and Acquity UPLC BEH C18 column (130 Å, 1.7 μm, 2.1 mm × 50 mm). Instrument control and data processing were performed using the Empower 3 software. Peak areas were obtained by integration at $\lambda = 240$ nm.

A mixture of H_2O: MeCN: TFA (2% v/v in H_2O) was used as mobile phase with the gradients described within each Chapter's experimental details.

7.2 Supplementary data for Chapter 2

7.2.1 Synthesis of compounds

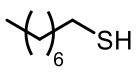

2a

1-octanethiol (**2a**): commercially available and was used without further purification.

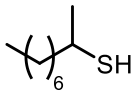

2b

2-nonanethiol (**2b**): was synthesised according to a literature procedure.[4]

^{1}H NMR (400 MHz, $CDCl_3$) δ 2.93 (hept, J = 7.0 Hz, 1H), 1.60 - 1.45 (m, 3H), 1.32 (d, J = 7.0 Hz, 3H), 1.31 - 1.22 (m, 10H), 0.91- 0.85 (m, 3H); ^{13}C NMR (101 MHz, $CDCl_3$) δ 41.0, 35.6, 31.8, 29.3, 29.2, 27.5, 25.6, 22.6, 14.1.

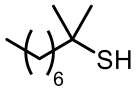

2c

2-methylnonane-2-thiol (**2c**): was synthesised according to a literature procedure.[4]

^{1}H NMR (400 MHz, $CDCl_3$) δ 1.67 (s, 1H), 1.58 – 1.52 (m, 2H), 1.46 - 1.39 (m, 2H), 1.37 (s, 6H), 1.33 - 1.23 (m, 8H), 0.89 (t, J = 7.0 Hz, 3H); ^{13}C NMR (101 MHz, $CDCl_3$) δ 44.6, 44.8, 32.8, 31.8, 30.0, 29.3, 25.4, 24.7, 14.1.

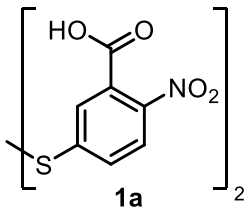

1a

5,5'-dithiobis(2-nitrobenzoic acid) (**1a**): commercially available and was used without further purification.

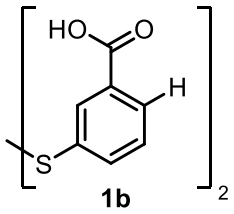

1b

3,3'-dithiobis(benzoic acid) (**1b**): A solution of commercial **4b** (1.85 g, 12.0 mmol, 1.0 equiv.) in DMSO (40 mL) was stirred at room temperature for 18 hours before acidification with 1 M aq. HCl (200.0 mL), forming a white precipitate. This was filtered and washed with 1 M aq. HCl (2 x 20 mL). The solid was dissolved in MeOH/$CHCl_3$ (1:1) at 40 °C, passed through a celite plug and the filtrate concentrated to dryness to give 3,3'-dithiobis(benzoic acid) (**1b**) as an off-white powder (1.636 g, 10.7 mmol, 89%).

^{1}H NMR (400 MHz, DMSO-d_6): δ 8.08 (t, J = 1.8 Hz, 2H), 7.85 (dt, J = 7.7, 1.3 Hz, 2H), 7.74 (ddd, J = 7.9, 2.1, 1.1 Hz, 2H), 7.51 (t, J = 7.8 Hz, 2H); ^{13}C NMR (101 MHz, DMSO-d_6): 166.7, 136.1, 133.0, 130.9, 129.7, 128.5, 127.5; HRMS (ESI+, m/z): [M-H]- calc. for $C_{14}H_9O_4{}^{32}S_2$, 304.9948; found, 304.9949; m.p. 249.9 - 250.4 °C

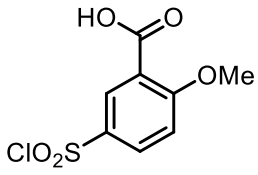

6

5-(chlorosulfonyl)-2-methoxybenzoic acid (**6**): 2-methoxybenzoic acid (2.50 g, 16.4 mmol, 1.0 eq.) was added to HSO_3Cl (4.92 mL, 73.8 mmol, 4.5 eq.) in portions over 10 minutes with ice cooling. After reacting at 0 °C for 30 minutes, $SOCl_2$ (1.19 mL, 16.4 mmol, 1.0 eq.) was added dropwise and the mixture stirred at room temperature for 3 hours. The solution was poured onto

ice and the precipitate collected by vacuum filtration with cold 1 M aq. HCl washings. Drying *in vacuo* gave **6** as a white powder (3.93 g, 96% yield).

^{1}H NMR (400 MHz, $CDCl_3$): δ 8.77 (m, 1H), 8.22 (dd, J = 9.0, 2.6 Hz, 1H), 7.25 (d, J = 9.0 Hz, 1H), 4.17 (s, 3H); ^{13}C NMR (101 MHz, $CDCl_3$): δ 173.2, 163.2, 137.4, 133.7, 133.4, 119.4, 113.1, 57.7; HRMS (ESI+, m/z): [M-H]- calc. for $C_8H_5O_5{}^{35}Cl{}^{32}S$, 248.9630; found, 248.9629; m.p. 145.6 - 147.7 °C Lit[5]: m.p. 138 - 140 °C, ^{1}H NMR ($CDCl_3$): δ 8.78 (s, 1H), 8.21 (s, 1H), 7.23 (d, 1H), 4.18 (s, 3H); 94% yield.

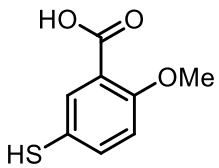

4c

5-mercapto-2-methoxybenzoic acid (**4c**): To a suspension of **6** (10.05 g, 40.1 mmol, 1.0 eq.) in AcOH (120.0 mL) was added a suspension of $SnCl_2$•$2H_2O$ (54.30 g, 240.6 mol, 6.0 eq.) in conc. HCl (37%, 60.0 mL) at room temperature. The mixture was then heated to 80 °C for 16 hours. The cooled solution was then poured onto ice and extracted with $CHCl_3$/MeOH (9:1, 5 x 50 mL) before washing of the combined organics with acidified brine (100 mL) and drying with $MgSO_4$. Concentration of the organic layer to dryness in vacuo gave **4c** as a pale yellow powder (6.65 g, 91% yield).

^{1}H NMR (400 MHz, acetone-d_6): δ 11.00 (s, 1H), 7.82 (d, J = 2.6 Hz, 1H), 7.53 (dd, J = 2.5, 8.7 Hz, 1H), 7.15 (d, J = 8.7 Hz, 1H), 3.97 (s, 3H); ^{13}C NMR (101 MHz, acetone-d_6): δ 165.9, 158.0, 136.1, 133.9, 123.2, 121.3, 114.4, 56.9; HRMS (ESI-, m/z): [M-H]- calc. for $C_8H_7O_3S$, 183.0121; found, 183.0120; m.p. 103.1 – 104.3 □C

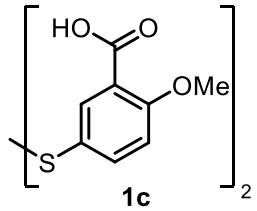

1c

5,5'-dithiobis(2-methoxybenzoic acid) (**1c**): was synthesised from **4c** (6.615 g, 35.9 mmol) in an analogous fashion to **1b** to give **1c** as a white powder (6.469 g, 98% yield).

^{1}H NMR (400 MHz, DMSO-d_6): δ 12.84 (br s, 1H), 7.72 (d, J = 2.5 Hz, 1H), 7.60 (dd, J = 8.7, 2.5 Hz, 1H), 7.16 (d, J = 8.8 Hz, 1H), 3.83 (s, 3H); ^{13}C NMR (101 MHz, DMSO-d_6): δ 166.3, 158.4, 134.7, 132.3, 126.3, 122.3, 113.8, 56.1; HRMS (ESI-, m/z): [M-H]- calc. for $C_{16}H_{13}O_6{}^{32}S_2$, 365.0159; found, 365.0158; m.p. 215.8 - 218.0 °C

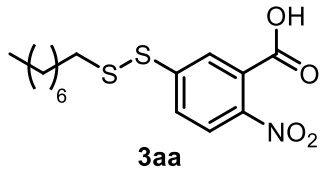

3aa

2-nitro-5-(octyldisulfaneyl)benzoic acid (**3aa**): To a solution of triethylamine (702 µL, 5.04 mmol, 2.0 equiv.) and **1a** (1.00 g, 2.52 mmol, 1.0 equiv.) in DCM (10 mL) was dropwise added a solution of triethylamine (351 µL, 2.52 mmol, 1.0 equiv.) and thiol **2a** (437 µL, 2.52 mmol, 1.0 equiv.) in DCM (10 mL). After 1 hour at room temperature, the reaction was diluted with 1 M aq. HCl (10 mL) extracted with DCM (3 x 20 mL). The combined organics were dried ($NaSO_4$) and the solvent removed *in vacuo*. The crude material was purified by column chromatography (methanol/chloroform (1:99)) to give **3aa** as a colourless oil (766.2 mg, 2.23 mmol, 88% yield).

^{1}H NMR (400 MHz, DMSO-d_6) δ 7.92 (d, J = 8.5 Hz, 1H), 7.83 (d, J = 2.0 Hz, 1H), 7.77 (dd, J = 8.5, 2.0 Hz, 1H), 2.82 (t, J = 7.0 Hz, 2H), 1.59 (p, J = 7.0 Hz, 2H), 1.37 – 1.27 (m, 2H), 1.27 –

1.12 (m, 8H), 0.83 (t, J = 7.0 Hz, 3H); ^{13}C NMR (101 MHz, DMSO-d$_6$) δ 166.0, 146.0, 143.6, 127.2, 125.9, 124.4, 120.8, 38.1, 31.1, 28.5, 28.2, 27.6, 22.0, 13.9; HRMS (ES-, m/z) calc. for $C_{15}H_{20}O_4N^{32}S_2$ [M-H]- 342.0828, found 342.0834. Data consistent with literature values.[3]

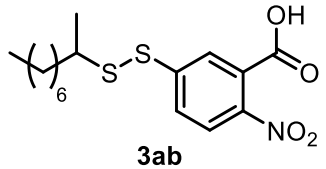

3ab

(±)-2-nitro-5-(nonan-2-yldisulfaneyl)benzoic acid (**3ab**): was synthesised in an analogous fashion to **3aa** from **1a** (494.6 mg, 1.25 mmol) and thiol **2b** (200.0 mg, 1.25 mmol) to give a colourless oil (408.5 mg, 1.114 mmol, 91% yield).

^{1}H NMR (400 MHz, DMSO-d_6) δ 8.02 (d, J = 8.5 Hz, 1H), 7.93 (d, J = 2.0 Hz, 1H), 7.90 (dd, J = 8.5, 2.0 Hz, 1H), 3.05 (hept, J = 6.5 Hz, 1H), 1.61 – 1.40 (m, 2H), 1.33 (p, J = 7.5 Hz, 2H), 1.24 (d, J = 6.5 Hz, 3H), 1.22 – 1.08 (m, 8H), 0.83 (t, J = 7.0 Hz, 3H); ^{13}C NMR (101 MHz, DMSO-d_6) δ 165.6, 145.7, 145.0, 128.8, 128.3, 125.9, 124.8, 46.9, 35.2, 31.2, 28.7, 28.5, 26.3, 22.0, 20.3, 13.9; HRMS (ES-, m/z) calc. for $C_{16}H_{22}O_4N^{32}S_2$ [M-H]- 356.0996, found 356.0993.

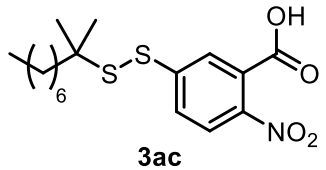

3ac

2-nitro-5-((2-methylnonan-2-yl)disulfaneyl)benzoic acid (**3ac**): was synthesised in an analogous fashion to **3aa** from **1a** (454.6 mg, 1.15 mmol) and thiol **2c** (200.0 mg, 1.15 mmol) to give a colourless oil (291.1 mg, 0.784 mmol, 68% yield).

^{1}H NMR (400 MHz, DMSO-d_6) δ 8.00 (d, J = 8.5 Hz, 1H), 7.94 (d, J = 2.0 Hz, 1H), 7.92 (dd, J = 8.5, 2.0 Hz, 1H), 1.52 – 1.45 (m, 2H), 1.29 – 1.12 (m, 14H), 1.10 – 1.01 (m, 2H), 0.83 (t, J =

7.0 Hz, 3H); ^{13}C NMR (101 MHz, DMSO-d_6) δ 165.6, 145.7, 145.2, 128.7, 126.3, 124.6, 53.7, 40.5, 31.2, 29.3, 28.5, 27.2, 24.2, 22.0, 13.9; HRMS (ES-, m/z) calc. for $C_{17}H_{22}O_4N^{32}S_2$ [M-H]- 370.1152, found 370.1149.

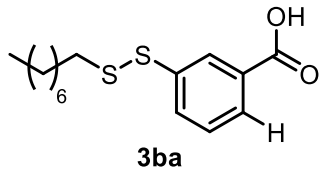

3ba

3-(octyldisulfaneyl)benzoic acid (**3ba**): was synthesised in an analogous fashion to **3aa** from **1b** (100.0 mg, 0.326 mmol) and thiol **2a** (56.5 µL, 0.326 mmol) to give a colourless oil (68.0 mg, 0.228 mmol, 70% yield).

^{1}H NMR (400 MHz, DMSO-d_6) δ 8.10 (t, *J* = 2.0 Hz, 1H), 7.82 (dt, *J* = 7.5, 1.5 Hz, 1H), 7.76 (ddd, *J* = 8.0, 2.0, 1.0 Hz, 1H), 7.51 (t, *J* = 8.0 Hz, 1H), 2.80 (t, *J* = 7.0 Hz, 2H), 1.58 (p, *J* = 7.0 Hz, 2H) 1.36 – 1.12 (m, 10H), 0.83 (t, *J* = 7.0 Hz, 3H), 0.83 (t, *J* = 7.0 Hz, 3H); ^{13}C NMR (101 MHz, DMSO-d_6) δ 166.6, 137.6, 131.9, 131.0, 129.5, 127.7, 127.1, 38.3, 31.1, 28.4, 28.4, 28.1, 27.5, 22.0, 13.9; HRMS (ES-, m/z) calc. for $C_{15}H_{21}O_2{}^{32}S_2$ [M-H]- 297.0988, found 297.0985.

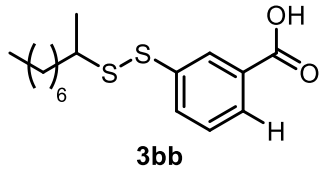

3bb

(±)-3-(nonan-2-yldisulfaneyl)benzoic acid (**3bb**): was synthesised in an analogous fashion to **3aa** from **1b** (100.0 mg, 0.326 mmol) and thiol **2b** (52.3 mg, 0.326 mmol) to give a colourless oil (56.9 mg, 0.183 mmol, 56% yield).

^{1}H NMR (400 MHz, DMSO-d_6) δ 8.12 (t, *J* = 2.0 Hz, 1H), 7.80 (dt, *J* = 7.5, 1.5 Hz, 1H), 7.76 (ddd, *J* = 8.0, 2.0, 1.0 Hz, 1H), 7.49 (t, *J* = 8.0 Hz, 1H), 2.97 (hept, *J* = 6.5 Hz, 1H), 1.59 – 1.44

(m, 1H), 1.43 – 1.38 (m, 1H), 1.33 – 1.04 (m, 13H), 0.83 (t, *J* = 7.0 Hz, 3H); ^{13}C NMR (101 MHz, DMSO-d_6) δ 166.6, 138.1, 131.0, 129.4, 127.6, 127.2, 46.6, 35.1, 31.1, 28.7, 28.4, 26.2, 22.0, 20.4, 13.9; HRMS (ES-, m/z) calc. for $C_{16}H_{23}O_2{}^{32}S_2$ [M-H]- 311.1145, found 311.1142.

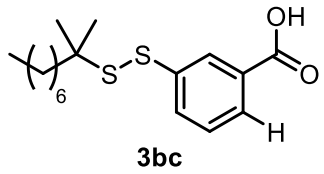

3bc

3-((2-methylnonan-2-yl)disulfaneyl)benzoic acid (**3bc**): was synthesised in an analogous fashion to **3aa** from **1b** (100.0 mg, 0.326 mmol) and thiol **2c** (56.8 mg, 0.326 mmol) to give a colourless oil (24.8 mg, 0.076 mmol, 23% yield).

^{1}H NMR (400 MHz, DMSO-d_6) δ 8.13 (t, *J* = 2.0 Hz, 1H), 7.82 – 7.76 (m, 2H), 7.48 (t, *J* = 8.0 Hz, 1H), 1.47 – 1.39 (m, 2H), 1.29 – 1.04 (m, 14H), 1.00 – 0.89 (m, 2H), 0.82 (t, *J* = 7.0 Hz, 3H); ^{13}C NMR (101 MHz, DMSO-d_6) δ 166.6, 138.4, 131.7, 129.2, 127.6, 127.6, 52.9, 40.5, 31.2, 29.2, 28.5, 27.2, 24.2, 22.0, 13.9; HRMS (ES-, m/z) calc. for $C_{17}H_{25}O_2{}^{32}S_2$ [M-H]- 325.1290, found 325.1299.

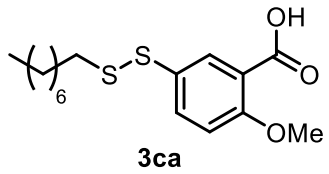

3ca

2-methoxy-5-(octyldisulfaneyl)benzoic acid (**3ca**): To a solution of **1c** (366.4 mg, 1.00 mmol) in HEPES buffer (40.0 mL, pH 8.00, 0.25 M) was added thiol **2a** (1.38 mL, 8.00 mmol). After 22 hours stirring (100 rpm) at room temperature, the reaction was diluted with 1 M aq. HCl (20 mL) extracted with MeOH/$CHCl_3$ (1:9, 5 x 50 mL). The combined organics were washed with acidified brine (100 mL), dried ($MgSO_4$) and the solvent removed *in vacuo*. The crude material

was purified by column and preparative thin layer chromatography (MeOH/$CHCl_3$ (3:97)) to give **3ca** as a clear yellow oil (188.1 mg, 0.69 mmol, 69% yield).

^{1}H NMR (400 MHz, DMSO-d_6): δ 7.77 (d, J = 2.6 Hz, 1H), 7.65 (dd, J = 8.6, 2.4 Hz, 1H), 7.15 (d, J = 8.7 Hz, 1H), 3.82 (s, 1H), 2.76 (t, J = 7.1 Hz, 2H), 1.59 (p, J = 7.2 Hz, 2H), 1.36-1.12 (m, 10H), 0.84 (t, J = 7.0 Hz, 3H); ^{13}C NMR (101 MHz, DMSO-d_6): δ 166.6, 157.9, 134.1, 131.6, 127.2, 122.4, 113.6, 56.0, 38.1, 31.2, 28.5, 28.5, 28.1, 27.6, 22.1, 14.0; HRMS (ESI-, m/z): [M-H]- calc. for $C_{16}H_{23}O_3{}^{32}S_2$, 327.1094; found, 327.1097

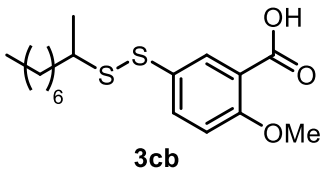

3cb

(±)-2-methoxy-5-(nonan-2-yldisulfaneyl)benzoic acid (**3cb**): was synthesised in an analogous fashion to **3ca** from **1c** (366.4 mg, 1.00 mmol) and thiol **2b** (380 µL, ca. 2.00 mmol), with a reaction time of 52 hours and stir rate of 500 rpm, to give a clear yellow oil (323.6 mg, 0.94 mmol, 94% yield).

^{1}H NMR (400 MHz, DMSO-d_6): δ 7.80 (d, J = 2.6 Hz, 1H), 7.67 (dd, J = 8.7, 2.6 Hz, 1H), 7.14 (d, J = 8.8 Hz, 1H), 3.81 (s, 3H), 2.92 (sextet, J = 6.7 Hz, 1H), 1.61-1.35 (m, 2H), 1.32-1.03 (m, 14H), 0.83 (t, J = 7.0 Hz, 3H),; ^{13}C NMR (101 MHz, DMSO-d_6): δ 166.5, 157.8, 133.8, 131.4, 127.7, 122.0, 113.5, 56.0, 46.4, 35.1, 31.2, 28.7, 28.5, 26.3, 22.0, 20.5, 13.9; HRMS (ESI+, m/z): [M+H]+ calc. for $C_{17}H_{27}O_3{}^{32}S_2$, 343.1396; found, 343.1397

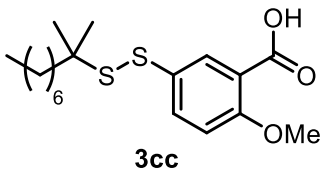

3cc

2-methoxy-5-((2-methylnonan-2-yl)disulfaneyl)benzoic acid (**3cc**): was synthesised in an analogous fashion to **3ca** from **1c** (366.4 mg, 1.00 mmol) and thiol **2c** (380 µL, ca. 2.00 mmol), with a reaction time of 71 hours and stir rate of 500 rpm, to give a clear yellow oil (251.1 mg, 0.70 mmol, 70% yield).

^{1}H NMR (400 MHz, DMSO-d_6): δ 7.81 (d, J = 2.5 Hz, 1H), 7.68 (dd, J = 8.8,2.6 Hz, 1H), 7.13 (d, J = 8.8 Hz, 1H), 3.81 (s, 3H), 1.47-1.38 (m, 2H), 1.26-0.91 (m, 16H), 0.83 (t, J = 7.1, 3H); ^{13}C NMR (101 MHz, DMSO-d_6): δ 166.4, 157.8, 133.8, 131.4, 128.0, 121.8, 113.4, 56.0, 52.6, 40.5, 31.2, 29.3, 28.6, 27.4, 24.3, 22.0, 13.9; HRMS (ESI+, m/z): [M+H]+ calc. for $C_{18}H_{29}O_3S_2$, 357.1553; found, 357.1554

7.2.2 NMR data

nonane-2-thiol (**2b**)

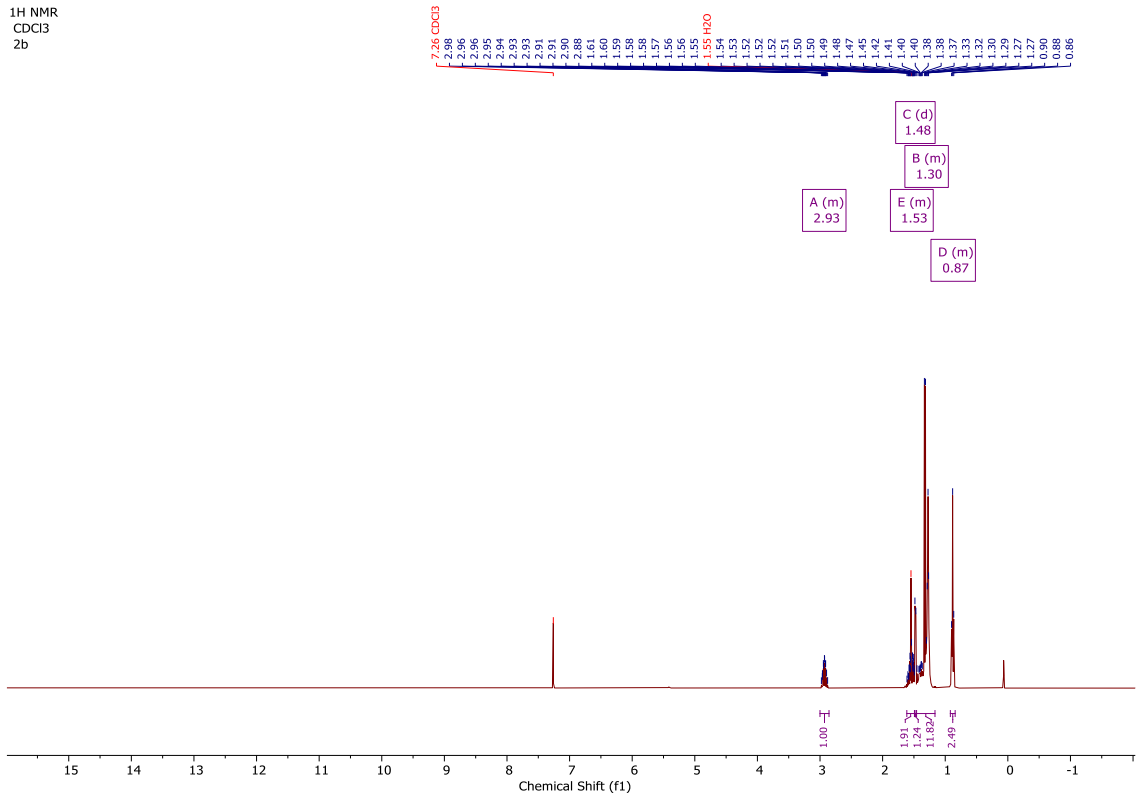

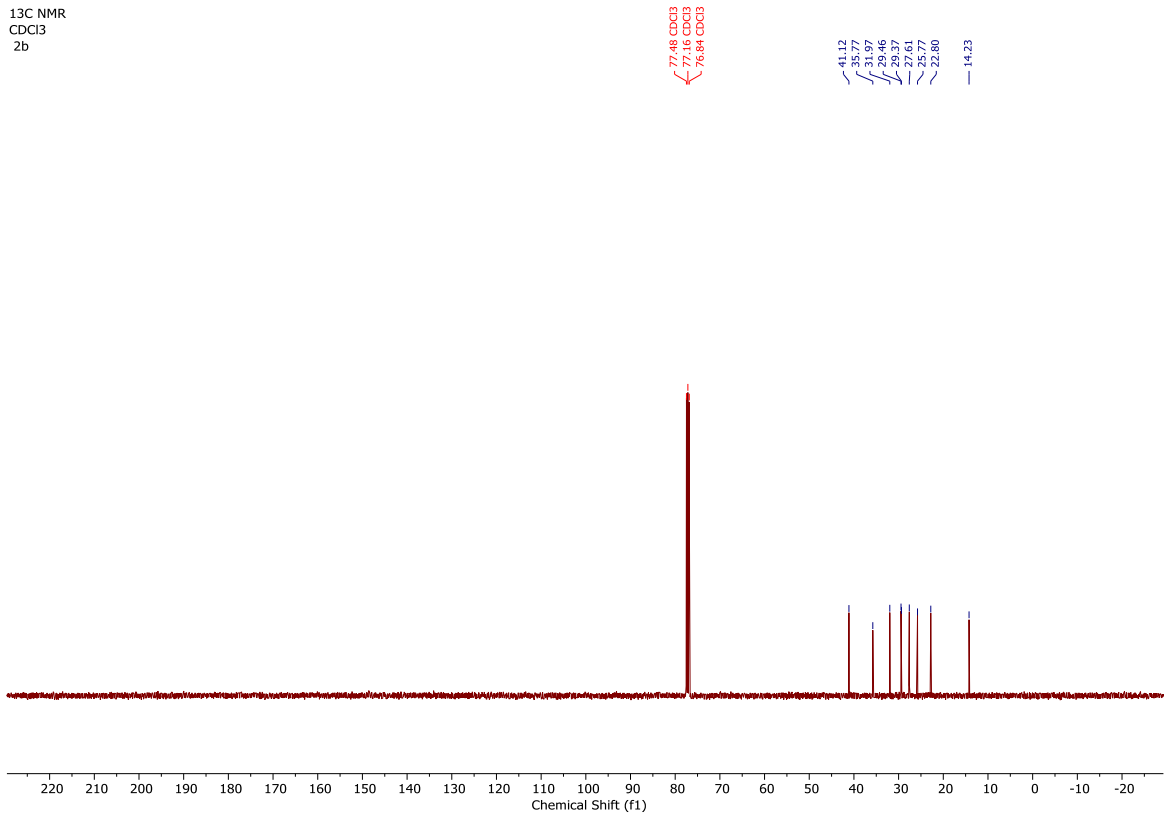

2-methylnonane-2-thiol (**2c**)

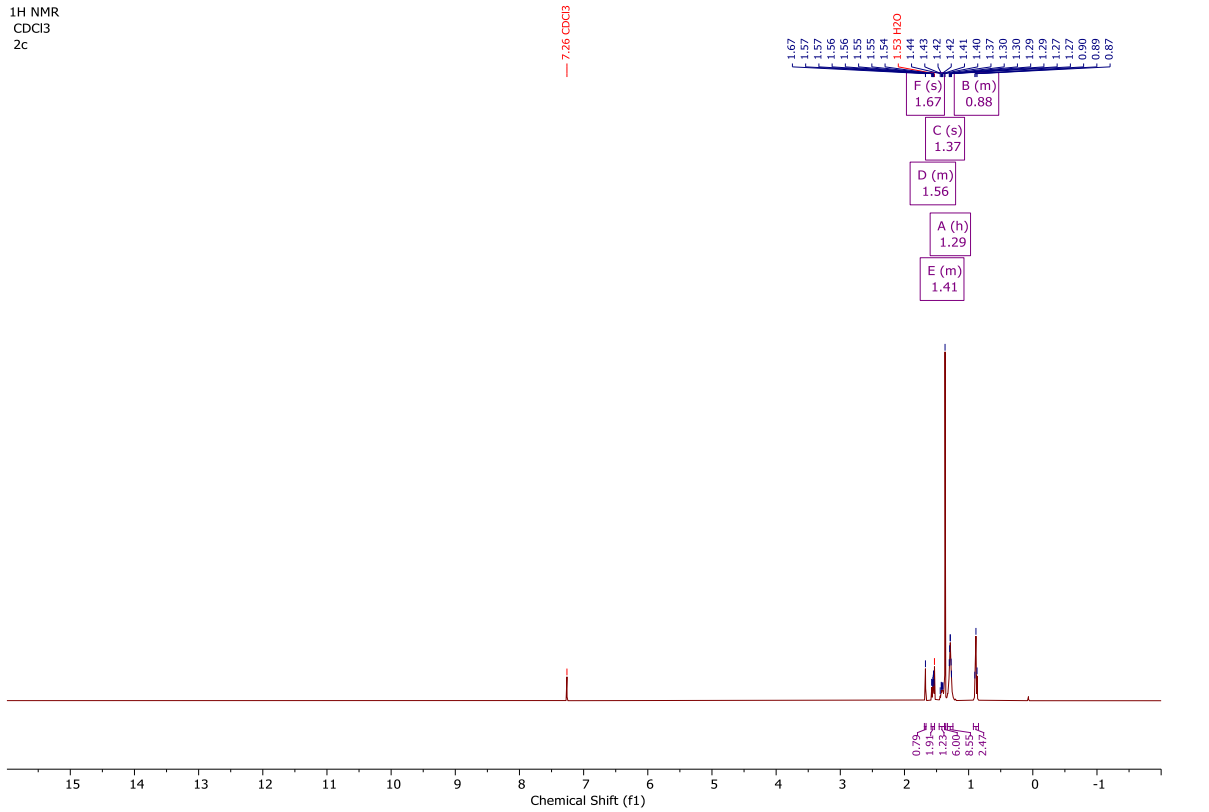

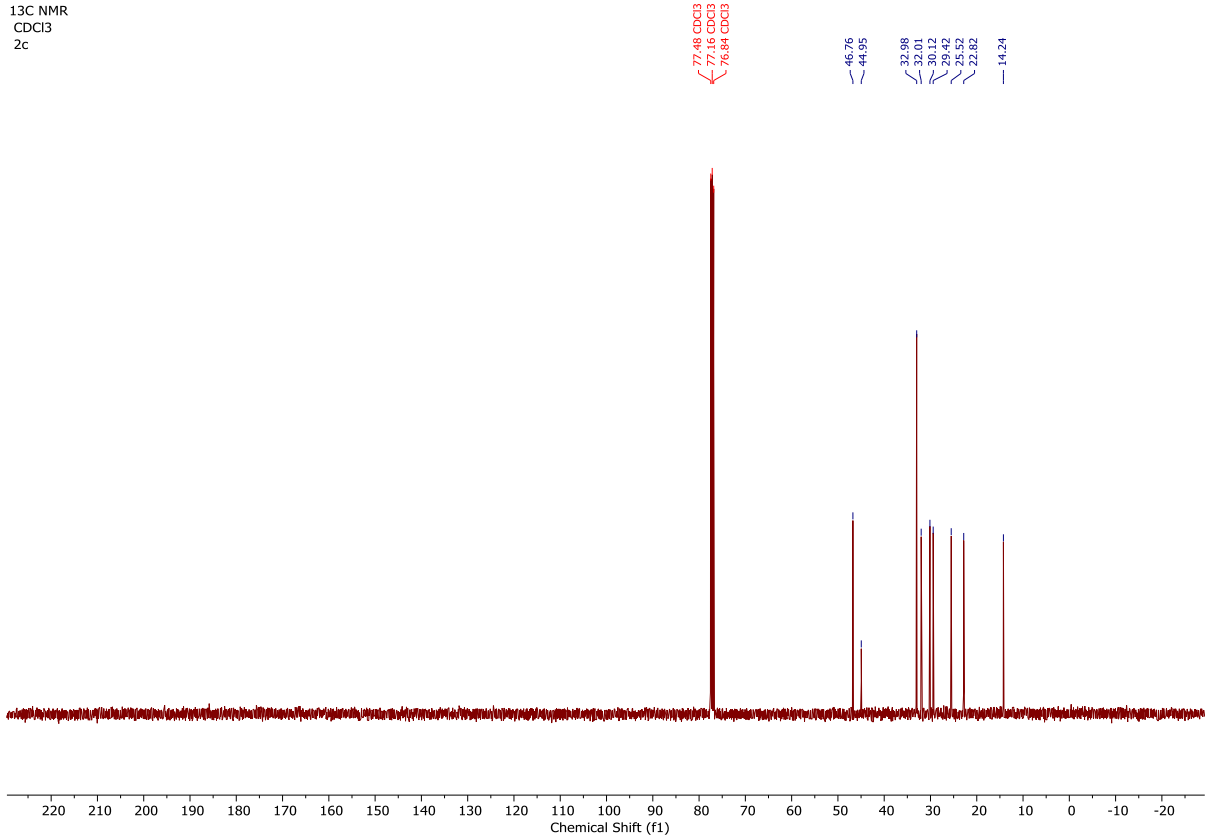

3,3’-dithiobis(benzoic acid) (**1b**)

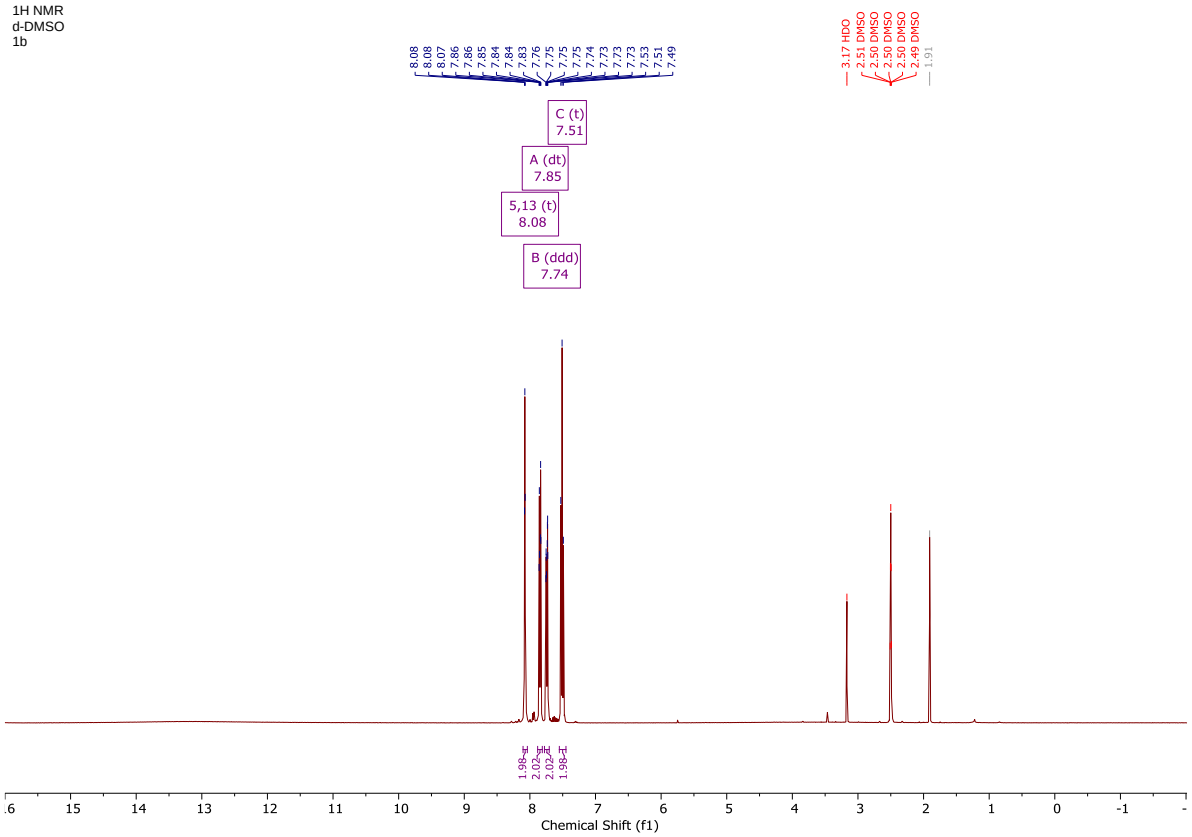

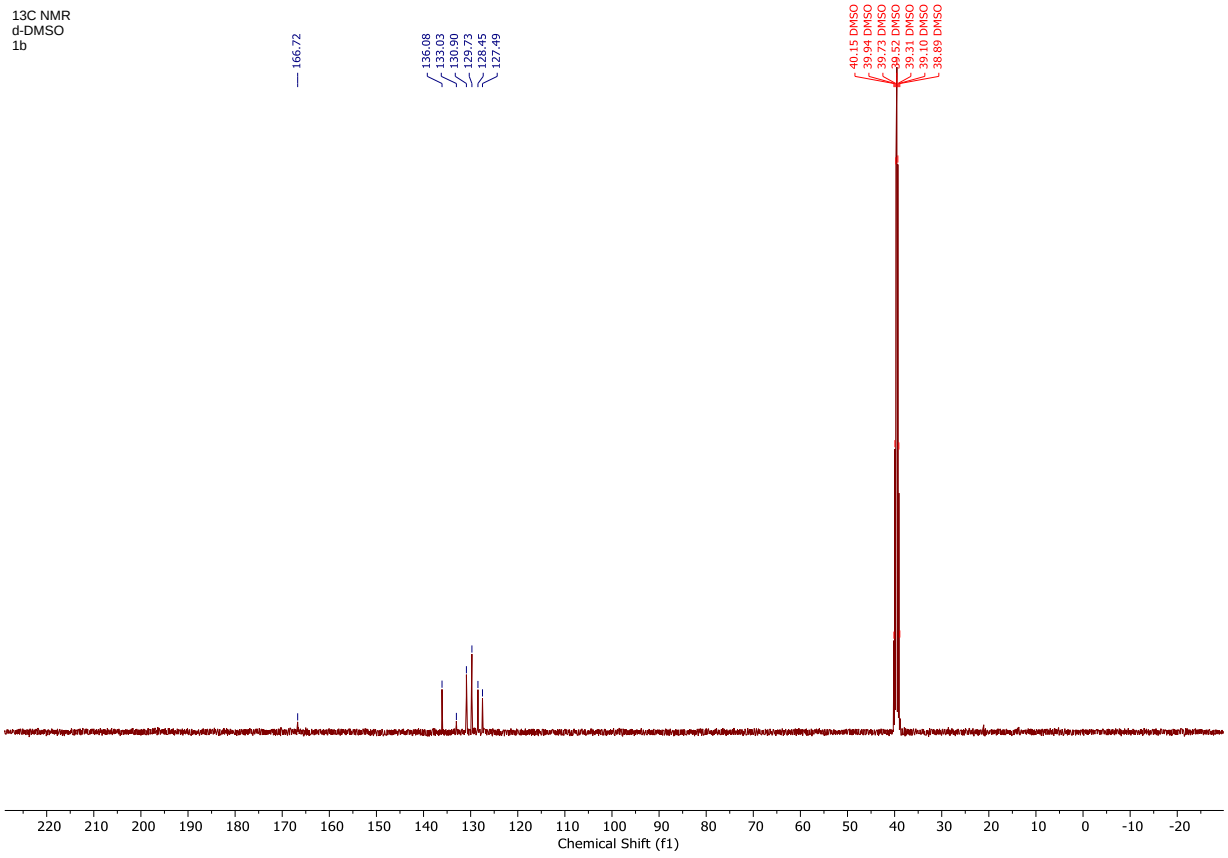

5-(chlorosulfonyl)-2-methoxybenzoic acid (**6**)

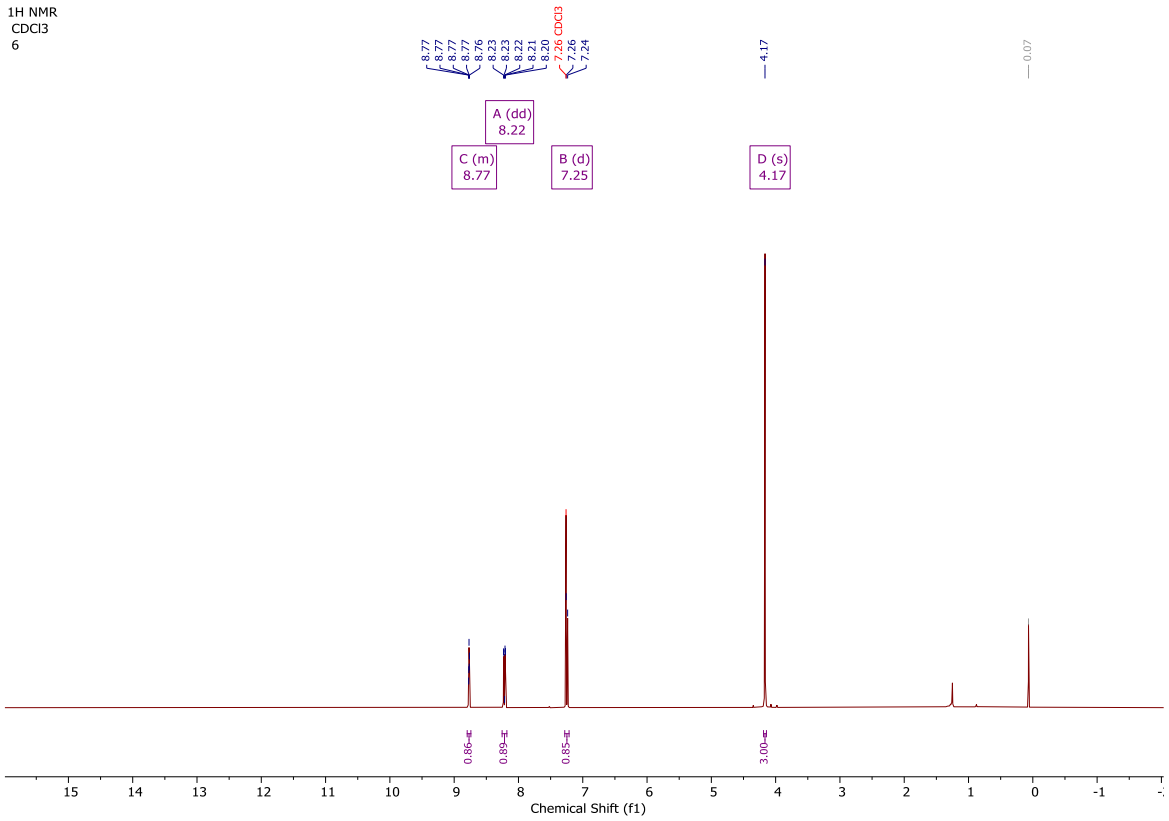

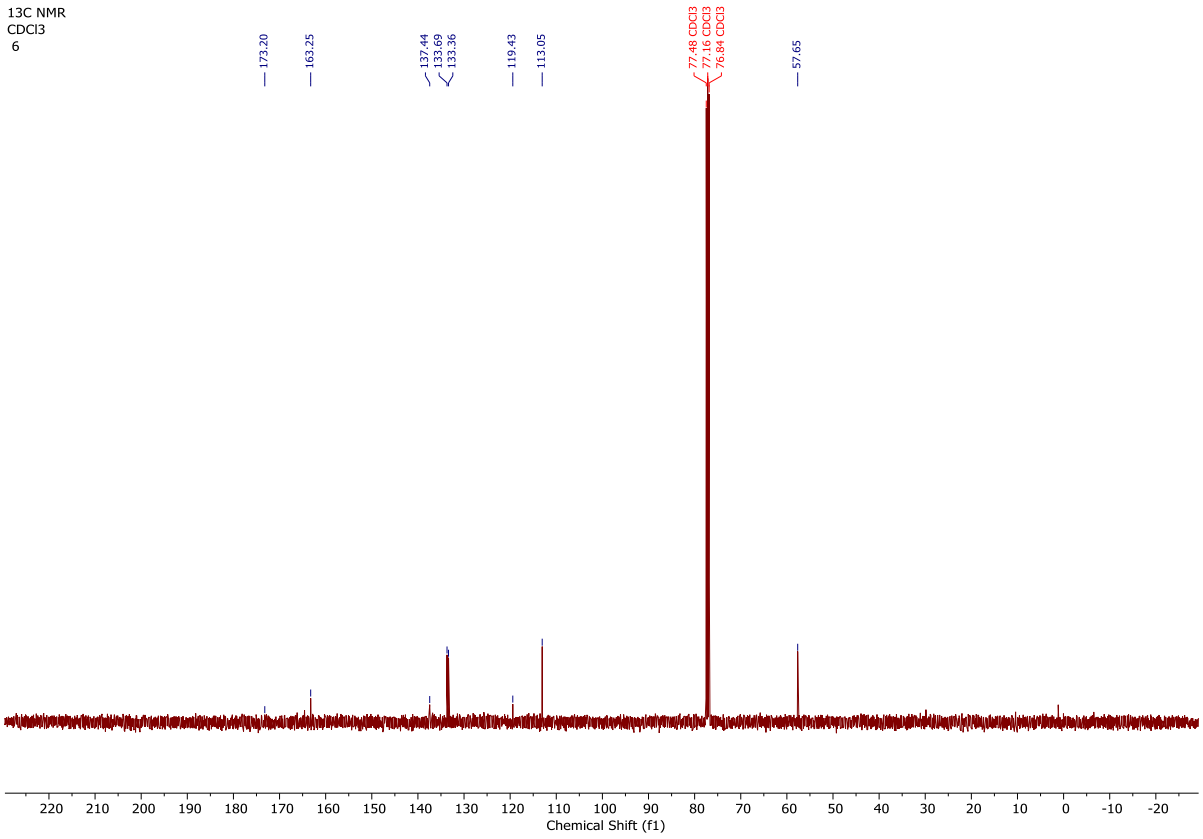

5-mercapto-2-methoxybenzoic acid (**4c**)

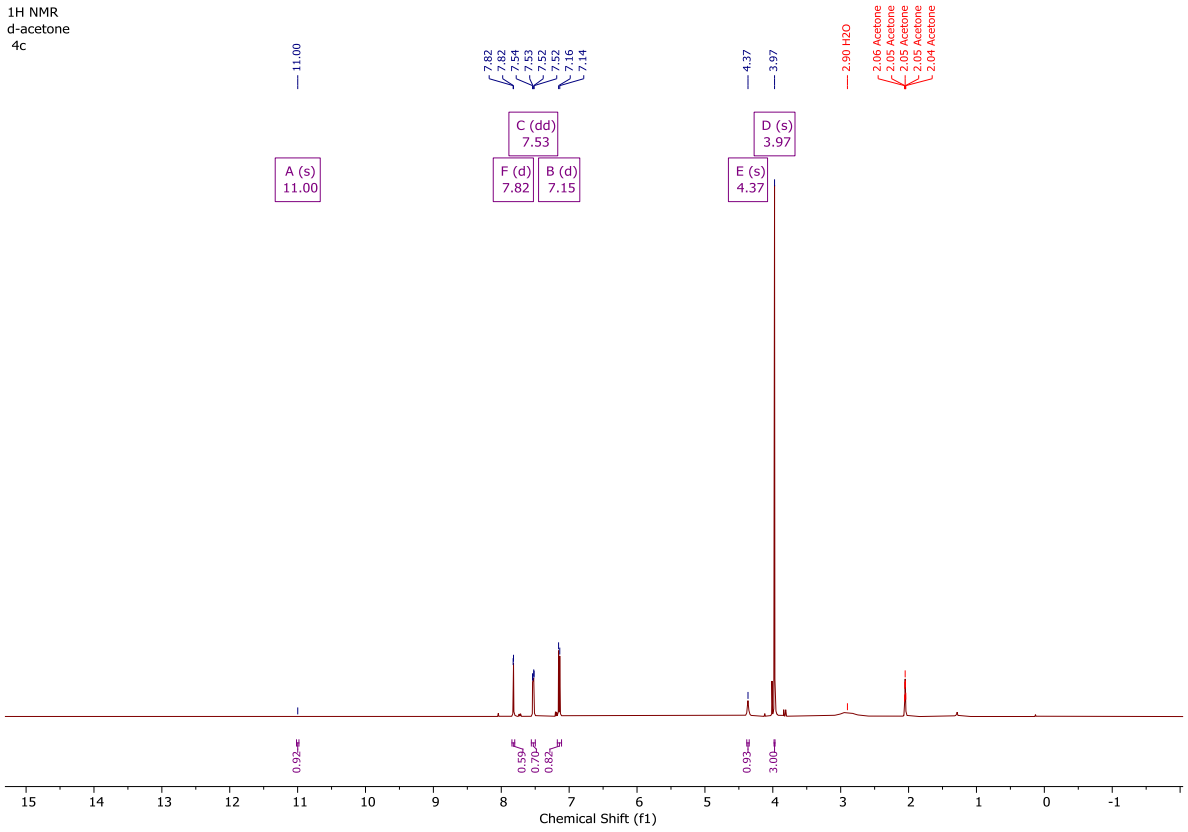

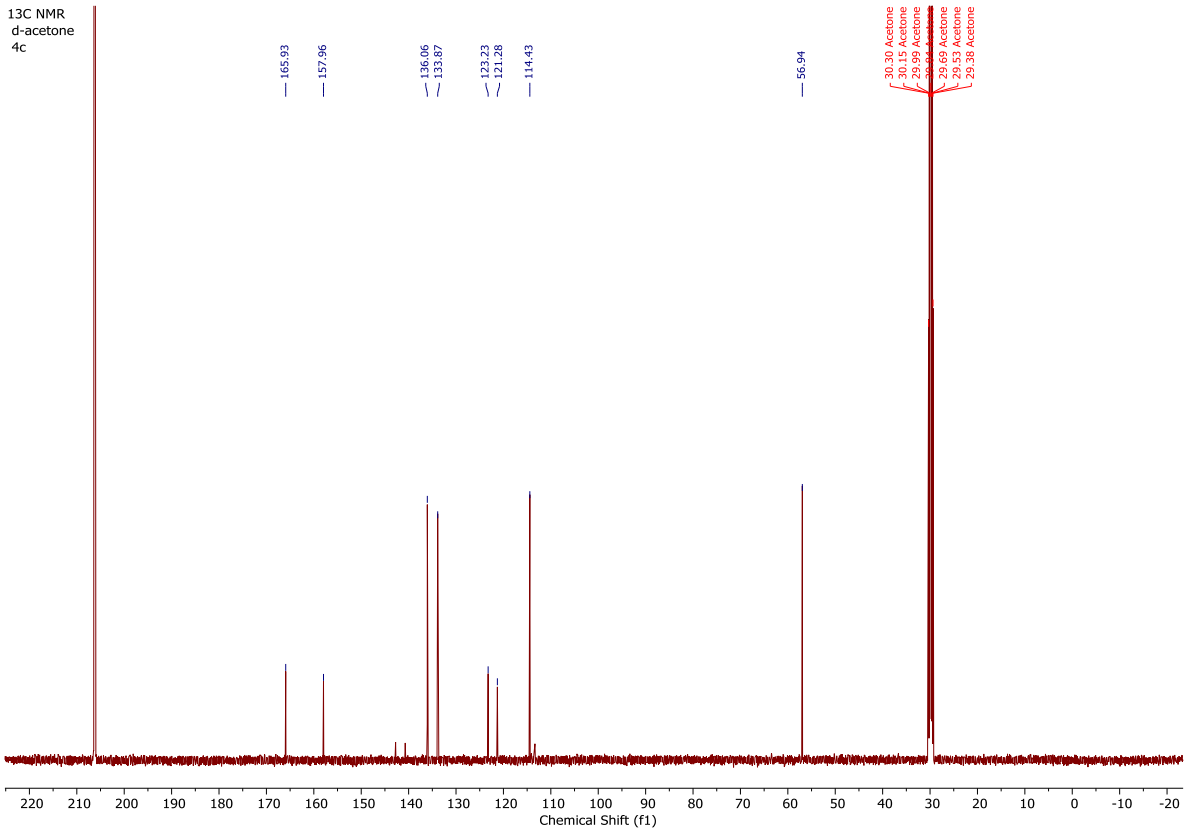

5,5’-dithiobis(2-methoxybenzoic acid) (**1c**)

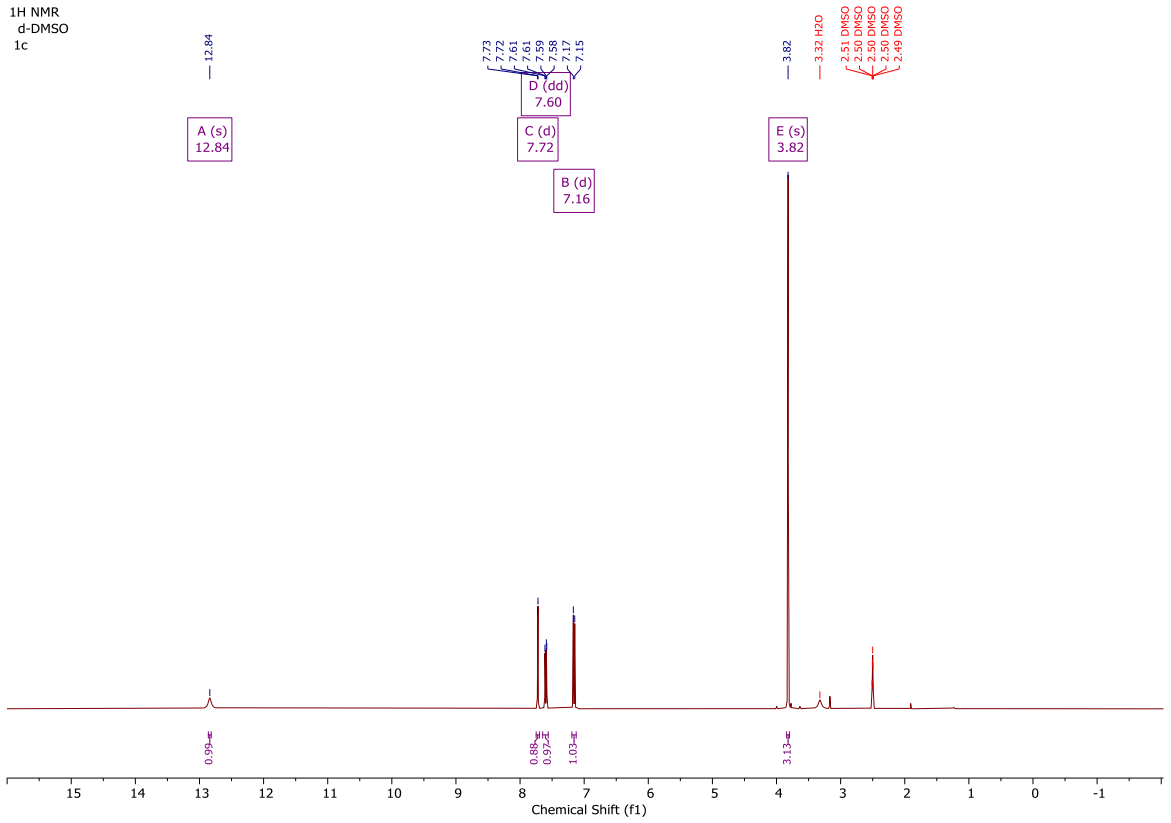

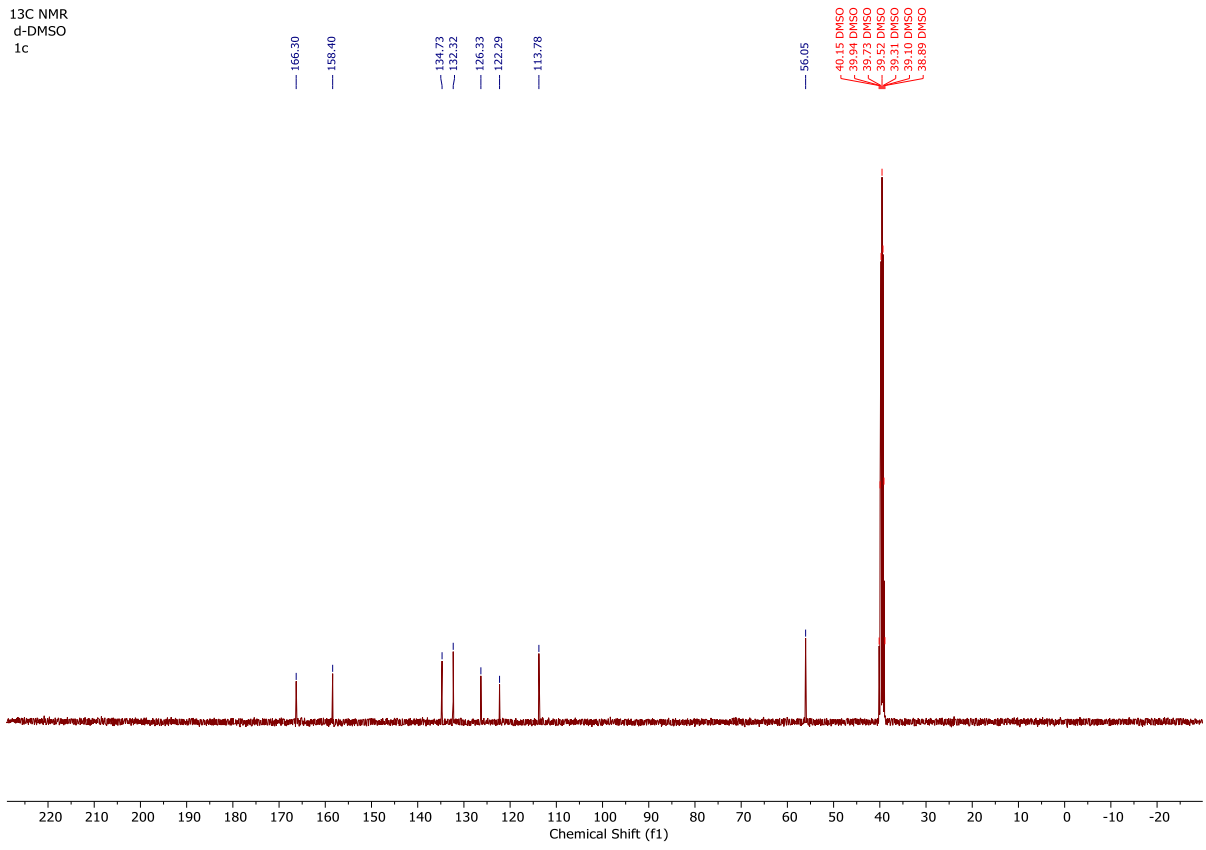

2-nitro-5-(octyldisulfaneyl)benzoic acid (**3aa**)

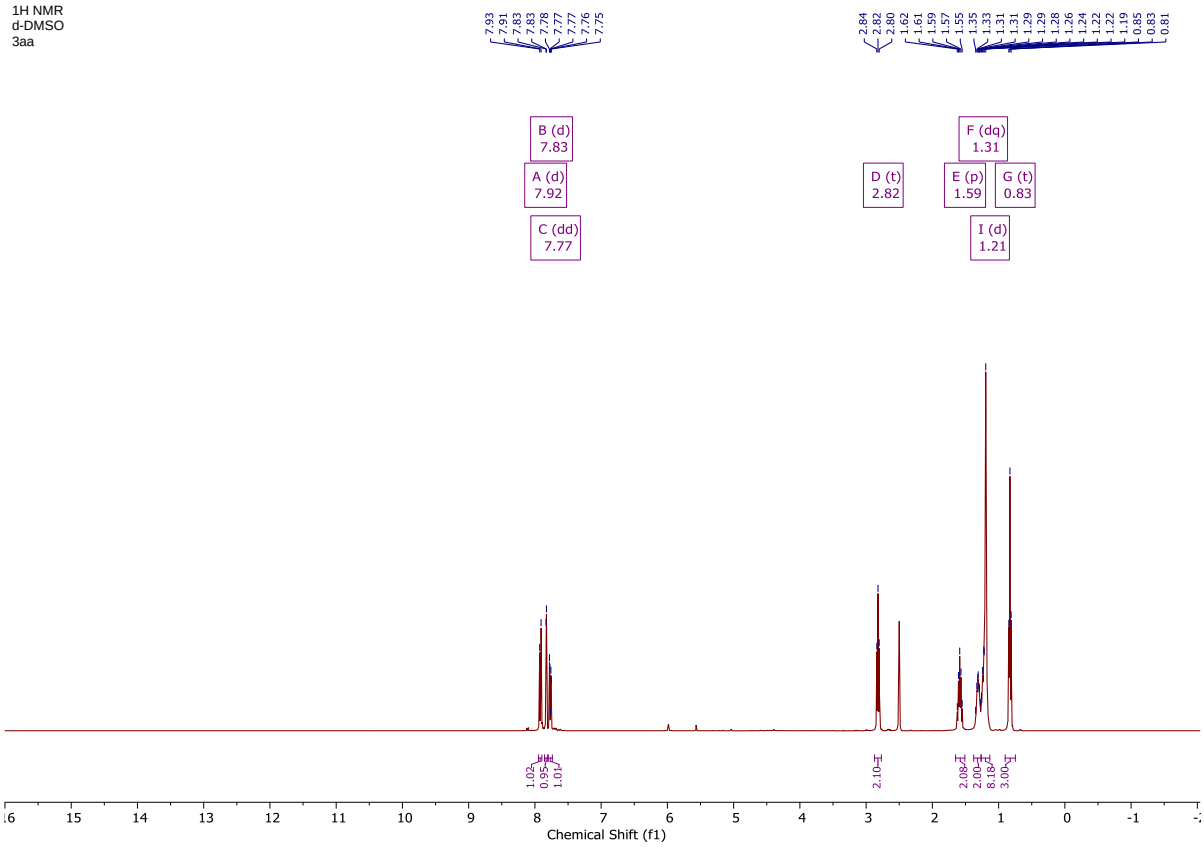

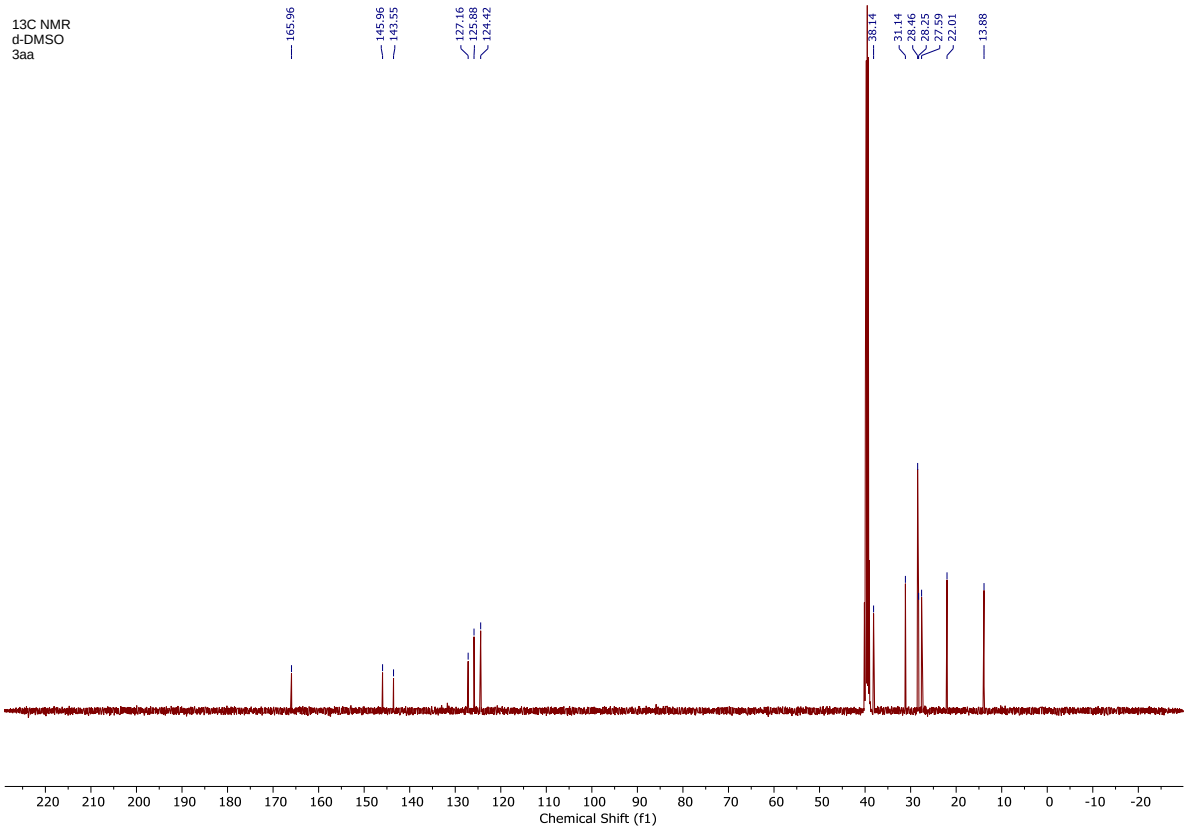

2-nitro-5-(nonan-2-yldisulfaneyl)benzoic acid (**3ab**)

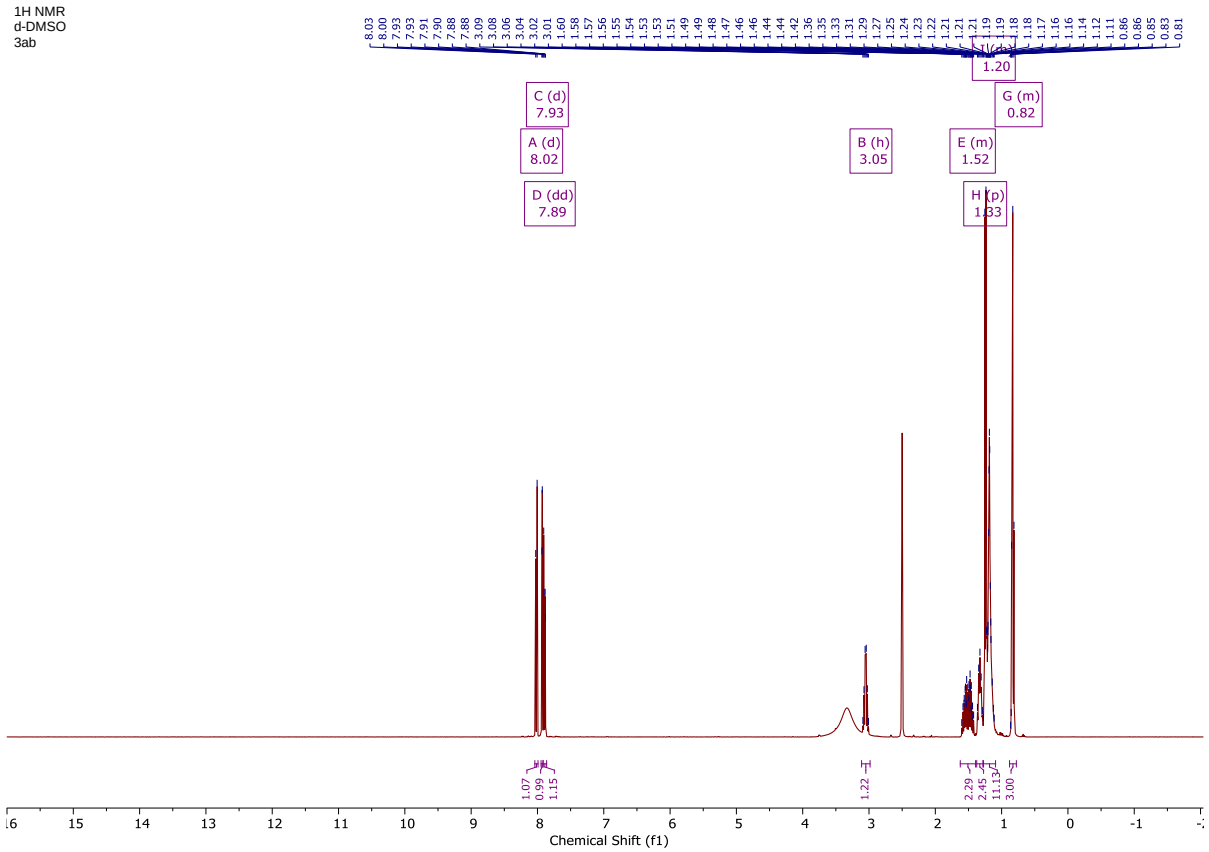

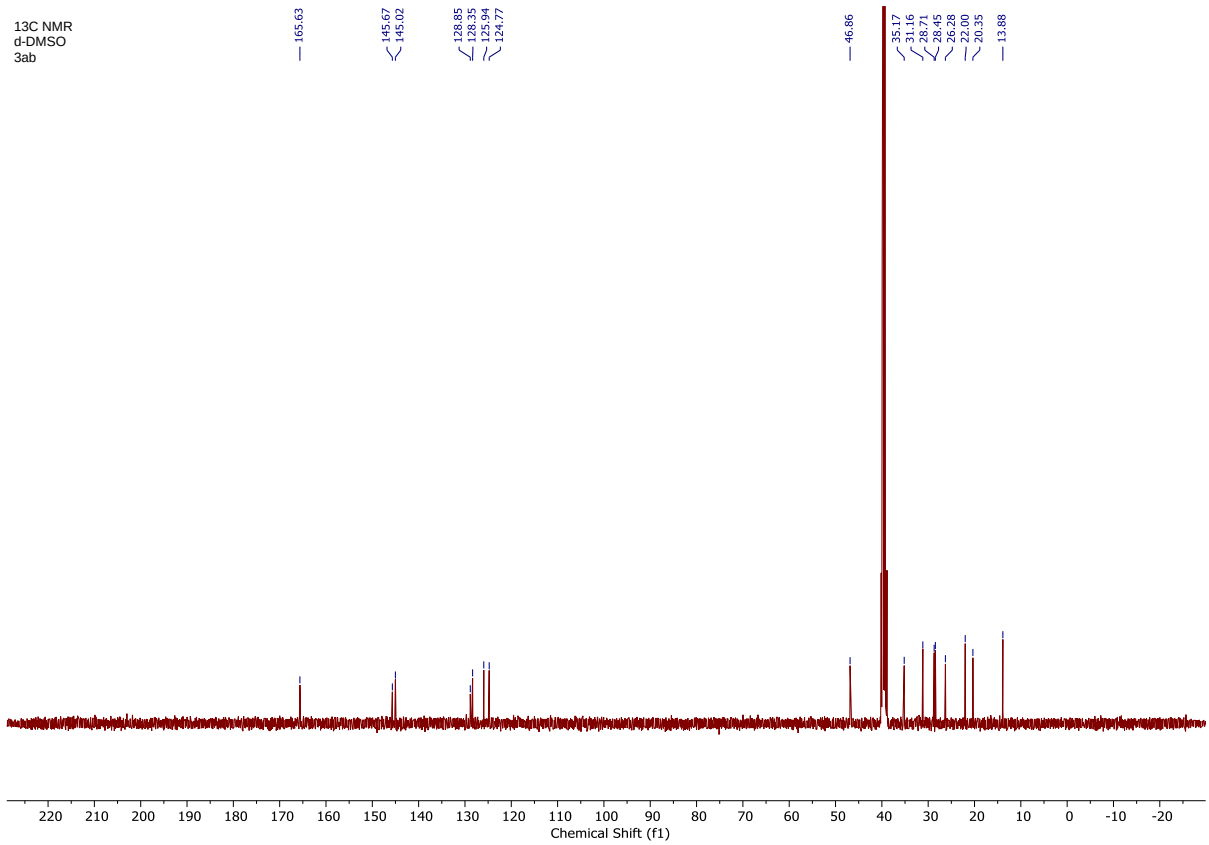

2-nitro-5-((2-methylnonan-2-yl)disulfaneyl)benzoic acid (**3ac**)

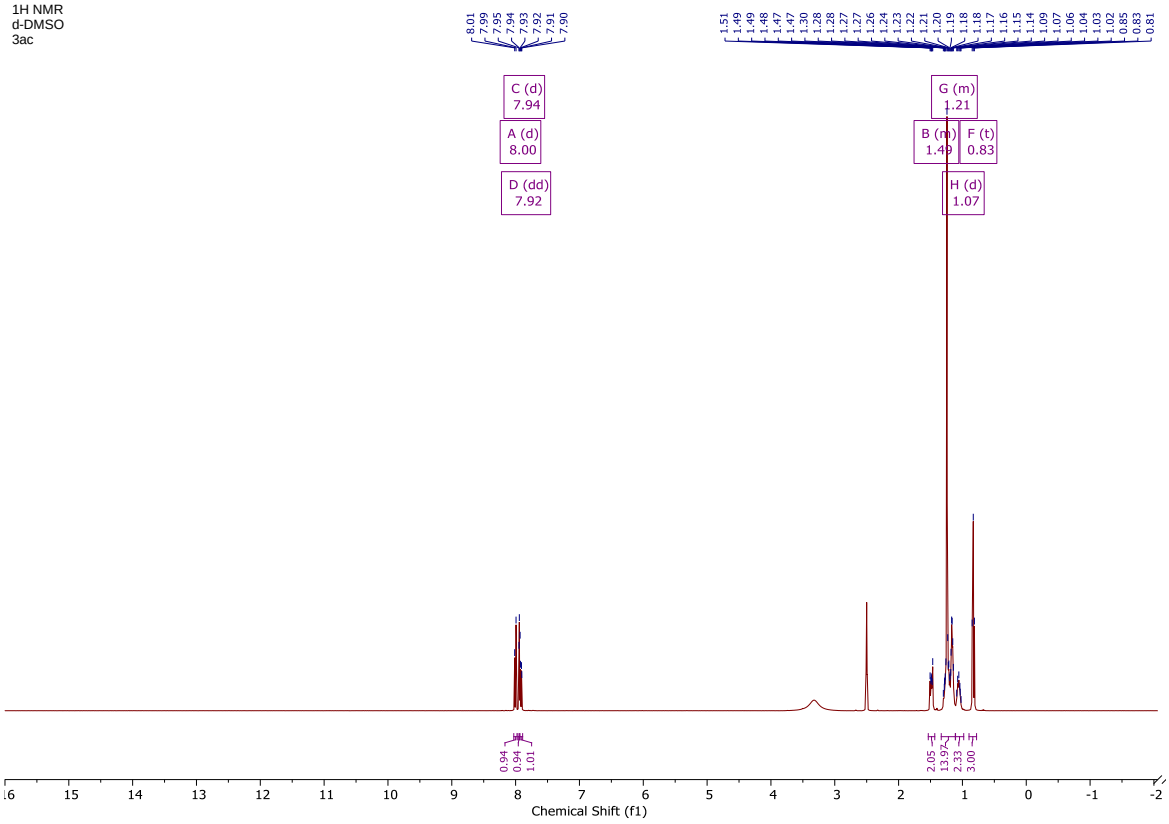

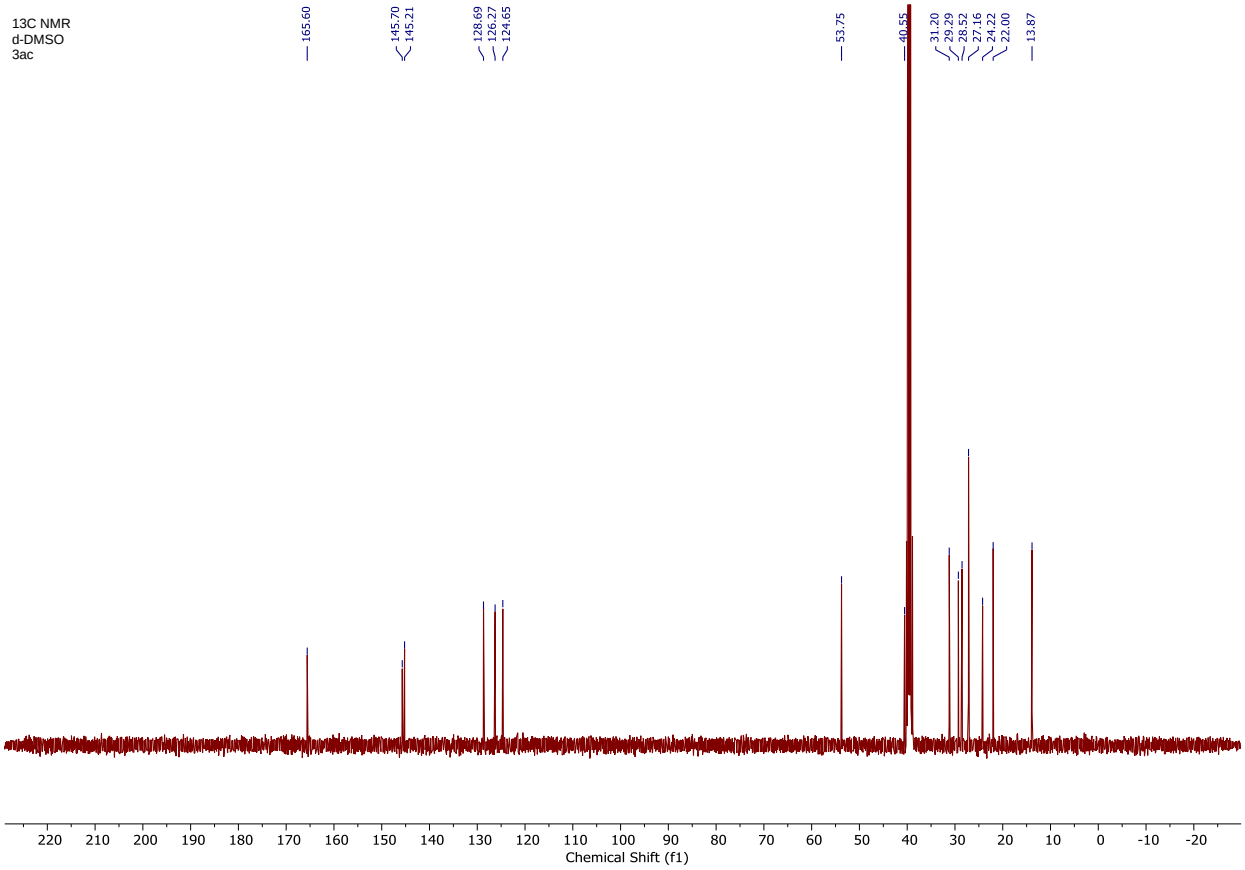

3-(octyldisulfaneyl)benzoic acid (**3ba**)

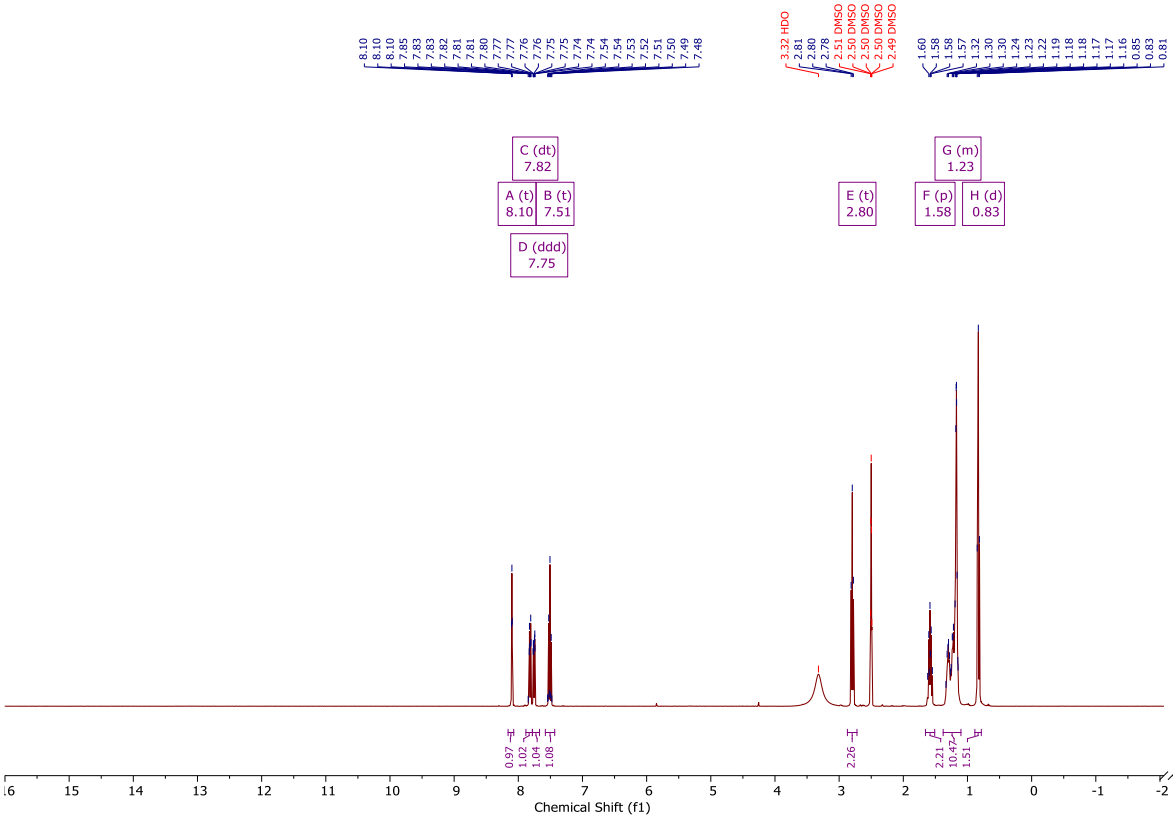

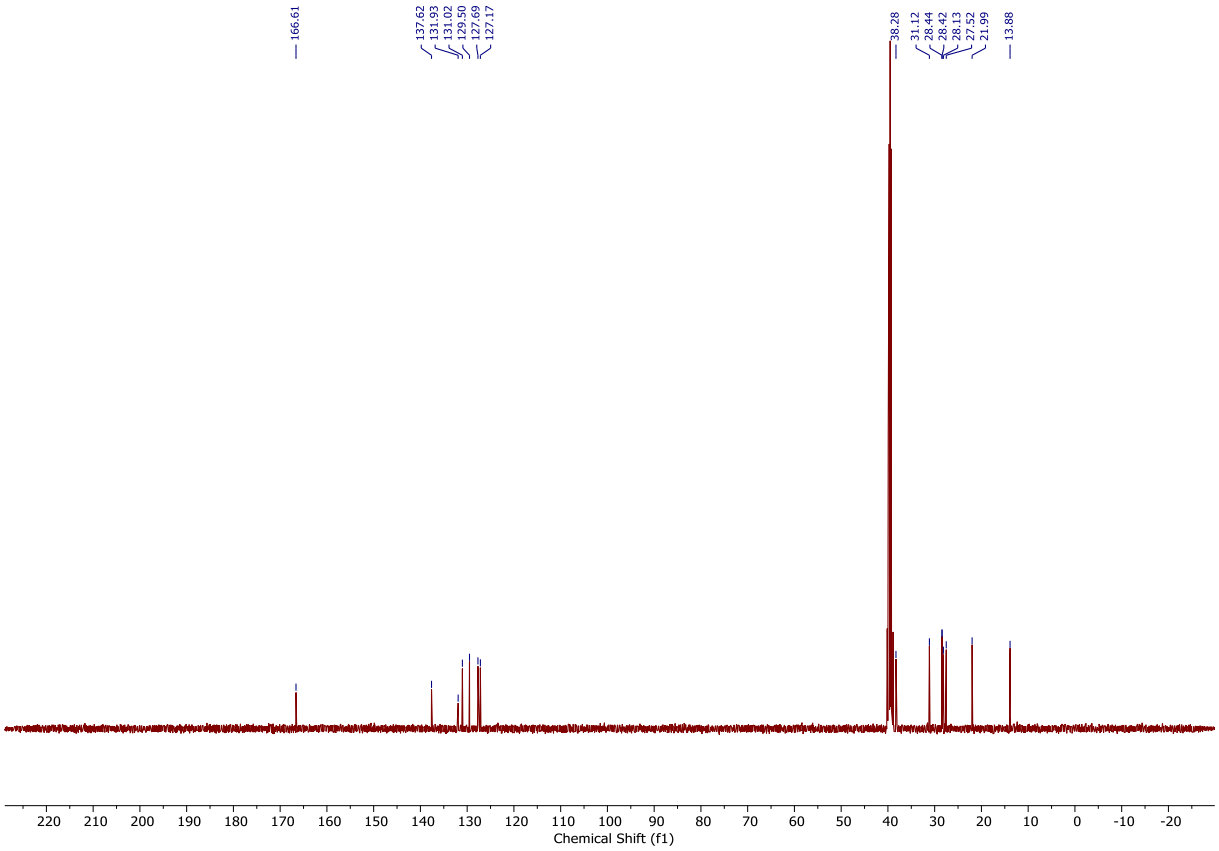

3-(nonan-2-yldisulfaneyl)benzoic acid (**3bb**)

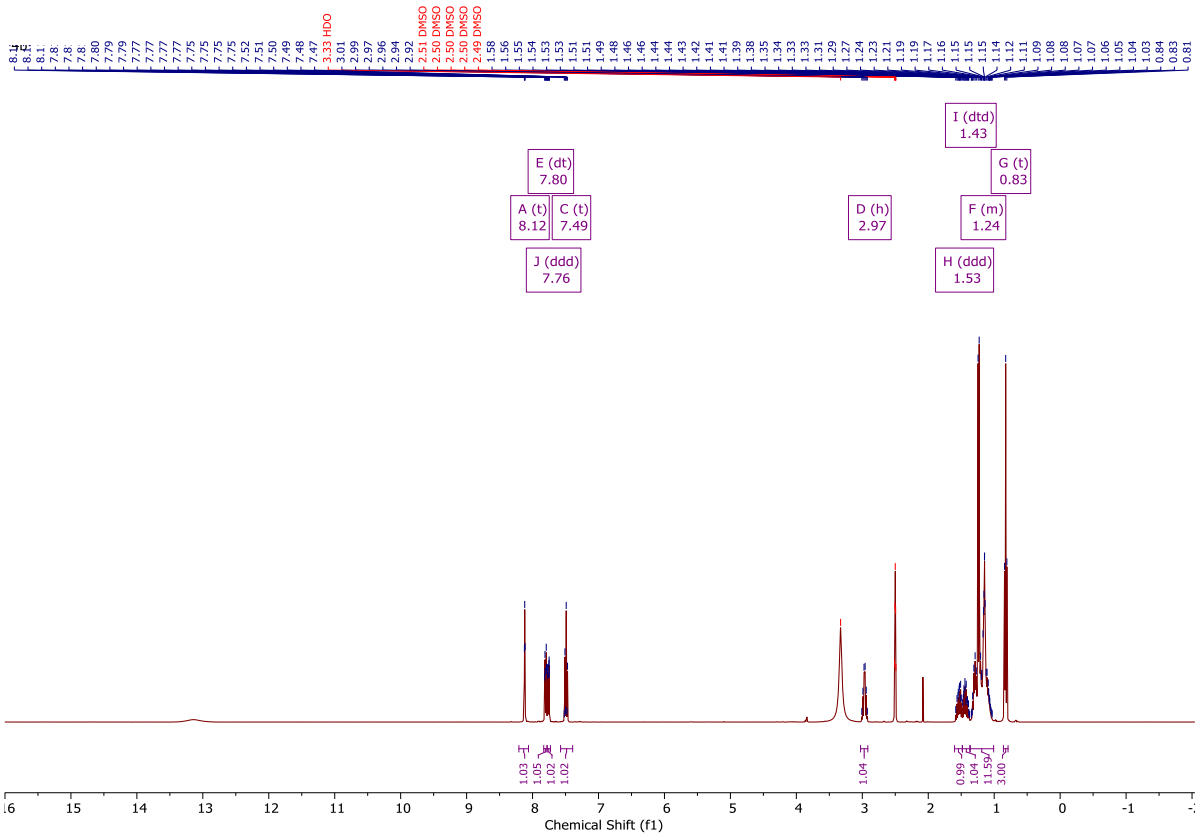

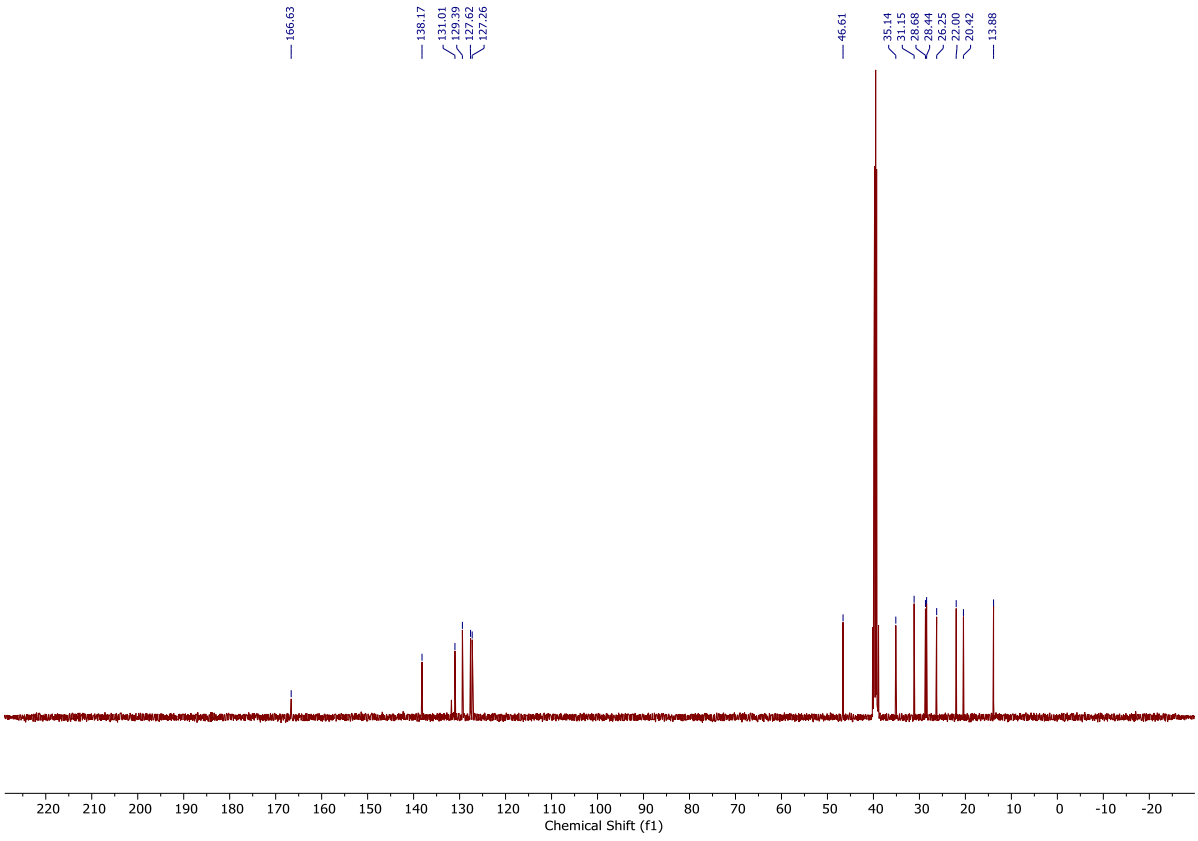

3-(2-methylnonan-2-yl)disulfaneyl)benzoic acid (**3bc**)

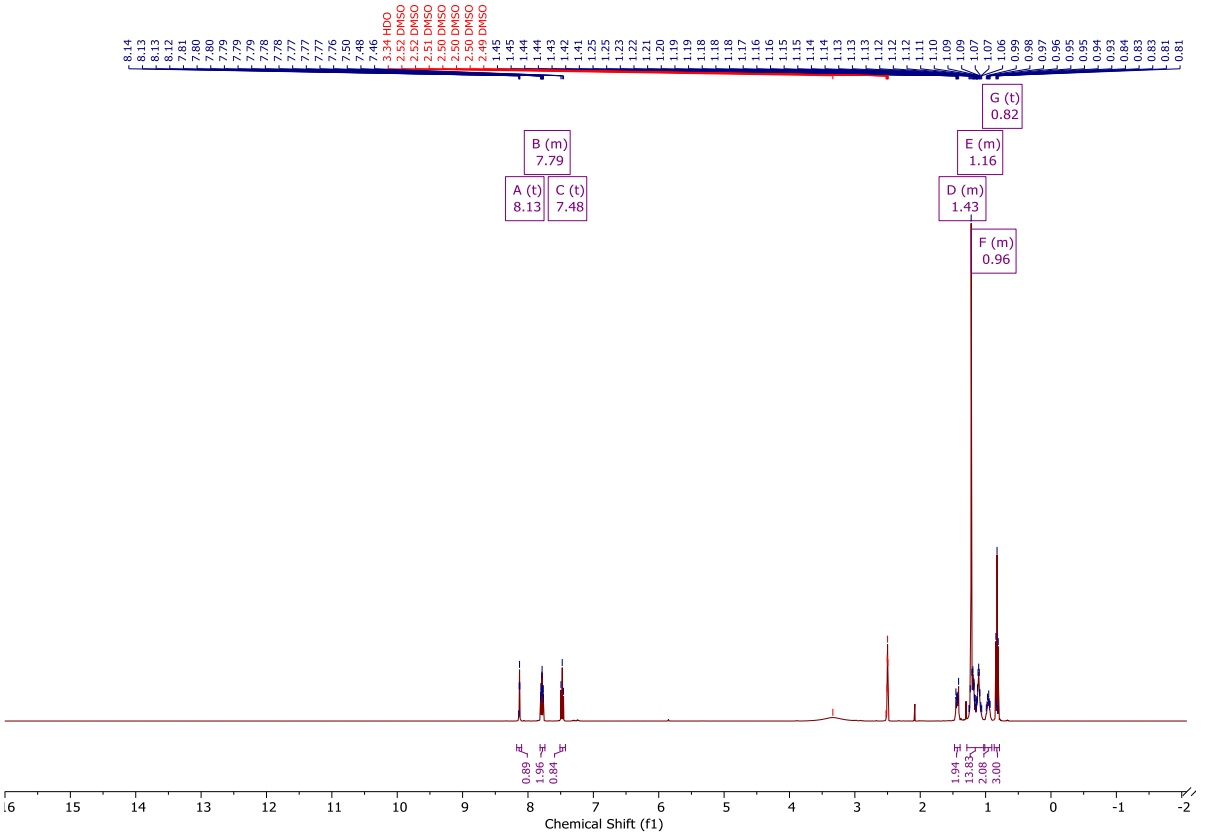

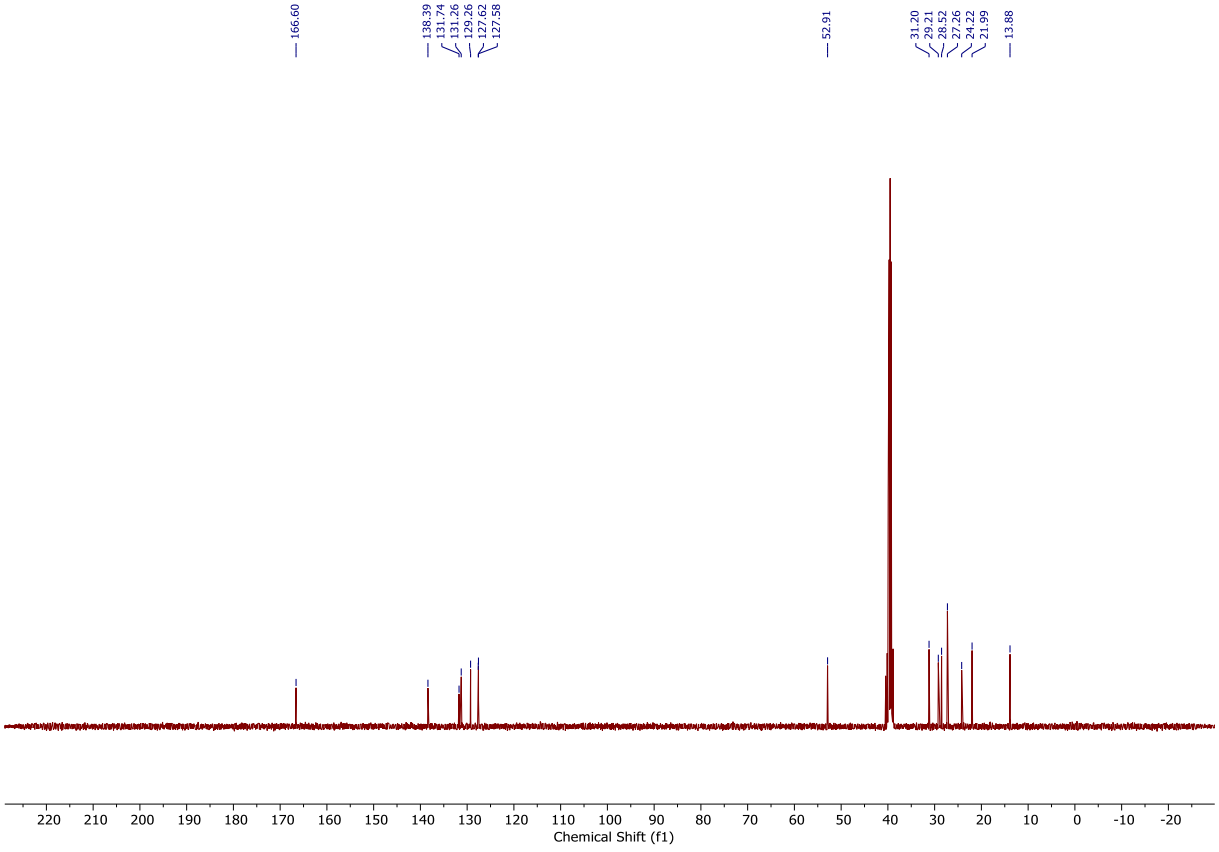

2-methoxy-5-(octyldisulfaneyl)benzoic acid (**3ca**)

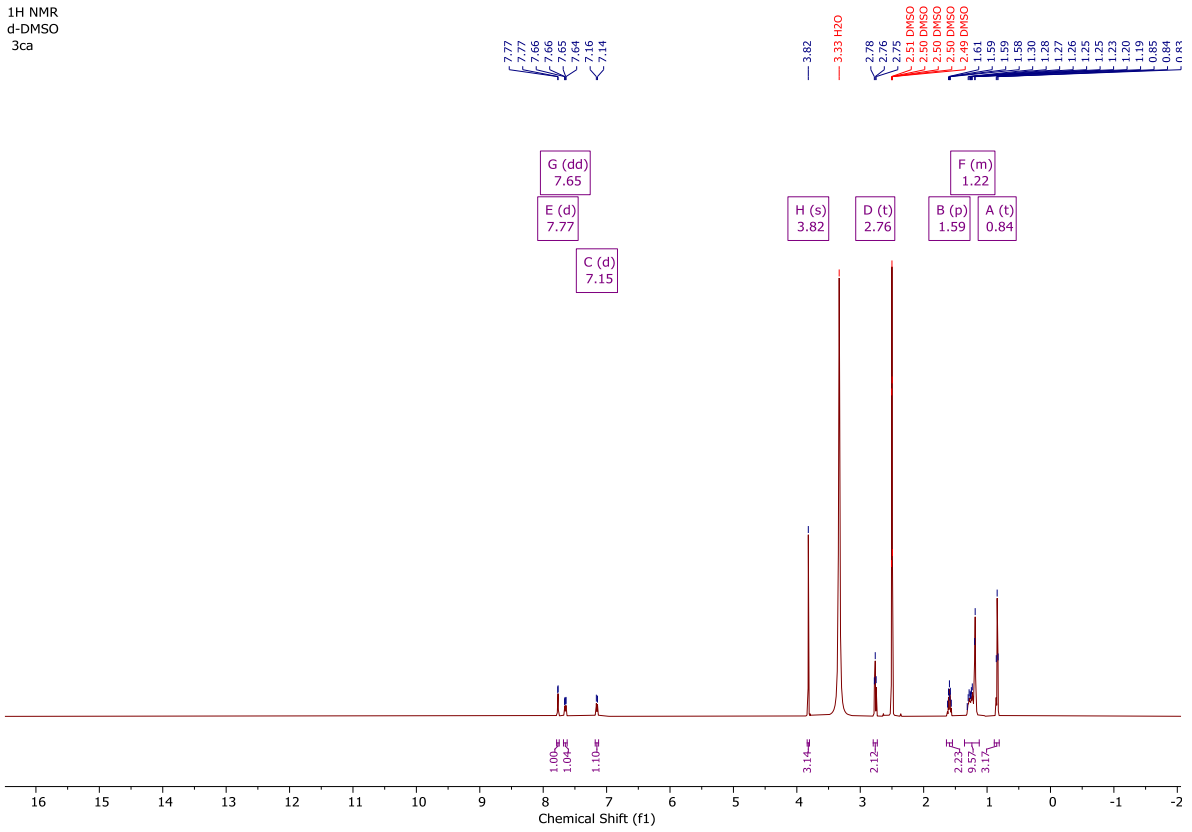

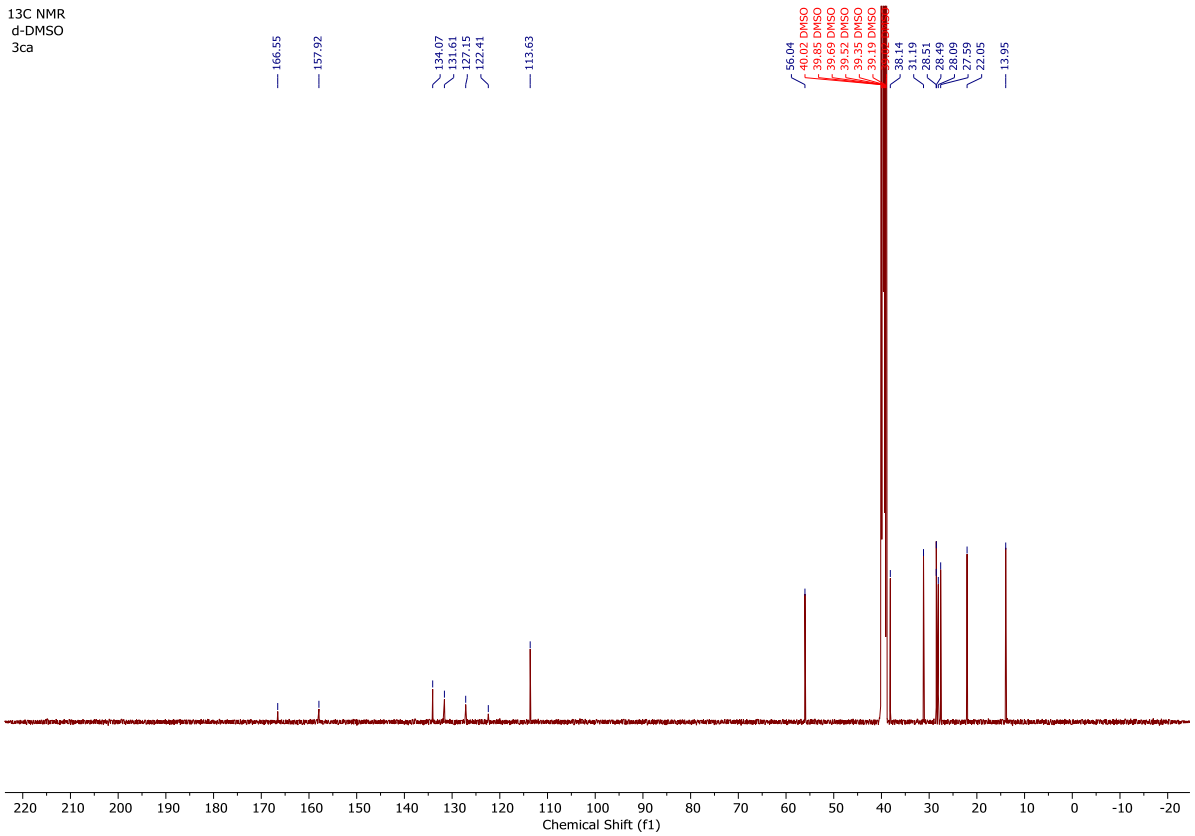

2-methoxy-5-(nonan-2-yldisulfaneyl)benzoic acid (**3cb**)

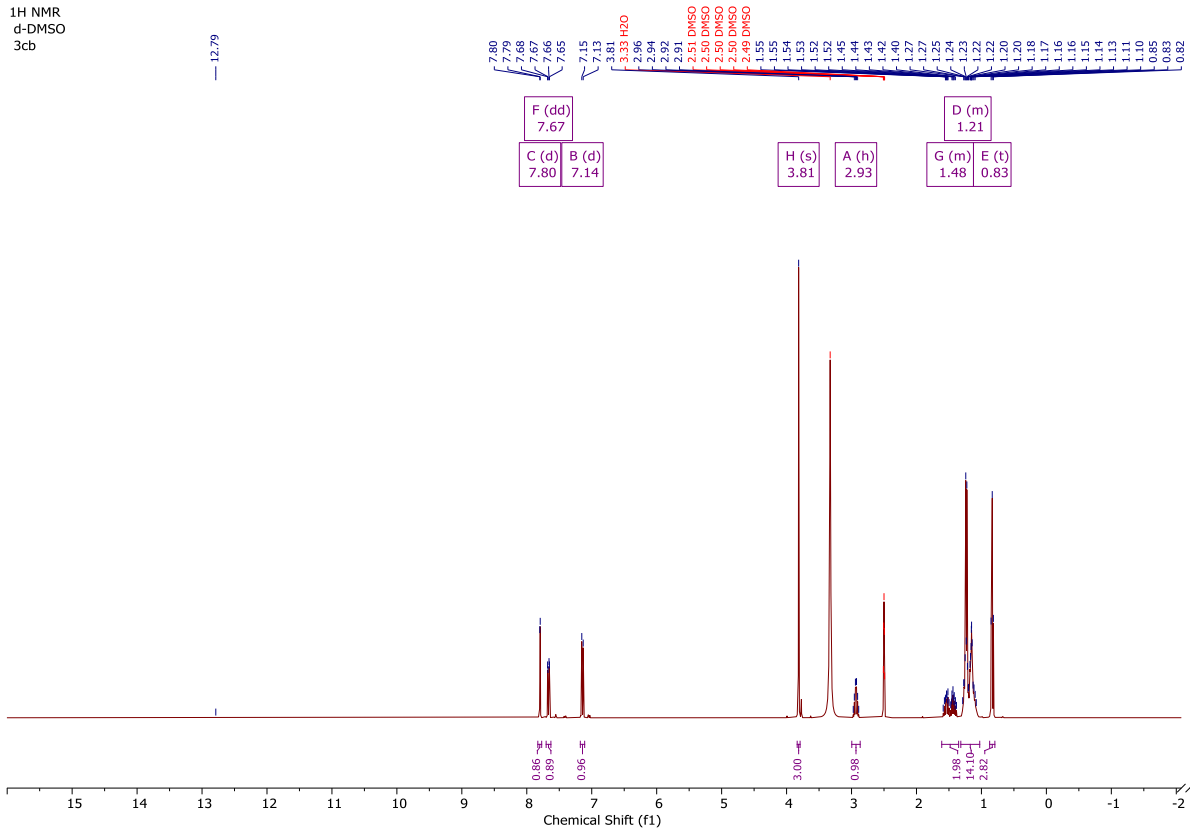

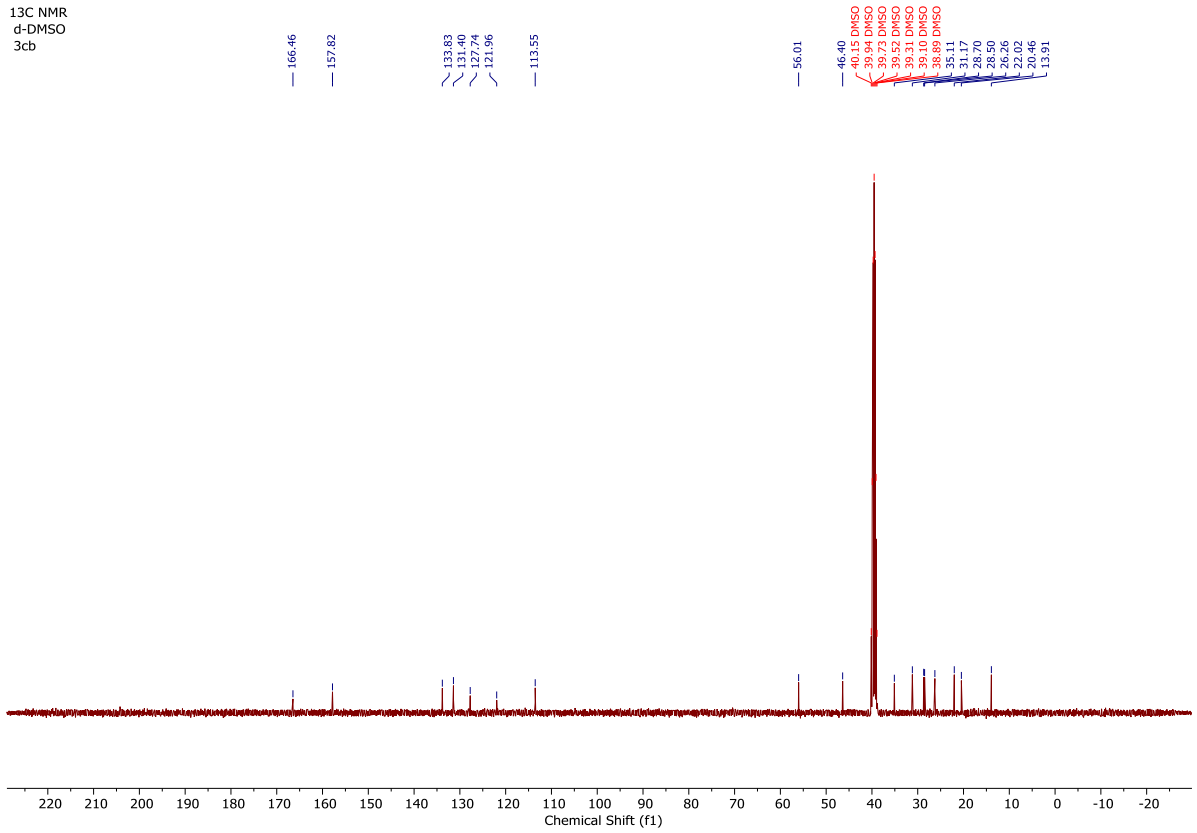

2-methoxy-5-(2-methylnonan-2-yl)disulfaneyl)benzoic acid (**3cc**)

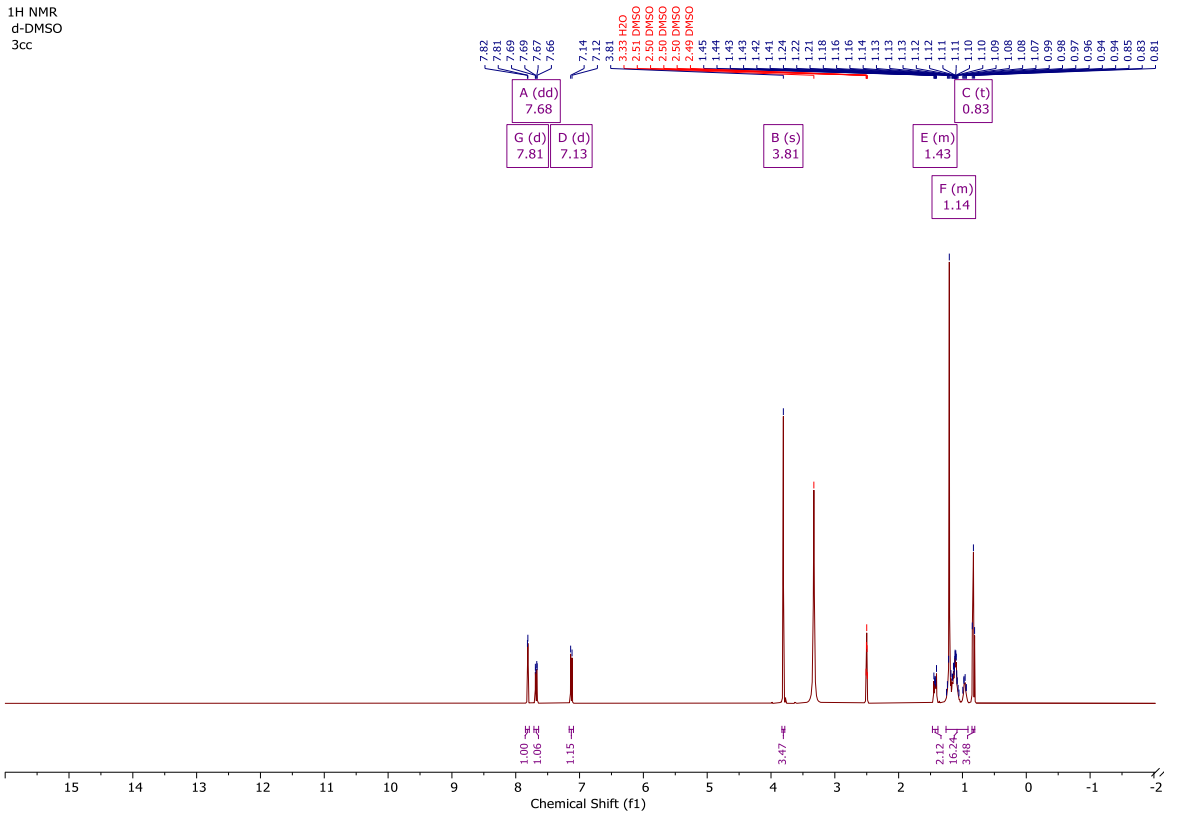

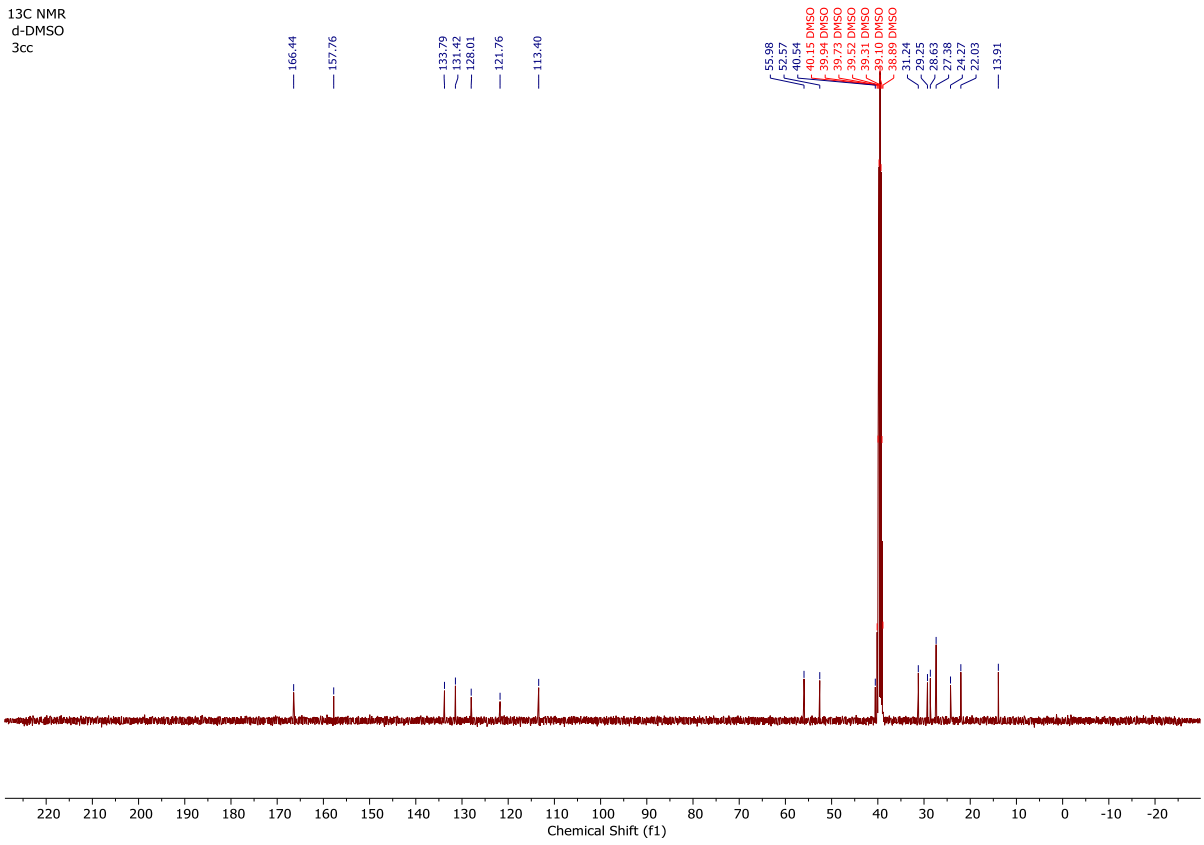

7.2.3 Procedures for kinetic experiments

Biphasic reaction setup: reactions were performed in 10 mL round bottom flasks using Fisherbrand oval 20 x 10 mm PTFE stir bars and were stirred using IKA RCT basic stir plates. At room temperature, once all the aqueous components were dissolved, the *appropriate thiol* (**2**) (1.0 or 8.0 eq.) was carefully layered onto an aqueous solution of the *appropriate disulfide* **1** (25 mM, 1.00 mmol, 1.0 eq.) in 4-(2-hydroxyethyl)-1-piperazineethanesulfonic acid (HEPES) aqueous buffer (pH 8.00, 4.0 mL) whilst stirring at 100 rpm. For reactions involving multiple aryl disulfides, the total initial concentration $[ArSSAr]_0$ was set as 25.0 mM and the aqueous solution was pre-stirred for 10 minutes prior to **2** addition. For reactions involving disulfide **1c**, experiments were set up under an inert atmosphere: buffer solutions and vessels were degassed by sparging with argon for a minimum of 1 hour and were sealed with a rubber septum and a positive argon pressure maintained, including during the sampling of aliquots.

Kinetic monitoring of reactions: all UV-active reaction species of interest were monitored and quantified by the UPLC analysis of aliquots. Reactions were sampled by withdrawing precisely 25 µL aliquots from the lower aqueous layer by microsyringe (Hamilton 25 µL Gastight) and quenching with precisely 1.0 mL of quench solution (maleimide, 6 mg/mL Milli-Q water) before injection into the UPLC instrument for quantification. Kinetics experiments were run in triplicate under identical conditions and occurred simultaneously, unless otherwise stated.

7.2.4 UPLC methods

UPLC gradients: mobile phases used in all methods are as follows: H_2O, MeCN, MeOH and 2% aqueous TFA. A multipurpose 5 minute gradient was used to monitor reactions containing only one aryl disulfide whereas further optimization was required for separating and quantifying more complex mixtures. The solvent gradients used are shown in the following tables, as are the retention times of species relevant to that gradient.

Table S1. Gradient 1.[a]

Time /mins	Flow rate /mLmin^{-1}	H_2O /%	MeCN /%	5% aq. TFA /%	Curve
0.00	0.600	93.0	2.0	5.0	Initial
0.25	0.600	93.0	2.0	5.0	6
4.00	0.600	2.0	93.0	5.0	6
4.40	0.600	2.0	93.0	5.0	6
4.50	0.600	93.0	2.0	5.0	10
5.00	0.600	93.0	2.0	5.0	10

[a] General purpose gradient that was used to monitor reactions containing one aryl disulfide.

Table S2. Retention time of relevant peaks for a typical elution using Gradient 1.

Compound	Retention time /mins
Aryl thiols **4**	1.84-1.90
Aryl disulfides **1**	2.63-2.74
Surfactant products (mixed disulfides) **3**	4.01-4.39

Table S3. Gradient 2.[a]

Time /mins	Flow rate /mLmin^{-1}	H_2O /%	MeCN /%	5% aq. TFA /%	Curve
0.00	0.250	88.0	2.0	10.0	Initial
0.25	0.250	88.0	2.0	10.0	6
0.75	0.250	58.0	32.0	10.0	6
8.50	0.250	58.0	32.0	10.0	6
8.60	0.250	2.0	93.0	5.0	6
9.90	0.250	2.0	93.0	5.0	6
10.00	0.250	88.0	2.0	10.0	10
10.50	0.250	88.0	2.0	10.0	10

[a] Specific gradient for mixtures of aryl disulfides, giving a distinct retention time for each one.

Table S4. Retention time of relevant peaks for a typical elution using Gradient 2.

Compound	Retention time /mins
homoaryl disulfide **1c**	5.45
heteroaryl disulfide **1f**	6.01
homoaryl disulfide **1a**	6.22
heteroaryl disulfide **1e**	6.49
heteroaryl disulfide **1d**	7.12
homoaryl disulfide **1b**	7.97

Table S5. Gradient 3a.[a]

Time /mins	Flow rate /mLmin^{-1}	H_2O /%	MeCN /%	5% aq. TFA /%	Curve
0.00	0.600	93.0	2.0	5.0	Initial
0.25	0.600	93.0	2.0	5.0	6
0.50	0.600	90.0	5.0	5.0	6
3.75	0.600	68.0	27.0	5.0	6
4.00	0.600	2.0	93.0	5.0	6
4.40	0.600	2.0	93.0	5.0	6
4.50	0.600	93.0	2.0	5.0	11
5.00	0.600	93.0	2.0	5.0	11

[a] Specific gradient for monitoring mixtures of aryl thiols, giving a distinct retention time for each one.

Table S6. Retention time of relevant peaks for a typical elution using Gradient 3a.

Compound	Retention time /mins
aryl thiol **4c**	2.65
aryl thiol **4a**	2.83
aryl thiol **4b**	2.89

Table S7. Gradient 3b.[a]

Time /mins	Flow rate /mLmin^{-1}	H_2O /%	MeCN /%	5% aq. TFA /%	Curve
0.00	0.450	93.0	2.0	5.0	Initial
0.25	0.450	93.0	2.0	5.0	6
0.50	0.450	90.0	5.0	5.0	6
3.75	0.450	72.0	23.0	5.0	6
4.00	0.450	2.0	93.0	5.0	6
4.40	0.450	2.0	93.0	5.0	6
4.50	0.450	93.0	2.0	5.0	11
5.00	0.450	93.0	2.0	5.0	11

[a] Alternative gradient for monitoring mixtures of aryl thiols, giving a distinct retention time for each one.

Table S8. Retention time of relevant peaks for a typical elution using Gradient 3b.

Compound	Retention time /mins
aryl thiol **4c**	3.35
aryl thiol **4a**	3.55
aryl thiol **4b**	3.65

Table S9. Gradient 4a.[a]

Time /mins	Flow rate /mLmin^{-1}	H_2O /%	MeCN /%	MeOH /%	5% aq. TFA /%	Curve
0.00	0.600	78.0	2.0	15.0	5.0	Initial
0.25	0.600	78.0	2.0	15.0	5.0	6
0.75	0.600	23.0	57.0	15.0	5.0	6
3.50	0.600	19.0	61.0	15.0	5.0	5
4.00	0.600	19.0	61.0	15.0	5.0	6
4.10	0.600	1.0	93.0	1.0	5.0	6
4.80	0.600	78.0	2.0	15.0	5.0	11
5.00	0.600	78.0	2.0	15.0	5.0	10

[a] Specific gradient for monitoring mixtures of surfactant products (mixed disulfides). When used in combination with Gradient 4b, a distinct, quantifiable peak was obtained for each product.

Table S10. Retention time of relevant peaks for a typical elution using Gradient 4a.

Compound	Retention time /mins[a]
3ca	2.58
3aa	2.63
3cb	2.82
3ac	2.91
3ba	2.91
3cc	3.01
3ac	3.14
3bb	3.23
3bc	3.50

[a] Well resolved, quantifiable peaks for this gradient are underlined. See Gradient 4b for remaining peaks.

Table S11. Gradient 4b.[a]

Time /mins	Flow rate /mLmin^{-1}	H_2O /%	MeCN /%	MeOH /%	5% aq. TFA /%	Curve
0.00	0.450	83.0	2.0	10.0	5.0	Initial
0.25	0.450	83.0	2.0	10.0	5.0	6
0.75	0.450	34.0	51.0	10.0	5.0	6
3.50	0.450	30.0	55.0	10.0	5.0	5
6.40	0.450	24.0	61.0	10.0	5.0	6
6.50	0.450	1.0	93.0	1.0	5.0	6
7.20	0.450	83.0	2.0	10.0	5.0	11
7.50	0.450	83.0	2.0	10.0	5.0	10

[a] Specific gradient for monitoring mixtures of surfactant products (mixed disulfides). When used in combination with Gradient 4a, a distinct, quantifiable peak was obtained for each product.

Table S12. Retention time of relevant peaks for a typical elution using Gradient 4b.

Compound	Retention time /mins[a]
3ca	4.93
3aa	5.19
3cb	5.63
3ba	5.80
3ab	6.00
3cc	6.17
3ac	6.40
3bb	6.40
3bc	6.62

[a] Well resolved, quantifiable peaks for this gradient are underlined. See Gradient 4a for remaining peaks.

UPLC calibration curves: concentrations were quantified using the calibration constants found in the calibration plots below. Calibration of the reaction components was achieved by multiple injections of accurate solutions to give a linear fit. For heteroaryl disulfides **1d-f**, calibration constants were obtained by taking the mean of the absorbances of the respective homoaryl disulfides from which they originate.

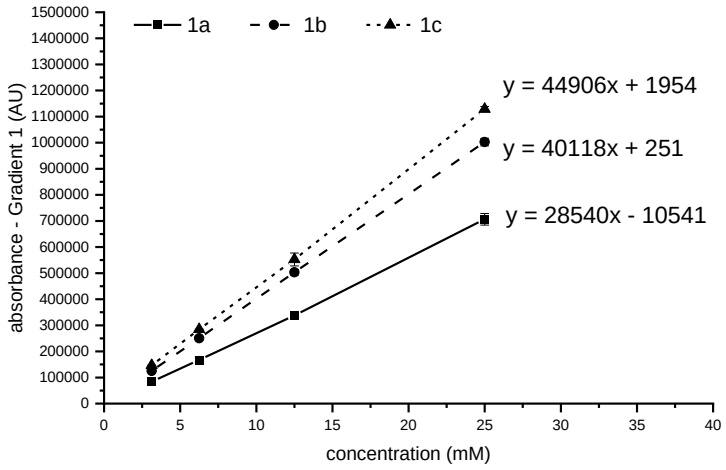

Figure S1: Calibration plot for compounds **1a-c** for UPLC analysis by Gradient 1. n = 3, error bars (where visible) represent the standard deviation

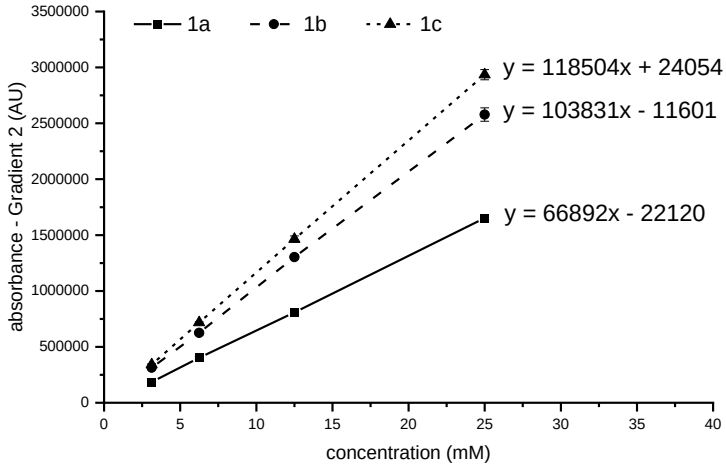

Figure S2: Calibration plot for compounds **1a-c** for UPLC analysis by Gradient 2. n = 3, error bars (where visible) represent the standard deviation

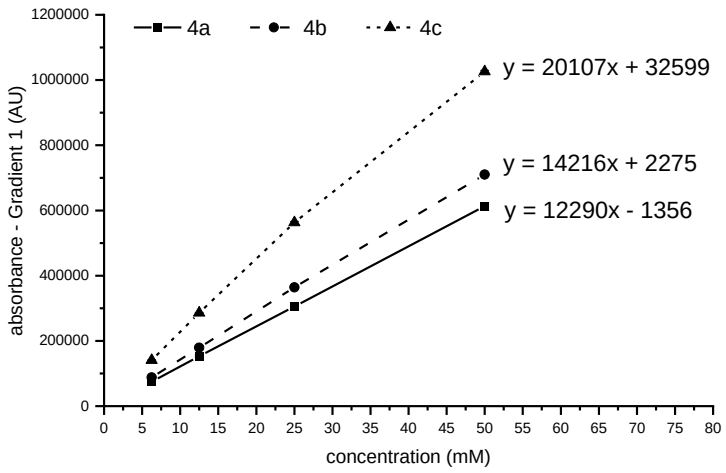

Figure S3: Calibration plot for compounds **4a**-**c** for UPLC analysis by Gradient 1. n = 3, error bars (where visible) represent the standard deviation

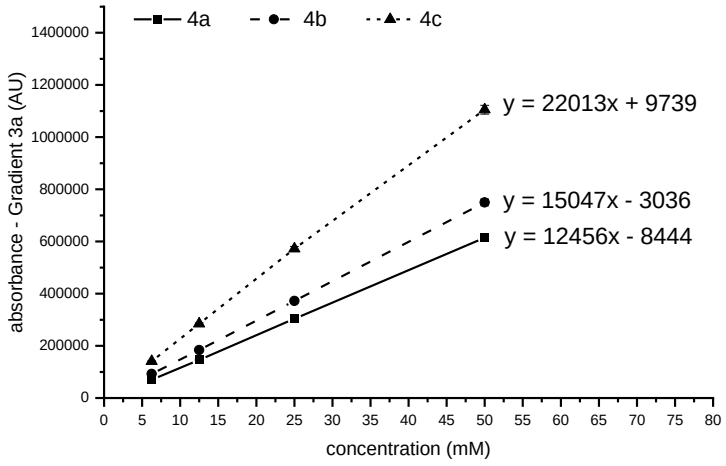

Figure S4: Calibration plot for compounds **4a**-**c** for UPLC analysis by Gradient 3a. n = 3, error bars (where visible) represent the standard deviation

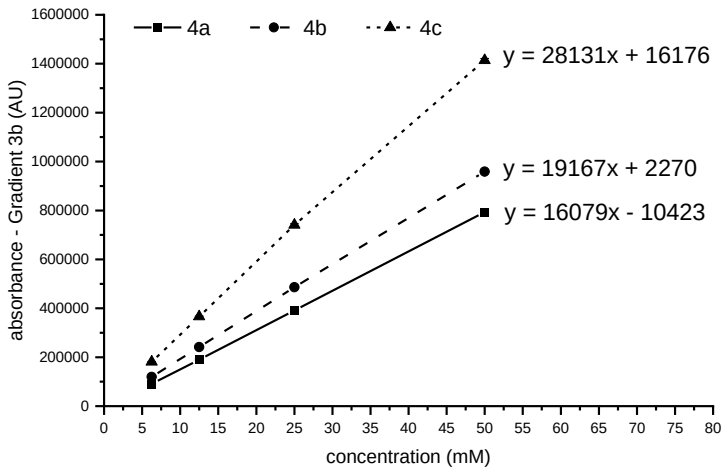

Figure S5: Calibration plot for compounds **4a-c** for UPLC analysis by Gradient 3b. n = 3, error bars (where visible) represent the standard deviation

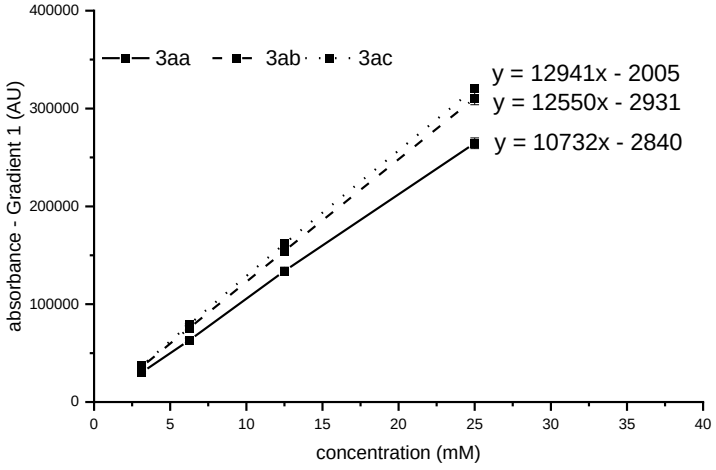

Figure S6: Calibration plot for compounds **3aa, ab, ac** for UPLC analysis by Gradient 1. n = 3, error bars (where visible) represent the standard deviation

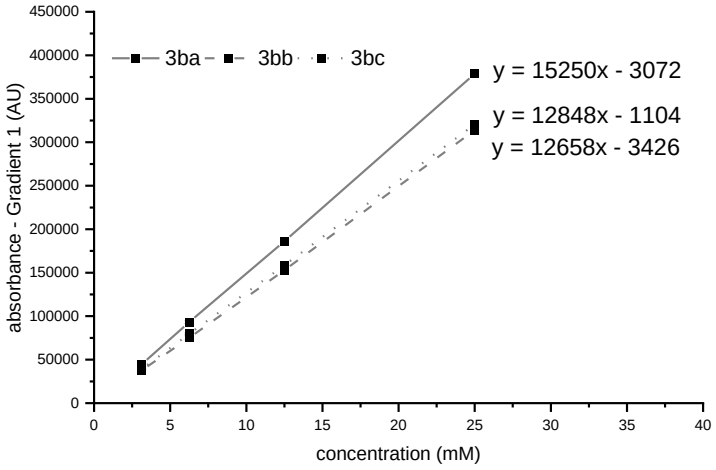

Figure S7: Calibration plot for compounds **3ba, bb, bc** for UPLC analysis by Gradient 1. n = 3, error bars (where visible) represent the standard deviation

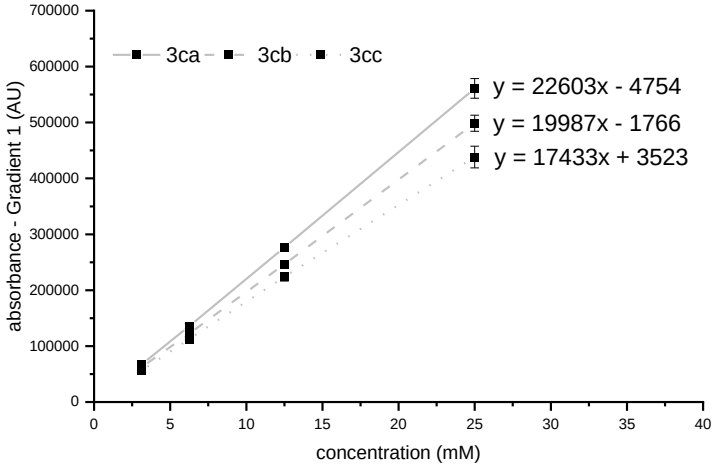

Figure S8: Calibration plot for compounds **3ca, cb, cc** for UPLC analysis by Gradient 1. n = 3, error bars (where visible) represent the standard deviation

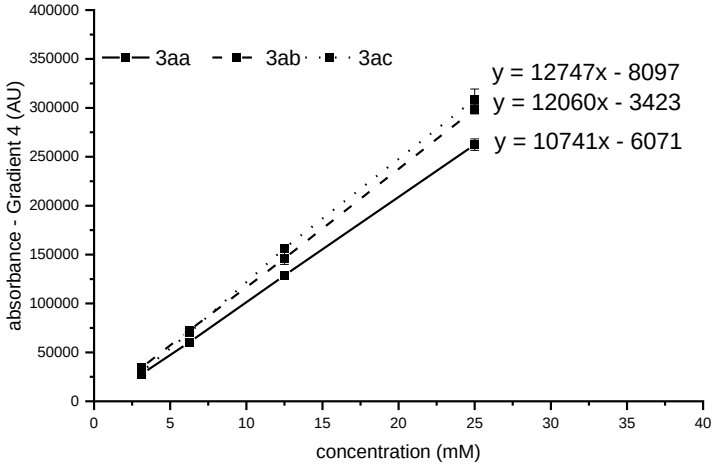

Figure S9: Calibration plot for compounds **3aa, ab, ac** for UPLC analysis by Gradient 4. n = 3, error bars (where visible) represent the standard deviation

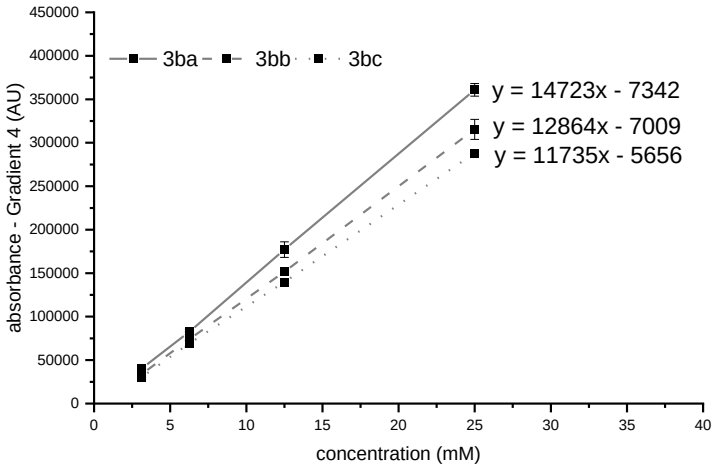

Figure S10: Calibration plot for compounds **3ba, bb, bc** for UPLC analysis by Gradient 4. n = 3, error bars (where visible) represent the standard deviation

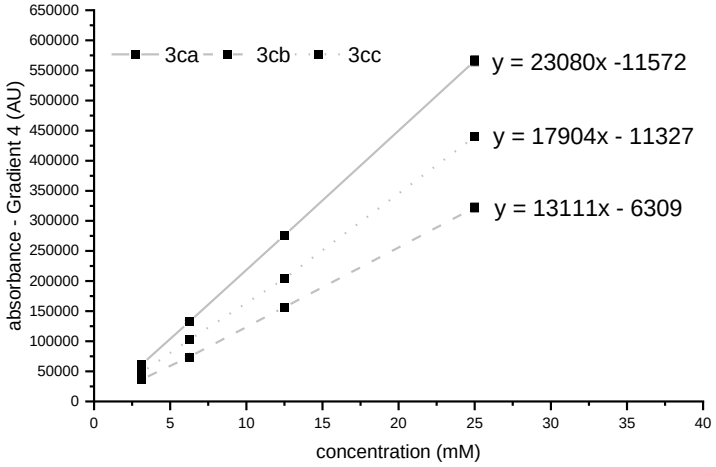

Figure S11: Calibration plot for compounds **3ca, cb, cc** for UPLC analysis by Gradient 4. n = 3, error bars (where visible) represent the standard deviation

7.2.5 Aggregate characterisation

Ring tensiometry measurements: The critical aggregation concentrations (CACs) of surfactants were determined with a Krus K10ST tensiometer. Measurements and calibration were performed at room temperature. Surface tensions were measured for a dilution series of each surfactant in HEPES buffer (0.25 M, pH 8.00), typically in a concentration range of 0.024-12.5 mM, using a volume of 3.0 mL per sample. Each measurement was performed in triplicate. CACs are found at the concentration which there is a change of linear regime between surface tension and natural logarithm of surfactant concentration. Solutions of the **3aa-ac** series all appeared transparent, whilst those of the other two series (**3ba-bc**, **3ca-cc**) appeared turbid, suggesting the presence of large aggregates such as vesicles.

Table S13. Critical aggregation concentrations (CAC) for all nine surfactants (**3**)

Compound	CAC /μM
3aa	473
3ab	294
3ac	83
3ba	290
3bb	234
3bc	188
3ca	560
3cb	284
3cc	156

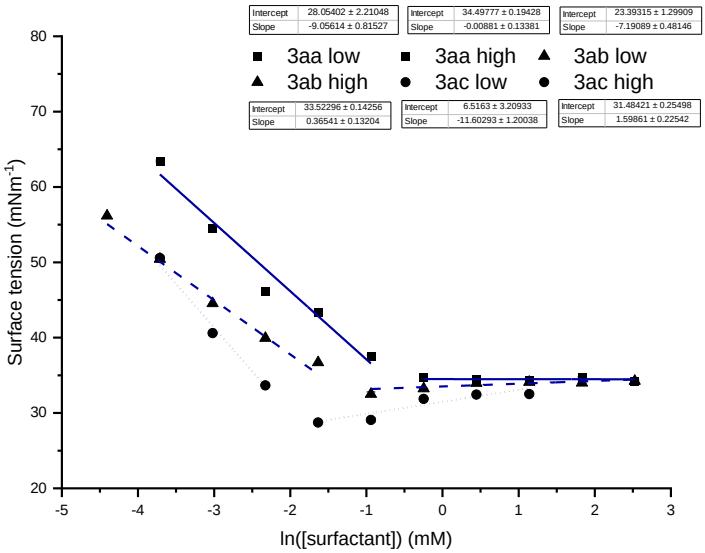

Figure S12: CAC determination by ring tensiometry for surfactants **3aa** (squares, solid line, 473 µM), **3ab** (triangles, dashed line, 294 µM) and **3ac** (circles, dotted line, 83 µM)

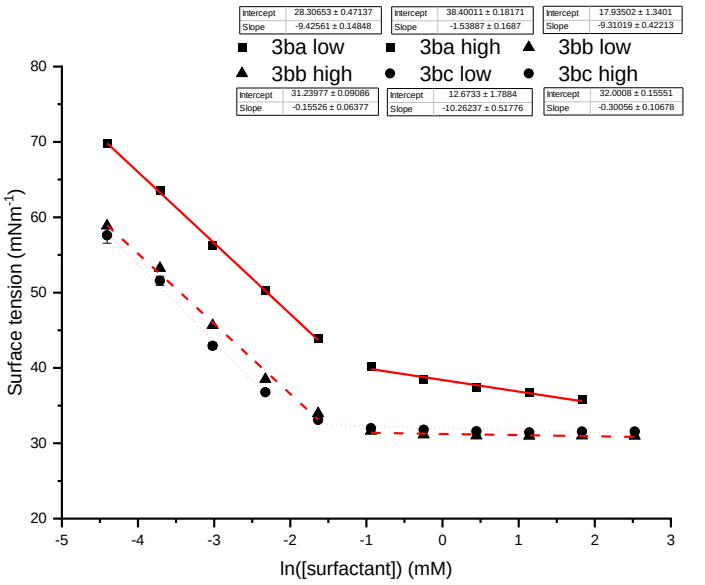

Figure S13: CAC determination by ring tensiometry for surfactants **3ba** (squares, solid line, 290 µM), **3bb** (triangles, dashed line, 234 µM) and **4cb** (circles, dotted line, 188 µM)

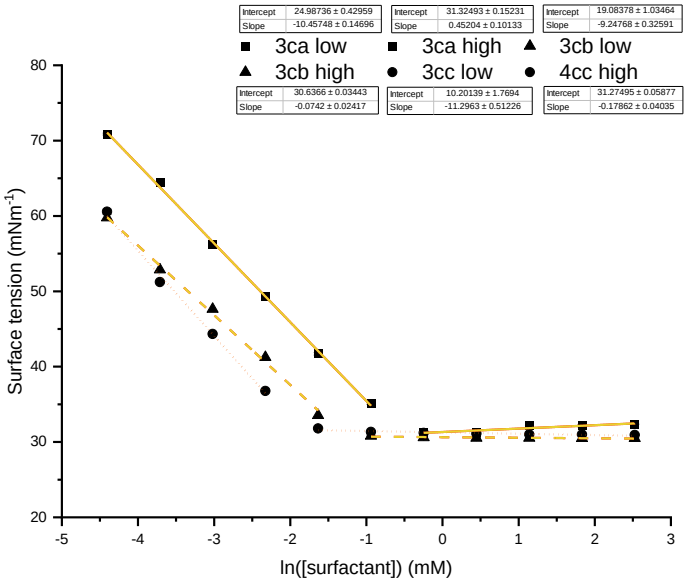

Figure S14: CAC determination by ring tensiometry for surfactants **3ca** (squares, solid line, 560 µM), **3cb** (triangles, dashed line, 284 µM) and **3cc** (circles, dotted line, 156 µM)

Dynamic light scattering (DLS): DLS measurements were recorded using a Malvern Zetasizer Nano ZEN5600 machine and Zetasizer software for data processing. Samples were prepared as a serial dilution in HEPES buffer (pH 8.0) from 25.0 mM to 0.049 mM. Three measurements were taken for each sample. Refractive index of 1.371 and viscosity of 1.0780 mPas were used in data processing. At the extremes of this concentration range, multiple scattering events and low signal to noise led to artifacts.

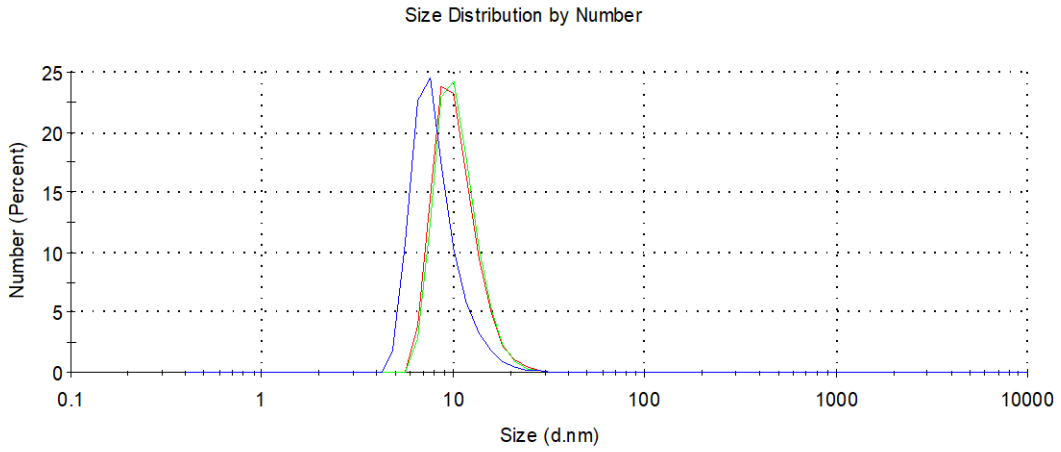

Figure S15: Size distribution of **3aa** (12.5 mM) by DLS. Mean aggregate size = 9.8 nm

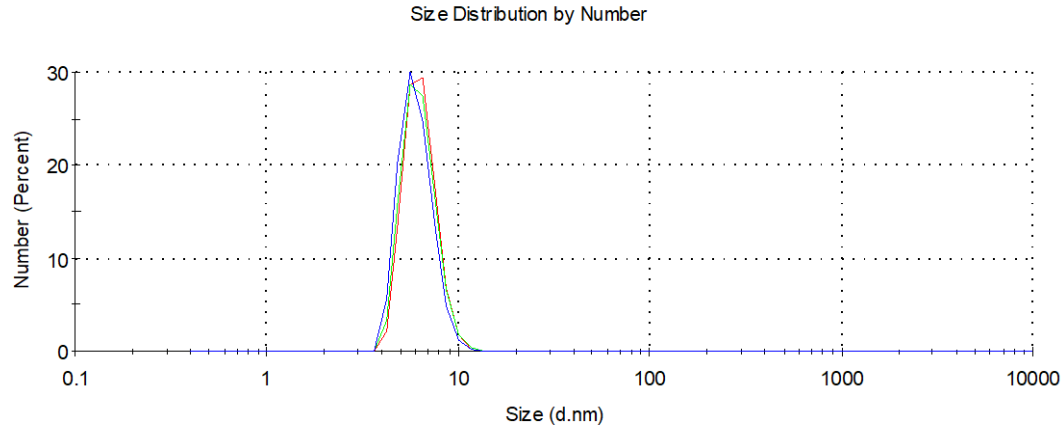

Figure S16: Size distribution of **3ab** (12.5 mM) by DLS. Mean aggregate size = 6.3 nm

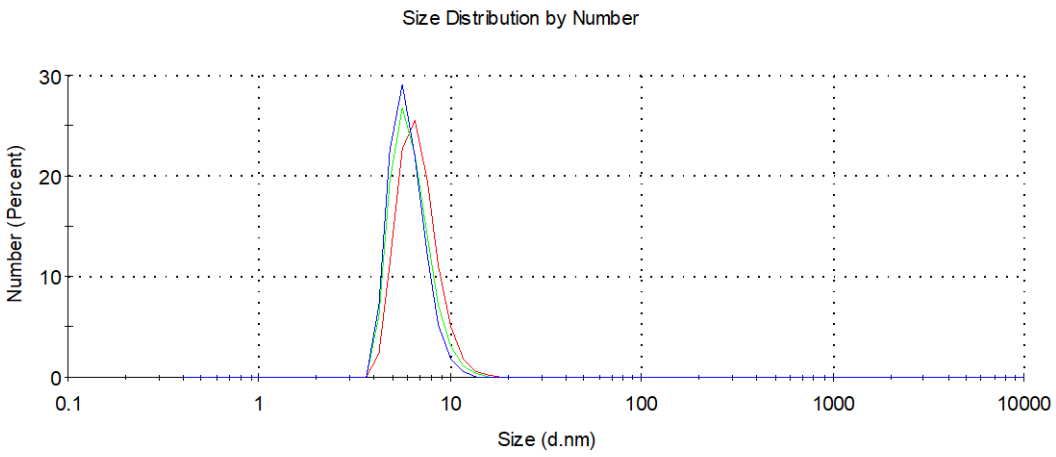

Figure S17: Size distribution of **3ac** (25.0 mM) by DLS. Mean aggregate size = 6.4 nm

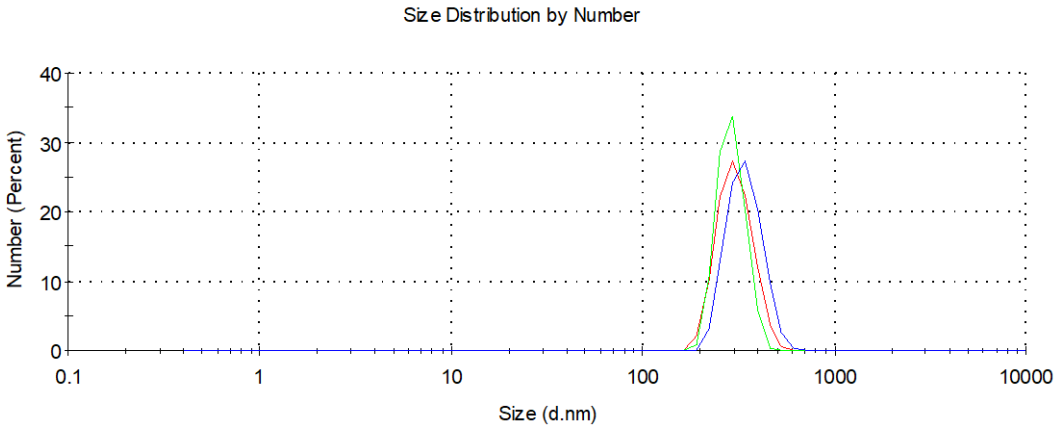

Figure S18: Size distribution of **3ba** (0.195 mM) by DLS. Mean aggregate size = 313.4 nm

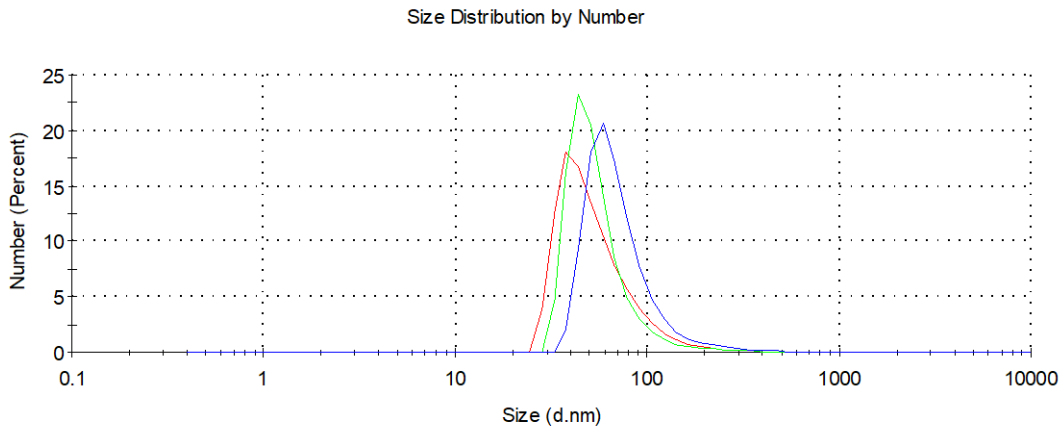

Figure S19: Size distribution of **3bb** (3.125 mM) by DLS. Mean aggregate size = 62.9 nm

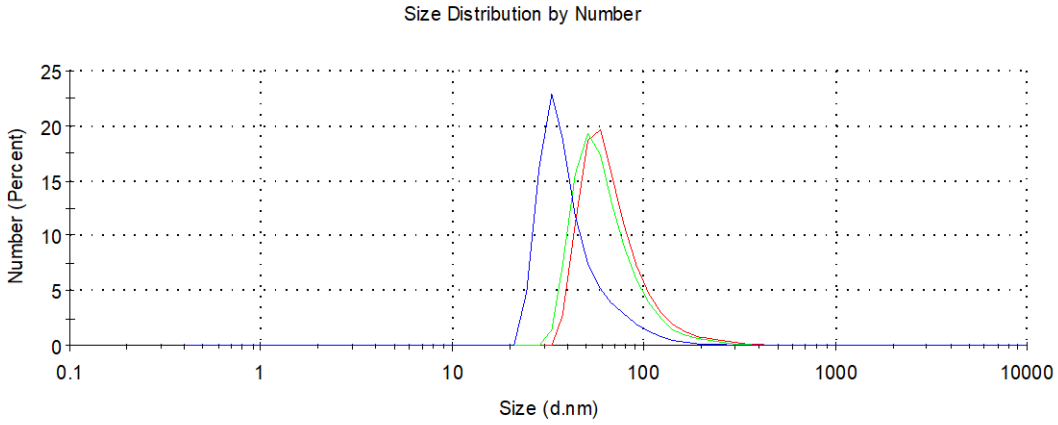

Figure S20: Size distribution of **3bc** (0.195 mM) by DLS. Mean aggregate size = 61.8 nm

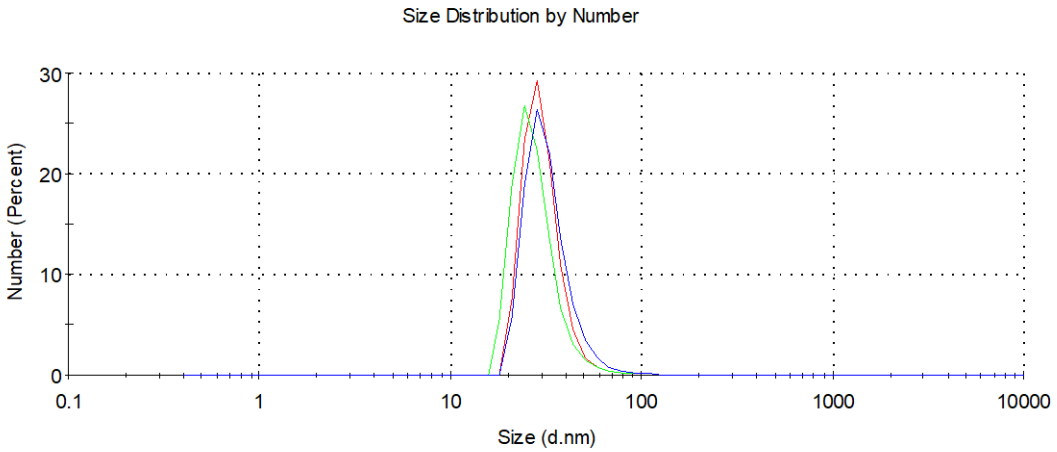

Figure S21: Size distribution of **3ca** (25.0 mM) by DLS. Mean aggregate size = 30.5 nm

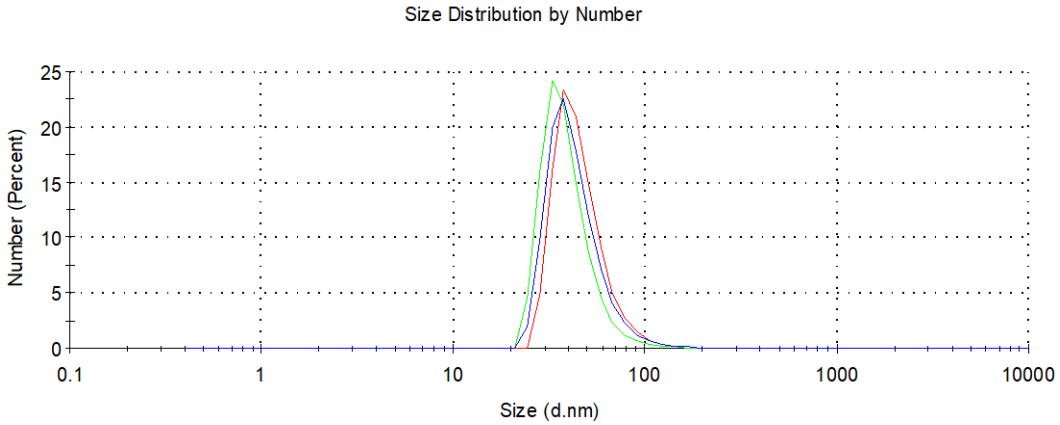

Figure S22: Size distribution of **3cb** (1.56 mM) by DLS. Mean aggregate size = 43.3 nm

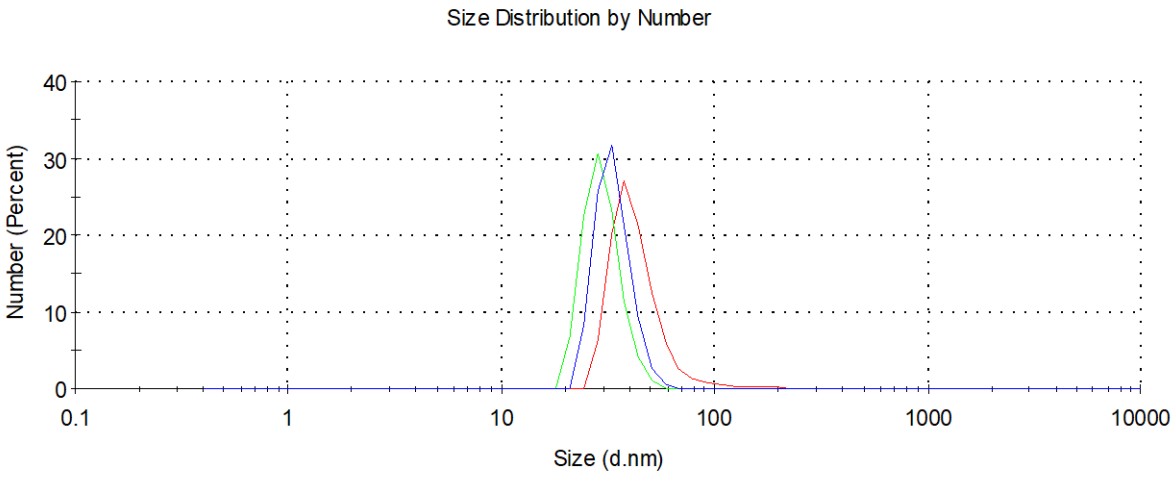

Figure S23: Size distribution of **3cc** (0.195 mM) by DLS. Mean aggregate size = 36.2 nm

7.3 Supplementary data for Chapter 3

7.3.1 Synthesis of compounds

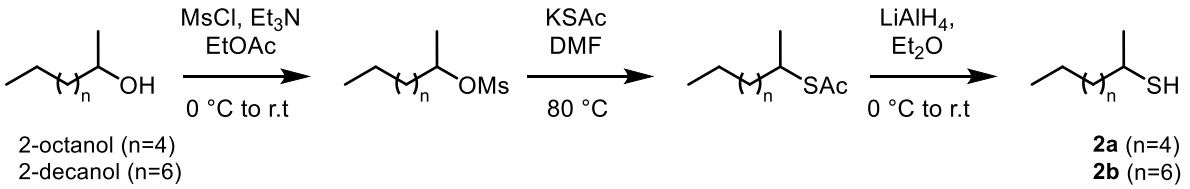

2a: The known title compound was synthesised according to a reported procedure from 2-octanol,[1] as depicted above, in 78% overall yield (14.44 g, 98.7 mmol).

2b: The known title compound was synthesised analogously to **2a** from 2-decanol in 76% overall yield (4.18 g, 24.0 mmol).

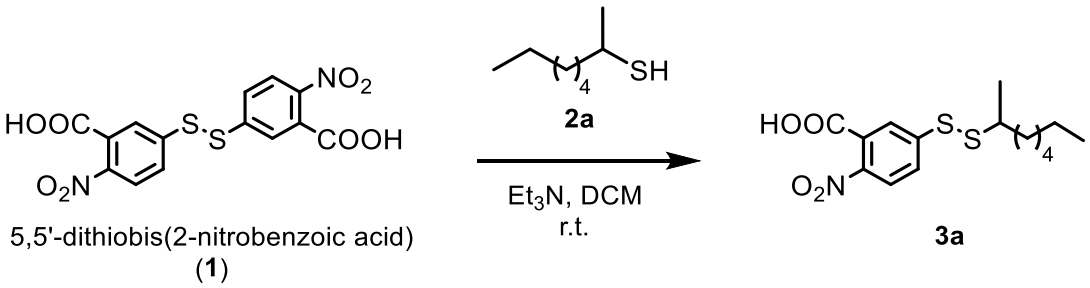

3a: To a stirred solution of 5,5'-dithiobis(2-nitrobenzoic acid) (**1**) (297 mg, 0.75 mmol) and Et_3N (314 uL, 3 eq.) in DCM (2.0 mL) was dropwise added a solution of **2a** (137 uL, 1.05 eq.) in DCM (1 mL) at room temperature. After 1 hour, the red solution was diluted with 1M aq. HCl (10 mL) and extracted with EtOAc (3x30 mL). The combined organics were washed with 1M aq. HCl (2x30 mL) and brine (50 mL), dried over $MgSO_4$ and filtered. After removal of the solvent, the crude oil was purified using flash column chromatography (0-2% MeOH/$CHCl_3$, 0.5% AcOH) to yield compound **3a** as a yellow oil (243 mg, 70%).

^{1}H NMR (400 MHz, $CDCl_3$) δ 7.95 (d, *J* = 2.1 Hz, 1H), 7.90 (d, *J* = 8.6 Hz, 1H), 7.79 (dd, *J* = 8.6, 2.1 Hz, 1H), 2.95 (sx, *J* = 6.7 Hz, 1H), 1.66 (ddd, *J* = 13.7, 8.1, 6.6 Hz, 1H), 1.52 (dq, *J* = 13.4, 7.0 Hz, 1H), 1.46 – 1.34 (m, 2H), 1.31 (d, *J* = 6.7 Hz, 3H), 1.29 – 1.21 (m, 6H), 0.87 (t, *J* =

6.8 Hz, 3H). ^{13}C NMR (101 MHz, $CDCl_3$) 170.1, 147.1, 145.9, 128.6, 127.3, 126.6, 124.7, 77.5, 77.2, 76.8, 47.8, 36.1, 31.8, 29.2, 27.1, 22.7, 20.7, 14.2. MS (ESI) Calc for $C_{15}H_{21}NNaO_4S_2$: 366.0804; found 366.0850 [M+Na]+

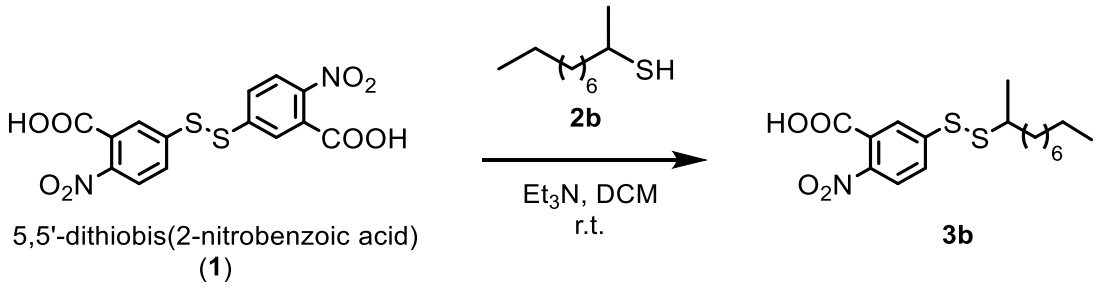

3b: The title compound was synthesised from **1** and **2b** analogously to **3a** (171mg, 46%).

^{1}H NMR (400 MHz, $CDCl_3$) δ 7.93 (d, *J* = 2.1 Hz, 1H), 7.90 (d, *J* = 8.6 Hz, 1H), 7.78 (dd, *J* = 8.6, 2.1 Hz, 1H), 2.94 (q, *J* = 6.7 Hz, 1H), 1.73 – 1.59 (m, 1H), 1.56 – 1.46 (m, 1H), 1.44 – 1.34 (m, 2H), 1.30 (d, *J* = 6.8 Hz, 4H), 1.25 (m, 10H), 0.91 – 0.83 (m, 3H). ^{13}C NMR (101 MHz, $CDCl_3$) δ 169.32, 147.11, 147.11, 145.81, 128.47, 127.56, 126.58, 124.72, 77.48, 77.16, 76.84, 47.74, 36.08, 31.98, 29.56, 29.53, 29.36, 27.16, 22.79, 20.67, 14.23. MS (ESI) Calc for $C_{17}H_{25}NNaO_4S_2$: 394.1117; found 394.1118 [M+Na]+

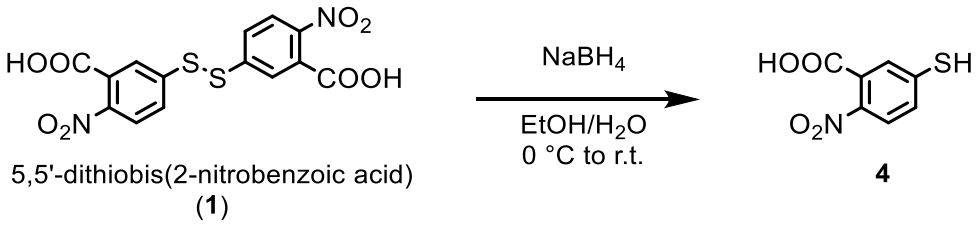

4: The known title compound was synthesised according to a reported procedure from **1** as depicted above.[2]

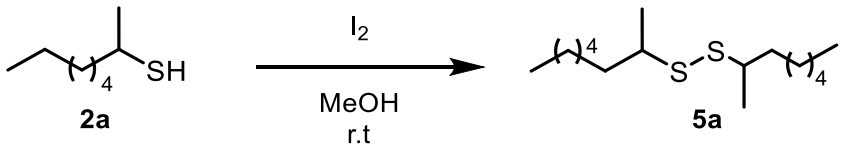

2a **5a**

5a: Iodine (500 mg, 2 mmol) in methanol (1 mL) was added dropwise to a solution of thiol **2a** (350 µL, 2 mmol) in 2 mL MeOH using a modified known procedure.[3] The solution was stirred for 1 hour, after which the reaction was quenched with aq. $NaHSO_3$. The solution was diluted with water and extracted with DCM (3x5 mL). The organic layer was washed with brine (5 mL) and dried using $MgSO_4$. After removal of the solvent, the crude product was purified using flash column chromatography (100% hexanes) to yield compound **5** as a colourless oil in quantitative yield.

^{1}H NMR (400 MHz, $CDCl_3$) δ 2.77 (sxd, *J* = 6.7, 2.0 Hz, 2H), 1.72 – 1.60 (m, 2H), 1.50 – 1.34 (m, 6H), 1.34 – 1.25 (m, 18H), 0.89 (m, *J* = 2.9 Hz, 6H). ^{13}C NMR (101 MHz, $CDCl_3$) δ 77.48, 77.16, 76.84, 46.88, 46.85, 36.38, 31.90, 29.32, 27.21, 22.77, 20.85, 20.80, 14.22. MS (ESI): no ionisation

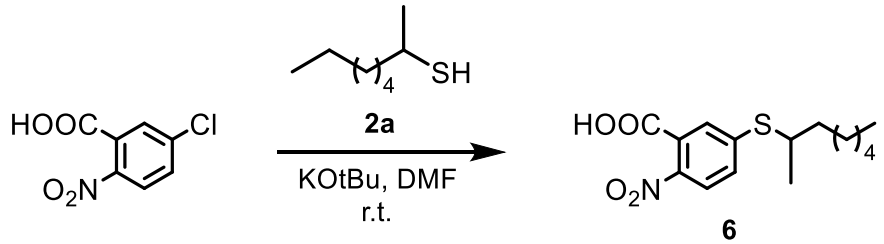

5-chloro-2-nitrobenzoic acid **6**

6: To a stirred solution of 5-chloro-2-nitrobenzoic acid (201 mg, 1 mmol) and KOtBu (336 mg, 3 eq.) in DMF (2.0 mL) was dropwise added a solution of **2a** (192 uL, 1.1 eq.) in DMF (0.5 mL) at room temperature. After 1 hour, the brown suspension was diluted with 1M aq. HCl (20 mL) and extracted with DCM (3x20 mL). The combined organics were washed with 1M aq. HCl (2x20 mL), brine (20 mL), dried over $MgSO_4$ and filtered. After removal of the solvent, the crude oil

was purified using flash column chromatography (0-3% MeOH/$CHCl_3$, 0.5% AcOH) to yield compound **6** as a waxy solid (212 mg, 68%).

^{1}H NMR (400 MHz, $CDCl_3$) δ 7.78 (d, *J* = 8.6 Hz, 1H), 7.56 (d, *J* = 2.1 Hz, 1H), 7.33 (dd, *J* = 8.6, 2.0 Hz, 1H), 3.45 (sx, *J* = 6.8 Hz, 1H), 1.71 – 1.50 (m, 2H), 1.48 – 1.38 (m, 2H), 1.33 (d, *J* = 6.6 Hz, 3H), 1.30 – 1.21 (m, 6H), 0.92 – 0.83 (m, 3H). ^{13}C NMR (101 MHz, $CDCl_3$) 171.1, 146.4, 144.1, 129.6, 129.4, 128.0, 124.4, 77.5, 77.2, 76.8, 42.0, 36.5, 31.8, 29.3, 27.0, 22.7, 21.0, 14.2. MS (ESI) Calc for $C_{15}H_{21}NNaO_4S$: 334.1084; found 334.1083 [M+Na]+

7.3.2 NMR data

Compound **2a**

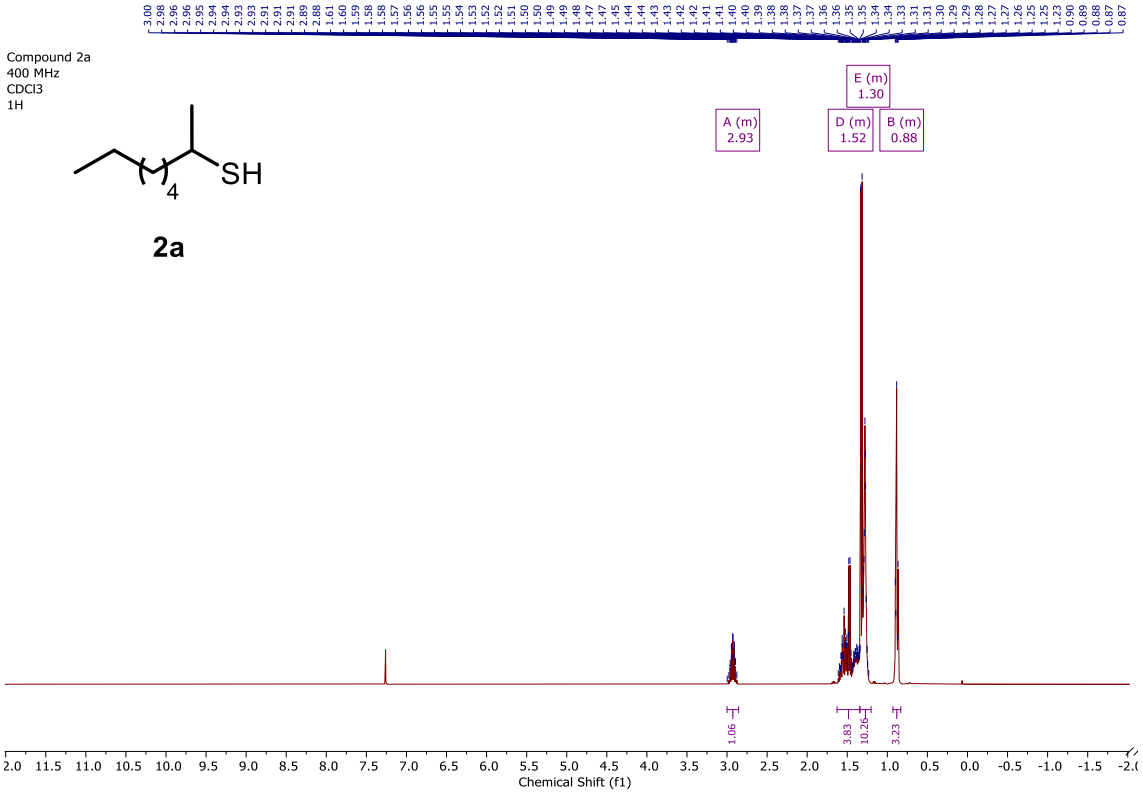

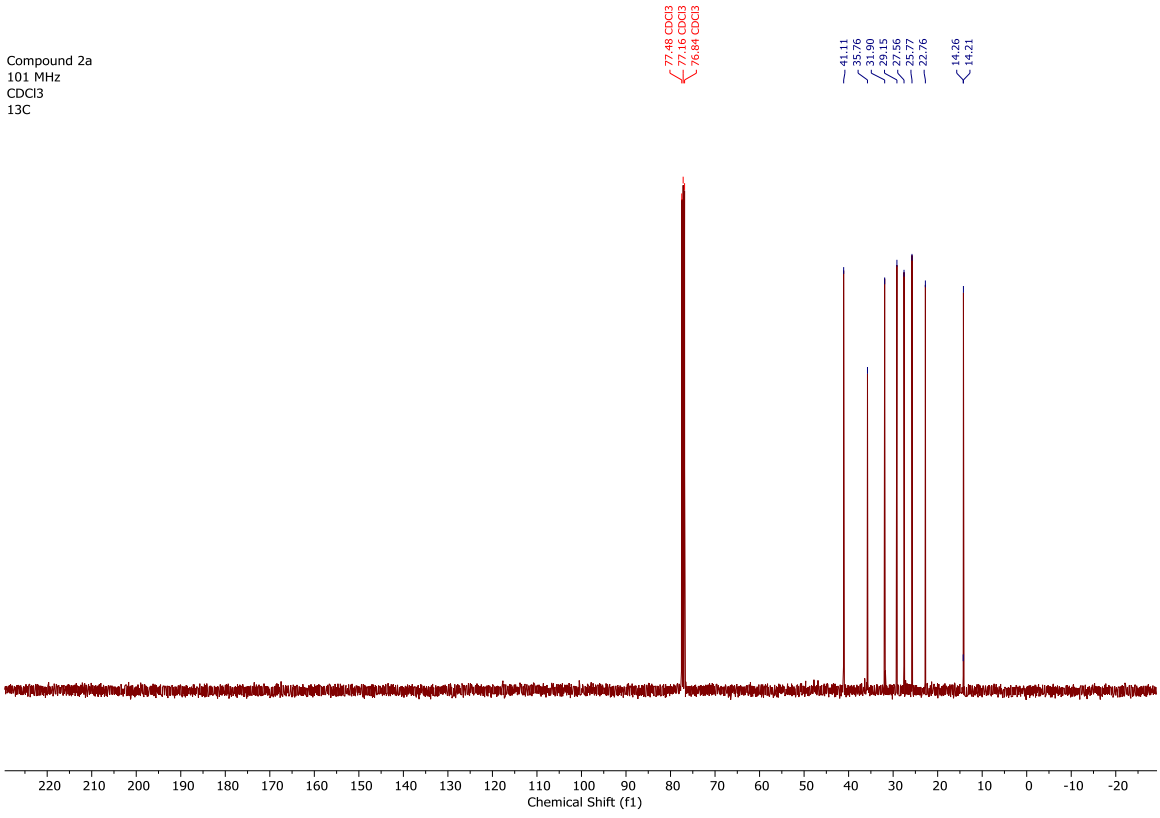

Compound **2b**

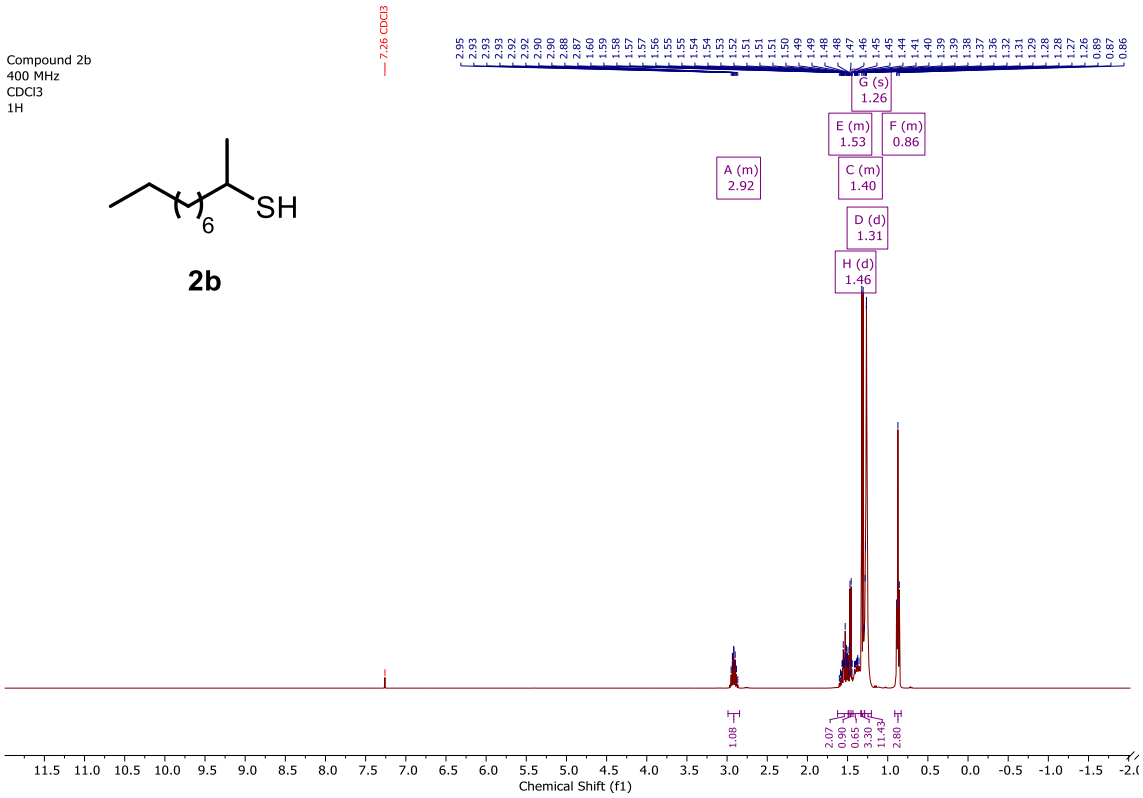
Compound 2b
400 MHz
CDCl3
1H
7.26 CDCl3
G (s)
1.26
E (m)
1.53
F (m)
0.86
A (m)
2.92
C (m)
1.40
D (d)
1.31
H (d)
1.46
1.08
2.07
0.90
0.65
3.30
11.43
2.80
Chemical Shift (f1)

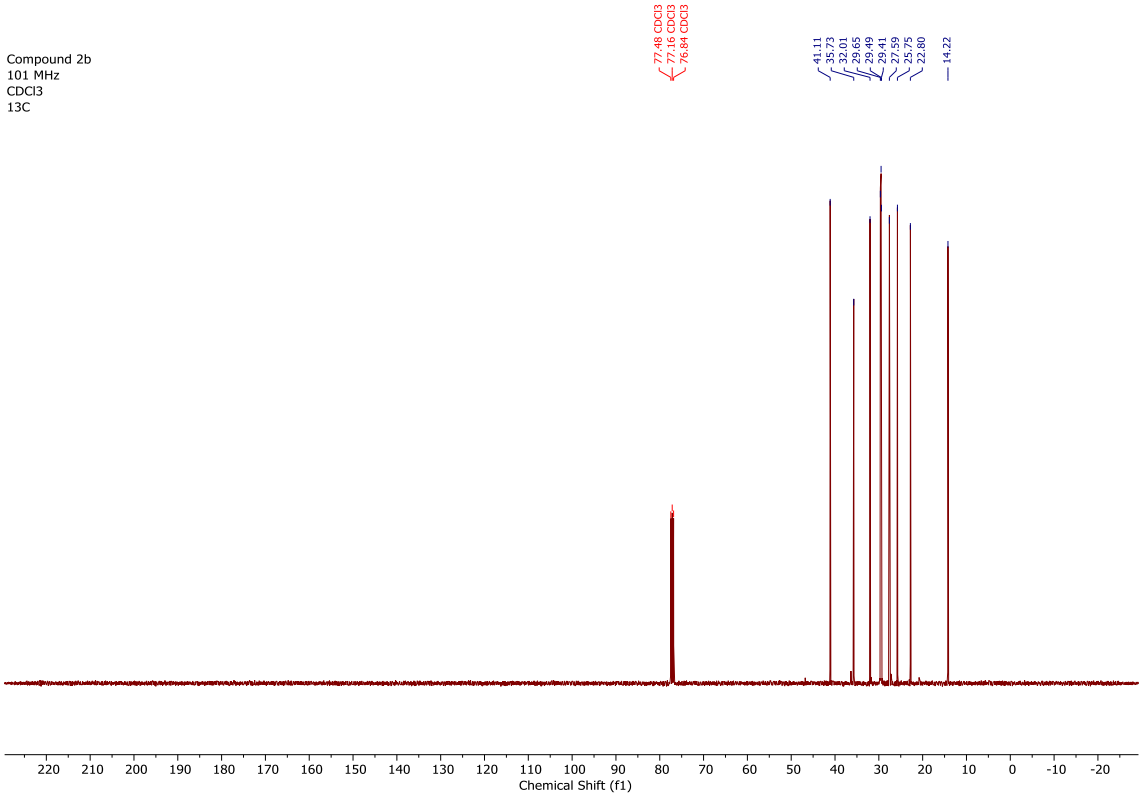
Compound 2b
101 MHz
CDCl3
13C
77.48 CDCl3
77.16 CDCl3
76.84 CDCl3
41.11
35.73
32.01
29.65
29.49
29.41
27.59
25.75
22.80
14.22
Chemical Shift (f1)

Compound **3a**

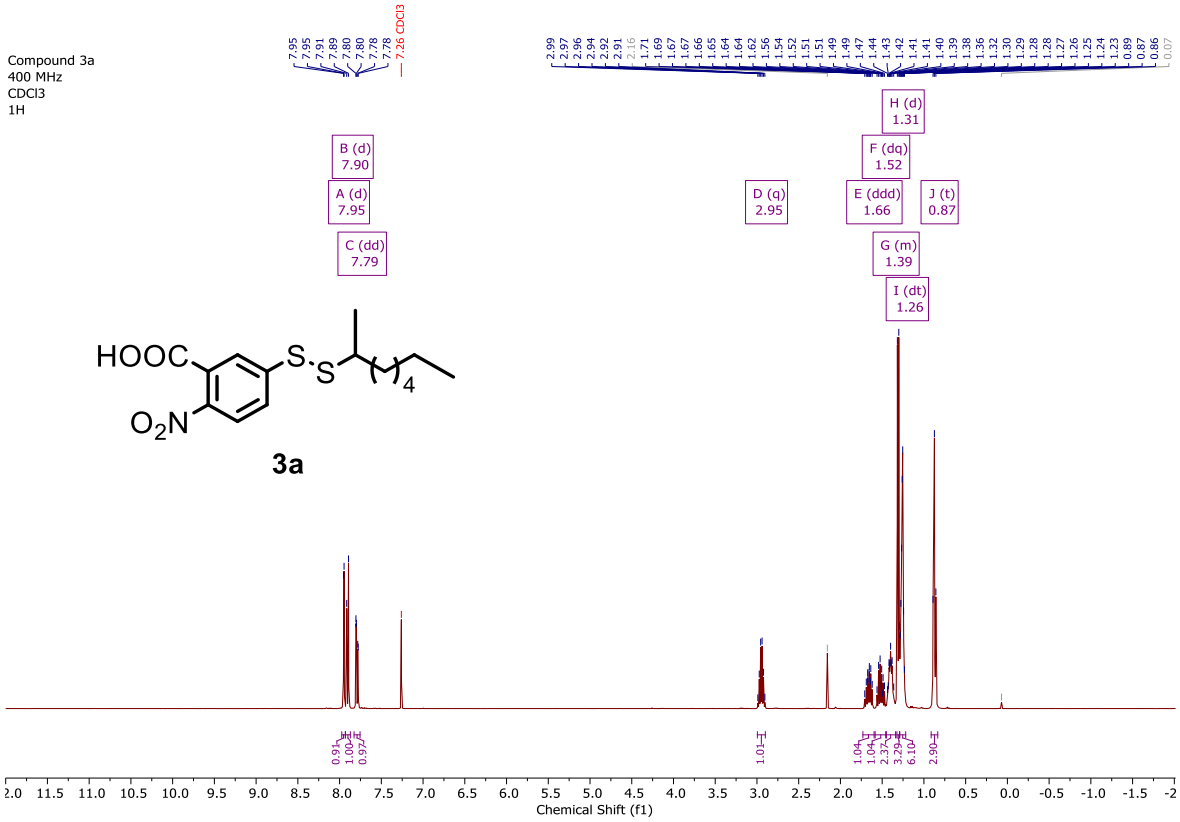
Compound 3a
400 MHz
CDCl3
1H
B (d)
7.90
A (d)
7.95
C (dd)
7.79
H (d)
1.31
F (dq)
1.52
D (q)
2.95
E (ddd)
1.66
J (t)
0.87
G (m)
1.39
I (dt)
1.26
HOOC
S
S
4
O2N
3a
Chemical Shift (f1)

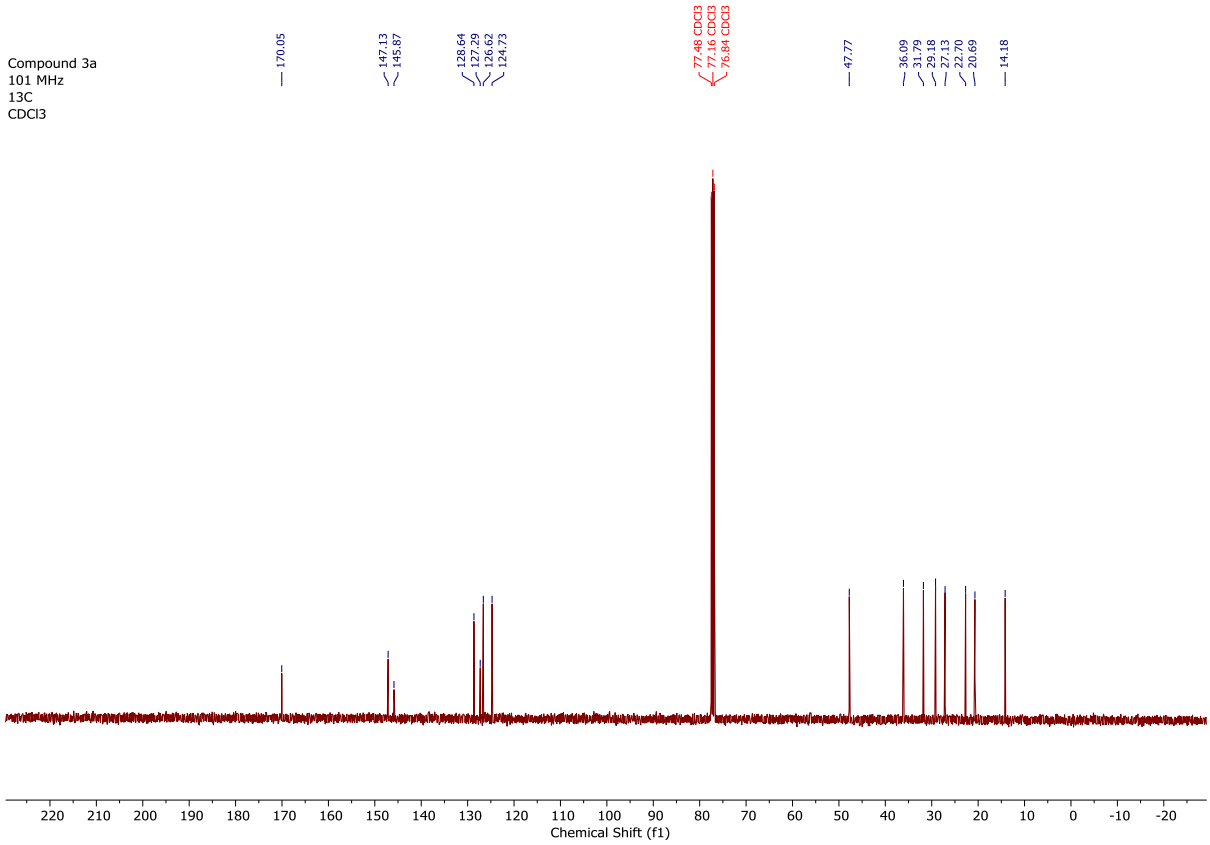
Compound 3a
101 MHz
13C
CDCl3
170.05
147.13
145.87
128.64
127.29
126.62
124.73
77.48 CDCl3
77.16 CDCl3
76.84 CDCl3
47.77
36.09
31.79
29.18
27.13
22.70
20.69
14.18
Chemical Shift (f1)

Compound **3b**

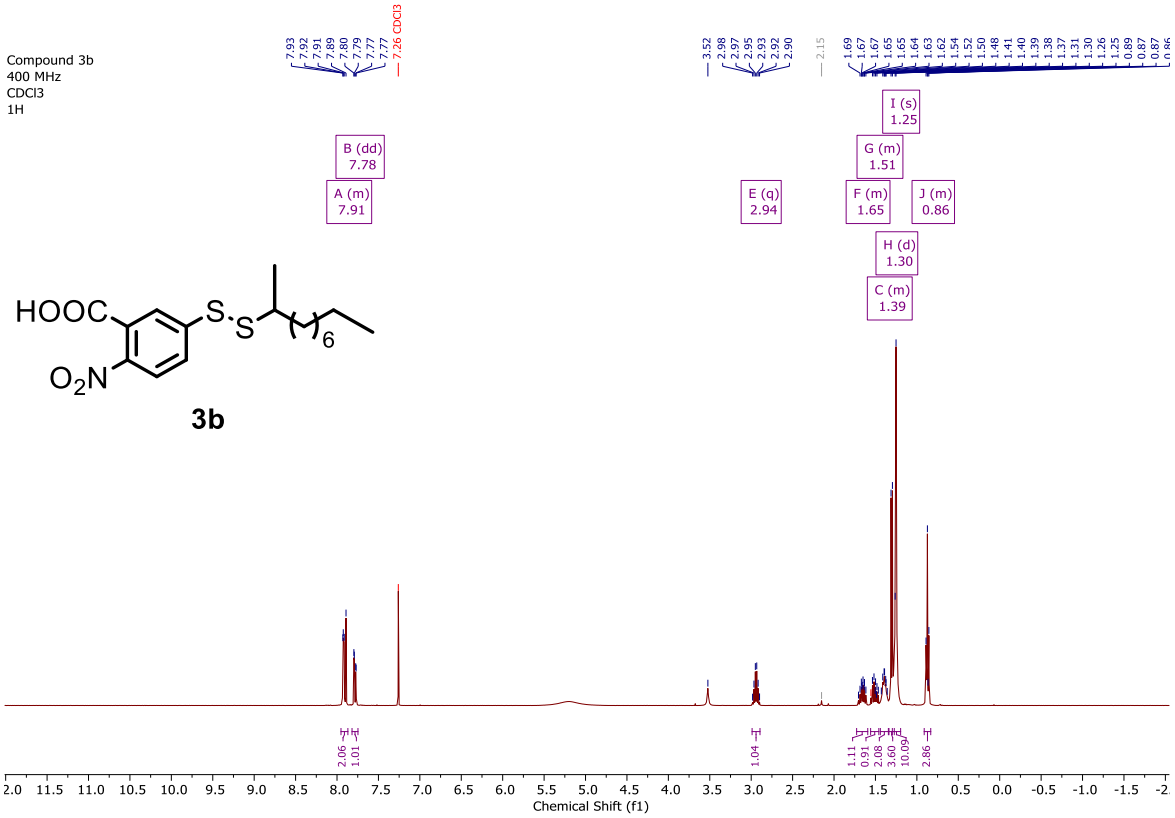
Compound 3b
400 MHz
CDCl3
1H
7.93
7.92
7.91
7.89
7.80
7.79
7.77
7.77
7.26 CDCl3
3.52
2.98
2.97
2.95
2.93
2.92
2.90
2.15
1.69
1.67
1.67
1.65
1.65
1.64
1.63
1.62
1.54
1.52
1.50
1.48
1.41
1.40
1.39
1.38
1.37
1.31
1.30
1.26
1.25
0.89
0.87
0.87
I (s)
1.25
B (dd)
7.78
G (m)
1.51
A (m)
7.91
E (q)
2.94
F (m)
1.65
J (m)
0.86
H (d)
1.30
C (m)
1.39
HOOC
S
S
6
O2N
3b
2.06
1.01
1.04
1.11
0.91
2.08
3.60
10.09
2.86
Chemical Shift (f1)

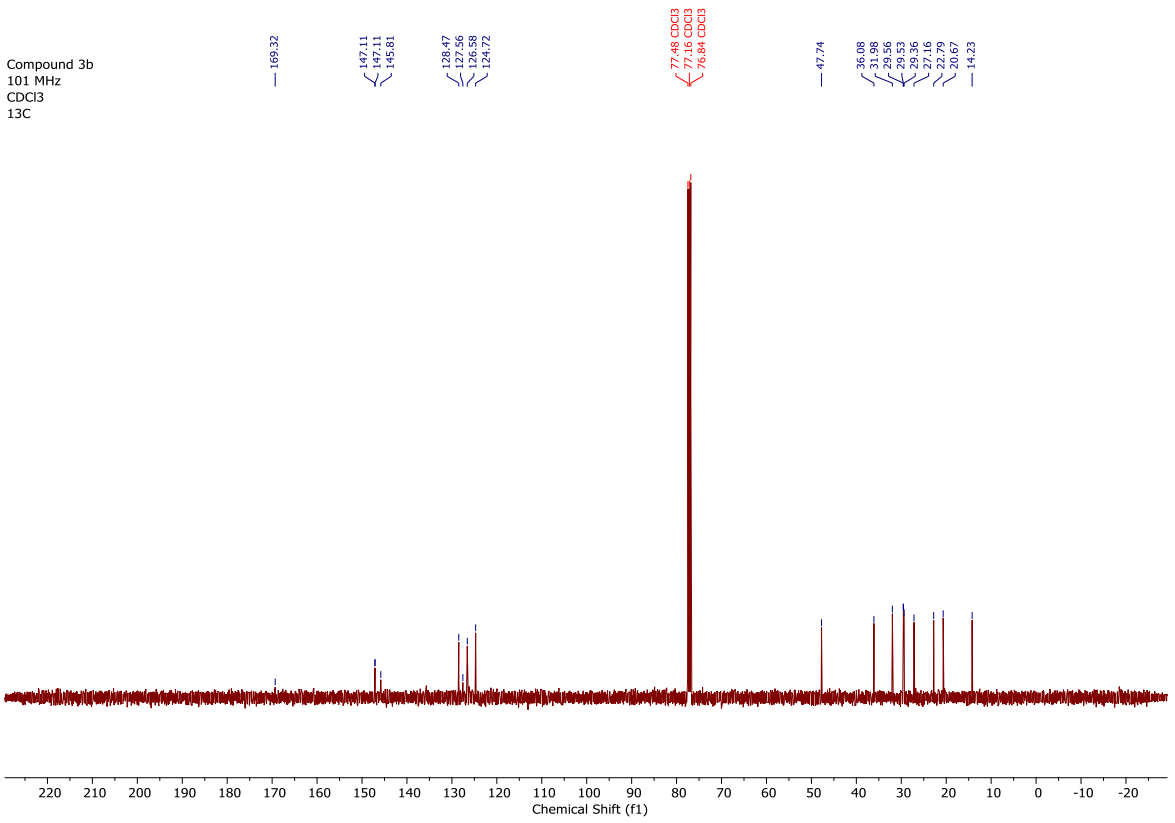
Compound 3b
101 MHz
CDCl3
13C
169.32
147.11
147.11
145.81
128.47
127.56
126.58
124.72
77.48 CDCl3
77.16 CDCl3
76.84 CDCl3
47.74
36.08
31.98
29.56
29.53
29.36
27.16
22.79
20.67
14.23
Chemical Shift (f1)

Compound **5**

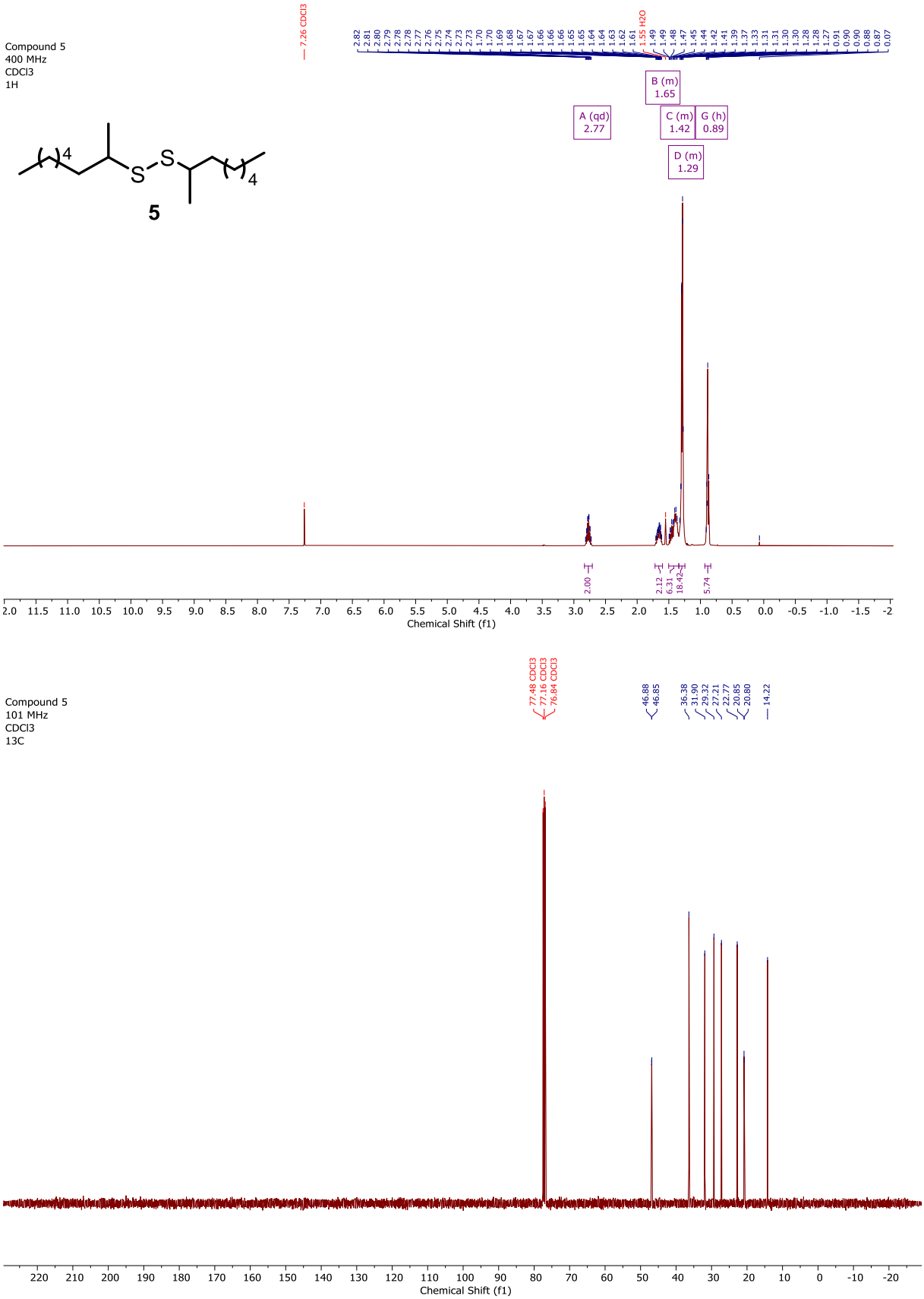
Compound 5
400 MHz
CDCl3
1H
5
7.26 CDCl3
1.55 H2O
B (m)
1.65
A (qd)
2.77
C (m)
1.42
G (h)
0.89
D (m)
1.29
2.00
2.12
6.31
18.42
5.74
Chemical Shift (f1)
Compound 5
101 MHz
CDCl3
13C
77.48 CDCl3
77.16 CDCl3
76.84 CDCl3
46.88
46.85
36.38
31.90
29.32
27.21
22.77
20.85
20.80
14.22
Chemical Shift (f1)

Compound **6**

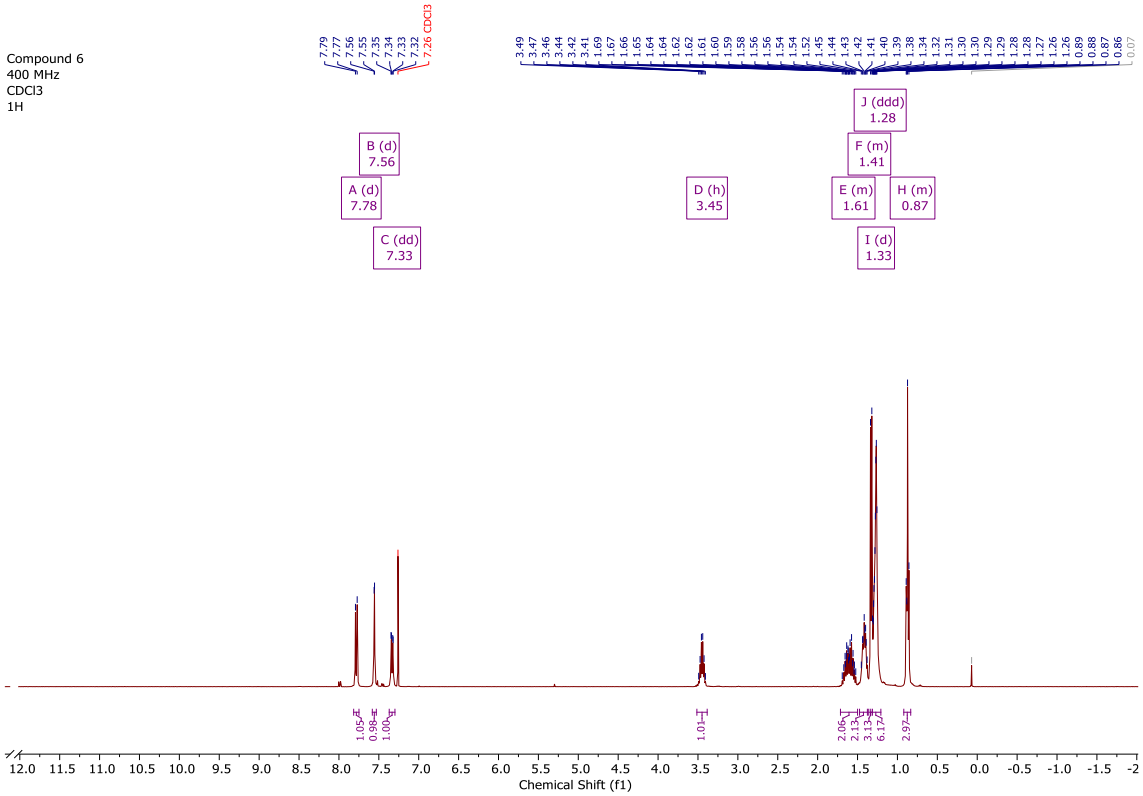
Compound 6
400 MHz
CDCl3
1H
B (d) 7.56
A (d) 7.78
C (dd) 7.33
D (h) 3.45
J (ddd) 1.28
F (m) 1.41
E (m) 1.61
H (m) 0.87
I (d) 1.33
Chemical Shift (f1)

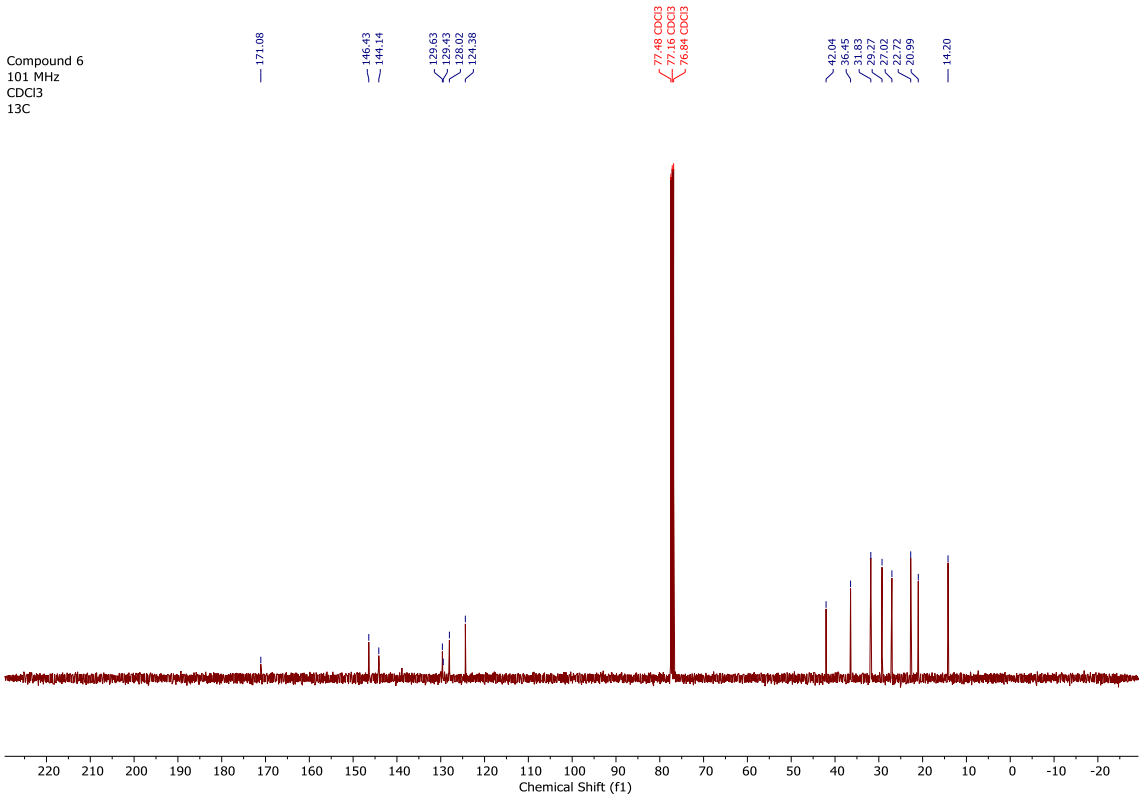
Compound 6
101 MHz
CDCl3
13C
Chemical Shift (f1)

7.3.3 Procedures for kinetic experiments

General oscillation experiment procedure

A solution of compound **1** (23 mg, 0.058 mmol) and DMAP (10 mg, 1.4 eq.) in 4 mL TRIS buffer (0.5 M, pH 9.00) was stirred at 800 rpm (oval stirring bar, *L*= 10 mm, ø= 5 mm) in a 10 mL round bottom flask at 40°C. Thiol **2a** (500 µL, 2.87 mmol, 50 eq.) was carefully placed on top of the aqueous layer and the addition of hydrogen peroxide (1.12 M, 45 µL/h) by syringe pump (AL-1000, WPI) was immediately started. The reaction was regularly sampled (every 3 mins) and analyzed as described in the UPLC section.

For the experiment in Figure 3.4, the H_2O_2 supply was modified (0.56 M, 270 µL/h) and 180 µL of 2-octanethiol (**2a**) and 14.3 mg DMAP was used.

For the experiments in Figure 3.7b, the H_2O_2 supply was halved (0.56 M, 45 µL/h), while 180 µL of 2-decanethiol (**2b**) instead of 2-octanethiol (**2a**) was added. Using thiols **2a** and **2b** results in similar oscillations with regards to surfactant **3a** and **3b**, but concentrations of **1** are higher and more easily monitored when using **2b**.

Reaction monitoring and UPLC analysis:

This general monitoring method is applicable to Chapters 3-5.

Aliquots were regularly taken by carefully extracting 20 µL of the aqueous layer by microsyringe. The aliquot was immediately added to 0.50 mL of a quench solution (maleimide, 62 mM, 3:1 H_2O:MeCN). A mixture of H_2O:MeCN: TFA (2% v/v in H_2O) was used as mobile phase with a gradient of 93:2:5 → 0:95:5 over 2.40 min.

UPLC calibration:

The concentrations of the different UV-active species that were analysed using UPLC and were calculated based on the calibration curves below.

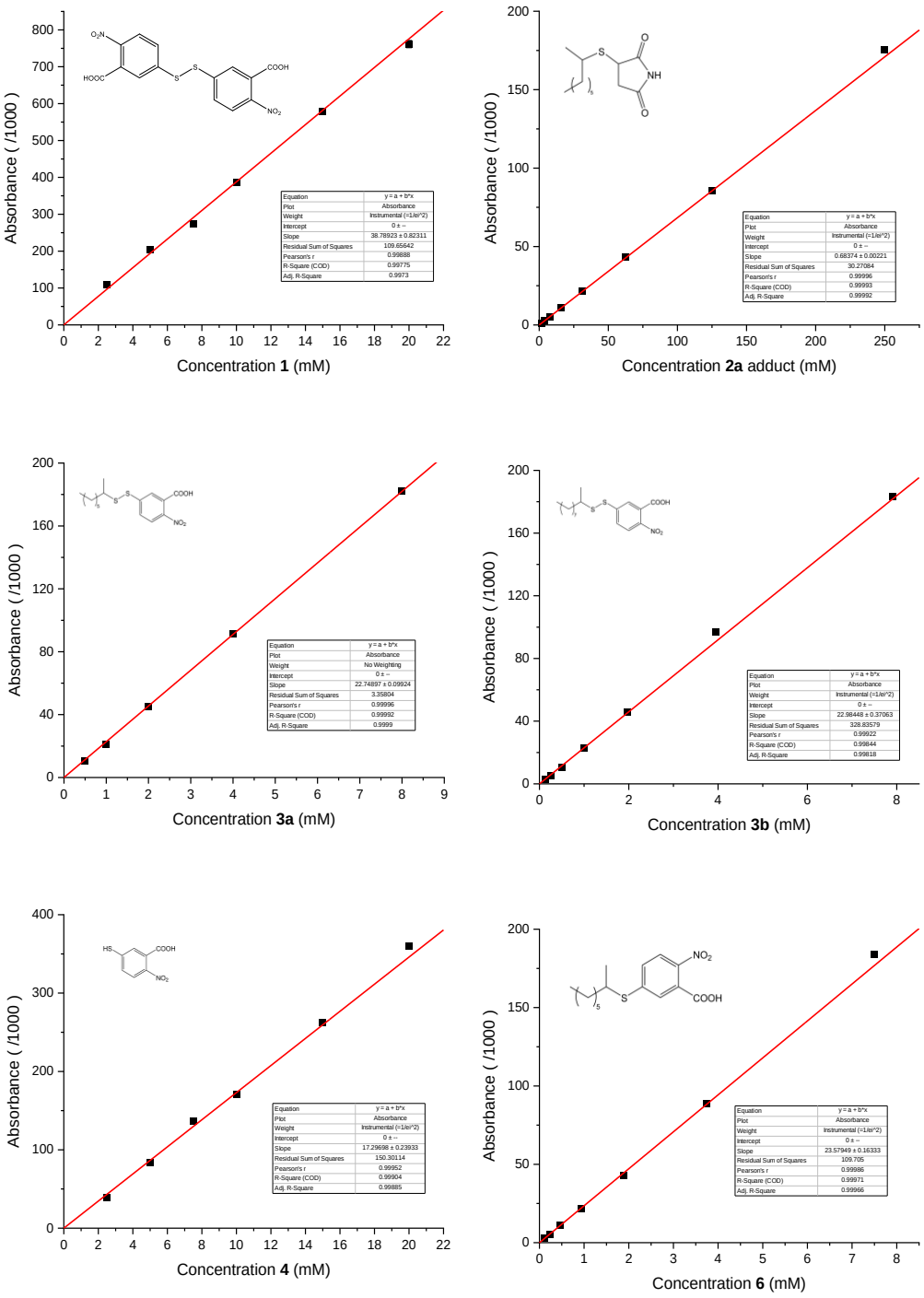

Figure S24: UPLC calibration curves for compounds **1**-**4** and **6** determined by injection of quenched samples from stock solutions.

7.2.4 Control experiments

<u>Oscillations in the absence of DMAP</u>

To show that DMAP is not essential to obtain oscillations, experiments were carried out in the absence of this compound. These experiments were set up as in the general oscillation procedure above but excluding DMAP. The reaction was regularly sampled (every 4 mins) and analyzed as described in the UPLC section. Removal of DMAP significantly increased the amplitude and period of these oscillations (Figure S24).

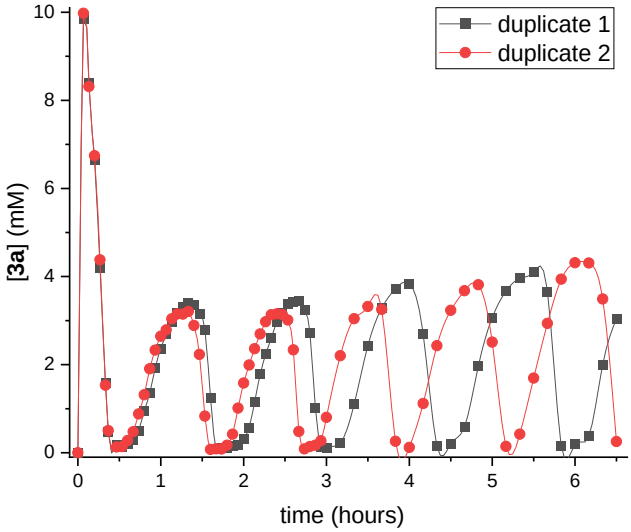

Figure S25: Oscillations in the absence of DMAP. DMAP is not required to obtain oscillations in the system centred on surfactant **3a,** but acts only as a catalyst.

Destruction control experiment (seeding, Figure 3.15):

To test the how destruction-seeding affected the oscillations, the general oscillation experiment was adapted to display longer periods. This was achieved by modifying the amounts of DMAP (12 mg), **2a** (300 µL) and oxidant flow (120 µL/h) while decreasing the stirring rate (to 400 rpm). Two identical reactions were set up in this manner with a 30 minute stagger, and decaying micelles (1 mL of reaction) were added to the other reaction that was experiencing growth.

Destruction control experiment (continuous surfactant addition, Figure 3.16):

In these experiments, the general oscillation procedure above was used but without DMAP and using **2b** instead of **2a**. After two hours of reaction, a second syringe pump was used to continuously add surfactant **3a** (38 mM, 200 µL/h) to the oscillating mixture. The reaction was regularly sampled (every 5 mins) and analyzed as described in the UPLC section.

7.2.5 iSCAT and other characterisation of the aggregates

Interferometric scattering microscopy (iSCAT) measurements:

The iSCAT experimental set-up is similar to that described by Young et al,[4] with a 532 nm diode laser used as the incident light source. Frames were recorded at 1 kHz with an exposure time of 0.98 ms, using a CMOS camera. Focus in the z axis is maintained using an autofocus system relying on the total internal reflection (TIRF) of a 638 nm beam. Instrument control was performed using the custom software written in LabView.

Data processing was performed using the custom software written in Python, as described elsewhere. In brief, differential imaging was achieved by subtracting sets of images temporally offset by a time Δt. The signal-to-noise ratio was then improved by spatially (3 x 3 binning) and temporally averaging the differential images (50 images). Particle detection was performed as described by Young et al. Briefly, diffraction-limited spots were identified by the software, and fitted to the 2D Gaussian function to give the ratiometric contrast value.

Glass microscope slides were cleaned by sequential sonication in Milli-Q water, isopropanol and Milli-Q water (5 min each) and dried under a stream of nitrogen. Sample wells were prepared by attaching silicone gaskets (reusable CultureWell™ gaskets, 3 mm x 1 mm, Sigma Aldrich) to the glass slide. All microscope slides and wells were cleaned and prepared on the day of the analysis.

Contrast-to-mass (C2M) calibration was performed in commercial PBS buffer solution. The calibration protocol included measurement of a protein oligomer solution, with masses of 90, 180, 360 and 540 kDa.

Each calibration experiment was analysed using the same software as described above. The mean peak contrast was determined in the software using Gaussian fitting. The mean contrast values from the calibration protein solution were then plotted and fitted to a line, $y=bx$, with y–contrast, x–mass and b–C2M calibration factor.

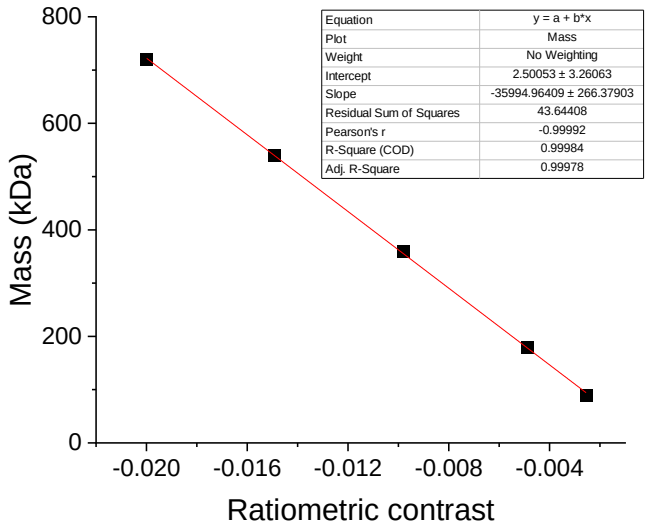

Figure S26: Size calibration for iSCAT measurements. Calibration curve for the conversion of ratiometric contrast to mass for a known protein oligomer standard. This calibration curve was used to estimate the average mass of the micelles of **3**.

Biphasic reaction between **1** and **2a** for iSCAT (Figure 3.10a and 3.10b):

Reactions for monitoring by iSCAT were set up using a modification of the general oscillation procedure above and with filtered stock solution filtered (0.22 µm microfilter) before addition to the round bottom flask. For both Figure 3.10a and 3.10b, thiol **2a** (180 µL, 18 eq.) was used. At given time intervals, 1.0

µL aliquots were taken from the aqueous layer, diluted with 499 µL of buffer (500-fold dilution), and 30 s iSCAT videos were recorded immediately. At the same time, 10 µL aliquots were taken for UPLC analysis.

Figure 3.10a: 5 mg DMAP per 4 mL TRIS buffer, hydrogen peroxide (0.56 M, 120 µL/h)

Figure 3.10b: 25 mg DMAP per 4 mL TRIS buffer, and hydrogen peroxide (0.56 M, 60 µL/h)

Cryo-EM measurements:

Grids were prepared using a Vitrobot mark IV (FEI) at 100% humidity. A volume of 3.5 µL at 5 mM concentration was applied to glow discharged Ultrafoil R2/2 200 mesh grids, blotted for 3.0 seconds and plunge frozen in liquid ethane.

Movies were taken at 150,000x microscope magnification, given a calibrated pixel size of 0.96 Å/px, with a total dose of around 60 e-/Å^2 and defocus values between 3.5 and 4.5 µm on a 200 kV Glacios (Thermo Fisher Scientific) microscope equipped with a Flacon III detector using EPU versions 2.5. Movies were aligned using full-frame motion correction in CryoSPARC-V3.1. CTF was estimated with GCTF and particles picked using blob picker, then extracted in 104 px box and submitted to a round of 2D classification.

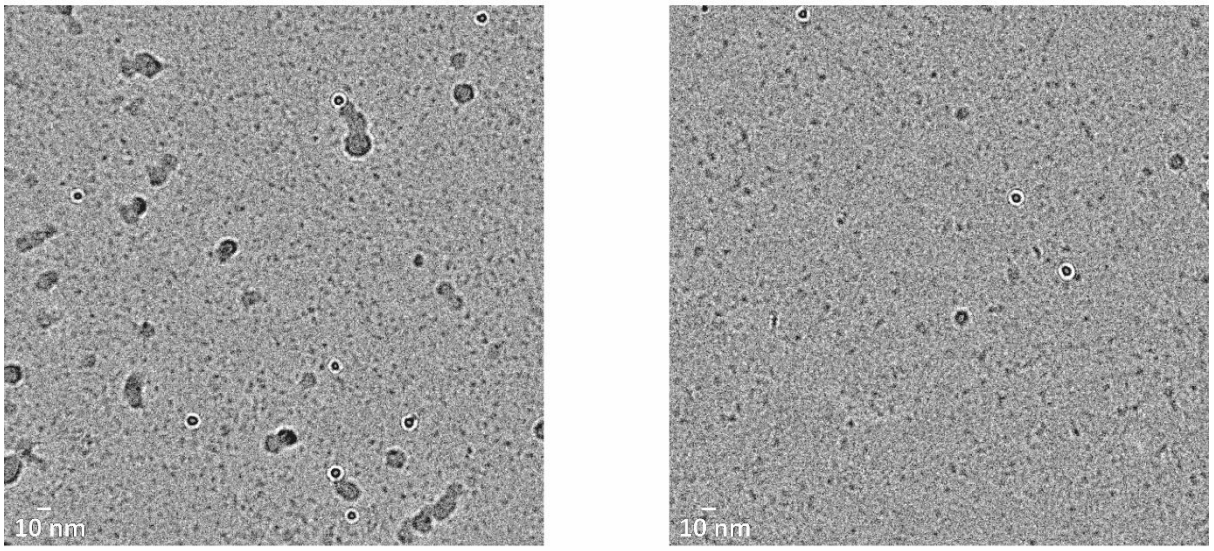

Figure S27: Cryo-TEM images of micelles composed of surfactants 3a and 3b. Images were recorded for 5 mM samples of compounds **3a** (left) and **3b** (right) in TRIS buffer (0.5 M, pH 9.00), showing micelles of approximately 10 nm in size.

Ring tensiometry measurements:

A dilution series of each surfactant was prepared in 0.5 M TRIS buffer (pH 9.0) and the surface tension of each sample recorded at room temperature using a Krus K10ST tensiometer. Surface tension is plotted against ln([surfactant]), with the concentration at which the surface tension no longer decreases corresponding to the critical micelle concentration (CMC). This can be calculated using the intercept of two lines on the curves of Figures S27. Note that these CMC values were determined at room temperature, while all oscillation experiments were carried out at 40°C.

Measured CMC of **3a** = exp(0.4458) = 1.56 mM
Measured CMC of **3b** = exp(-0.6481) = 0.52 mM
Measured CMC of **6** = exp(0.5798) = 1.79 mM

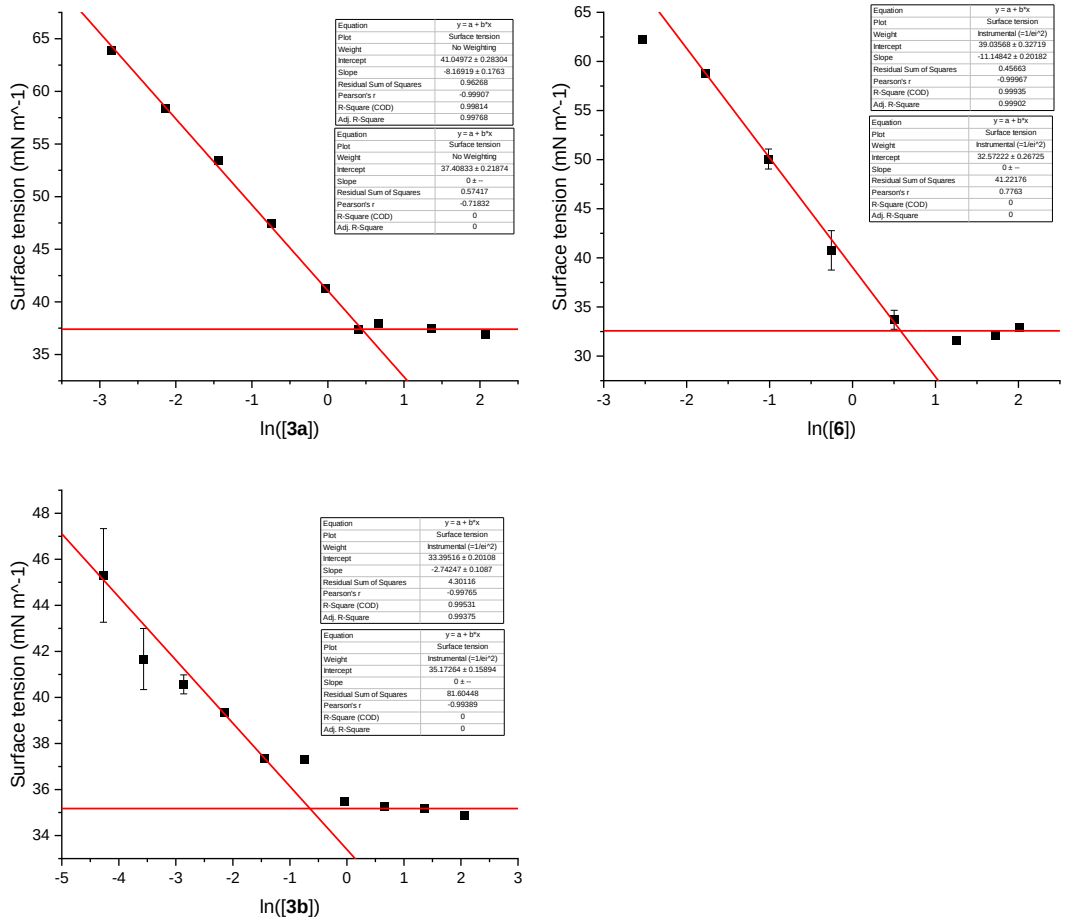

Figure S28: Ring tensiometry measurements on compounds **3a**, **3b** and **6**. Plot of the surface tension versus ln(concentration) in a TRIS buffer (0.5 M, pH 9.00). The intercept of the two lines corresponds to the critical micelle concentration (CMC).

Dynamic Light Scattering measurements:

DLS measurements were recorded using a Malvern Zetasizer Nano ZEN5600 machine and Zetasizer software for data processing. Samples of **3a** and **3b** were prepared as a serial dilution in 0.5 M TRIS buffer (pH 9.0). Three measurements were taken for each sample. Refractive index of 1.371 and viscosity of 1.0780 mPas were used in data processing. All samples were filtered using a microfilter (pore size, 0.22 µm) before measurement. Disposable plastic cuvettes were used with 1.0 ml of sample solution.

			Size (d.n...	% Intensity:	St Dev (d.n...
Z-Average (d.nm):	6.609	Peak 1:	8.192	97.9	3.404
PdI:	0.231	Peak 2:	3972	2.1	1091
Intercept:	0.827	Peak 3:	0.000	0.0	0.000
Result quality	Good				

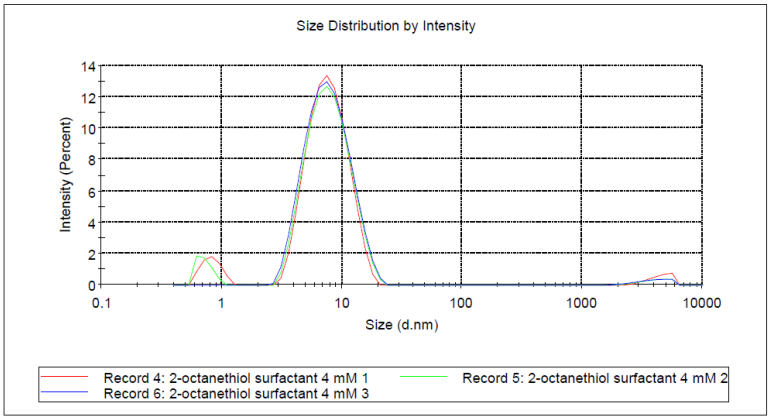

Figure S29: DLS measurement on a 4 mM solution of compound **3a** at pH 9.00.

			Size (d.n...	% Intensity:	St Dev (d.n...
Z-Average (d.nm):	8.850	Peak 1:	10.61	98.8	4.371
PdI:	0.192	Peak 2:	4270	1.2	977.7
Intercept:	0.918	Peak 3:	0.000	0.0	0.000
Result quality	Good				

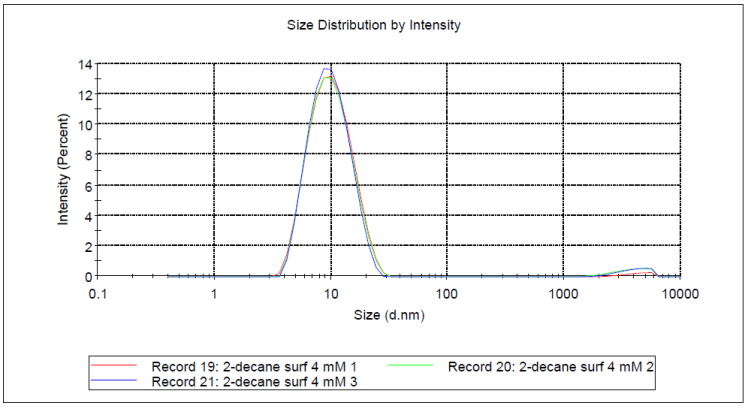

Figure S30: DLS measurement on a 4 mM solution of compound **3b** at pH 9.00.

7.4 Supplementary data for Chapter 4

7.4.1 Synthesis of compounds

Compounds **2a** and **4** were prepared as previously described in Experimental Section 7.3.

7.4.2 Procedures for kinetic experiments

General oscillation experiment procedure: A solution of compound **4** (57 mg, 0.29 mmol) and DMAP (30 mg, 0.25 mmol) in 10 mL TRIS buffer (0.5 M, pH 9.00) was prepared. From this solution, 4 mL was added to a 10 mL round bottom flask and stirred at 800 rpm at 40°C (oval stirring bar, *L*= 10 mm, ø= 5 mm). Thiol **2a**, 2-octanethiol (1.6 mL, 9.2 mmol) was carefully placed on top of the aqueous layer and the addition of hydrogen peroxide (0.56 M) by syringe pump (AL-1000, WPI) was immediately started at the desired addition rate. Reactions were regularly sampled (every 3 mins) and analysed as described in the Chapter 3 UPLC monitoring section.

Oxidant supply variation experiments (Figure 4.2a):

Data for Figure 4.2a were obtained according to the general oscillation experiment procedure above but with a reduced amount of DMAP (24 mg, 0.20 mmol) in the 10 mL TRIS buffer stock and a reduced amount of thiol **2a** (0.5 mL). The addition rate of hydrogen peroxide (0.56 M) was varied in this experiment, increasing from 50 to 100 to 200 µL/h.

Stirring rate variation experiments (Figure 4.2b):

Data for Figure 4.2b were obtained according to the general oscillation experiment procedure above but with a reduced amount of DMAP (24 mg, 0.20 mmol) in the 10 mL TRIS buffer stock and a reduced amount of thiol **2a** (0.5 mL) and with hydrogen peroxide (0.56 M) added at 100 µL/h.

Morse code experiment (Figure 4.4):

Data for Figure 4.4 were obtained according to the general oscillation experiment procedure above using thiol **2a** (2.0 mL, 11.5 mmol). The addition rate of hydrogen peroxide (0.56 M) was varied between 0,

130 and 300 µL/h. Oxidant rates were switched during the experiment based on the analysis of reaction aliquots by UPLC in real time.

Codon encoding experiment (Figures 4.5 and 4.6):

Data for Figures 4.4-4.5 were obtained as described in the general oscillation experimental procedure above. Oxidant and stirring rates were switched based on the analysis of reaction aliquots by UPLC in real time. The following sets of stirring rate and oxidant supply were used to obtain the four peak shapes:

Base:	Peak shape:	Stirring rate /rpm	Oxidant supply /µLh^{-1}
A	Short, sharp	1200	90
C	Tall, sharp	1200	160
G	Short, broad	600	50
T/U	Tall, broad	300	80

7.5 Supplementary data for Chapter 5

7.5.1 Procedures for kinetic experiments

General U-tube oscillation experiment procedure

5.0 mL of a stock solution of compound **4** (70 mg, 0.35 mmol) in 10 mL TRIS buffer (0.5 M, pH 9.00) was carefully added to a glass U-tube vessel containing a disc-shaped stir bar (ø= 13 mm) heated at 50 °C and stirred at 900 rpm. To this, separate organic layers (1.50 mL each) were carefully introduced, followed by a H_2O_2 addition needle into the aqueous phase. The LHS (donating) phase usually being 1-heptanethiol and the RHS (receiving) phase usually being n-dodecane. The apparatus is adjusted to allow for consistent stirring and the addition of H_2O_2 (0.51 M, 60 µL/h) by syringe pump (AL-1000, WPI) was then started. The reaction was regularly sampled every 10 mins from the aqueous phase and analyzed as described in the UPLC section. Samples of the organic phases were taken every 20 minutes and analysed by HPLC.

The experiment in Figure 5.1 was conducted according to a modification of the Chapter 3 general oscillation procedure where the H_2O_2 supply was modified (0.56 M, 150 µL/h), a reduced amount of DMAP (6.25 mg, 0.35 equiv.) used and the reaction conducted at room temperature. Indigo (2.5 mg) was included in the TRIS buffer stock as a suspension prior to initiation of the reaction.

The data in Figure 5.4 was obtained according to a modification of the general U-tube oscillation procedure with the following changed parameters: stirring rate of 800 rpm, temperature of 40 °C and H_2O_2 addition rate of 200 µL/h (0.22 M).

The data in Figure 5.5 was obtained as a triplicate according to the general U-tube oscillation procedure.

The data in Figure 5.8 was obtained according to the general U-tube oscillation procedure using saturated solutions of the cargo molecules in 1-heptanethiol at 40 °C as the donating organic layer.

The data in Figure 5.16 was obtained according to a modification of the general U-tube oscillation procedure with the following changed parameters: H_2O_2 addition rate of 60 µL/h (0.525 M) and organic layer volumes of 1.80 mL.

1 Polster, J. & Schieberle, P. Structure-Odor Correlations in Homologous Series of Alkanethiols and Attempts To Predict Odor Thresholds by 3D-QSAR Studies. *J. Agric. Food Chem.* **63**, 1419-1432 (2015). https://doi.org:10.1021/jf506135c

2 Morrow, S. M., Colomer, I. & Fletcher, S. P. A chemically fuelled self-replicator. *Nature Communications* **10**, 1011 (2019). https://doi.org:10.1038/s41467-019-08885-9

3 Tanner, D. D., Zhang, L., Vigneswaran, M. & Kandanarachchi, P. The Regioselective Reaction of Atomic Hydrogen with Unsymmetric Disulfides and Sulfides. *The Journal of Organic Chemistry* **60**, 4481-4487 (1995). https://doi.org:10.1021/jo00119a027

4 Young, G. *et al.* Quantitative mass imaging of single biological macromolecules. *Science* **360**, 423-427 (2018). https://doi.org:10.1126/science.aar5839